The Effect of an Embedded VSC-HVDC link on the Transient stability of the Dutch and German Transmission Systems

Polykarpos-Antre Christoforidis

Master of Science Thesis

Faculty of Electrical Engineering, Mathematics and Computer Science
Department of Electrical Sustainable Energy
Specialization in
Intelligent Electrical Power Grids

Supervisors

Dr. dipl-ing. Marjan Popov
Dipl-ing., MSc Mario Ndreko
Ir. Jorrit Bos

Delft, November 2014

Abstract

Driven mainly by the Kyoto Protocol and the EU climate action (20-20-20 targets), the country members of the European Union have taken actions towards the reduction of emissions and the increase of the electricity generated by Renewable Energy sources (RES) **[49]**. According to studies of the European Network of Transmission System Operators for Electricity (ENTSOE), the participation of RES generation in the generation mix of Europe will be majorly increased compared to the present situation **[2].** According to these studies a major contributor to this RES increase will be Germany. The German government's energy transition plan **[5]**, intends to replace most of the country's nuclear generation with renewable energy generation. A large part of the renewable energy generation will come from offshore wind parks. These windparks will be located in the north of Germany, in the North and Baltic seas. This change in generation mix will affect the geographical distribution of Germany's generation sites leading to possible threats for the secure operation of the German transmission system **[3]**. In order to overcome congestions in the transmission system the German Transmission System Operators (TSOs) have proposed the construction of four High Voltage Direct Current (HVDC) transmission corridors which will be embedded in the German transmission system. These HVDC corridors (termed A, B, C and D) will span from the north to the south of the country and will facilitate the transmission of the large offshore wind generation in the north to the large load centers in the south.
This MSc thesis focuses on studying the effect of Corridor A on the transient stability of the transmission system. Due to the proximity of Corridor A to the German border with the Netherlands and thus the proximity of its HVDC converter stations to the Dutch transmission system it is interesting to see if and how this HVDC corridor affects the transient stability of the German as well as the Dutch transmission system.
An analysis of the control parameters of the VSC-HVDC under various faults in the AC system is implemented in order to examine their effect on the voltage of the AC network and the rotor angles of the system's online generators. The grid code compliance of Corridor A with the short circuit current contribution and its effect on the system's voltage and rotor angle response of its generators will be observed. Additionally this thesis studies the effect a sudden loss of Corridor A will have on the power tie-line power between the Dutch and German power systems and the rotor angle stability of generators located both in the Nethrlands and Germany. In order to perform the aforementioned studies time-domain simulations will be performed using Siemens PTI's software tool Power System Simulator for Engineers (PSS®E).

The results of the study show that the higher the short circuit reactive current contribution the more effective the voltage support during a disturbance. However the effect of the short circuit reactive current contribution on the rotor angle responses of the generators is not always that clear due to the many factors that can affect it. Additionally the results show that the influence of the HVDC converters is regional. Therefore the effects of the short circuit current contribution of the HVDC converters, is more pronounced in the German transmission system than in the Dutch. These results will lead to recommendations for the HVDC converter parameters in order to achieve the best results for the voltage profile and rotor angle stability of the generators of the system.

1. Introduction

1.1 Background

Driven mainly by the Kyoto Protocol and the EU climate action (20-20-20 targets), the country members of the European Union have taken actions towards the reduction of emissions and the increase of the electricity generated by Renewable Energy sources (RES) **[49]**.

ENTSO-E's Scenario Outlook and Adequacy Forecast (SO&AF) is an annually published report that analyses the adequacy of the pan-European power system by providing an overview of generation adequacy for all ENTSO-E members, for regions and for individual countries at a mid- and long- term time horizon **[1].** These reports present two bottom-up scenarios, one conservative and one best estimate, as well as a top-down scenario based on the EU 2020 targets. 2012's SO&AF report predicts a major increase in the Renewable Energy Sources (RES) participation in the generation mix. In figure 1.1 the generation mix for 2012 and for 2020 is shown. **[2]**

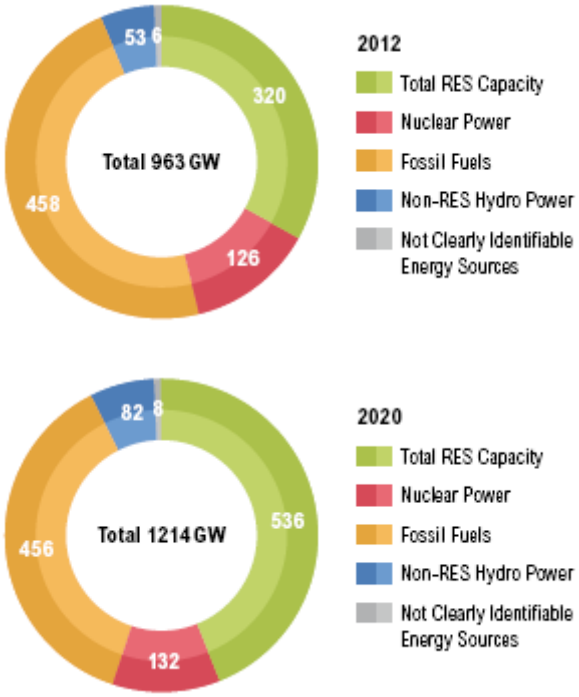

Fig. 1.1 generation mix in 2012 and 2020 (top down) [2]

According to the 2012 SO&AF report the total generation capacity in the EU will increase by 250 GW by 2020 reaching a total of 1214 GW (top-down scenario). The increase will be mainly due to the large penetration of RES generation and specifically wind and solar power. A great increase of RES generation is predicted also by the bottom-up scenario, although lower by 22 GW.

A great, if not the main, contributor in this renewable energy boom will be Germany. After 2011's nuclear accident in Fukushima, Japan, the German government decided to speed up the long term nuclear power phase out initially

planned, by shutting down 8 of its 17 reactors immediately. **[5]** The rest of them are planned to be shut down by the year 2022. This conventional generation, will be replaced by increasing for the major part wind power generation and in a smaller degree fossil fuel based generation.

Germany's RES generation 2023 (GW)					
Onshore wind	**Offshore wind**	**Photovoltaic**	**Biomass**	**RES hydro**	**Other RES generation**
49.3	14.1	61.3	8.5	4.8	1.5

Table 1.1 Prediction of Germany's RES generation according to the reference scenario for 2023 [3]

Germany's offshore wind generation is located in the North and Baltic seas.
According to **[33]** the total offshore wind generation as in March 2014 is 628.3 MW, of which 577.5 MW are located in the North Sea and 50.8 MW in the Baltic Sea.

North Sea offshore wind generation (March 2014)					
Project	Hooksiel	Aplpha Ventus	BARD offshore 1	ENOVA Offshore Ems-Emden	Riffgat
Capacity (MW)	5	60	400	4.5	108
Total (MW)	577.5				

Table 1.2 North sea offshore wind generation in March 2014 [33]

Baltic Sea offshore wind generation (March 2014)		
Project	Baltic 1	48.3
Capacity (MW)	Rostock	2.5
Total (MW)	50.8	

Table 1.3 Baltic sea offshore wind generation in March 2014 [33]

The German government's energy transition plan named *Energiewende*, will affect greatly the grid in Germany as well as the ones in its neighbouring countries. As of March 2014 a number of offshore wind projects of a total capacity of 7.8 GW in the North sea and 1.2 GW in the Baltic sea has been authorised and many other offshore wind generation projects are awaiting for approval **[33]**. The offshore wind targets are to reach a capacity of 11.000 MW by the year 2022. From the above it is clear that a large amount of power generation will be concentrated in the northern part of Germany while major load centers are located in the center (Ruhr) and south. The penetration of large amounts of wind power in the north will change the up to now generation-load distribution throughout the country therefore creating possible congestions in the existing AC grid **[3], [4], [5].** Therefore the main problem lies in how to transfer this concentrated amount of offshore wind power from the generation sites to the large load centers in an efficient way without compromising the transmission system's security.

Figure 1.2 shows that if the German generation in 2023 changes according to Energiewende, many lines of the German transmission system will be overloaded if no actions are taken to reinforce it. The percentage in the figure represents the loading of the transmission lines.

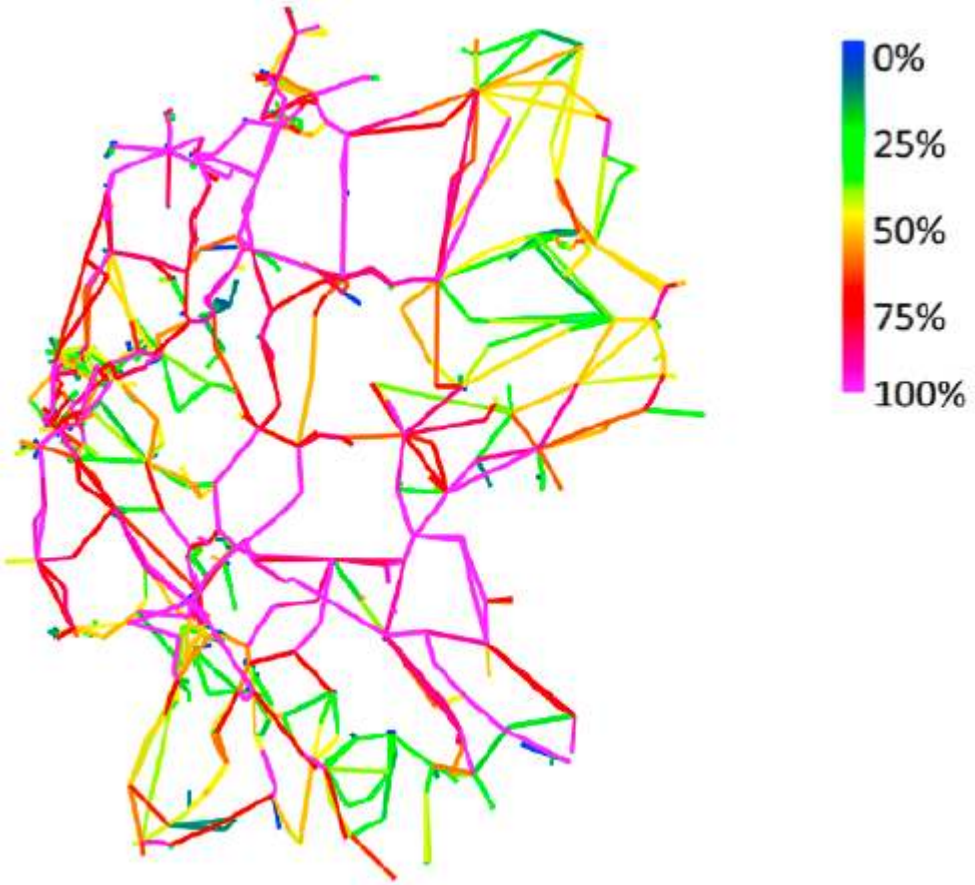

Fig. 1.2 German transmission system (as in 2013) line loadings for a typical scenario of high wind generation and high load in 2023 [3]

Since 2012 the four German Transmission Network Operators (TSO's), 50 Hertz, Amprion, TenneT and TransnetBW have been working on the expansion of the existing transmission grid on land in order to ensure stable grid operation for the new generation mix mentioned above. The expansion plan focuses on high power north-south connections. The requirements for new construction include 1500 km of AC transmission lines and 2100 km of corridors for High Voltage DC (HVDC) transmission lines. The four DC corridors (A,B,C and D) will have a total transmission capacity of 12 GW. **[3]**

The selection of HVDC technology over HVAC for the bulk transfer of power from the north of Germany to the south is justified by the following reasons.

Even though HVDC terminal station costs are quite high due to the conversion equipment, overall savings in capital cost arise due to lower cost of transmission lines. This happens because less conductors are needed for DC transmission than in 3-phase AC transmission. Also DC conductors are in principle thinner than AC ones because DC transmission doesn't suffer from skin effect. Furthermore if overhead line transmission is used, the HVDC transmission towers are smaller and simpler than the AC ones. **[6]**

Benefits in using HVDC are also present when using underground cables instead of overhead lines. Due to the proximity of cables to each other or to the ground, an unavoidable capacitance, known as stray capacitance, occurs. Due to their structure the stray capacitance of underground cables is much higher than that of an overhead line. This would pose a problem if the cable were to transmit AC current because the

polarity change in each cycle would charge and discharge the cable creating a charging current which utilizes a large part of the transfer capability of the cable. In the case of HVDC transmission the cable draws no charging current allowing power to be transmitted over any cable length, limited only by the cable cost and Ohm losses. **[6]**

It can be seen in figure 1.3 that the initial investment (for zero transmission distance) is quite higher for HVDC systems than for AC transmission systems. This difference is due to the high cost of the converter station equipment. However the rate of increase of the investment cost for HVDC transmission systems is lower than for AC transmission systems mainly due to the need for line compensation of the latter. Therefore the investment cost of the two transmission technologies becomes equal at a specific transmission distance known as break-even distance. For transmission distances above the break-even distance HVDC is a more economically viable solution than HVAC.

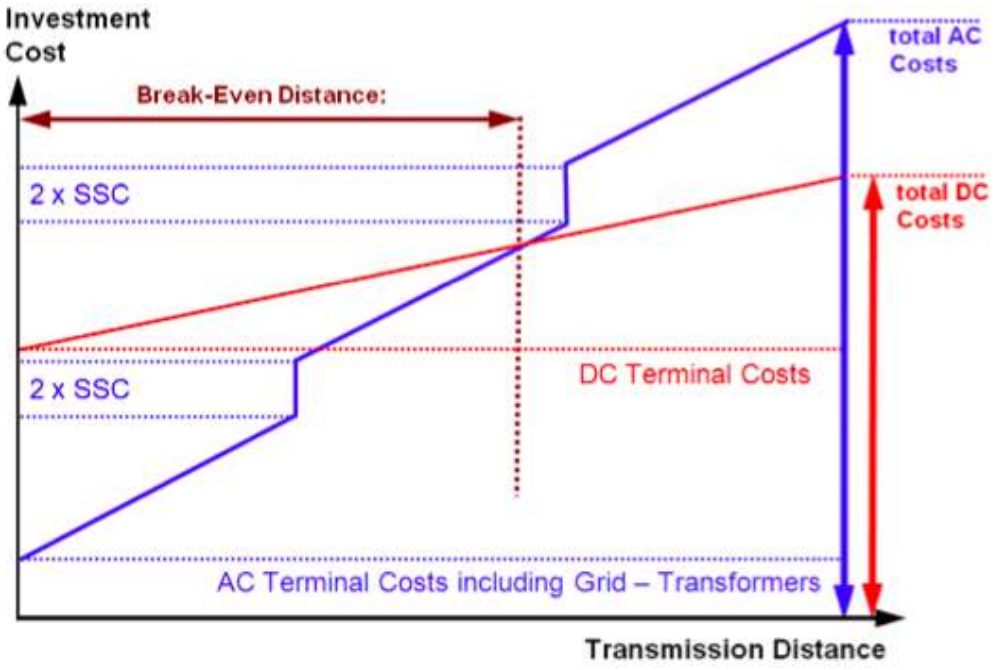

Fig. 1.3 Investment cost vs. transmission distance for HVAC and HVDC lines [7]

Another important reason why HVDC was preferred is the fact that DC transmission can provide greater controllability to an AC system. Given the fast control of power electronics used in the converter stations power flow control is easily implemented in HVDC technology which can lead to reducing loop flows and bottlenecks. This high controllability can be accomplished by using Voltage Source Converters (VSC) for power conversion of DC links. Their four quadrant operation allows VSCs to not only control active power flow but also provide an independent control of the reactive power output. Therefore through the appropriate controllers the VSC-HVDC converters can provide ancillary services such as frequency control, reactive power and voltage control. Such services might improve the stability of the AC transmission system in case of a disturbance. **[8]**

1.2 Problem definition and thesis objectives

As mentioned in paragraph 1.1 the German TSOs are planning to construct four HVDC corridors in order to ensure the secure operation of the network after the planned changes in Germany's generation mix and geographical distribution.
The location of these corridors (coloured purple) is shown in figure 1.4.

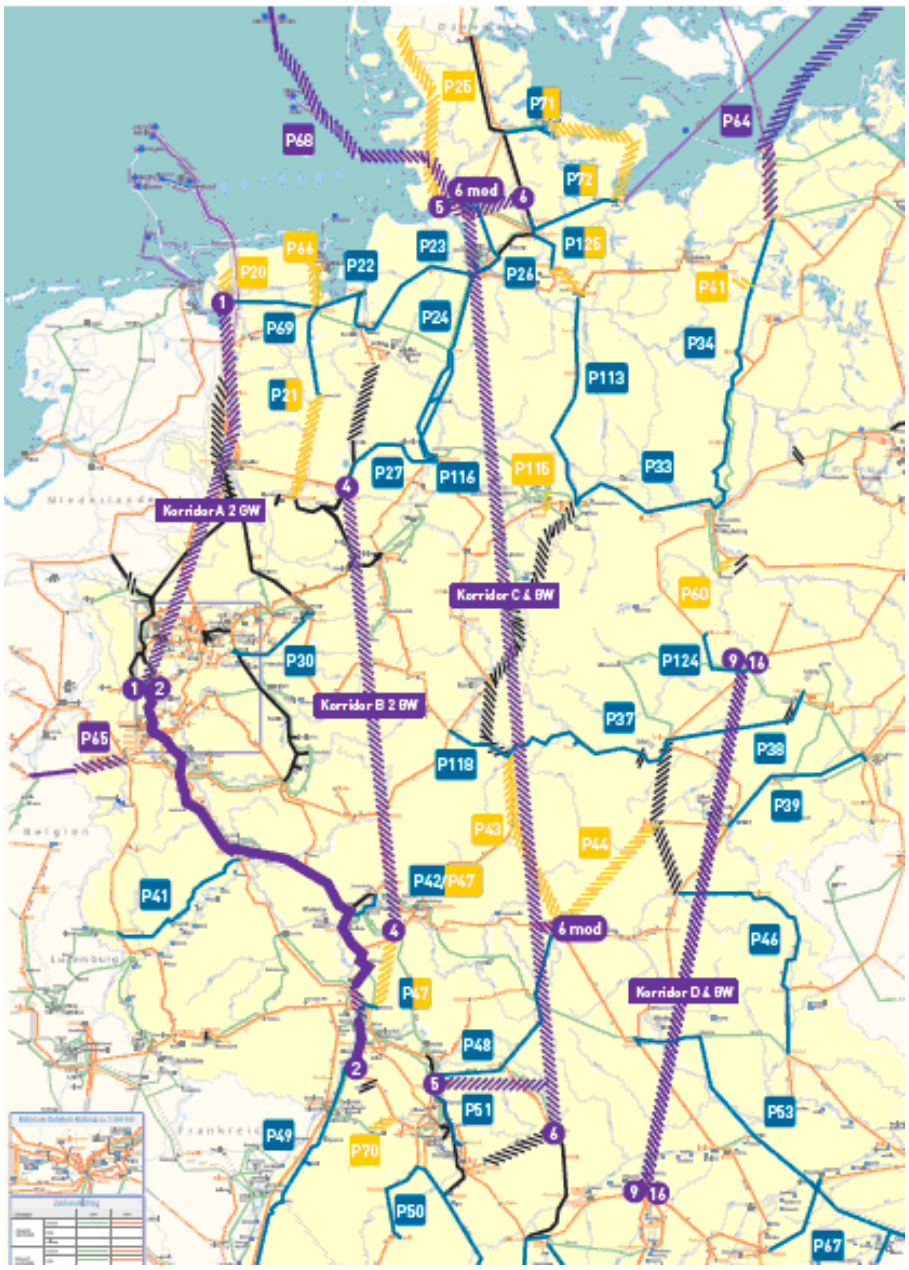

Fig. 1.4 HVDC corridor locations [3]

As can be seen Corridor A is located in the west of Germany, very close to the borders with the Netherlands and Belgium. Due to its proximity to the Dutch borders Corridor A might influence the Dutch transmission system.

It will consist of two sections, the first section will span from Emden, a connection point for offshore wind parks under construction, to Osterath and the second section will continue from Osterath and end up in Philippsburg which is located in the south, close to large load centers of Germany. The total length of Corridor A will be

approximately 660 km and it will have a transfer capacity of 2 GW. The second section of corridor A (Osterath-Philippsburg) will follow an existing transmission path and will be implemented by switching from AC to DC transmission. The transmission path followed by the other section (Emden-Osterath) is not yet specified. The planned year of commissioning of the Emden-Osterath section is 2019-2020 and of the Osterath-Philippsburg section is 2018. The converter technology used will be that of VSC. **[3]**

As will be analyzed in chapter 2, the fast acting controls of the HVDC system converters combined with the four-quadrant operation of the VSC technology can provide voltage support to the grid during steady state operation and under sytem faulted conditions. Therefore besides alleviating congestions, Corridor A's behaviour during faults may have an influence on the stability and system security of the Dutch grid. This thesis studies Corridor A and its effect on the Dutch grid emphasizing on transient stability issues.

Studies so far, regarding HVDC links embedded in AC transmission systems, show that VSC-HVDC links are capable of improving the operation of the transmission system. Authors in **[9]** and **[10]** show that the reactive power support of the VSC-HVDC can help increase the maximum power transfer and also maintain the voltage in the Point of Common Connection (PCC) of the HVDC with the AC system within acceptable limits thus avoiding voltage collapse due to lack of reactive power. Another study **[11]** shows that the VSC-HVDC could help increase the Critical Clearing Time (CCT) of generators located near the PCC and also help increase the voltage recovery rate of the PCC after a fault, which is important for the stability of the system. Increase of CCT by embedding a VSC-HVDC link into an AC system is also noted in **[7]**. Other studies such as **[12]** and **[13]** show that through reactive power support, VSC-HVDC links can help improve system stability by supporting the voltage of Line Commutated Converter-HVDC (LCC-HVDC) in a multi-infeed system, and the voltage of dynamic loads such as induction motors during faults. The aforementioned references usually use radial systems or simplified test systems to conduct the dynamic studies.

Authors in **[14]** study the effect of the short circuit reactive current control of VSC-HVDC connected wind generation plants on the system's voltage profile and transient stability. It is shown that short circuit current injection may lead the system to instability if not properly handled. The similarity of controls of the converters of VSC-HVDC connected wind parks and poin-to-point VSC-HVDC lines makes it possible to extend the study results to the operation and transient stability of point-to-point embedded HVDC links.

In **[37]**, the authors examine various sensitivity parameters affecting the short-circuit reactive current contribution of VSC-HVDC connected wind power plants and their effect on the transmission system's voltage and transient stability after a disturbance.

It can be concluded from the above studies that the capability of VSC-HVDC links to provide reactive power support can be beneficiary to the system's voltage profile during faults and under post-fault conditions. Additionally it is observed that VSC-HVDC voltage support can affect the transient stability of the system. Therefore the present study will focus on the control characteristics and capabilities of VSC-HVDC Corridor A and particularly those related to reactive power and voltage support.

A sensitivity analysis of the control parameters of the VSC-HVDC under various faults in the AC system will be implemented in order to examine their effect on the voltage stability of the AC network and the rotor angle stability of the system's

generators. The grid code compliance of the Corridor A with the fault ride-through and short-circuit current contribution will be observed. In more detail, the effect of the amount of additional short-circuit reactive current injection as a function of the voltage dip during a fault, on the system's voltage and rotor angle stability will be examined. Due to the limited capability of power electronic equipment in the VSC converters to high currents, the converters have a limited short-circuit current contribution and thus through appropriate switching actions, known as current limitation strategies, the converter current is maintained below the critical current value. In **[37]** and **[38]** it is seen that the various current limitation strategies and the way the active and reactive converter current components are prioritised affect the system voltage as well as the rotor angle stability of generators. Consequently the effect of current limitation strategies on the voltage and rotor angle responses will also be examined. Finally the effect of the current limit itself will also be examined. Through this study, recommendations on network code requirements of the VSC converter stations of Corridor A will be given.

First an IEEE multi-machine benchmark system will be used and then the study will be extended to a real case study such as the transmission system of Germany and its neighboring countries.

In the aforementioned sensitivity analysis, the effect of the transmission system modelling on the results will be examined.

Finally, another study that will be implemented is the examination of a sudden and permanent loss of Corridor A and the impact it will have on the power flow of the interconnecting lines between Germany and the Netherlands and the rotor angle stability of the system's generators.

The dynamic simulations will be run using a dynamic model representing the situation of the Dutch transmission network and that of its neighbouring countries in the year 2020. The software tool that will be used is Power System Simulator for Engineering (PSS®E) developed by Siemens, PTI.

1.3 Network code for HVDC

Besides the inherent characteristic of DC transmission of not generating or absorbing reactive power and therefore not needing line compensation, the advancements in the field of power electronics have provided HVDC transmission systems with flexibility and fast control over power flow. These characteristics of HVDC can prove quite beneficiary for applications such as bulk power transmission over long distances, submarine and underground cable transmission, connection of asynchronous areas etc. Due to network development and the shift towards renewable power generation such applications are becoming common in modern power systems and thus the installation of HVDC systems is increasing. **[7]** Existing but also upcoming HVDC links in Europe, such as the France-Spain interconnector, the Allegro HVDC link (Belgium-Germany) the four HVDC transmission corridors in Germany and numerous other projects for the connection of offshore wind parks with the AC transmission grid have increased the impact of HVDC transmission systems on the operation of the AC transmission system. This increasingly important role of HVDC systems has given rise to the need for common rules and requirements for HVDC system owners and power generating facility owners of DC-connected power park modules in order to contribute to the efficient functioning of the European electricity market and ensure the system's secure operation. To this end, ENTSO-E has recently published a Network Code requirement for HVDC connections and DC-connected power park

modules **[15]**. These network code requirements tackle issues such as active power control and frequency support, reactive power control and voltage support, fault ride through, power system restoration and other. ENTSO-E's Network Code on HVDC, aims in giving general guidelines for the acceptable operation of HVDC links. The TSO's of each country can further specify the network requirements while respecting the guidelines given in **[15]** by ENTSO-E.

This study focuses on requirements regarding reactive power control and voltage support as well as fault ride through of HVDC transmission systems, therefore this chapter will present only the relevant grid codes.

1.3.1 Reactive short circuit current contribution during faults

During three-phase faults the converter station shall be capable to provide additional reactive short circuit current in order to maintain as high as possible the voltage at the PCC. The amount of reactive current depends on the deviation of the voltage from its nominal value. The relevant TSO should specify the time by which the 2/3 of the additional reactive current should be provided. The relationship between voltage deviation and additional reactive current must be linear. The slope of the curve is to be specified. The voltage set-point can have a deadband from zero to 5%.

According to the German grid code the additional reactive current should follow the characteristic presented in fig. 1.5.

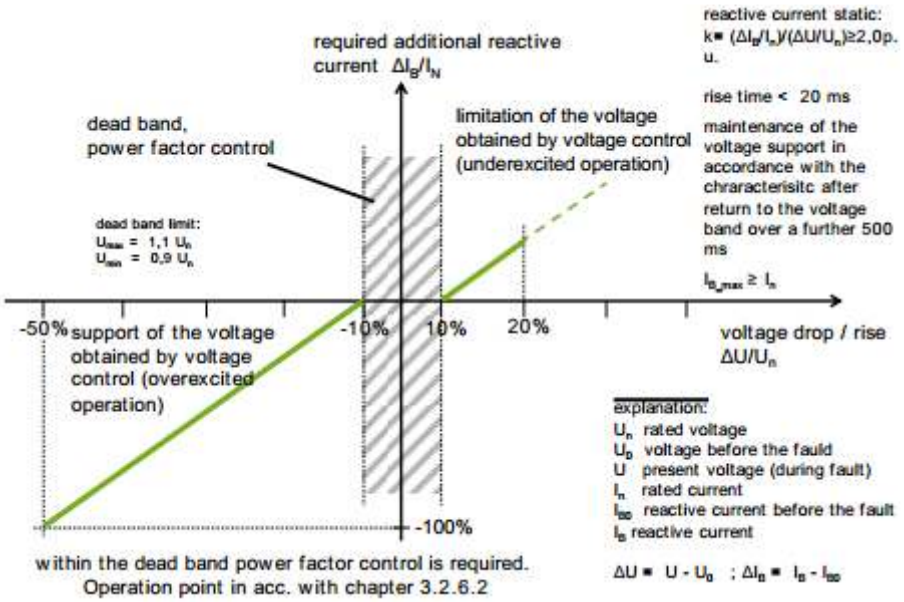

Fig. 1.5 Additional reactive current as a function of voltage deviation [16]

In the case of faults or low/high voltage operation the relevant TSO shall decide whether active or reactive current contribution has higher priority.

1.3.2 Fault ride through

A voltage-against-time profile at the PCC is provided in order to specify the operation of the converter station during a symmetrical (3 phase) fault.

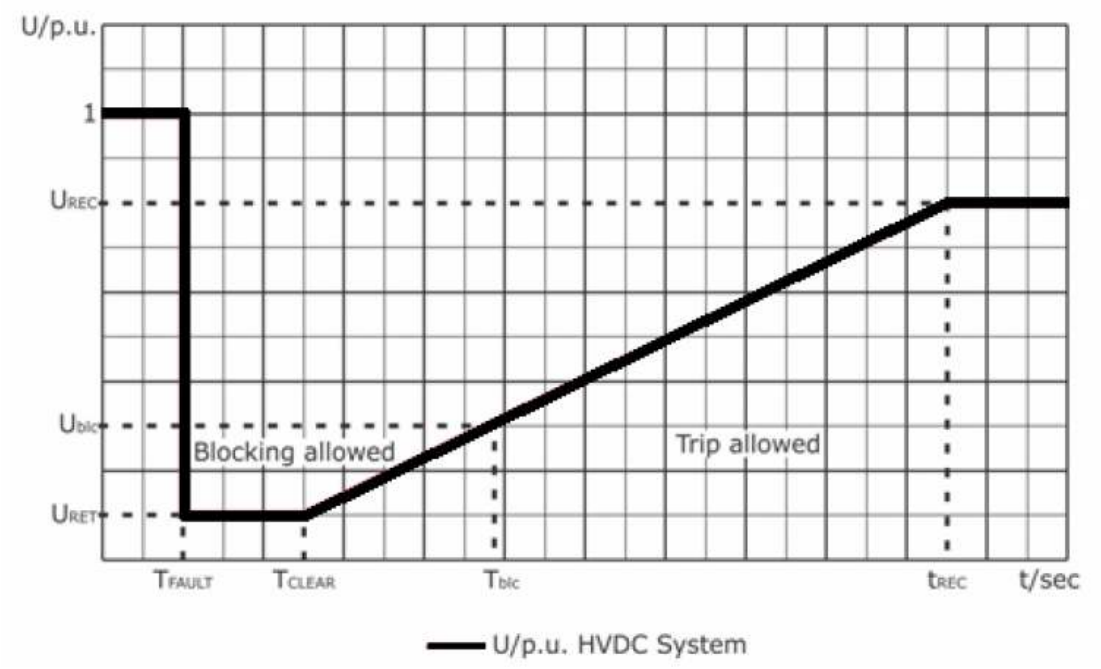

Fig. 1.6 U-t profile at connection point of the HVDC converter station with the AC grid [15]

The curve in fig. 1.6 shows the course of the minimum allowable voltage at the PCC, in pre-fault, fault and post-fault conditions. As long as the phase-to-phase voltage at the PCC stays above this curve, the HVDC converter station must stay connected to the AC grid. In fig. 1.6 the voltage is expressed in per unit (voltage base equals to the nominal voltage at the PCC). U_{ret} is the retained voltage during the fault, t_{fault} is the time the fault occurs and t_{clear} is the time the fault is cleared. Below U_{blc} the HVDC converter is allowed to be blocked, meaning it stays connected to the grid but without providing any active or reactive power. U_{rec} refers to the recovered voltage after the fault clearance and t_{rec} is the time at which it is reached.

The parameters mentioned above can range through a set of values specified in table 1.4.

Voltage parameters (p.u)		**Time parameters (seconds)**	
$\mathbf{U_{ret}}$	0-0.3	$\mathbf{T_{clear}}$	0.14-0.25
$\mathbf{U_{rec}}$	0.85	$\mathbf{T_{rec}}$	1.5-10
$\mathbf{U_{blc}}$	0-0.75	$\mathbf{T_{blc}}$	as defined by the U-t profile

Table 1.4 Parameters for fault ride through of HVDC converter station [15]

1.4 Thesis layout

In chapter 2 a presentation and comparison of the existing HVDC transmission technologies is presented. Main emphasis will be given on the VSC-HVDC technology and the general topologies and components of this technology will be presented. Additionally in this chapter a brief explanation of the concept of power system stability will be given.

Chater 3 begins by introducing the controllers of the VSC converters. Next the VSC-HVDC line model that is used for the dynamic simulations is introduced and

explained. Finally the validation of the model and an introduction to the sensitivity parameters that will be examined for Corridor A, are done on a smaller system model, the IEEE 39 bus system.

In chapter 4, the results of the simulations described in paragraph 1.2 will be presented. A thorough analysis of the results follows. The result presentation will start with the results of the sensitivity analysis. The effect of Corridor A's examined parameters on the Dutch and German transmission systems will be presented. Next the effect of the transmission system modelling assumptions on the results will be examined. The main focus will be on the modelling approach of wind power plants of the system. Finally the effect of the sudden and permanent loss of Corridor A on the transmission system's stability will be presented and analyzed.

Finally in chapter 5 the conclusions of the results presented in chapter 4 will be drawn. Recommendations for future research work on the present topic will also be done.

2. HVDC Transmission

2.1 HVDC technologies

The application of HVDC transmission in power systems has been increasing in the recents years, however DC transmission is not a new concept. It was first attempted in 1889 by Rene Thury. This DC system was an electromechanical system which consisted of a series connection of DC generators and motors. This concept was applied in a number of projects in Europe, the best example of which is the DC interconnection of Moutiers and Lyon with a transmission capacity of 20 MW at 125 kV over 230 km. However, the complexity of the system and the difficulty to connect with high speed steam turbine generators, were significant drawbacks for this technology.

In 1902 the mercury-arc valve was invented by Peter Cooper Hewit. This was a technology that allowed rectification and inversion of large currents. It was initially used for industrial and railway applications. The first commercial application of this technology for HVDC transmission was in 1954, in the Gotland 1 project, in Sweden which was a submarine link that connected the island Gotland to the mainland and had a transmission capacity of 20 MW at 100 kV. This technology's main problems were arc-backfire (conduction on the opposite direction), the uneven voltage distribution across the valve and the handling of limited voltages (150 kV). **[17]**

HVDC transmission as known and used today is based on electronic power conversion. In this way conversion of AC voltage to DC voltage and vice versa is accomplished by using converters based on solid-state devices such as thyristors, IGBTS etc. The available HVDC technologies nowadays use either Line Commutated Converters (LCC, also know as current source converters) or Voltage Source Converters (VSC, also known as self-commutated converters). HVDC schemes using LCCs are known as Classical HVDC.

The basic module of LCCs and VSCs (two-level) is the Graetz bridge.

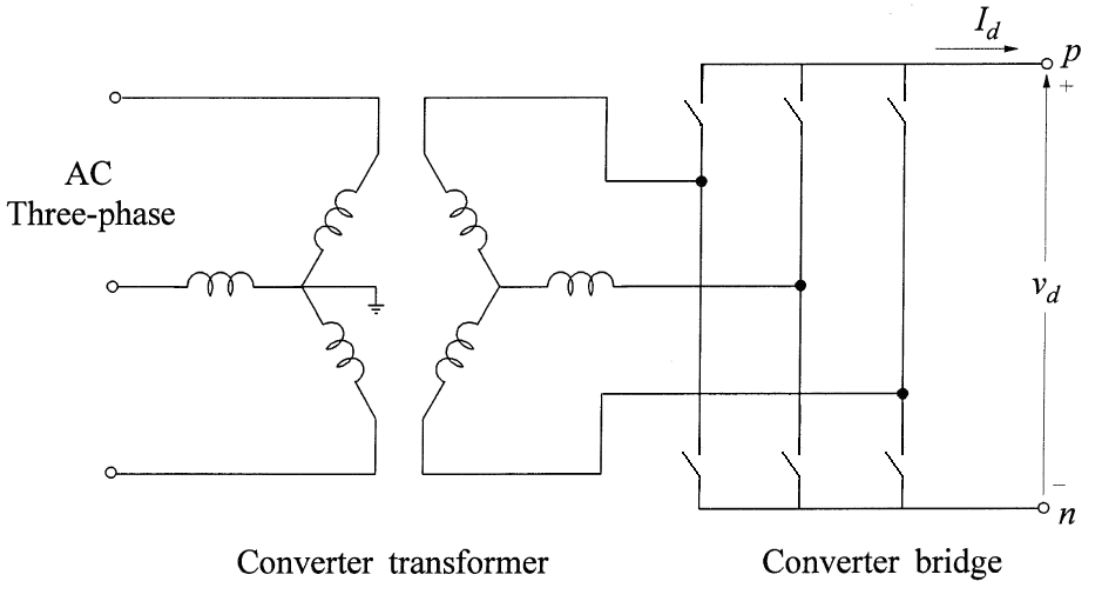

Fig. 2.1 Graetz bridge [18]

LCCs use thyristors as switching devices in the bridge, while VSCs use devices with both turn-on and turn-off capability such as IGBTs and GTOs.

2.1.1 LCC converters

LCCs are also known as line commutated converters. The name indicates that the conversion depends on the line voltage of the AC system. This happens because the switching device used in this type of converters is a thyristor.

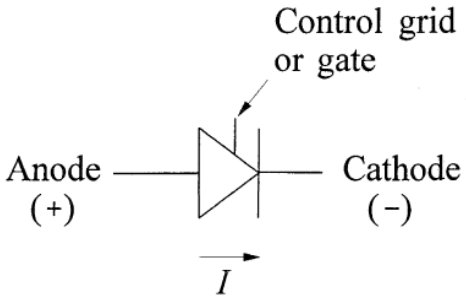

Fig. 2.2 Thyristor representation [18]

For a thyristor to conduct two conditions need to be satisfied. Firstly the thyristor must be forward biased, i.e the anode's potential must be positive relatively to the cathode and a triggering signal must be sent to its gate. Turn off of the thyristor cannot be controlled and is only accomplished once current drops to zero and tries to reverse. Hence the thyristor conduction depends on an existing AC voltage and this is why thyristor based converters are known as line commutated converters. **[18]** Modern thyristors have a blocking voltage capability of 8.5 kV. In order to achieve high voltage levels needed for HVDC transmission applications, each thyristor valve of the converter bridge consists of a series connection of a number of thyristors. For typical applications 24 to 30 thyristors are connected in series to create a valve. For ultra high voltage applications (around 800 kV) a valve may contain 60 series connected thyristors. **[19]**

The output voltage on the DC side of the Graetz bridge is shown in fig. 2.3.

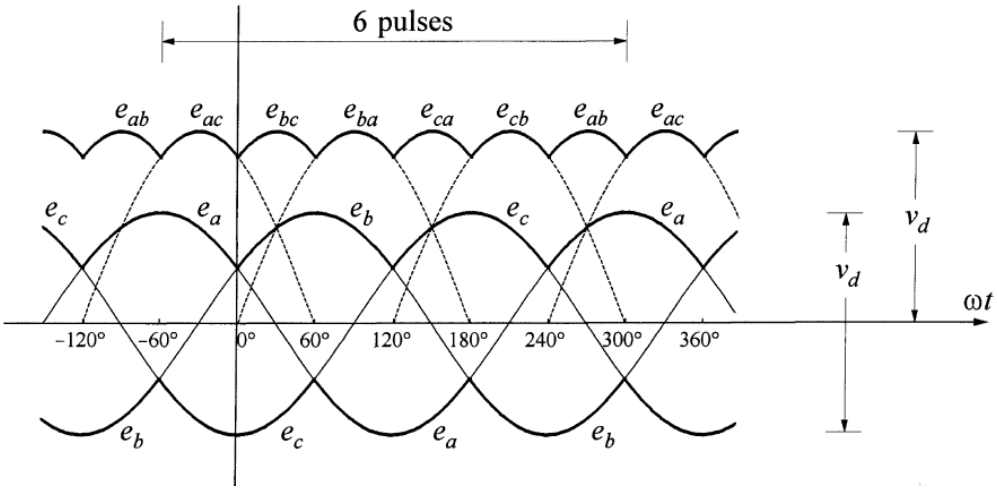

Fig. 2.3 AC side line-to-line voltages and DC side voltage of Graetz bridge [8]

During one electrical period the output voltage V_d of the bridge contains 6 pulses, therefore the Graetz bridge is also known as a 6-pulse bridge. In order to achieve higher and smoother DC voltages but also to decrease the harmonic content of the AC output voltage, classical HVDC systems use multiple bridge converters. This means that two or more 6-pulse converters are connected through Y-Y and Y-Δ transformers in order to achieve 12-pulse, 24-pulse or higher pulse outputs. Although the higher the number of pulses, the fewer harmonics usually classical HVDC uses the 12-pulse configuration. The complexity of the transformer connections for higher pulse configurations is the main reason for this choice. **[18]**

Regarding the mode of operation LCCs operate in the two lower quadrants of the P-Q plane. This means that they can provide or absorb active power but only absorb reactive power.

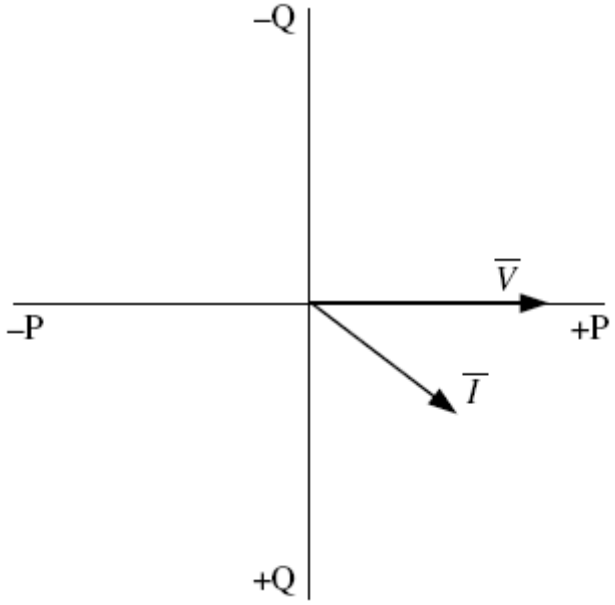

Fig. 2.4 Four quadrant diagram of converter with the voltage as reference [8]

This is due to the gate control of the thyristor which can be used to delay the "ignition" of the thyristor and control the magnitude of the DC voltage. The ignition angle α, results in a phase shift between the AC voltage and the fundamental frequency component of the converters current. For $\alpha=0^o$, the phase displacement is zero and it increases as α increases. Also the commutation delay due to the converter transformer's reactance results in a phase shift between voltage and current. These phase shifts have as a consequence the converter to absorb reactive power whether it operates as a rectifier or an inverter. The reactive power consumption of CSC converters is usually about 50% to 60% of the active power transferred **[8]**, **[18]**. Due to this reactive power consumption reactive power sources, such as shunt capacitors, must be connected at the terminals of the converters. Besides the reactive power compensation needed, the high reactive power absorption of LCCs makes the connection of classical HVDC to weak AC systems problematic.

A development in the CSC converters is the so called, Capacitor Commutated Converter (CCC). In this configuration capacitors are connected in series between the converter and the converter transformer in order to compensate the reactance of the transformer and assist the commutation voltage. In this way the converter absorbs less

reactive power reducing the size of the shunt capacitor banks and helping the operation of the converter when connected to relatively weak systems. **[8]**

2.1.2 VSC converters

The main disadvantage of LCCs is that the thyristor valves have only one degree of freedom, meaning that only their turning-on can be controlled. This means that the commutation process, from one switch to the other, depends on the AC network voltage and therefore the LCC cannot inject reactive power to a passive network. VSCs use solid state devices that their switching-on and switching-off are fully controlled. Depending on the needed switching frequency these devices can be IGBTs (for high switching frequency) or thyristor-type devices such as GTOs or IGCTs (for low switching frequencies). **[8]** This allows VSCs to operate on the four quadrants of the P-Q plane and therefore can generate or absorb reactive power in contrast to LCCs which only absorb. VSCs were first used in an HVDC transmission application in 1997 for the connection between Hallsjon and Grangesberg **[20].** This project was carried out by ABB. A detailed comparison of the LCC and VSC HVDC technologies can be found in appendix B.

There are three types of VSCs used in HVDC applications, two-level, three-level and modular multilevel converters. The categorization is done based on the voltage levels produced in the AC output of the converter, before it is filtered.

According to **[4]**, the VSC technology that will be used for Corridor A will be that of midular multilevel converters. Therefore a description of this technology is presented in this paragraph. Details on the other VSC technologies (two and three-level) can be found in appendix B.

Multilevel converters

Three-level converters are a first step towards multilevel conversion. Although the diode neutral point clamped and the flying capacitor converter topologies can achieve a higher number of voltage levels than three their use for this purpose is avoided. The main reasons for this is the considerably high number of clamping diodes (for the NPC converter) or clamping capacitors (for the flying capacitor converter) and the higher control and circuit complexity. **[8]**

A promising topology for multilevel conversion is the modular multilevel converter (MMC). A basic characteristic of this topology is its modularity. For this reason no central components are present. Therefore there is no common DC side capacitor as in the case of the two or three-level VSC. Each module contains its own capacitor which is connected to the terminals of a half-bridge **[24]**. The submodule topology is presented in fig.2.5 (a) and the three-phase converter topology is presented in fig. 2.5 (b).

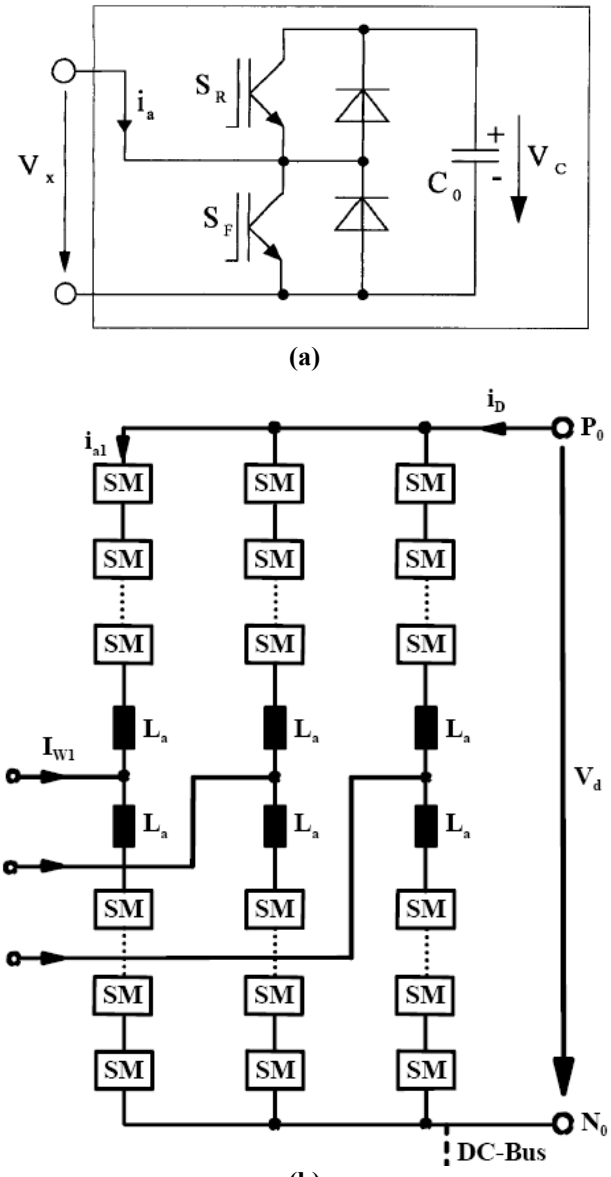

Fig. 2.5 (a) MMC submodule topology, (b) Three-phase MMC topology [25]

Each submodule's output can be either equal to zero or to the capacitor's voltage (V_C). In more detail when switch S_R is turned on and S_F is turned off then the submodule's output is V_C when S_F is turned on and S_R is turned off the submodule's output is zero and finally when both S_R and S_F are turned off the submodule is blocked. By adjusting the number of the switched submodules in the upper and lower arm, the output of each phase arm is adjusted.
The output of a MMC is shown in figure 2.6.

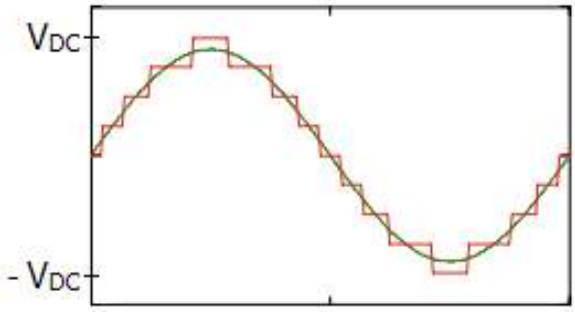

Fig. 2.6 MMC voltage output [35]

The inductances L_a, in each phase arm of the converter operate as chokes that limit the AC current in case of a DC fault. **[25]**

Since the MMC is modular, high voltage and power ratings can be easily accomplished. Also a high number of voltage levels can be achieved therefore the AC output approaches a sinusoid and therefore little or even no filtering is required. **[28]** This helps to further reduce the footprint of the converter stations.

Thanks to the small steps of the multilevel output, the switching frequency is low (150 Hz), leading to switching losses that are considerably lower compared to the two-level VSC. Low switching losses result in high efficiencies of the MMC, around 99.5%. A drawback of the MMC is that it involves complex design and control because each submodule must be controlled separately in order to achieve the desired voltage output. **[25], [27]**

2.2 HVDC link configurations

HVDC schemes can be classified in two types, Back-to-Back schemes and Transmission schemes. **[6]**

Back-to-back schemes are usually used to interconnect two AC networks with different frequencies. Both the converters in this scheme are located in the same location and no transmission line is used between them. Because no DC conductor is used back-to-back schemes are operated with high currents (3-4 KA) in order to minimize the cost and losses of the converter equipment. Figure 2.7 shows a typical back-to-back circuit configuration. Midpoint grounding (between the two converters) can be used in order to reduce the stress of the converter transformers.

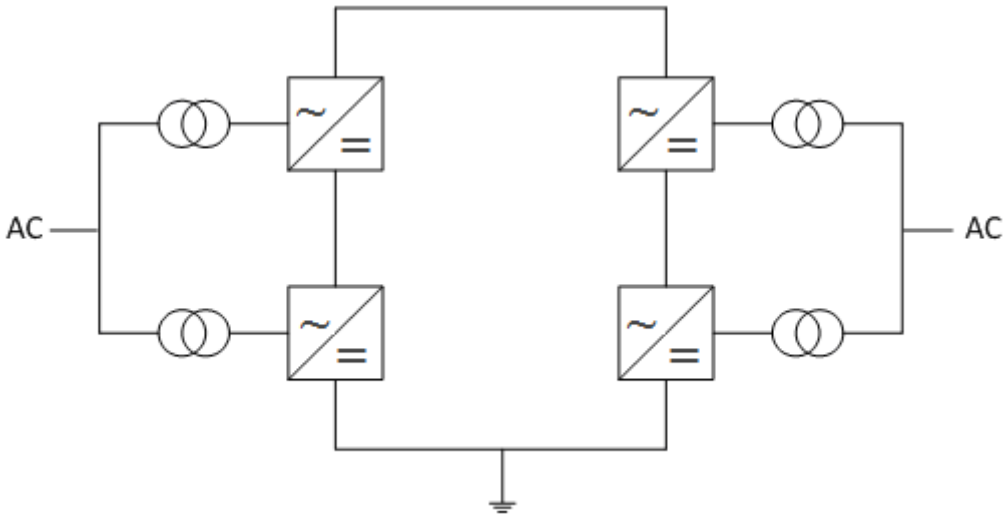

Fig. 2.7 Back-to-back scheme

On the other hand transmission schemes are used for bulk energy transmission over long distances. The two converter stations are connected through a DC conductor, either a transmission line or an underground/submarine cable. Two configurations are usually used for this scheme, the monopolar and bipolar configuration.

The monopolar configuration is the simplest of both. There is only one converter in each end of the DC conductor. The return is accomplished either by ground or sea (depending on the application) or by a metallic conductor. Monopolar links can also be the first stage in the development of a bipolar link. These two types of monopolar HVDC links are shown in figures 2.8 and 2.9.

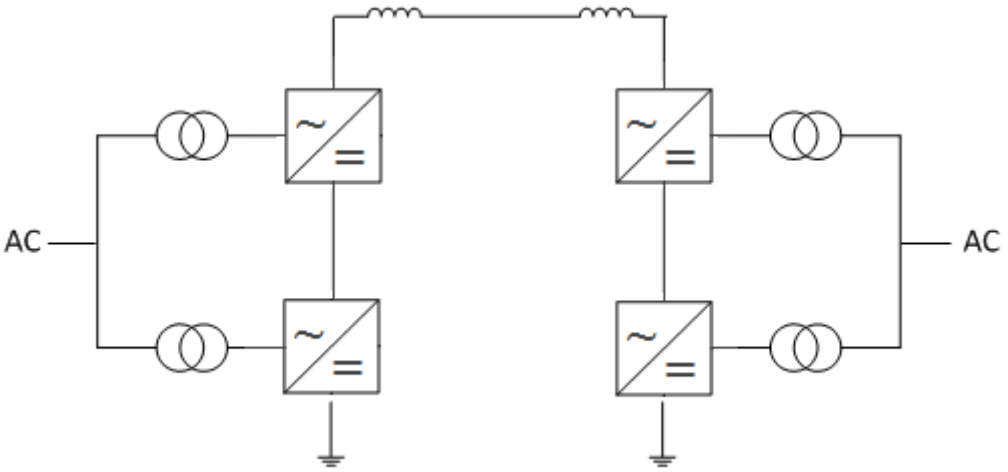

Fig. 2.8 Monopolar HVDC link with ground return

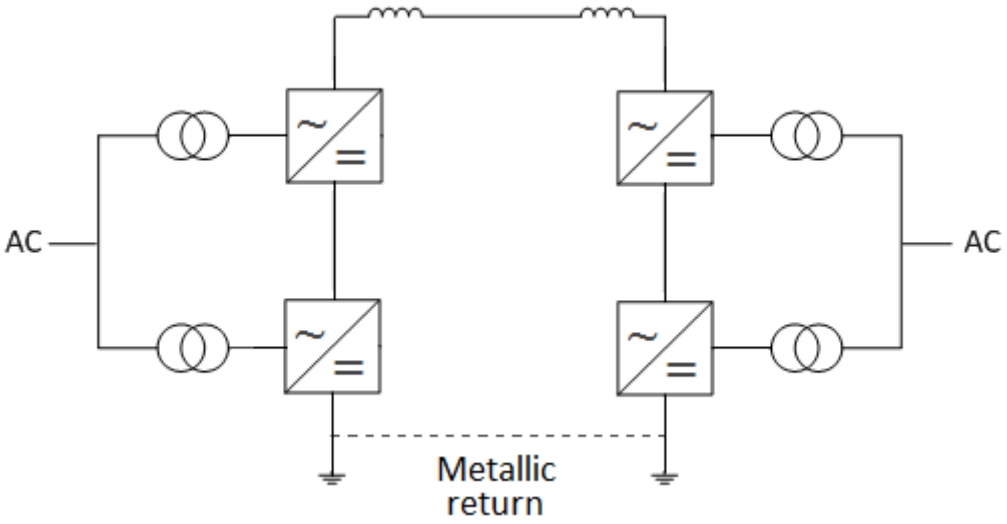

Fig. 2.9 Monopolar HVDC link with metallic return

The ground return has a lower cost since one conductor less is used. However when the earth resistivity is too high or interference with other underground or undersea metallic structures is possible, metallic return is preferred. **[18]**

The bipolar configuration has two independent poles, each consisting of an independent converter. This configuration uses two conductors, one has positive polarity while the other negative. Power flow can be in one or both directions. The bipolar configuration is arranged in such a way that the return currents cancel each other out. Each pole can operate separately or in a master slave configuration. In the case of a line fault in one line the other line can continue transferring power if separate control is used. If large ground return current is undesired then, given the appropriate DC side arrangements, the link could operate as a monopolar metallic return HVDC link. Also using separate control the direction of power flow can be selected for each pole irrespective of the settings on the other pole. The bipolar configuration is shown in figure 2.10. **[6]**, **[18]**

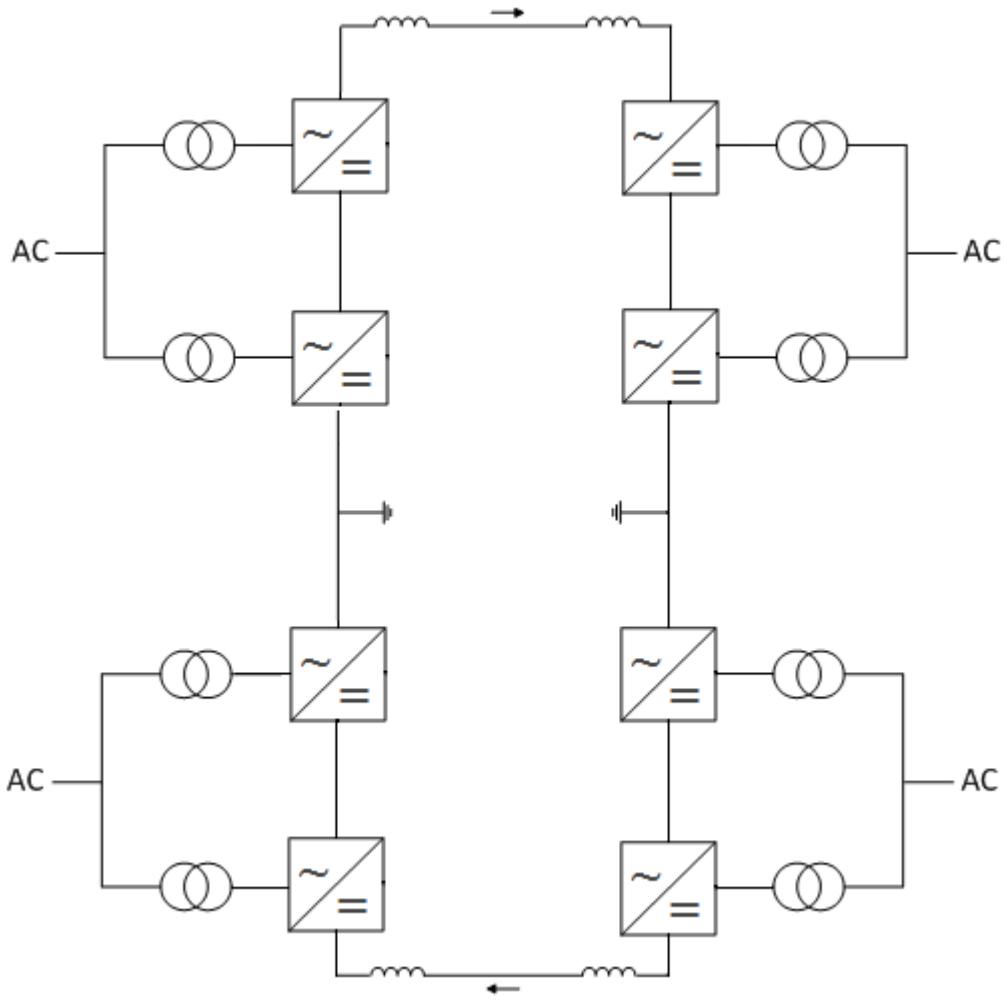

Fig. 2.10 Bipolar HVDC link

2.3 VSC-HVDC link components

VSC-HVDC links consist of the converter station and the DC conductor. Converter stations include many and different components in order to provide acceptable power quality (reduced harmonics, reduced DC current ripple, etc.) and high controllability of transferred power. In this paragraph each component is introduced and its role is briefly explained. As can be expected the main component of the converter station is the converter which rectifies the AC current in the sending point and inverts the DC current in the receiving point. The technology used for the converter affects the rest of the equipment used in the converter station as will be seen below.

As mentioned in paragraph 2.1, VSCs are the second, newer type of converters used for HVDC transmission. Due to their different behaviour and way of operation the components of an HVDC link using VSCs differ from those using an LCC. A single-line diagram of a VSC-HVDC link is shown in figure 2.11. **[32]**

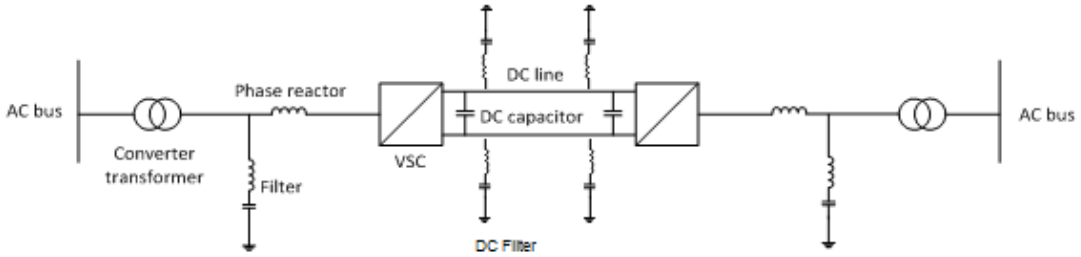

Fig. 2.11 Typical VSC HVDC link [32]

VSC converter

The existing topologies and operational principles of VSCs, besides the modular multi-level type, can be found in appendix B.

As mentioned earlier the VSC can operate in the four quadrants of the PQ plane. The VSC can operate, in steady state, in any point in the PQ plane that is located inside of its capability chart. Three main factors shape this capability curve: maximum current through the switches, maximum voltage generated from the converter and thermal limit of the converter cables.

There is a maximum amount of current that can flow through the converter switches during steady state. If higher current flows for a long time period the switches will be destroyed. During faults switches are blocked in order to be protected; the fault current flows through the freewheeling diodes. The locus of maximum switch current in the PQ plane, is a circle with its center at the origin (P=0, Q=0) and a radius equal to $U_s \cdot I_{max}$ (U_s is the grid voltage at the connection point and I_{max} is the maximum allowed current in the switches). Note that during voltage dips in the AC side the radius decreases which leads to reduced converter capability.

The voltage generated by the converter is limited. In case PWM is used this is due to the limited modulation index that the converter can achieve. The locus of the overvoltage limiting factor is again a circle with its centre located in the point P=0, $Q=-\frac{U_s^2}{X}$ (X is the phase reactor impedance) and of radius $\frac{U_s \cdot U_c}{X}$ (U_c is the voltage at the converter's AC side).

The final limiting factor is the maximum current across the converter cables, which translates into their thermal capability limit. The locus of this limit in the PQ plane is a vertical line.

In practice there is also an under-voltage reactive power limit. This limit is imposed by the main-circuit design and the necessity for a minimum voltage level for the transmission of active power. Typical values for Q_{max} and Q_{min} are 0.5 p.u and -0.5 p.u respectively per unit of the converter's MVA rating. **[41]**

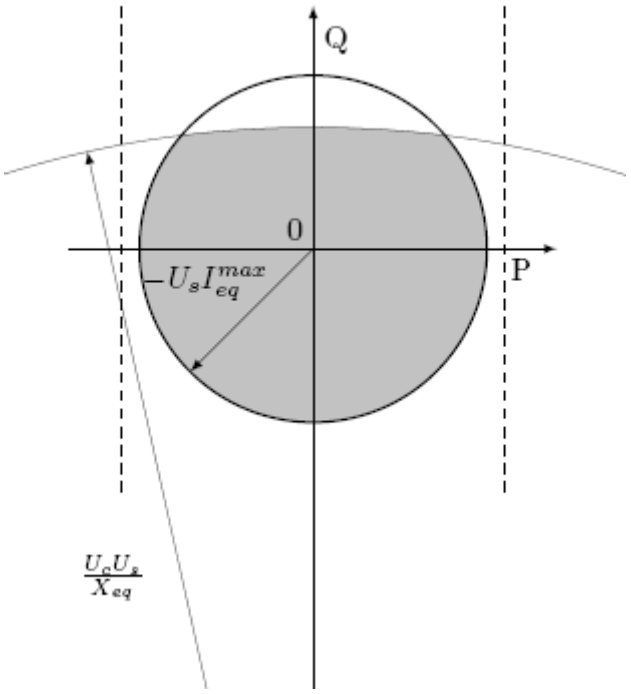

Fig. 2.12 VSC capability chart [32]

Converter transformer

Just like in the case of LCC-HVDC links converters in VSC-HVDC schemes are connected to transformers that adjust the AC voltage to a level appropriate for the converter. In LCC applications converter transformers need special design because they are subject to current harmonics and small DC current components. However in the case of VSC the harmonic filters are installed between the converter and the transformer and consequently a common AC transformer can be used. The transformer's tap changer helps the VSC optimize its operation and reduce losses **[32]**

Phase reactor

The phase reactor is a large inductive element with low resistance. Its role is to control the current in the AC side. By doing so it controls both active and reactive power. This makes it one of the most important elements in the AC side. It is also a part of the AC filter. It is an important element in the vector control of the VSC-HVDC converters. The way the phase reactor influences the power flow control can be better understood through equations 2.1 and 2.2 which are the power flow equations applied between the converters AC output and the point of connection to the grid.

$$P = \frac{U_s \cdot U_c \sin(\delta_c)}{X} \tag{2.1}$$

$$Q = -\frac{U_s^2}{X} + \frac{U_s \cdot U_c}{X}\cos(\delta_c) \tag{2.2}$$

U_s is the grid voltage at the connection point, X is the phase reactor's reactance and U_c and δ_c are the magnitude and angle of the AC side converter voltage.

By controlling the voltage magnitude the converter controls the reactive power flow, while the active power flow is controlled through the converter's AC voltage angle.
More details on the role of the phase reactor on the VSC converter control can be found in paragraph 3.1.

Filters

Just as in the LCC case, filters are needed in order to block harmonics in the converter's output reach the AC grid. Together with the phase reactor a low pass filter is created. If needed a high pass filter can be installed. The filter is located between the converter and the converter transformer. Filters in VSC-HVDC schemes are much smaller than in LCC-HVDC schemes due to the smaller harmonic content of the VSC converter output.

DC capacitor

These capacitors are placed on the DC side of the converter. Their main function is to keep the DC side voltage within a narrow band by charging or discharging. They also reduce the DC voltage ripple. Their size affects the dynamics of the DC side circuit.

DC filters

These filters are placed in parallel to the DC capacitors and filter harmonics in the DC voltage.

DC conductor

Usually VSC-HVDC links are used in underground or submarine transmission scenarios. In VSC HVDC schemes mostly XLPE cables are used. XLPE cables use polymeric insulation that can withstand high forces and repeated flexing. This type of cable cannot be used in LCC-HVDC transmission because reversal of power is accomplished by polarity reversal of the voltage and this can create problems due to the space charging phenomenon. In VSC-HVDC transmission the voltage polarity is constant and power flow reversal is accomplished through current reversal. **[8]** In contrast to liquid insulated cables, XLPE cables weigh less and therefore can be transported and installed easily. Also since their insulating material is solid there is no danger of it spilling in the sea or the ground as is the case for oil filled cables.
Present standard voltages for XLPE cables in recent HVDC schemes are 84 and 150 kV but ratings of 300 kV have also been developed.

3. VSC-HVDC model validation

3.1 The PSS®E library model (VSCDCT)

In Appendix C the general concept of modeling a VSC-HVDC line is introduced. In the present paragraph the VSC-HVDC model used for this study will be presented. The VSC-HVDC line model used in the present work is PSS®E's library model, VSCDCT. This model can be used for the representation of either point to point or back to back HVDC configurations. The understanding of how the model works is important and for this reason an explanation of the model's structure and functions is given in the present paragraph.

3.1.1 Power flow model

PSS®E contains a library model for the power flow representation of VSC-HVDC lines. This model is not only used for power flow studies but also provides VSCDCT with the initial values needed for dynamic simulations.

The power flow model enables the user to control the VSC power outputs. In more detail, the VSCs can control the active and reactive power output. The VSC's reactive power output can be controlled either by controlling their power factor or a specified bus' voltage. The reactive power setpoints of the VSCs are independent from one another. In a sense VSCs have a similar behavior, in power flow, as a synchronous generator which also has the capability of controlling its active power output and its terminal voltage. **[50]** Each converter can be set either in active power control mode or in DC voltage mode.

The reactive power capabilities of the VSCs have to be specified by the user and should be based on the VSC capability chart presented in paragraph 2.3.2.

The DC line is represented by a resistance specified by the user. This resistance is used to calculate the transmission losses of the VSC-HVDC line. The converter losses, both constant and current dependent, are calculated using a linear loss model.
The VSC-HVDC model represents only the converters and the DC line. Converter transformers and filters must be modeled separately by the user.

3.1.2 Dynamic model

The VSCDCT, PSS®E model is a time-averaged model and is therefore intended to be used in order to study the effect of the VSC-HVDC on the network on the electro-mechanical time frame.

In general VSC-HVDC models can be either detailed or time-average. In detailed models, all the components of the VSC-HVDC line, such as all the semiconducting components, are modeled. Special electromagnetic transient software tools, such as PSCAD, ATP etc, are needed in order to perform simulations with these models. These models can be used to study the behavior of different HVDC topologies, PWM techniques or high frequency component harmonics.

On the other hand, time-average models do not model in such detail the HVDC components. Also there is no distinction made between different topologies or switching techniques. All phenomena related to the fundamental switching frequency can be studied adequately. The main principle of time-average models is that the

HVDC line is represented as controllable three-phase voltage sources on the AC side and a controllable current source on the DC side. Time-averaged models can be used both by electromagnetic transient programs as well as power flow simulation tools, such as PSS®E, Power Factory etc. **[45]**

Since the VSCDCT model is used for electro-mechanical time frame studies only the outer controllers are represented. The inner control loop and the DC side characteristics have a much faster response than the time scale of PSS®E. Therefore the DC side dynamics are modeled in an approximate way while the inner current controller is not modeled at all. The active and reactive current components are assumed to take instantaneously their reference values created by the outer controllers.

The VSCDCT model consists of three modules, two of which represent the VSCs and the other the DC line. The converter modules have modeled the outer controllers and enable the user to control AC voltage or reactive power, DC voltage or active power as well as to apply current limitation strategies. Additional features are active power ramping and converter blocking.

Regarding active power control, the DC line module coordinates the power flow between the two converters and is therefore responsible for creating a power order for each converter and assigning it to each VSC module. In the case of a current limitation in the network of a converter, e.g a fault in the AC system close to one of the converters, an imbalance in the power flows of the converters will occur resulting in a change of the DC voltage. The active power reference of the VSC modules will be lowered appropriately, by the DC line module, in order to bring the active power exchange between the converters in balance once again. The DC line module also is responsible for taking into account the DC transmission losses. It creates the appropriate active power reference in order to compensate these losses. The losses are compensated in the DC voltage controlling converter. By changing the appropriate setpoint value in the VSCDCT model, active power ramping is performed by the DC line module.

When the current output of a converter exceeds its nominal value then by appropriate switching, the converter can reduce its current. The total current reduction of a converter can be achieved through various current limitation strategies which reduce the current components (active and reactive) by a different amount. The main current limiting strategies found in literature are the active, reactive and equal priority current limitation and are further explained in section 3.3.3. These current limitation strategies can be achieved by the VSC modules by using the appropriate value of a weighting factor which determines the amount by which each converter current component will be reduced when it exceeds its limit.

As mentioned above, VSCDCT gives also the possibility to control either AC voltage at a bus or the converter's reactive power output. When in AC voltage control mode, the converter module changes its reactive power setpoint in order to maintain the voltage at a bus. By default the controlled bus is the filter bus, which is the bus at which the AC side of the HVDC line is connected. If desired, another bus' voltage can be controlled by changing the appropriate parameter in the model. VSCDCT also enables the user to use a droop, when two or more VSC-HVDC lines are set to control the voltage of the same bus. Without the provision of this droop the converters could be driven to their limits while attempting to control the bus' voltage.

Instead of AC voltage control the VSCDCT model can be set to reactive power control during dynamic studies. The setpoint of the reactive power can be changed by

the user during the simulation. Additionally during simulations it is possible to change from AC voltage control to reactive power control and vice versa. **[50]**

3.2 IEEE 39 bus system

The test system used to validate the VSCDCT model is the IEEE-39 bus system. This is a well tested system which exhibits dynamic responses similar to those of real power systems.

The system is presented in figure 3.1. The generation consists of twelve generators, ten of which are conventional generators supplying 5984 MW and the remaining two are wind turbines generating 1600 MW. The conventional generators are modeled as round rotor synchronous generators (GENROU) and the wind turbines as type 3, doubly fed induction generators. The conventional generators use exciter (ESDC1A) and governor (TGOV1) models.

As can be seen from figure 3.1, the point-to-point HVDC link is connected between areas 1 and 3 at buses 3 and 21. Buses 42 and 101 are the HVDC's filter buses. The system model had initially an AC connection between buses 16 and 17. By adding the point-to-point HVDC line areas 1 and 3 become more coupled and the effect of a fault in area 1 affects considerably area 3 and vice versa. The coupling of the two areas was decreased by removing the line between buses 16 and 17 in order to examine in more efficient way, the effect of each HVDC converter on its area. This situation is similar to the situation regarding Corridor A, in which the HVDC converters are electrically far from each other and therefore the areas surrounding the converters can be seen as loosely coupled areas of the transmission system.

The total power transfer of the VSC-HVDC line is set to 600 MW at a DC voltage of 300 kV. The direction of flow in the HVDC is from area 3 to area 1, so the converter connected at bus 42 is the sending converter and the converter at bus 101 is the receiving converter. Both HVDC converters are set to AC voltage control mode. The reactance of the converter transformers were modeled separately since, as explained in paragraph 3.1.1, PSS®E's VSCDCT model does not contain a transformer record.

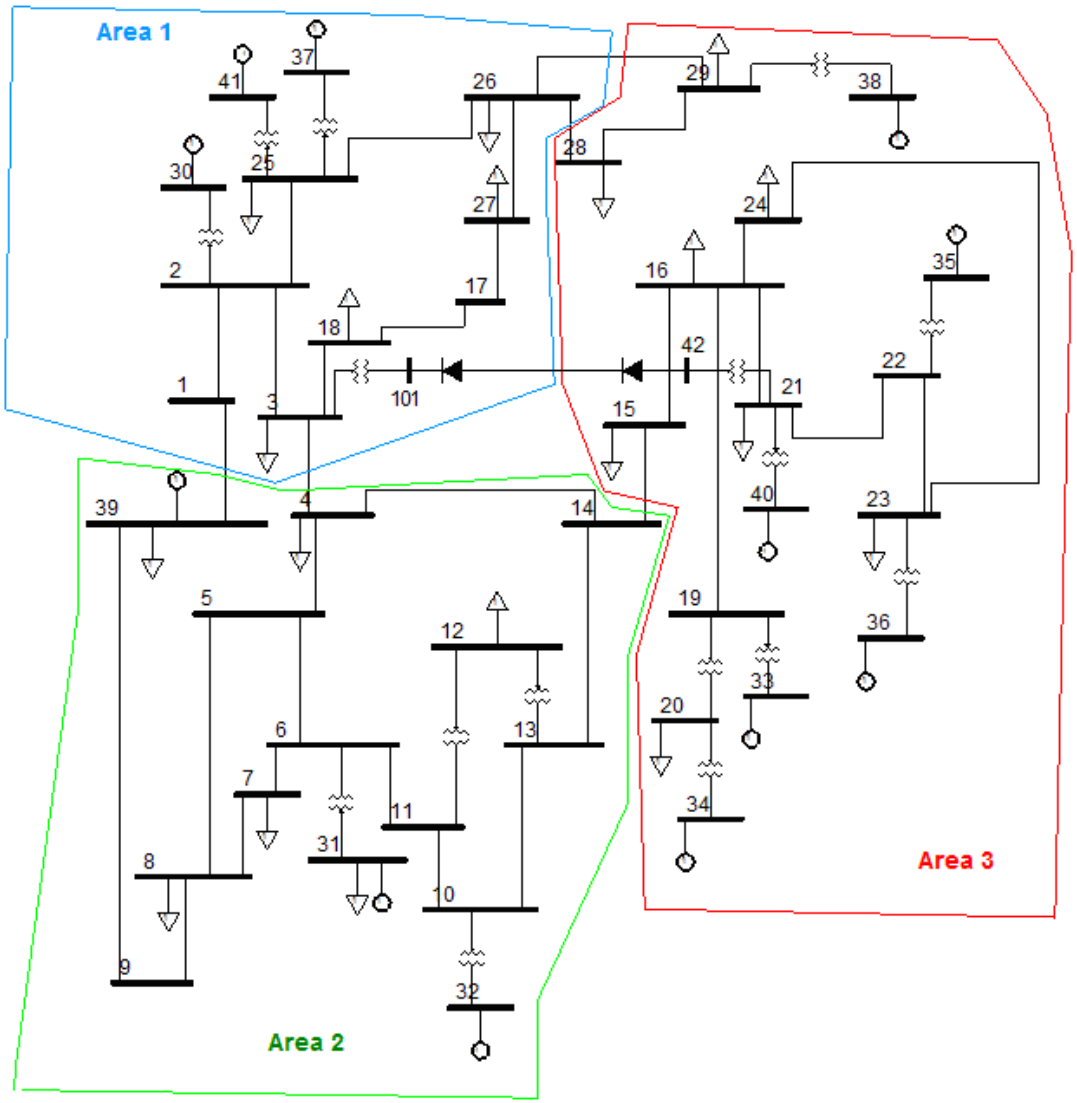

Fig. 3.1 IEEE 39 bus system with VSC-HVDC line connected between areas 1 and 3

3.3 Sensitivity analysis of reactive power and AC voltage control parameters

The purpose of this chapter is to validate the operation of the PSS®E VSCDCT library model and introduce the sensitivity of a transmission system to the parameters of the reactive power and AC voltage controllers implemented on the VSC-HVDC transmission system. For this purpose a VSC-HVDC link connecting two areas is placed in the IEEE 39 bus system, as explained in paragraph 3.2. The analysis of the reactive and AC voltage controller parameters on the AC system performance will be presented through time domain simulations.

3.3.1 Effect of the k gain on the system

As explained in paragraph 1.3.1 the Network code for VSC-HVDC, requires that during a three phase fault the VSC-HVDC provides additional short circuit reactive current in order to maintain the voltage at the PCC as close as possible to its steady

state value. In addition the short circuit current contribution assists the fault detection and protection schemes in the AC system. The amount of additional reactive power depends on the PCC's voltage deviation from its nominal value. The k gain, as given by the grid code **[15]**, is therefore defined as the slope of the additional reactive current versus the PCC voltage deviation curve, as can be seen in fig. 1.5.

In more practical terms, the k gain is actually the proportional gain of the converter's AC voltage controller. As can be seen in fig. 1.5 the curve may have a deadband around zero voltage deviation, however this deadband is not taken into account in the present study because the VSCDCT model has no such provision. However, it is expected that by disregarding the deadband the AC system's dynamic response will be improved according to **[47]**.

In order to show the effect of the k factor to the system a series of time domain simulations is performed for various values of k (2, 4 and 6). The case of a three-phase bus fault in bus 27 will be examined. The bus fault is cleared after 150 ms. In these simulations the over-current capability of the HVDC converters is assumed to be equal to I_{max}=1.15 p.u (in the converter's current base) **[37]** and the current limiting strategy is assumed to be that of reactive current priority. The HVDC converter connected to bus 21 is the sending end and the VSC connected to bus 3 is the receiving end of the VSC-HVDC link. The converters are set to control the voltage of their respective filter buses (buses 42 and 101).

3.3.1.1 Response of HVDC converters to faults for different values of k

In paragraph C.1.1 of Appendix C it is explained that the total current of a VSC-HVDC converter can be analyzed in two components according to the d-q reference system. These components are the active (d-axis component) and reactive (q-axis component) current components. It was also explained that the AC voltage of the converter is mainly influenced by changes in the reactive current component of the converter. The k gain affects the injection of additional reactive current during faulted conditions and therefore affects the AC voltage profile of the system during and after a system's disturbance. It is interesting therefore to see how different values of the k gain affect the voltages of the AC system.

By improving the AC system voltages through reactive current injection during a fault, the impact of a fault on the system's dynamic response becomes less severe. The effect on the severity of the fault will also influence the generator response during and after a fault. It is therefore of interest how the rotor angles of the system's generators will behave after a fault for different values of the k gain.

The presentation of the simulation results will start by showing the response of the sending HVDC converter connected to bus 21 and that of the receiving converter connected to bus 3 of the system.

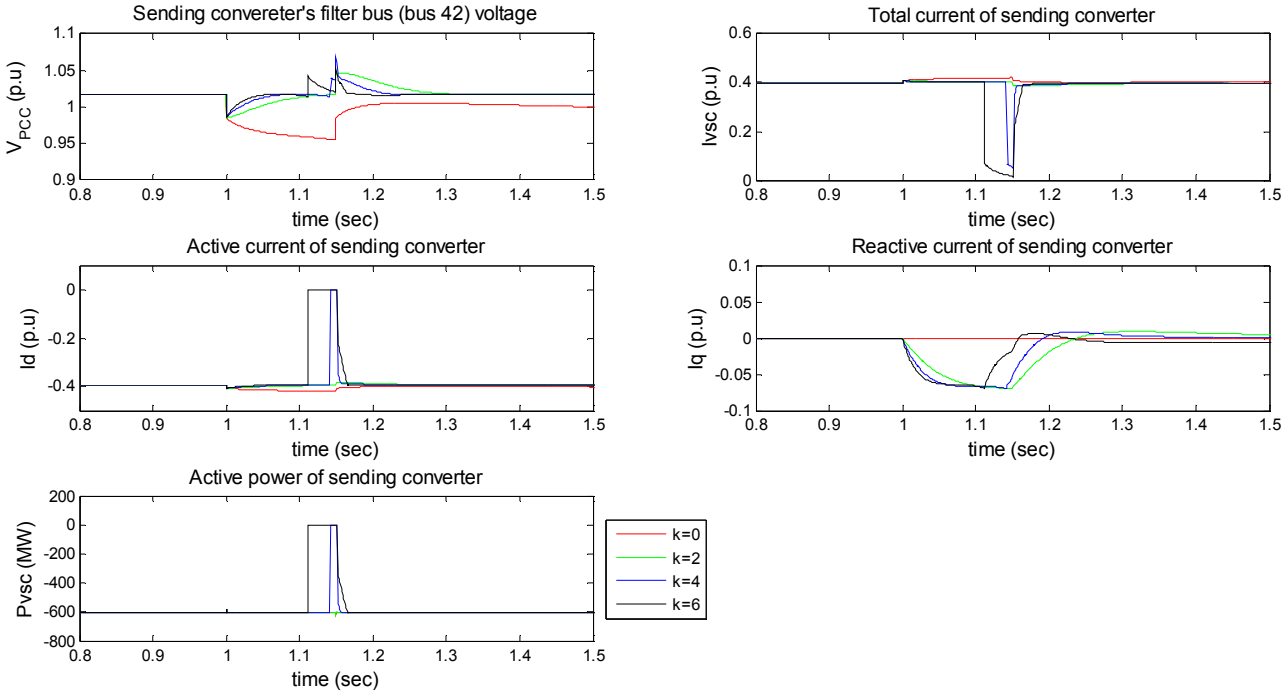

Fig. 3.2 Response of sending converter (bus 21) for different values of k gain for a fault in bus 27

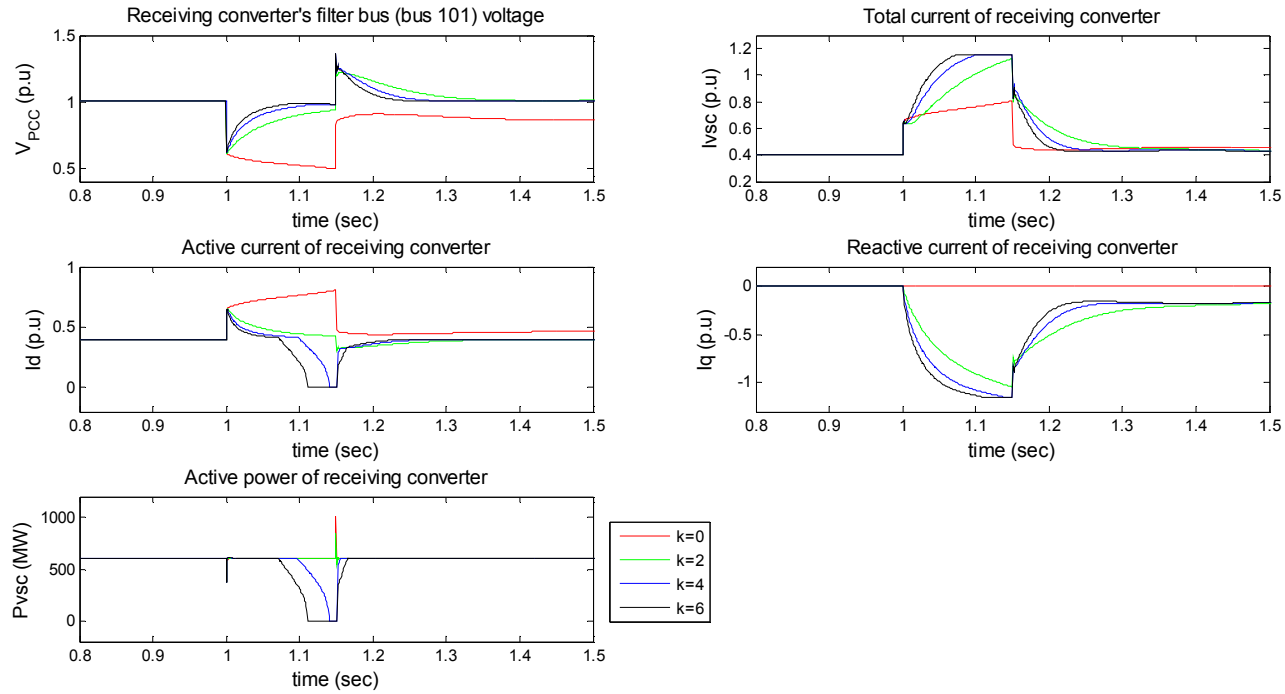

Fig. 3.3 Response of receiving converter (bus 3) for different values of k gain for a fault in bus 27

Observing the converter responses it can be seen that the voltage dip in the receiving converter's filter bus (bus 101) is much larger than that in the sending converter's filter bus (bus 42). This is expected since the fault is located closer to the receiving converter in bus 3 (they are both located in area 1) than to the sending converter in bus 21. The higher voltage dip in area 1 will lead the receiving converter

to generate a higher amount of additional reactive short-circuit current in order to maintain the voltage in bus 101 as close as possible to the voltage controller's reference value.

This leads the receiving converter to reach its current limit of 1.15 p.u, for values of k equal to 4 and 6. When k equals zero, the converter controllers do not offer voltage support during the fault and thus their reactive current component remains unchanged during and after the fault. On the other hand, the sending converter does not reach its current limit for any value of the k gain.

When the receiving converter reaches its current limit it will have to reduce its current components according to the current limitation strategy (CLS). In this case the converter CLS is set to reactive current priority, so the only current component that will be reduced is the active current component. In the case of high k values (4 and 6), the reactive current component of the receiving converter will increase the most and will eventually reach the current limit. In this case, the receiving converter's active current component will reduce to zero. In order to maintain the DC voltage at a constant value, the energy exchange between the converters must be in balance. Therefore the active current output of the sending HVDC converter must be reduced by the same amount.

It has to be mentioned at this point that PSS®E's VSC-HVDC line model has a weakness regarding the active current reduction in the non-limit-reaching converter. As can be seen from the sending converter (which doesn't reach its current limit during the fault) in figure 3.2, its active current will not reduce to zero gradually as it does in the receiving converter, but it will drop suddenly to zero when limit-reaching converter's active current reaches its zero value. In reality however, the non-limit-reaching converter's active current should decrease gradually to zero following the limit-reaching converter's active current reduction. This sudden reduction to zero, of the non-limit reaching converter's active current does not result in a considerable distortion of the simulation results because the time constants of the HVDC outer controllers are small and thus the actual rate of reduction of the active current components is already steep. However there is a small effect of the sudden active current reduction on the simulation results and it is manifested as a small voltage jump in this non-limit reaching converter's filter bus voltage. This behavior can be seen in the sending converter's filter bus voltage in figure 3.11 for k=4 and 6. The voltage jump can be seen clearer in figure 3.4. The time instances t_1 and t_2 are the instances the active current of the sending converter drops suddenly to zero for k=4 and k=6 respectively, while t_{clear} is the time instant the fault is cleared.

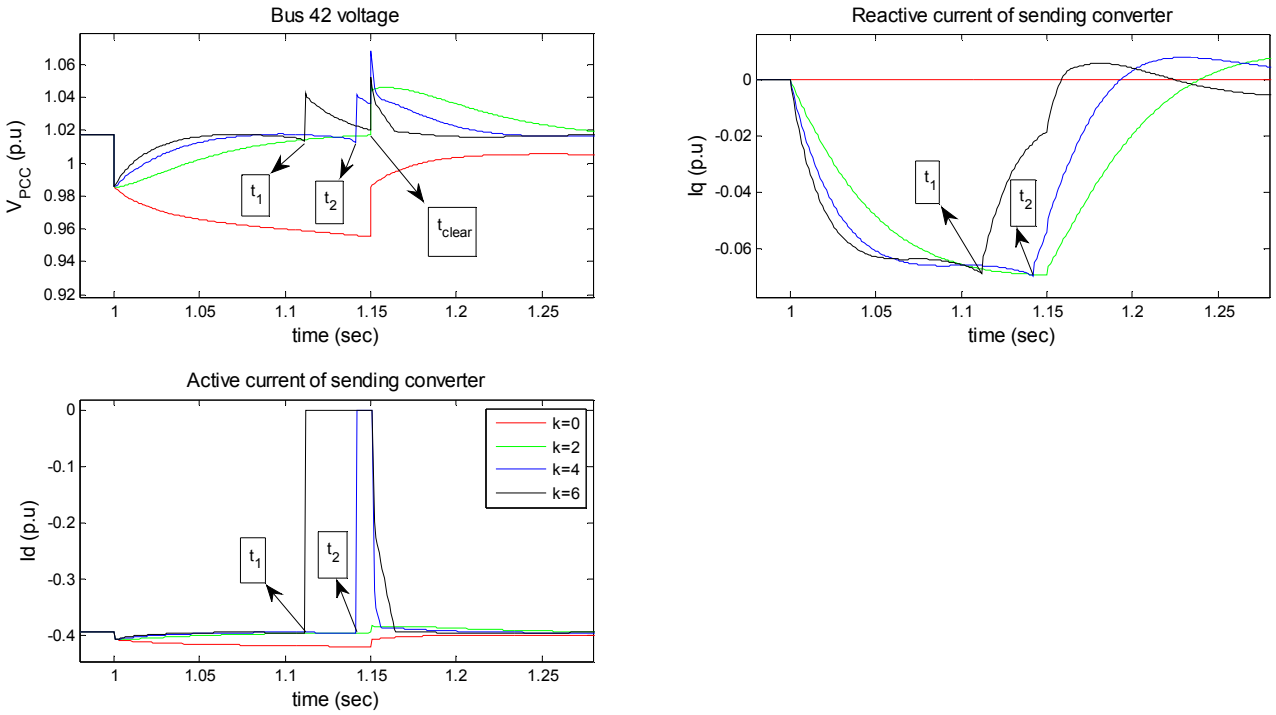

Fig. 3.4 Effect of the sending converter's sudden active current drop on its filter bus voltage

The voltage drop across the phase reactor of the HVDC converter depends on both reactive and active power (equation C.27, Appendix C). However due to the high X/R ratio in transmission systems, the effect of active power is usually neglected. This is indeed true in the case of the examined system since the X/R ratio in bus 42 is 27.4 and in bus 101 it is 24.6 which are quite high. Therefore the effect of the active current reduction on the system voltages is expected to be small. This small effect of active power and thus active current on the AC system voltage justifies the small voltage jump witnessed in figure 3.4 in the sending converter's filter bus. Since the reduction of the active current is sudden in the sending converter, the change in voltage in the sending converter's area will appear as a sudden jump. A similar, but even smaller, voltage jump appears also in the buses in the area close to the non-limit-reaching converter. Due to the voltage jump, the reactive current of the converter will suddenly drop at time instances t_1 and t_2.

Finally regarding the active current component of the converters it can be seen that it has its highest value when no reactive current current support is given during the fault, i.e when k=0. In this case the value of the converter's AC voltage is the lowest and thus according to equation C.15, of Appendix C, a higher active current component will be needed in order to maintain the DC power closer to its reference value. In the case of the receiving converter, there is an additional reason why the active current component is higher when k=0. For k=0 the reactive current does not increase, therefore there will be more room for the active current to increase.

3.3.1.2 Effect of the k gain on the AC system's bus voltages

In this paragraph the effect of the HVDC converter voltage support during and after the fault will be presented. The selected buses, the voltage of which is monitored, are buses 18, 2, 22, 16, 8 and 10. Buses 18 and 2 are located in area 1, which is the area in

which the receiving HVDC converter is located and also the fault occurs. Buses 22 and 16 are located in area 3 which is the sending end area of the HVDC line. Finally buses 8 and 10 are located in area 2. The voltage plots of the aforementioned buses are presented in figure 3.5.

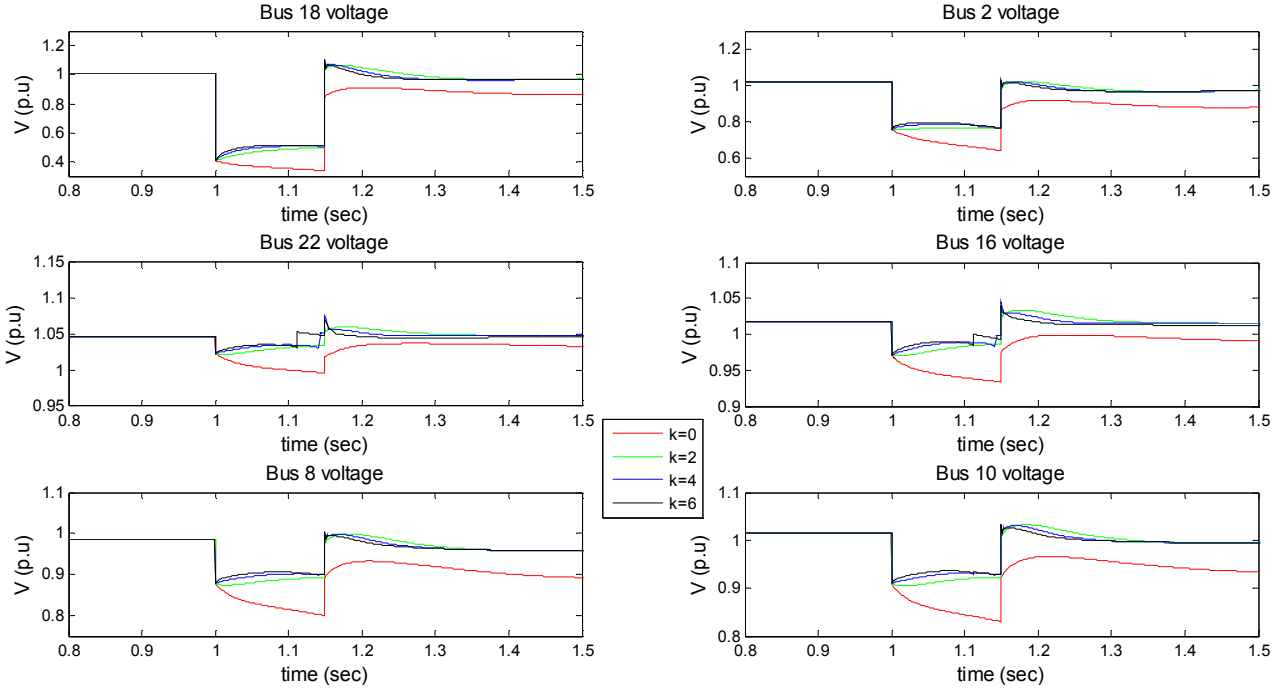

Fig. 3.5 Effect of the k gain on the bus voltages

By observing figure 3.5 two things can be noticed immediately. First of all, for values of k higher than zero, i.e when the HVDC converters support the AC voltage by injecting additional short-circuit reactive current into the system, the voltages during the fault are higher than the case where k=0. Secondly the effect of the fault is more severe in area 1 where the fault occurs. The voltage dip in buses 18 and 2, which are located in area 1, is higher than in the buses of other areas. It should be noted that the scale of the graphs in figure 3.5 is not the same for each bus. The presentation of these plots is done in order to show with as much detail as possible the behavior of the voltage for each selected bus. In order to make a clear comparison between the different buses and quantify the voltage dip and the improvement of the voltage for each value of the k factor the average voltage dip ΔV% is defined as:

$$\Delta V_{\%} = \frac{V_{prefault} - \overline{V}_{fault}}{V_{prefault}} \cdot 100\% \qquad (3.1)$$

where, $V_{prefault}$ is the prefault value of the bus' voltage and $\overline{V}_{fault}$ is the average value of the bus' voltage during the fault. The average voltage dip for each selected bus is shown in table 3.1.

	Bus 18 (area 1)	Bus 2 (area 1)	Bus 22 (area 3)	Bus 16 (area 3)	Bus 8 (area 2)	Bus 10 (area 2)
k	**ΔV%**	**ΔV%**	**ΔV%**	**ΔV%**	**ΔV%**	**ΔV%**
0	64.455	33.790	4.243	7.301	16.782	16.300
2	52.866	25.127	1.661	3.582	10.240	9.872
4	50.539	23.521	1.186	2.929	8.899	8.617
6	49.727	23.055	0.748	2.579	8.419	8.198

Table 3.1 Effect of k gain on the average voltage dip

As can be seen from the values of table 3.1, the voltage dip in area 2 is higher than in area 3. This shows that area 2 is more coupled to area 1 than area 3 is to area 1.
The most important observation however is that the higher the value of the k gain, the lower the voltage dip. A higher k gain means the HVDC converter injects a higher amount of reactive current into the system which was already seen in previous paragraphs that is used to control the AC voltage. The voltage improvement is almost the same for k=4 and 6 since in both cases the reactive current component reaches the current limit.

The voltage profile improvement is evident for all the buses of the system. However, the voltage improvement is higher for buses located close to the receiving HVDC converter which is the one affected most by the fault and thus injects a higher amount of short-circuit reactive current. This observation shows that the effect of the converter voltage support is regional in the sense that the farther a bus from a voltage supporting HVDC converter, the lower the voltage support it receives.

3.3.1.3 Effect of the k gain on the rotor angle response of generators

Next, the effect of the HVDC converter voltage support on the rotor angles of the generators will be examined. The rotor angles of selected generators will be monitored. The selected generators are generators connected to buses 30 and 37 from area 1, generators connected to buses 35 and 36 from area 3 and generators connected to buses 31 and 32 from area 2.

The rotor angle plots of these generators are shown in figure 3.6.

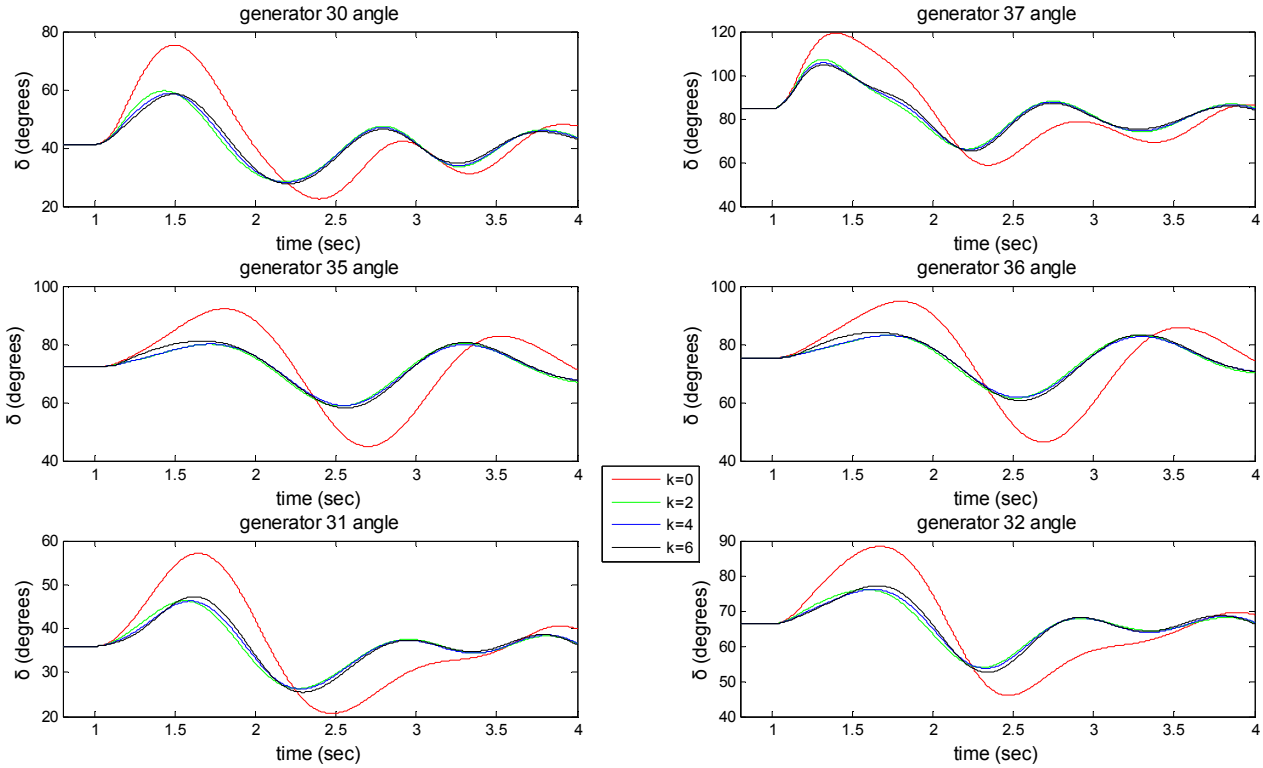

Fig. 3.6 Effect of k gain on the generators rotor angles

Figure 3.6 shows that when voltage support is offered by the HVDC converters (k>0), the rotor angle stability of the generators improves, i.e the peaks of the rotor angle oscillations become smaller. This is explained by the fact that due to voltage support, the voltage dip in the system's voltage becomes smaller. Consequently the impact of the fault becomes less severe and thus the rotor angle oscillations will become smaller.

The scale of the plots for each generator in figure 3.6 is not the same. In order to compare the rotor angle response of the generators and to see clearer the effect of different k gain values and to quantify it, the maximum first peak rotor angle deviation is defined by equation 3.2.

$$\Delta\delta_{\max\%} = \frac{|\delta_{prefault} - \delta_{peak}|}{\delta_{prefault}} 100\% \qquad (3.2)$$

where, $\delta_{prefault}$ is the generator's rotor angle before the fault occurs and δ_{peak} is the peak value of the rotor angle's first oscillation after the fault occurs. The thesis focuses on the first swing rotor angle stability and therefore only the first peak of the rotor angles is of interest.

The maximum rotor angle deviations for the selected generators are shown in table 3.2.

	generator 30 (area 1)	generator 37 (area 1)	generator 35 (area 3)	generator 36 (area 3)	generator 31 (area 2)	generator 32 (area 2)
k	$\Delta\delta_{max\%}$	$\Delta\delta_{max\%}$	$\Delta\delta_{max\%}$	$\Delta\delta_{max\%}$	$\Delta\delta_{max\%}$	$\Delta\delta_{max\%}$
0	82.914	40.862	27.572	26.005	58.728	33.353
2	44.695	26.562	10.732	10.378	28.719	14.853
4	42.531	24.837	10.766	10.379	28.574	14.818
6	42.032	23.749	12.295	11.704	31.348	16.442

Table 3.2 Effect of k gain on the maximum rotor angle deviation

The values of table 3.2 show that the higher k gain values do not necessarily decrease the rotor angle peaks. It can be seen that for the generators in area 3 the rotor angle peaks increase for k equal to 4 and 6. By closer examination it can be seen that the deterioration of the rotor angle oscillation appears when the active current of the HVDC converters is reduced. The sending converter of a point-to-point HVDC converter is viewed by the system as a load, on the other hand the receiving converter is equivalent to a generator. When active power reduction occurs in the sending converter, a surplus of power will be created in the sending converter's area (in this case area 1). This surplus of power will cause the regional generators to accelerate. This acceleration, induced by the active current reduction, will be superimposed to the acceleration or deceleration of the generators due to the fault.

On the receiving side of the point-to-point HVDC line a similar situation takes place. The active current reduction of the receiving converter will result in a deficiency of active power in the receiving converter's area (in this case area 3). This active power deficiency will lead local generators to decelerate. The response of the rotor speeds can be seen in figure 3.7.

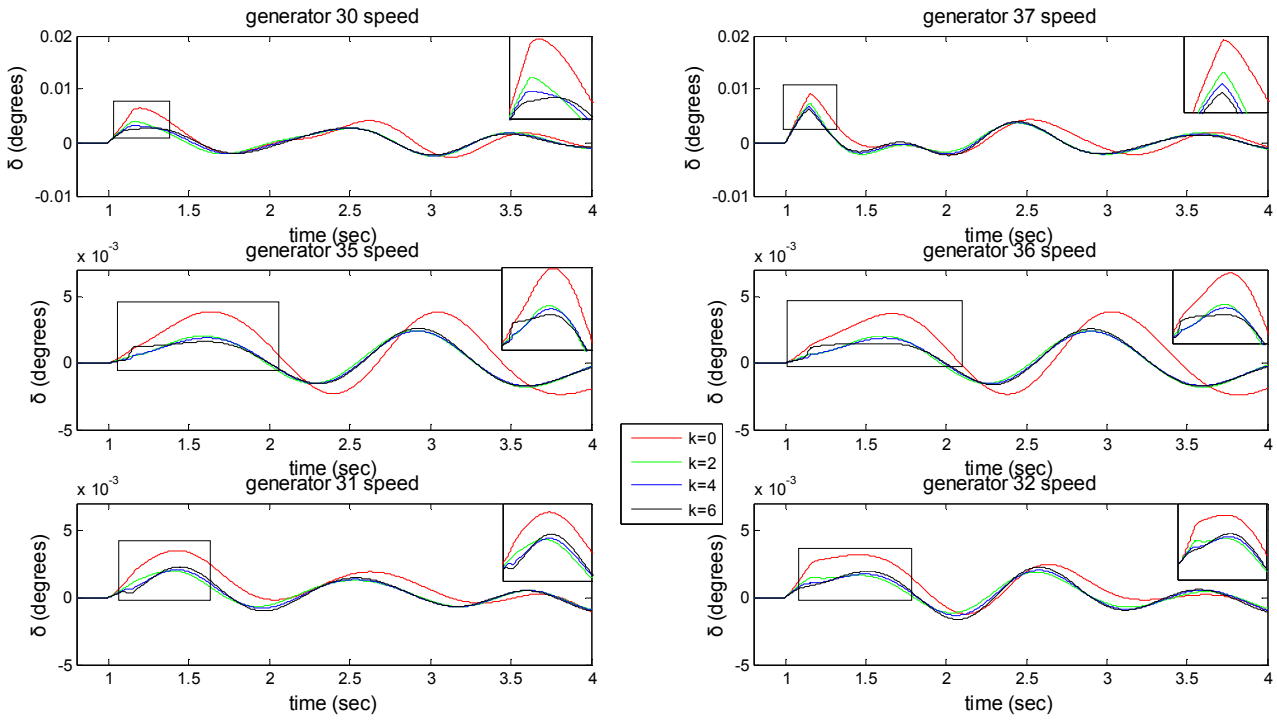

Fig. 3.7 Effect of k gain on the generators rotor speeds

As can be seen by figure 3.7, for k=0, the response of all the monitored generators is to accelerate due to the fault and therefore their rotor angle will increase. The generator acceleration due to the active current reduction of the converter in area 3 will be superimposed on the fault-induced acceleration. This creates a sudden speed increase that is more visible for k=6 in generators 35 and 36. This sudden speed increase will lead to a higher first peak of the rotor angles of generators in area 1. This can be validated by the rotor angle deviations of generators 35 and 36 for k equal to 4 and 6. On the other hand, the active current-induced deceleration in area 1 will be superimposed to the fault induced acceleration leading to a smaller rotor speed. This leads to a smaller rotor angle deviation. Again the values of table 3.2 for generators 30 and 37 for k equal to 4 and 6 agree with this explanation.

Regarding the generators in area 2 (31 and 32) it is seen that the rotor angle response improves (lower first rotor angle peak) for k=4 but deteriorates (higher rotor angle peak) for k=6. The situation in area 2 is not so clear because although IEEE's 39 bus system has three different areas the system is quite small and quite meshed, so there is some degree of interaction between the areas. It appears that the voltage profile improvement for k=4 influences more the rotor angles than the reduction of active current leading to an improvement of the rotor angles in area 2. On the other hand when k=6, the active current will be reduced faster and the effects of this reduction will be more severe than for k=4. It appears that the effect of the active current on the rotor angles prevails against the voltage profile improvement and its effect on rotor angle stability. It can be seen that reaching a conclusion regarding generator rotor angle response in areas other than those of the sending and receiving converters is difficult due to the difference in the effect of the relevant factors. For this reason the analysis, regarding rotor angle response, will be focused from now on generators near the HVDC converters.

3.3.2 Effect of converter over-current capability on the system

As was explained in chapter 1 one of the limiting factors of a VSC's active and reactive output is the current flowing through its power electronic components. During faulted conditions the converter switches may tolerate higher currents than the nominal value for the short duration of the fault. The value of this current is usually found in literature to be 1.15 p.u **[37]**. HVDC converters through appropriate switching actions, manage to maintain the current below this limit.

In paragraph 3.3.1 it was found that increasing the VSC's, k factor in order to increase the additional reactive current injection to the system during faults has little effect in the system if the converter's current limit is reached. Additionally it was seen that the active current component reduction that takes place when the current limit is reached (and the limitation strategy is not set to active current priority), the rotor angle response of the system's generators is affected. Therefore an interesting sensitivity is to see how the current limit of the HVDC converters affects the system. For these simulations two values of the current limit will be used. In the first case the over-current capability is equal to 1.15 p.u and in the second equal to 1.3 p.u. The value selected for the k factor is equal to 6, which is a large value in order to reach the converter's current limit for the studied case. The current limiting strategy is set to that of reactive current priority. The fault location is once again bus 27.

3.3.2.1 Response of HVDC converters to faults for different over-current capabilities

Just as in paragraph 3.3.1 for the case of the k gain sensitivity, the result presentation will start by the response of the HVDC converters to the fault. The responses of the sending and receiving converters are presented in figures 3.8 and 3.9 respectively.

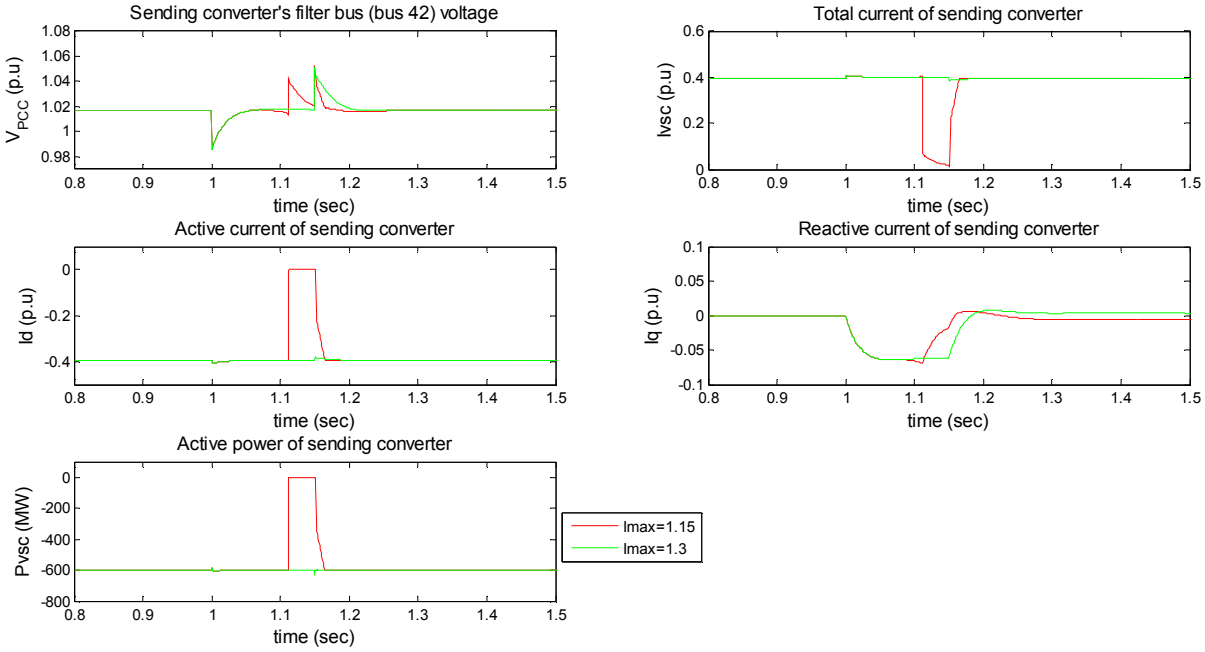

Fig. 3.8 Response of sending converter (bus 21) for different current capabilities for a fault in bus 27

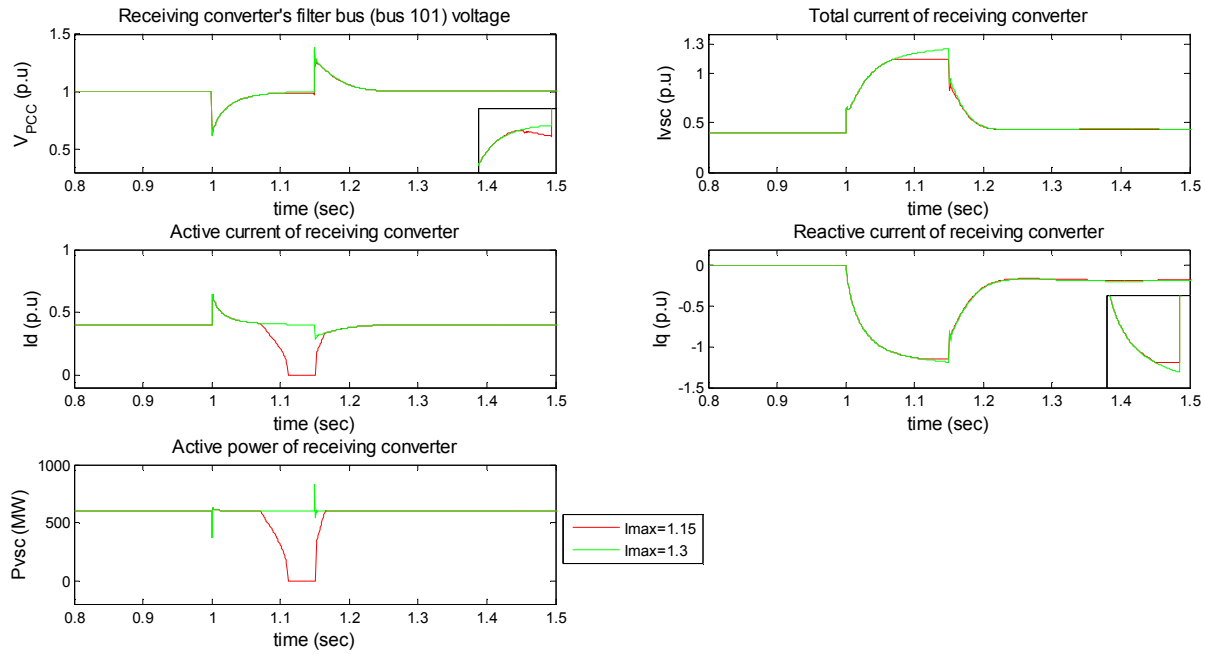

Fig. 3.9 Response of receiving converter (bus 3) for different current capabilities for a fault in bus 27

Figures 3.8 and 3.9, show that only the limit reaching converter (the receiving converter in this case) is benefited by the higher current limit. This makes sense since a higher current limit cannot offer any improvement if the limit is not reached.

The higher value of the current limit improves slightly the bus voltage in the filter bus of the receiving converter (101) since there is a higher over-current capability for the reactive current component to increase.

As can be observed by figure 3.9 the receiving converter does not reach the current limit when it is set to the higher value of 1.3 p.u. Therefore no current reduction will take place. This can be witnessed by the active current components for both the sending and receiving converters for I_{max}=1.3 p.u. Therefore the voltage jump that was witnessed in the sending converter's filter bus for I_{max}=1.15 p.u does not occur for the higher value of I_{max}. The only voltage jump that occurs in the sending converter's filter bus for I_{max}=1.3 p.u is the one due to the fault clearance at t=1.15 sec.

3.3.2.2 Effect of the over-current capability on the AC system's bus voltages

Next the effect of the different current capabilities on the AC system's bus voltages will be presented. The selected buses are 3, 18, 17 and 4. As can be noticed, the focus is mainly on the voltage profile of buses located close to the limit-reaching converter (receiving converter connected in bus 3). As was seen in paragraph 3.3.2.1, the effects of a higher current limit cannot be observed in the area of a converter that does not reach its limit. Therefore only buses from area 1 (buses 3, 18, 17) and a bus from area 2 (bus 4) that is located close to the receiving converter will be examined. The plots of the bus voltages are presented in figure 3.10.

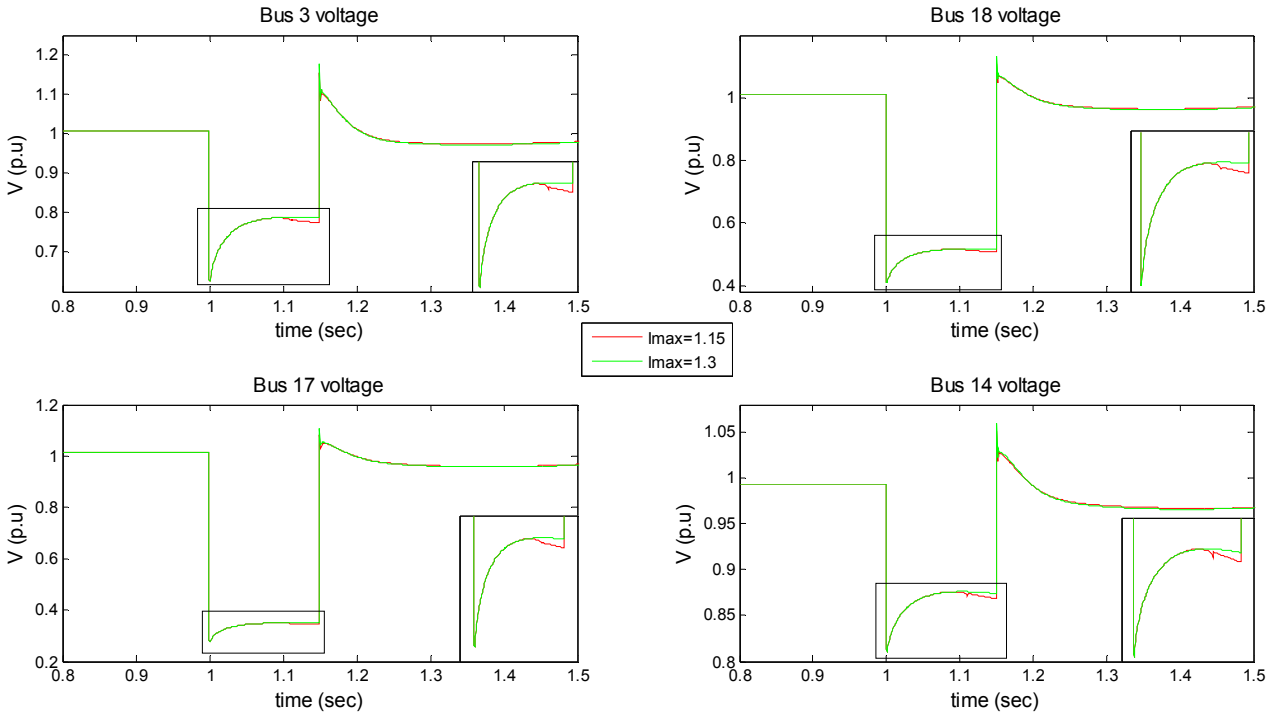

Fig. 3.10 Effect of the current limit on the bus voltages for a fault in bus 27

The plots of figure 3.10 indicate that a higher current limit can help improve the voltage profile since a higher reactive current value can be achieved. The improvement however appears to be small.

The average voltage dip is presented in table 3.3 in order to quantify the voltage improvement.

	Bus 3 (area 1)	**Bus 18 (area 1)**	**Bus 17 (area 1)**	**Bus 4 (area 2)**
I_{max}	**ΔV%**	**ΔV%**	**ΔV%**	**ΔV%**
1.15	24.103	50.425	66.470	12.857
1.3	23.804	50.230	66.338	12.737

Table 3.3 Effect of the over-current capability on the average voltage dip for a fault in bus 27

The values of table 3.3 show that the improvement of the voltage during the fault is small. In all of the cases it is less than 0.5%.

3.3.2.3 Effect of the over-current capability on the rotor angle response of generators

Finally the effect of the over-current capability on the rotor angle response to a fault is examined. The selected generators are from areas 1 and 3 since, as mentioned in paragraph 3.3.1.3, clear conclusions on the effect of HVDC converters on the rotor angles can be drawn only for generators near the converters. The selected generators are the generators connected in buses 30 and 37 from area 1 and 35 and 36 from area 3.

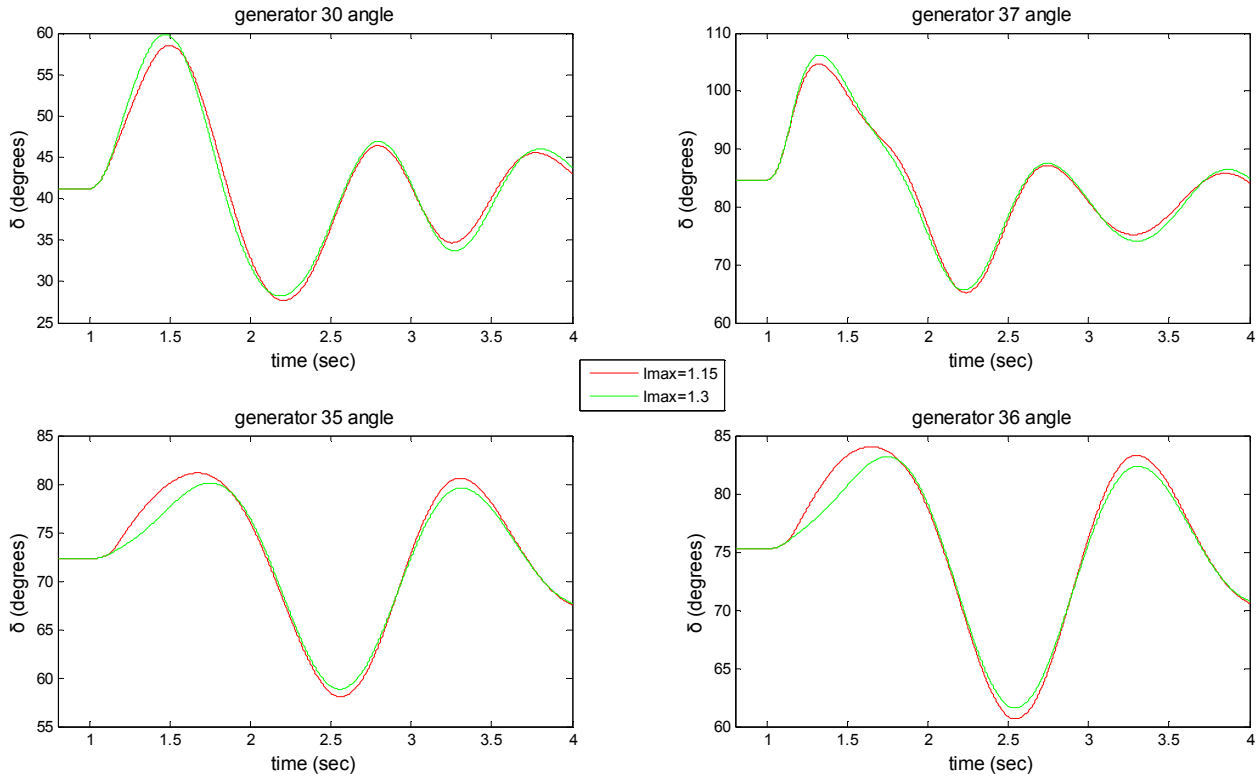

Fig. 3.11 Effect of over-current capability on the generators rotor angles for a fault in bus 27

The results of figure 3.11 show that the effect of an increase in the current limit of the converters is to increase the first peak of the rotor angle oscillation of the generators 30 and 37 which are located in the receiving converter's area. On the other hand the first peak of the rotor angle oscillation decreases for a higher value of the current limit for generators 35 and 36 in the sending converter's area. This can also be seen by the values of table 3.4.

	generator 30 (area 1)	**generator 37 (area 1)**	**generator 35 (area 3)**	**generator 36 (area 3)**
Imax	$\Delta\delta_{max\%}$	$\Delta\delta_{max\%}$	$\Delta\delta_{max\%}$	$\Delta\delta_{max\%}$
1.15	42.032	23.749	12.295	11.704
1.3	45.245	25.510	10.875	10.578

Table 3.4 Effect of over-current capability on the maximum rotor angle deviation for a fault in bus 27

This behavior is related to the active current reduction of converters. In paragraph 3.3.1.3 it was explained that an active current reduction of the converters, when they reach their current limit, will lead to an acceleration of generators in the sending area and a deceleration of generators in the receiving area. As explained higher speed peaks, due to acceleration, lead to a higher first peak of the rotor angle oscillation. This active current reduction-induced acceleration/deceleration is superimposed on the acceleration or deceleration a generator experiences due to the fault. Taking into account all of the above it was shown that the active current reduction decreases the rotor angle peaks of generators in area 1 while it increases them in area 3. By increasing the current limit to 1.3 p.u the receiving converter will not reach the new current limit as was seen in paragraph 3.3.2.1. This means that no active current reduction will take place in either of the converters. Since there is no active current reduction the effects of it will not influence the rotor angle stability of the generators in areas 1 and 3. Therefore the generators in area 1 will not benefit anymore from the active current reduction leading to a higher first-rotor angle peak for I_{max}=1.3, while the first-rotor angle peak for generators in area 3 will be smaller since there is no active current reduction to further accelerate those generators.

3.3.3 Effect of the converter current limitation strategy on the system

As explained earlier in paragraph 3.3.2, the power electronic components of the VSC are sensitive to currents above their nominal value. In paragraph 2.3.2 it was explained that the converter's phase reactor can reduce possible currents during faults. Additionally the converter has the ability to limit further the current, if needed, by appropriate switching actions. There are various current limitation strategies (CLS) that determine how each current component (active and reactive) is reduced. Some of the CLSs found in literature **[37]** are that of active current priority, reactive current priority and equal current priority.

In the case of active current priority, when the converter current exceeds the over-current capability, priority is given to the active component of the current. This means that only the reactive current component will be decreased until the total current is again within the current limits. The active current component will retain the same value it had before current limitation. In the case that the active current component is

also larger that the current limit then the active current component is reduced to become equal to the current limit and the reactive current component becomes zero.

The reactive current priority limiting strategy is similar to the active current limitation strategy. However, in this case, priority is given to the reactive current component.

In the equal current priority limiting strategy, both the active and reactive currents components are reduced until the total converter current is equal to the current limit. The amount by which each current component is reduced is such at each time the ratio of the active and reactive currents remains constant and equal to their ratio before the current limit was reached.

The concept of the strategies is depicted in figure 3.12.

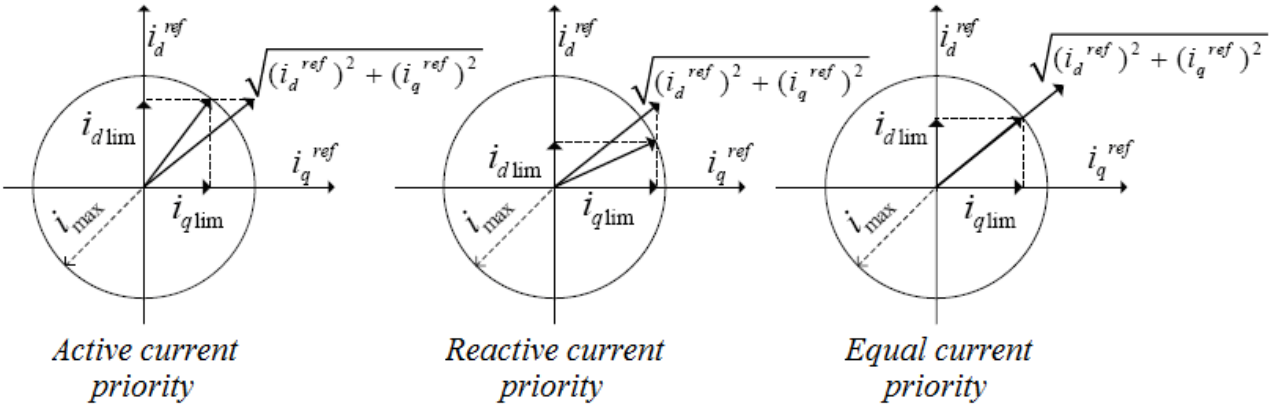

Fig. 3.12 Current limitation strategies

Since different current limitation strategies result in different active and reactive current components during the fault it is interesting to see how this affects the system. The simulations are performed for active, equal and reactive current priority. Once again, the studied disturbance is a three-phase fault at bus 27, cleared 150 ms after the occurrence. The over-current capability of the HVDC VSCs is set to I_{max}=1.15 p.u and the k factor is equal to k=6. These values are adequate for the study since for a fault applied in bus 27, the receiving VSC reaches its current limit and the effect of the current limitation strategies can be observed.

3.3.3.1 Response of HVDC converters to faults for different current limitation strategies

Just as in the previous sensitivity parameters examined, the result presentation will start with the response of the HVDC converters to the fault. Figures 3.13 and 3.14 present the response of the sending and receiving converters.

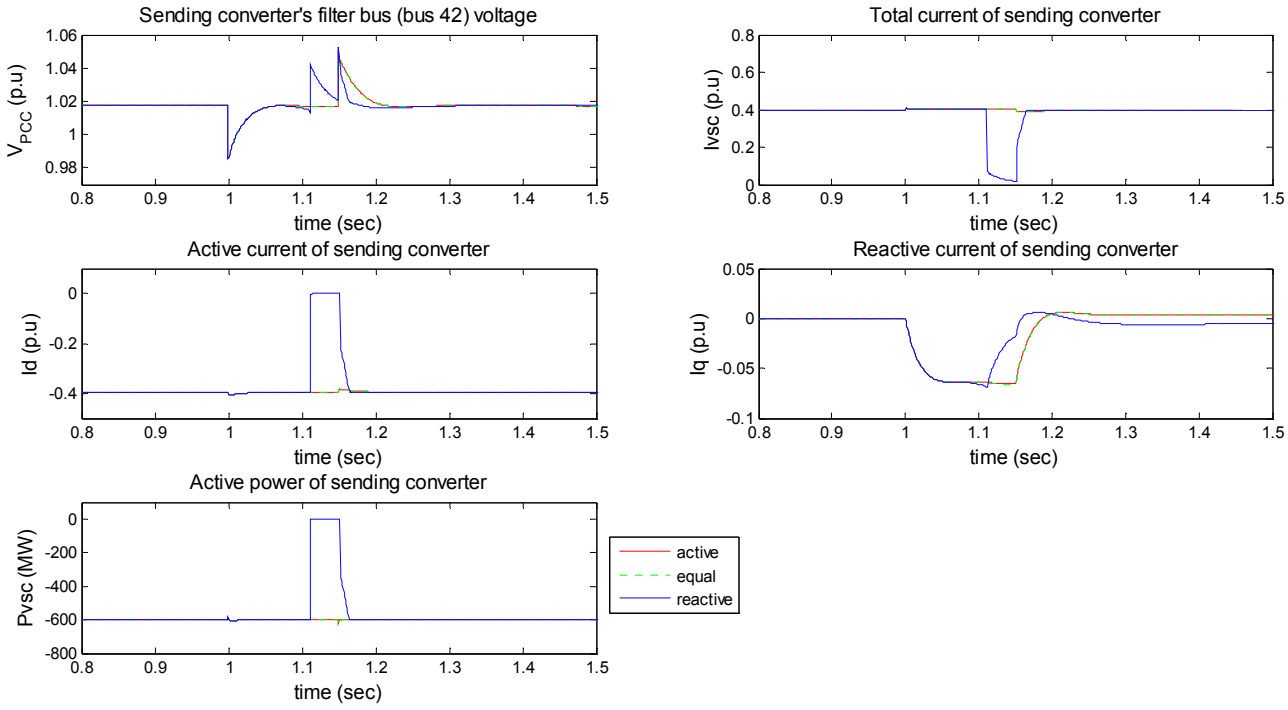

Fig. 3.13 Response of sending converter (bus 21) for different current capabilities for a fault in bus 27

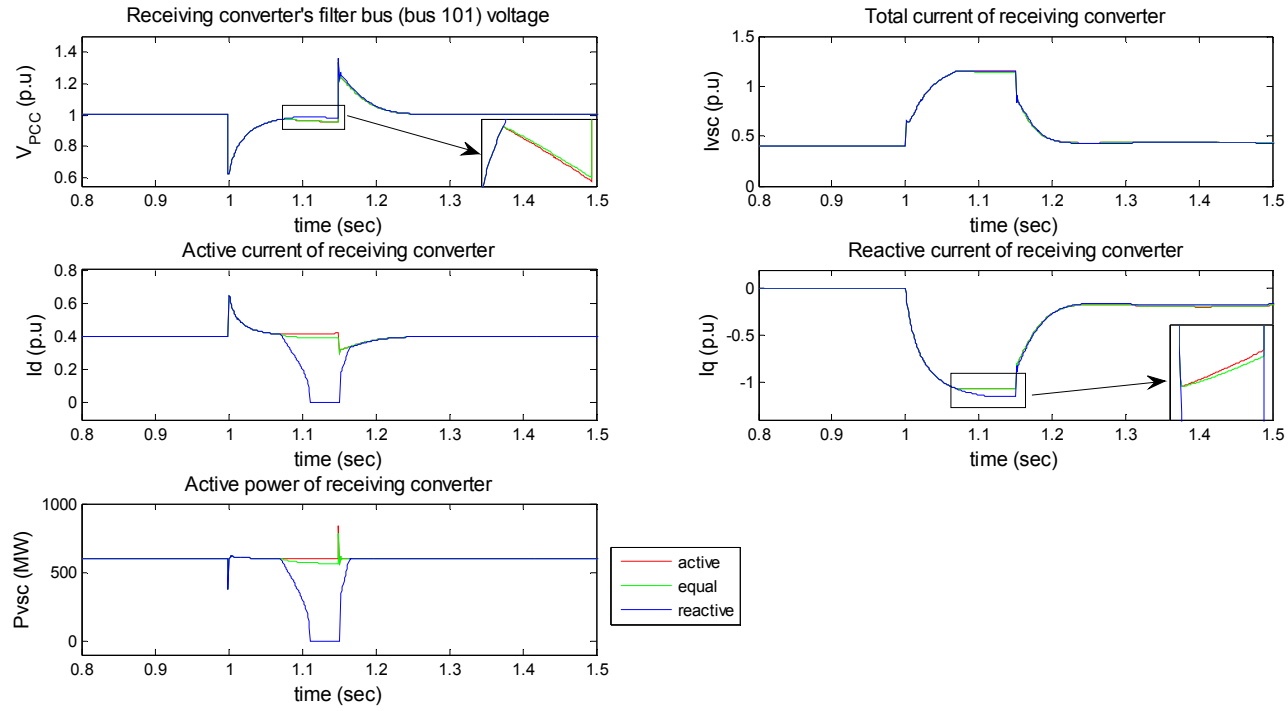

Fig. 3.14 Response of receiving converter (bus 3) for different current capabilities for a fault in bus 27

Figure 3.13 reveals that any effect the CLSs have on the non-limit-reaching converter (sending converter in this case) are related to the active current reduction

that takes place in the limit-reaching converter (receiving converter in this case). This can be seen for example by the voltage jump at bus 42 for a CLS of reactive current priority.

Besides that the CLS does not affect the response of the sending converter because it does not reach its current limit for the specific fault location.

The true effects of the CLS can be seen in the receiving converter's response presented in figure 3.14. In this figure it can be observed that the reactive current priority leads to a higher voltage in the filter bus of the receiving converter. This is expected since in reactive current priority the reactive current is not reduced at all. The lowest filter bus voltage is observed for the active current priority, where the reactive current component is reduced the most. Equal current priority results in a slightly better voltage profile for the filter bus compared to the case of active current priority.

As expected the highest active current component and thus highest DC power transfer during the fault is achieved for the active current priority. Reactive current priority leads to the reduction of the active current to zero while equal current priority leads to a much smaller active current reduction.

It must be mentioned that due to the weakness of the model, explained in paragraph 3.3.1.1, active current reduction takes place in the non-limit-reaching converter (sending converter) only for reactive current priority where the active current component of the limit-reaching converter is reduced to zero. In equal current priority, where the active current of the limit-reaching converter is reduced but doesn't reach zero, the active current of the non-limit-reaching converter is not reduced. This behavior will affect the results but only little because the active current reduction in equal priority is small either way.

3.3.3.2 Effect of the current limitation strategy on the AC system's bus voltages

The effect of the CLS on the AC voltage of the system's buses will be shown. The selected buses are the same as those in paragraph 3.3.2.2 since the impact of the CLS can mainly be observed in the area near the limit reaching converter. The voltage plots are presented in figure 3.15.

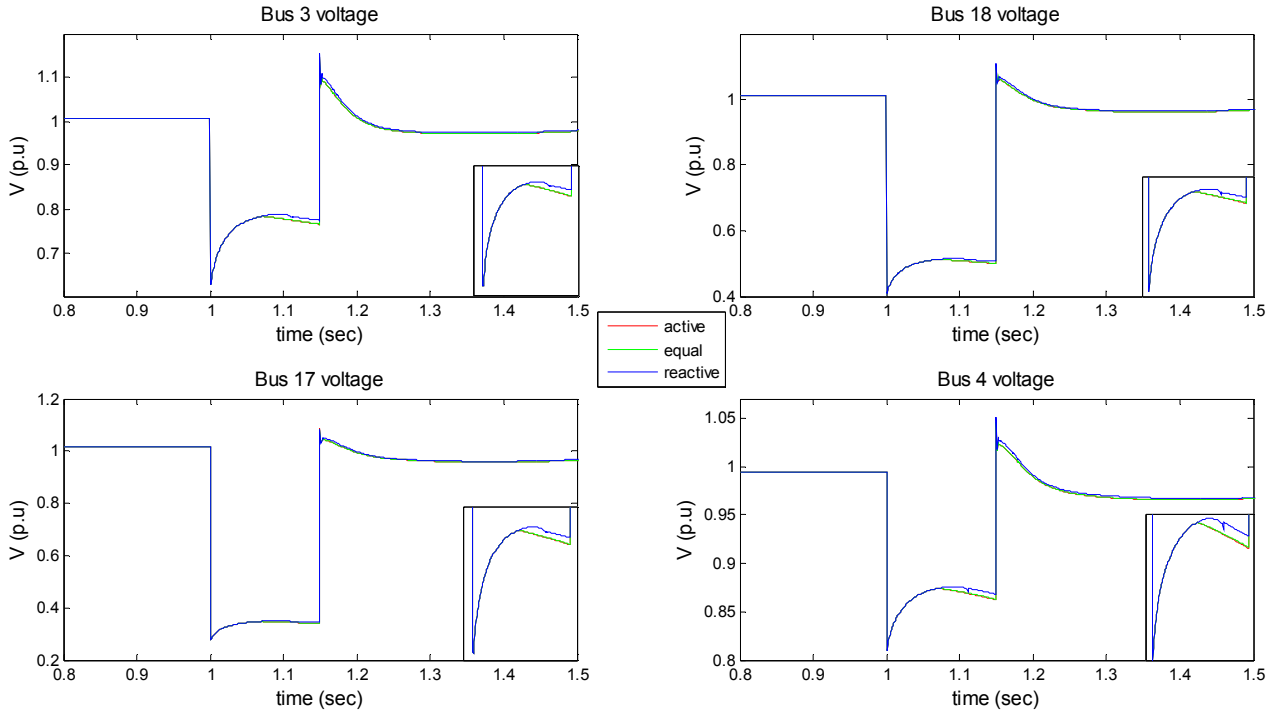

Fig. 3.15 Effect of the current limitation strategy on the bus voltages for a fault in bus 27

Figure 3.15 shows that the effect of different current limitation strategies is smaller, especially between the active and equal current priorities. The differences between the various CLSs can be better seen by the values of table 3.5.

	Bus 3 (area 1)	**Bus 18 (area 1)**	**Bus 17 (area 1)**	**Bus 4 (area 2)**
CLS	**ΔV%**	**ΔV%**	**ΔV%**	**ΔV%**
active	24.504	50.689	66.648	13.103
equal	24.485	50.677	66.640	13.087
reactive	24.103	50.425	66.470	12.857

Table 3.5 Effect of the current limitation strategies on the average voltage dip for a fault in bus 27

The results show that the less a current limitation strategy reduces the converter's reactive current component the higher the voltage in the system's buses will be during a fault. Therefore the highest fault voltage is achieved for reactive current priority, next for equal current priority and finally active current priority results in the lowest bus voltages during the fault. The difference however between the various CLSs is small.

3.3.3.3 Effect of the current limitation strategy on the rotor angle response of generators

Finally the effect of the CLSs on the rotor angles of generators will be presented. The criteria for selecting the generators to monitor are the same as in paragraph 3.3.2.3. Therefore the monitored generators are the generators connected to buses 30

and 37 from area 1 and 35 and 36 from area 3. The rotor angle plots are presented in figure 3.16.

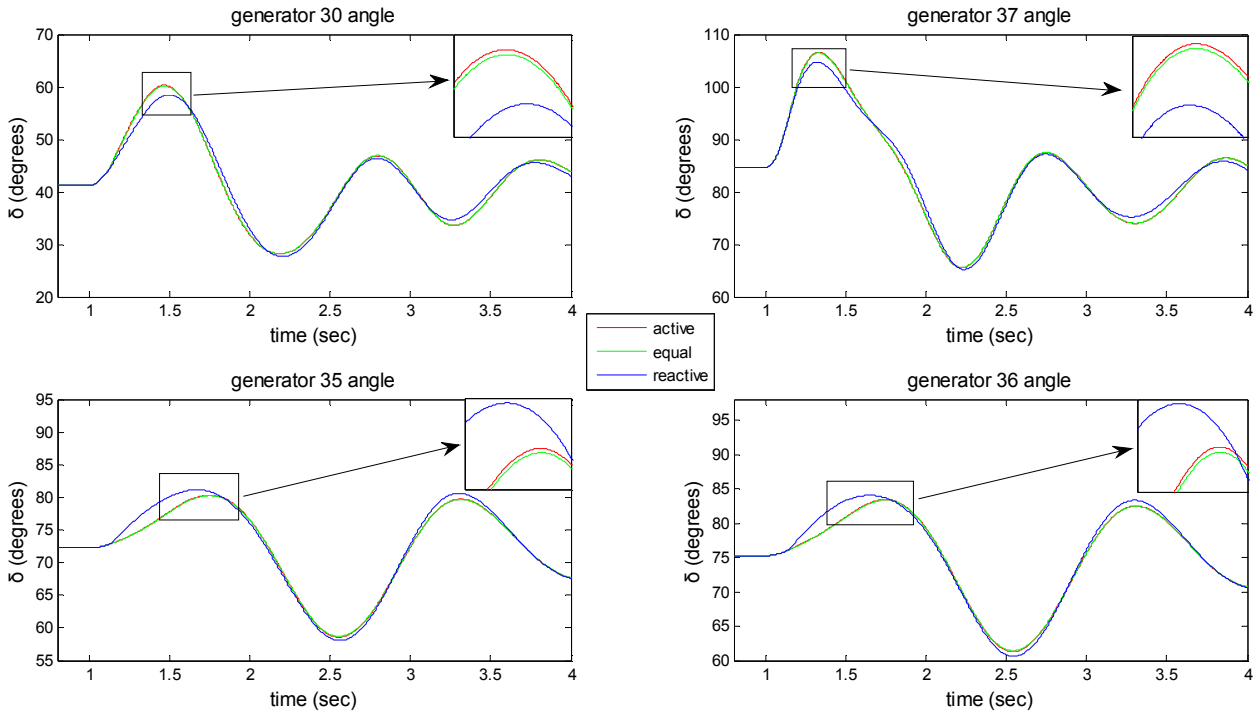

Fig. 3.16 Effect of current limitation strategy on the generators rotor angles for a fault in bus 27

Figure 3.16 indicates once again the effect active current reduction has on the rotor angles of the generators in areas 1 and 3. The effect of the CLSs on the rotor angles is quantified by the maximum first peak rotor angle deviations presented in table 3.6.

	generator 30 (area 1)	**generator 37 (area 1)**	**generator 35 (area 3)**	**generator 36 (area 3)**
CLS	$\Delta\delta_{max\%}$	$\Delta\delta_{max\%}$	$\Delta\delta_{max\%}$	$\Delta\delta_{max\%}$
active	46.301	25.965	11.193	10.875
equal	45.903	25.801	11.091	10.777
reactive	42.032	23.749	12.295	11.704

Table 3.6 Effect of current limitation strategy on the maximum rotor angle deviation for a fault in bus 27

In paragraph 3.3.1.3 it was seen that the active current reduction improved the rotor angle stability of the generators in area 1, while the rotor angle stability of generators in area 3 deteriorated. Observing the maximum rotor angle deviations of generators 30 and 37 it is seen that the smallest rotor angle peak is achieved for reactive current priority. This happens because this CLS results in the highest active current reduction (active current eventually reduces to zero). The next smallest rotor angle deviation is achieved for equal current priority since active current reduction again takes place but it is smaller compared to the reactive current priority CLS. The highest rotor angle deviation occurs for active current priority where no active current reduction takes place.

The situation for generators in area 3 is as expected for the case of active and reactive current priorities. Active current priority results in the lowest rotor angle deviation since active current reduction deteriorates the rotor angle stability of generators in area 3, while the highest rotor angle deviation occurs for reactive current priority. The rotor angle deviation for the equal current priority is smaller compared to active current priority. This is unexpected since in equal priority, active current reduction does occur. The reason for this unexpected result is the weakness of the VSCDCT model, presented in paragraph 3.3.1.1. As was explained in paragraph 3.3.3.1, the HVDC line model's weakness leads the active current of the non-limit-reaching converter to not reduce unless the limit-reaching converter's active current is reduced to zero. Since equal current priority does not lead to a reduction of the receiving converter's active current to zero, active current reduction will not occur in the sending HVDC converter. Therefore the rotor angle stability of the generators in area 3 appears improved, compared to active current priority, due to the improved voltage profile equal current priority offers. In reality however the rotor angle deviation of the generators in area 3 should be worse than the case of active current priority but better than the case of reactive power priority.

The study presented in this chapter reveals that the sensitivities seen in **[37]** are not seen in this case. The authors in **[37]** study similar sensitivities as in this thesis but for HVDC links connecting offshore wind farms to the AC system. This is the main reason for the observed differences. HVDC links connecting offshore wind farms to the grid absorbs power from the offshore grid and inject it to the AC power system. However, embedded HVDC lines absorb and inject power from the same AC system (from different areas though). Therefore the HVDC line affects the AC system in the sending side in a different way than it affects it on the receiving side. This makes it difficult to account for the general transient stability of the whole AC system.

4. Results and Analysis

In chapter 3 PSS®E's library model for representing point-to-point VSC-HVDC lines was introduced and its verification was done by using it in time domain simulations with the IEEE 39 bus system. In this chapter, the same VSC-HVDC model will be used to represent Corridor A, in the German transmission system. A series of time domain simulations will be performed in order to specify the effect of Corridor A on the German and Dutch transmission systems.

This chapter contains a description of the transmission system model used for the studies. Next the results of the dynamic simulations are presented. The results discuss the influence of VSC-HVDC system control parameters during AC faulted conditions. Emhasis is given on the voltage and rotor angle responce. The examined parameters as introduced in Chapter 3 and are namely the k gain, the converter's over-current capability and the applied current limitation strategy. Finally the sudden loss of Corridor A, e.g due to an HVDC converter failure, will be studied in order to determine its impact on the AC transmission system.

4.1 The Dutch transmission system model

The power system model used for the dynamic simulations is the Dutch AC transmission system (110-380 kV) and those of its neighboring countries (Belgium, Luxemburg, France and Germany) on the 220 kV and 380 kV voltage levels, for the year 2020. The grid model has been developed by TenneT and DNV GL in the PSS®E version 33.3.

4.1.1 Modeling assumptions

The starting point for the model is ENTSOE's 2020 grid. The Dutch transmission system is replaced with a more detailed model. The power flow model of the Netherlands is based on the "Business as usual" scenario of KCD 2012-2020 for the years 2013, 2016 and 2020. The source for the foreign countries power flow model is the ENTSOE RGNS model. Some additions and changes were made in the above model to represent large future projects that might affect the Dutch grid and that weren't already included. An example of such a change is the AC connection between Doetinchem in the Netherlands and Niederrhein in Germany.

For the creation of the dynamic model, the generators present in the power flow model are linked to dynamic models. These models additionally contain excitation and turbine governor models. In some cases under-excitation limiters and power system stabilizer models are added to the generator models. All generators use PSS®E's library model GENROU. For most of the large generator units (above 200 MVA) in the Netherlands, the owners have provided models and values for the model parameters. For the rest of the units in the Netherlands and abroad the following modeling assumptions are made:

- For units where no specific parameters are known, generic data is used. The inertia constant H, is arbitrarily chosen between 1.5 and 5.5 seconds.

- Units in the Netherlands with an apparent power larger than 50 MVA are provided with an excitation system model (SEXS) and a turbine governor model (TGOV1 for steam turbines and GAST for gas turbines).
- Units smaller than 50 MVA are not modeled at all for dynamic studies.
- Large, influential units outside the Netherlands are provided with excitation system and turbine governor models (SEXS and TGOV1 respectively).
- All other units are provided only with an excitation system model (SEXS).

Regarding wind park models, their dynamic behavior differs from that of conventional generators depending on the wind turbine type. During and at post-fault conditions, the fault-ride-through and subsequent power recovery characteristics must be modeled specifically. However in the present transmission system model wind parks are not modeled using specific models. The wind generation in the Netherlands is modeled as negative static loads. Wind generation outside the Netherlands is modeled as conventional generators again using the GENROU model.

During faults both conventional generators and wind turbines provide short circuit reactive current injection to the system in order to maintain the voltages at their connection points as close as possible to the reference value of their voltage controller. However the current capability of generators is substantially higher than the current capability of the wind turbine converters. This has not been taken into account in DNV GL's system model and may influence the results. For this reason a number of simulations have been performed also with a modified system model where the wind turbines in Germany have been replaced with negative static loads. These simulations examine the effect the wind turbine modeling has on the results. The modeling of wind turbines as static loads may not represent the realistic case, since static loads do not contribute at all short circuit reactive current in the case of a fault. However this case represents a concervative scenario and will reveal the effect of the wind turbine fault current contribution when compared to the case where the wind turbines are modeled as synchronous generators. Having the wind turbines modeled as loads will result in a concervative scenario where only the HVDC line's effect is examined. The results of this analysis can be found in appendix E.

Due to the uncertainty regarding the exact dynamic behavior of loads in the Netherlands an approximation is used for their modeling. For dynamic studies a fraction of the load is converted to follow a constant current or constant admittance characteristic. Frequency dependence of the loads is neglected.

The existing HVDC connections of the Netherlands with Great Britain (BritNed), Norway (NorNed) are modeled as negative static loads. The HVDC cable Cobra, connecting the Netherlands and Denmark, which is not commissioned yet, is also modeled, again as a negative load.

4.1.2 Additions and changes in the transmission system model

For the purpose of the present study, Corridor A was added in TenneT and DNV GL's Dutch transmission system model. The VSC-HVDC model used, is PSS®E's library model VSCDCT, which was introduced and validated in chapter 3. As mentioned in paragraph 1.2, Corridor A will span from the North of Germany to the south and will consist of two sections. The HVDC corridor's converter stations are planned to be located in Emden, Osterath and Philippsburg (see figure 4.1). These connection points were also used for the present study. Henceforth Corridor A's

section from Emden to Osterath will be addressed as *EMD-OST section*, while the section from Osterath to Philippsburg will be addressed as *OST-PHLP section*.

The generation of the offshore wind parks in the North Sea was initially set to 2938 MW. This generation was increased by 1500 MW while at the same time the load in Germany was also increased accordingly. This change in Germany's generation and load was done in order to represent a realistic scenario were a large power flow from north to south would be facilitated by Corridor A.

Currently the Emden substation is part of the 220 kV grid in Germany. In TenneT and DNV GL's model, Emden's substation is also modeled as a 220 kV bus. After calculating the short-circuit ratio (SCR) of the Emden bus it was found to be equal to 2.67. This SCR was considered low and therefore the Emden bus was upgraded to a 380 kV bus. This bus upgrade is also in accordance with the plans of TenneT-Germany which intends to upgrade the Emden bus to 380 kV before the connection of Corridor A. This bus upgrade led to a SCR equal to 5.44 which is moderate.

When applying faults near the Emden HVDC converter station the dynamic simulation failed to converge during the fault application. The moderate SCR was thought to be the problem. The SCRs in the other two connection points in Osterath and Philippsburg are quite high and are equal to 17.87 and 15.06 respectively. Emden's SCR was further increased by adding an additional connection between the 380 kV buses of Emden and Diele. The new SCR in Emden became equal to 9.05 and approached the SCRs of Osterath and Philippsburg. The divergence problem was indeed solved by this change. The addition of the extra Emden-Diele connection is not an actual project TenneT Germany has mind and it will have an effect on the power flows. However the accuracy of the dynamic simulations is not expected to be greatly influenced.

4.2 Methodology

In this paragraph the methodology used in the simulations will be explained. The thesis focuses on two subjects:

- Influence of the embedded VSC-HVDC link's control parameters on the Fault-Ride-Through and voltage response of the Dutch and Geramn network. The study is performed taking HVDC network code requirements **[15]** as a boundary condition.
- The impact of the loss of Corridor A on the transient rotor angle stability of the Dutch and German transmission system.

Regarding the sensitivity analysis, the voltage support related parameters that are examined were presented in chapter 3 and are the voltage controller's *k gain*, the HVDC converter's *over-current capability* and *current limiting strategy*.

In order to observe the influence of these three parameters on the transmission system's dynamic behavior, three-phase bus faults are applied on 380 kV buses both in the Dutch and the German transmission systems. The fault is cleared after 150 ms. For each fault location a number of simulations is run where each time the value of one of the examined parameters is changed. The criterion for choosing the fault locations is their distance from Corridor A's converters. In the Netherlands, fault locations both close and far from the converters are examined. The chosen fault

locations can be seen in figure 4.1. The red dots signify the fault locations and the black ones Corridor A's converter locations.

Fig. 4.1 Fault locations in the Netherlands

In Germany the faults locations are selected to be close to the converters in order to ensure that the converters reach their current limit. By reaching their current limit the maximum influence of Corridor A on the system can be examined. An additional reason why the converters must reach their current limit during the fault is that the sensitivities of the over-current capability and current limitation strategy can only be seen when the current limit is reached. The selected fault locations in Germany can be seen in figure 4.2. As can be seen from figure 4.2, three zones have been defined. These zones represent the areas near Corridor A's converters. Only faults inside the zones are examined.

The snapshot of the system is such that the generation of the offshore wind parks in the North Sea is large and the load in the south of Germany is also increased. Therefore Corridor A is set to transfer power from the north of Germany to the south. Consequently Zone 1 is a "sending" zone, Zone 2 is both a "sending and receiving" zone and Zone 3 is a "receiving" zone. The importance of whether a zone is sending or receiving has been seen in chapter 3, since it determines how local generators will react to a power reduction of the HVDC line's power transfer.

Fig 4.2 Fault locations in Germany

Finally as mentioned above, the last case study is the influence of the loss of Corridor A on the transmission system's transient rotor angle stability. This study assumes an internal converter fault which results in the switching off of the relative Corridor A section. So the disconnection of the EMD-OST section and the OST-PHLP section of Corridor A will be examined. Focus will be given on the rotor angle stability of large generators and the power flow in the AC interconnection lines between the Netherlands and Germany.

4.3 Sensitivity analysis: Three-phase bus faults in Germany

In this paragraph, the results of the sensitivity analysis for faults in Germany will be presented. In paragraph 4.3.1 the effect of the HVDC voltage controller's k gain on the system will be. Next, the effect of the HVDC converters' over-current capability will be examined in paragraph 4.3.2. Finally in paragraph 4.3.3 the converter current limitation strategy on the transmission system will be examined.
Simulations will be preformed for all the fault locations presented in figure 4.2 in order to get a more holistic view on the effect of the HVDC converters on the dynamic behavior of the system.

4.3.1 The effect of the k gain on the AC system for faults in Germany

As explained in paragraph 3.3 the k gain is the amount of additional reactive current injection supplied by the HVDC converter, for voltage support during the disturbance period. This is given as a function of the voltage dip. As shown in figure 1.5 this function is a straight line and therefore the k gain is its slope.

The examined values of k are 0, 2, 4 and 6. When the k gain is equal to 0 the HVDC converter offers no additional reactive current to support the voltage. As the k gain increases the amount of additional reactive current from the converter increases.
The other sensitivity parameters remain unchanged. The over-current capability of the converter is set to 1.15 per unit on the converter's nominal current and the current limiting strategy is set to reactive current priority.

The HVDC converters are set to control their filter bus' voltage. The filter bus is the bus that is connected in the AC side of the converter where the AC side harmonic filters are connected, as shown in figure 2.12 in paragraph 2.3.2.
The active power transferred by Corridor A is set to 2000 MW.

4.3.1.1 Response of Corridor A's HVDC converters to faults for different values of k

First a symmetrical self-cleared fault is applied in Dorpen in Zone 1. Dorpen is located near Emden and the borders with the Netherlands. Its 380 kV bus is connected directly to Diele's 380 kV bus which is an interconnection point between the Netherlands and Germany. It is also planned as a connection point for offshore wind parks in the North Sea. This location was selected due to its proximity to the Dutch transmission system and to Emden's HVDC converter.

The response of Emden's converter to a fault in Dorpen is shown in figure 4.3. Osterath's converter response is shown in figure 4.4. Despite the fact that Osterath is located far from Zone 1 its response is shown in order to demonstrate the interaction between the two HVDC converters and also to observe how severe the impact of a fault in Zone 1, is at Zone 2. The response of the converters of the OST-PHLP section of Corridor A will not be presented since their distance from the fault is large and thus the fault will have a small impact on the system there.

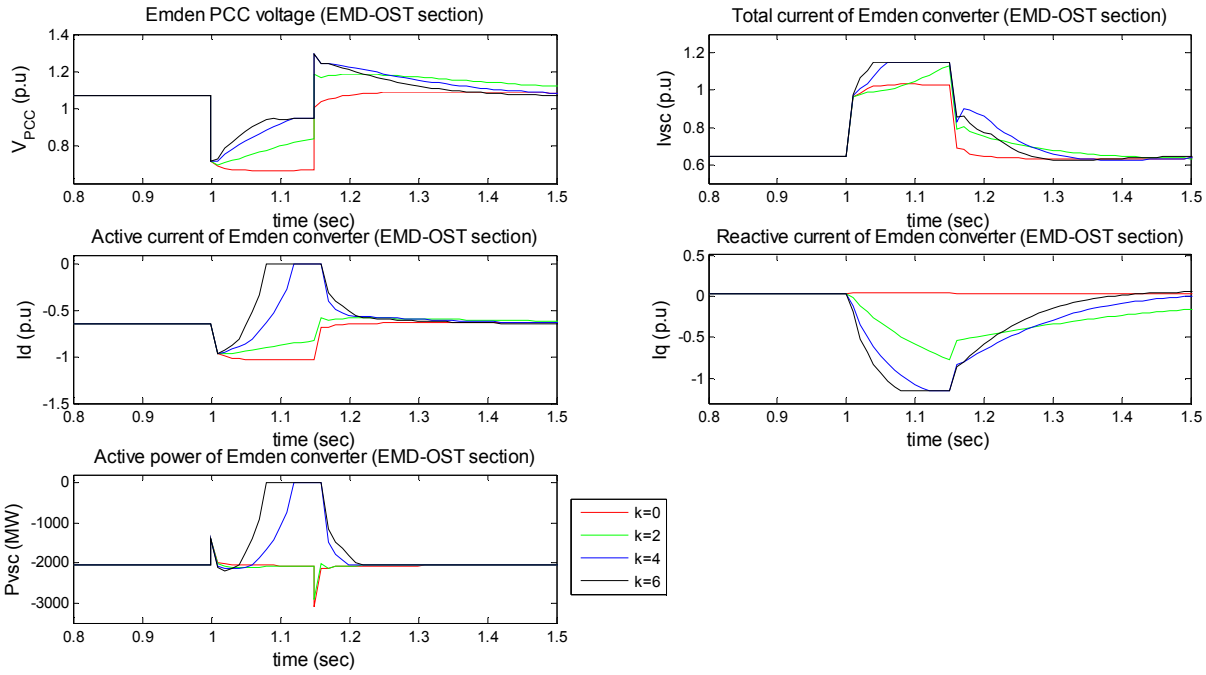

Fig. 4.3 Response of Emden's converter (EMD-OST section) to a 3-phase bus fault in Dorpen (Zone 1) for different values of k

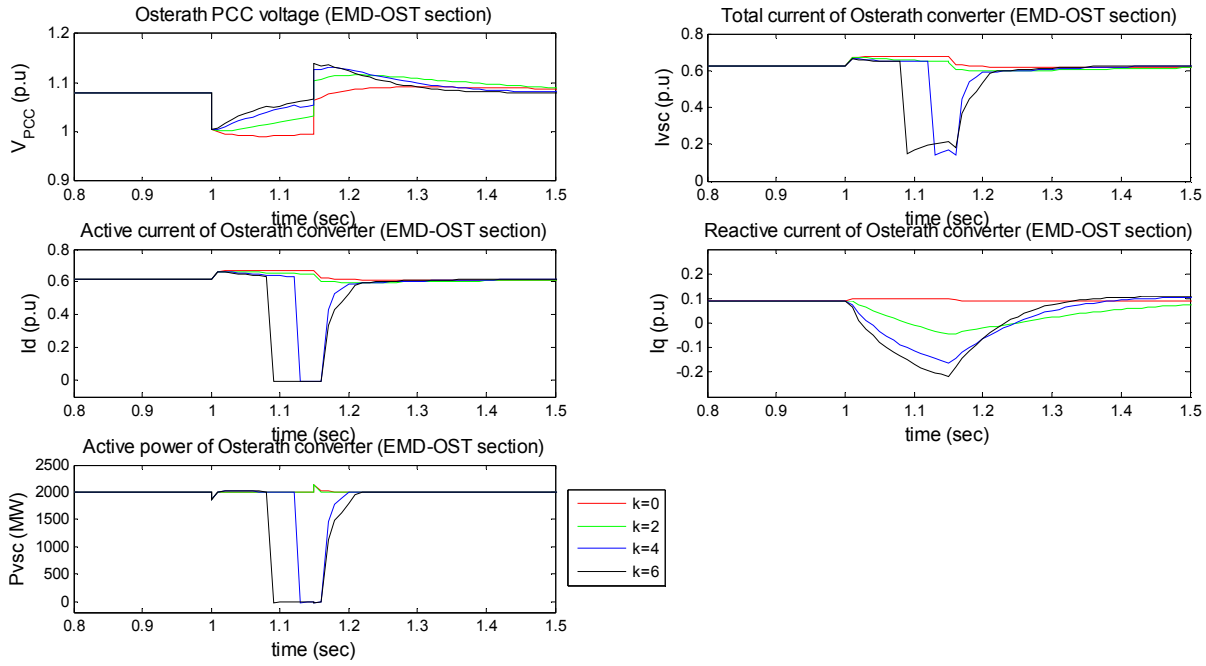

Fig. 4.4 Response of Osterath's converter (EMD-OST section) to a 3-phase bus fault in Dorpen (Zone 1) for different values of k

The first thing to notice in figures 4.3 and 4.4 is that voltage boost at the filter buses in Emden and Osterath during the fault is higher for higher values of k, i.e for higher additional reactive short circuit current. This effect was expected and was also seen in paragraph 3.3.1. The voltage drop during the fault in Osterath's filter bus is much smaller than in Emden since the fault is located far from Osterath.

As can be seen by the converter's total current, Emden's converter reaches its current limit during the fault for k equal to 4 and 6. Osterath's converter on the other

hand doesn't reach its current limit. This happens because the fault is located close to Emden and far from Osterath.

For k equal to 4 and 6, the reactive current component in Emden surpasses the converter's current limit during the fault and is therefore chopped to 1.15 p.u, which is the current limit used in these simulations. At the same time the active current component of Emden's converter is reduced to zero. This happens because the converter's current limitation strategy is set to reactive current priority. In this current limiting strategy, as explained in paragraph 3.3.3, once the converter's current surpasses its current limit the converter reduces the active current component and doesn't change the reactive component. When the reactive current component becomes equal to the current limit all of the converter's current capability is given to the reactive current component leaving no "room" for an active current component and thus it becomes zero. As can be seen in figure 4.4, despite the fact that Osterath's converter does not reach its current limit, its active current component also becomes zero for k equal to 4 and 6. This happens because Emden's converter has reduced its active current component to zero. As explained in paragraph 3.3.1.1, in order to maintain the DC voltage at a constant value, the energy exchange between the converters must be in balance. Therefore when for some reason the active current output of one converter is reduced, the active current output of the other HVDC converter must be reduced by the same amount.

As is observed in figure 4.4, due to the VSCDCT's weakness explained in paragraph 3.3.1.1, the active current of Osterath's converter (which doesn't reach its current limit during the fault), will not reduce to zero gradually as it does in Emden's converter, but it will drop suddenly to zero when Emden's active current reaches its zero value. This behavior is a limitation of the model due to the lack of the DC circuit representation. In reality however, the non-limit-reaching converter's active current should decrease gradually to zero following the limit-reaching converter's active current reduction. This sudden reduction to zero, of the non-limit reaching converter's active current, results in a voltage jump in this converter's filter bus voltage. This behavior can be clearly seen in figure 4.5. The time instances t_1 and t_2 are the instances the active current of Osterath's converter drops suddenly to zero for k=4 and k=6 respectively.

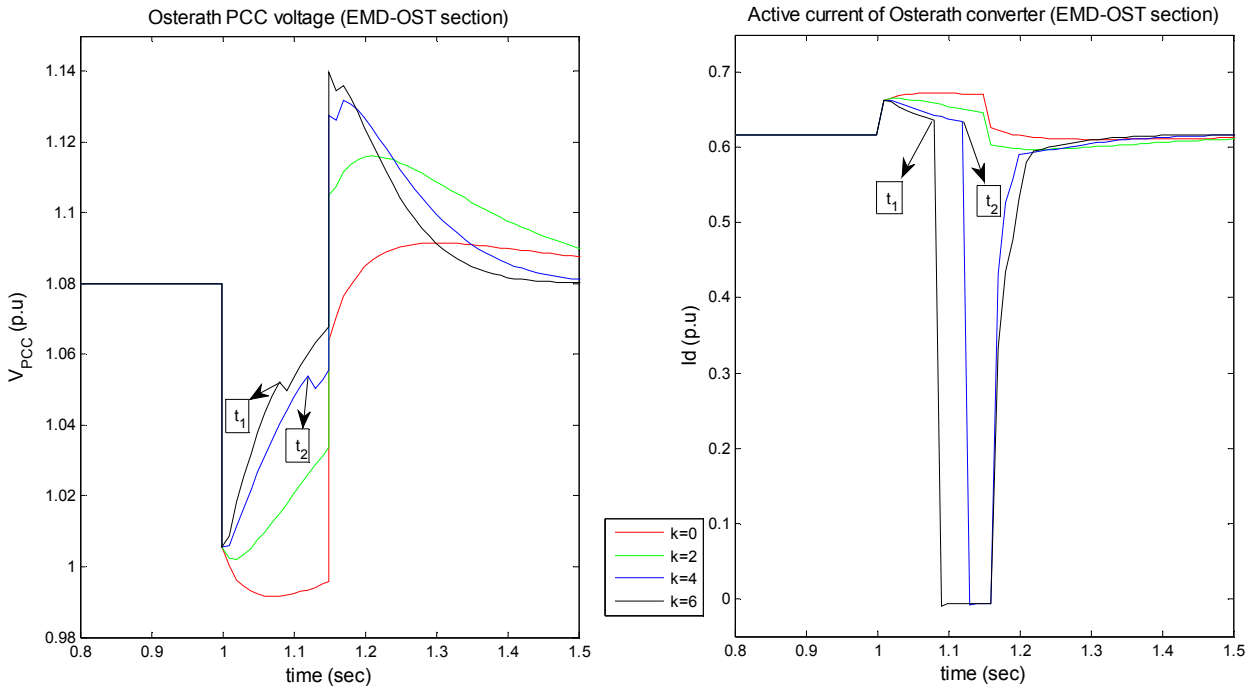

Fig. 4.5 Effect of Osterath's sudden active current drop on its filter bus voltage

Looking at the reactive current curves of figures 4.3 and 4.4 one can see that during the fault their values initially decrease. One would expect that the reactive current of the converter would have to increase during the fault in order to maintain the voltages. However this is not exactly true and it depends on whether the converter is absorbing or generating reactive power during steady state. In the simulations the HVDC converters are set to voltage control mode controlling their filter buses at values lower than the values they would normally have if no device controlled their voltage. Therefore the converters have to absorb reactive current in order to accomplish this. When the fault occurs the bus voltage will decrease. Thus the converter will try to increase the controlled bus' voltage meaning that the additional reactive current during the fault needs to be generated and not absorbed contrary to the steady state case. The net result in the converter's reactive current output is an initial decrease in its value and that is what is seen in figures 4.3 and 4.4.

Regarding the converter active power output, it can be seen in figure 4.3 that the converter's active power is 2069 MW which means that it is higher than the 2000 MW Corridor A is supposed to transfer. This happens because the sending end HVDC converter, in our case the one located in Emden, is set to compensate for the converter and DC line losses. In other words, the active power reaching Osterath is set to be 2000 MW and not less due to losses. This can be verified in the active power curve of the Osterath HVDC converter, in figure 4.4

Next the response of Corridor A's converters for a fault in Sechtem will be shown. As seen in figure 4.2, Sechtem is located in Zone 2, i.e near Osterath's HVDC converters. Osterath is the intermediate converter station of Corridor A. A fault near Osterath will have effect on both the EMD-OST and OST-PHLP sections of Corridor A.

Only the response of the two Osterath HVDC converters will be shown since those are the converters affected most from the fault. The response of Emden's and Philippsburg's converters can be found in appendix D. The response of Osterath's

receiving converter (EMD-OST section) is shown in figure 4.6 while that of Osterath's sending converter (OST-PHLP) is shown in figure 4.7.

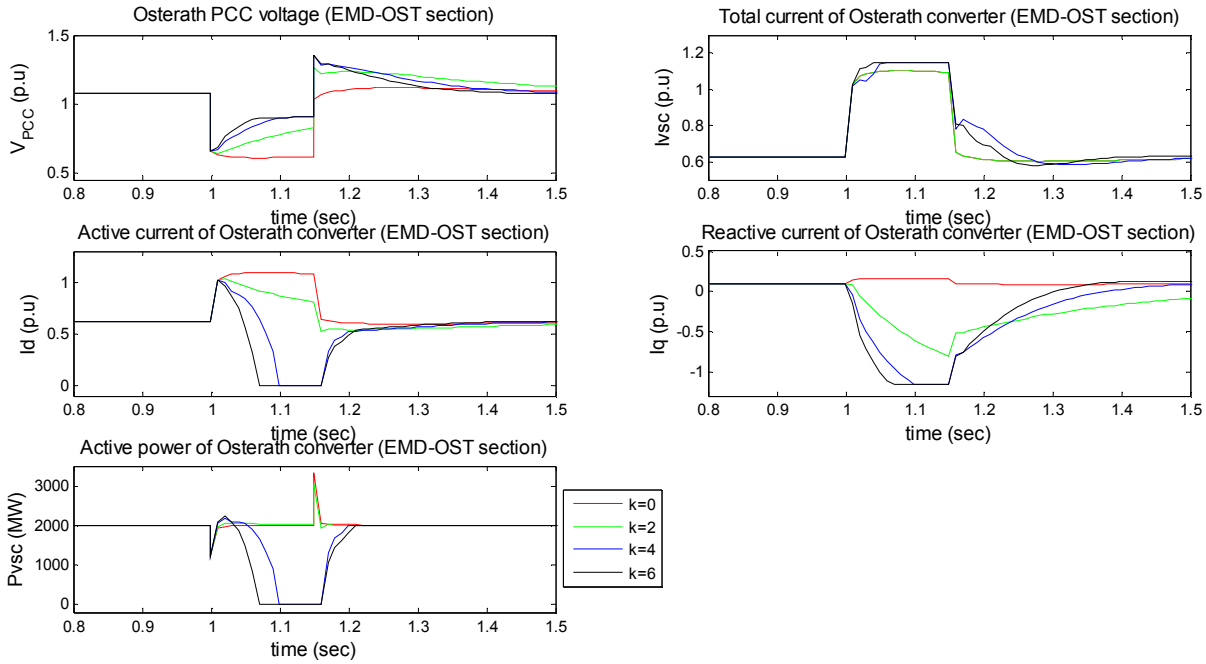

Fig. 4.6 Response of Osterath's converter (EMD-OST section) to a 3-phase bus fault in Sechtem (Zone 2) for different values of k

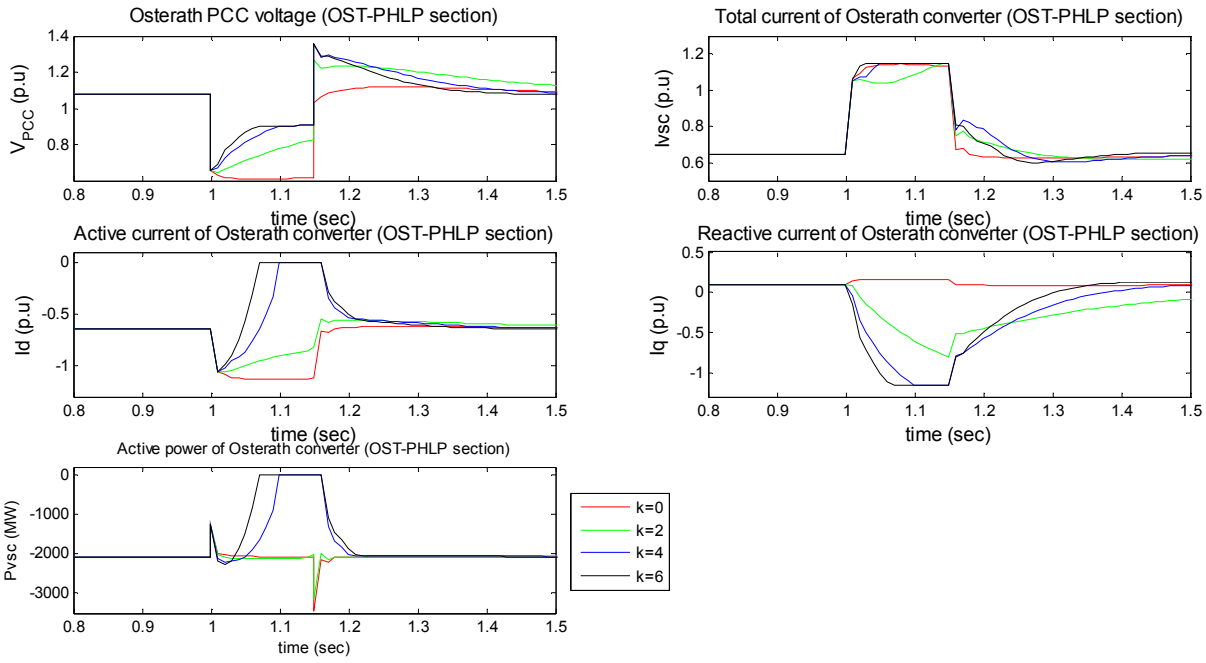

Fig. 4.7 Response of Osterath's converter (OST-PHLP section) to a 3-phase bus fault in Sechtem (Zone 2) for different values of k

The same observations for Emden's converter for a fault in Dorpen can be done for figures 4.6 and 4.7. In more detail, Osterath's converters which are located in the same zone as the fault are affected the most by the fault. This happens because the fault causes a large voltage dip in Zone 2's voltages and therefore on the filter buses of the converters. In order to counteract this large voltage dip the converters will

increase their reactive current outputs and will reach the converter current limit for k=4 and 6. The active currents in these cases will drop to zero in both of Osterath's converters but also in Emden's and Philippsburg's converters in order to maintain the DC voltage in the EMD-OST and OST-PHLP sections. It can also be seen again that the higher the value of the k gain the better the voltage support in the filter buses in Osterath.

Finally, the fault in Hopfingen, in Zone 3 will be examined. The response of Philippsburg's HVDC converter is shown in figure 4.8.

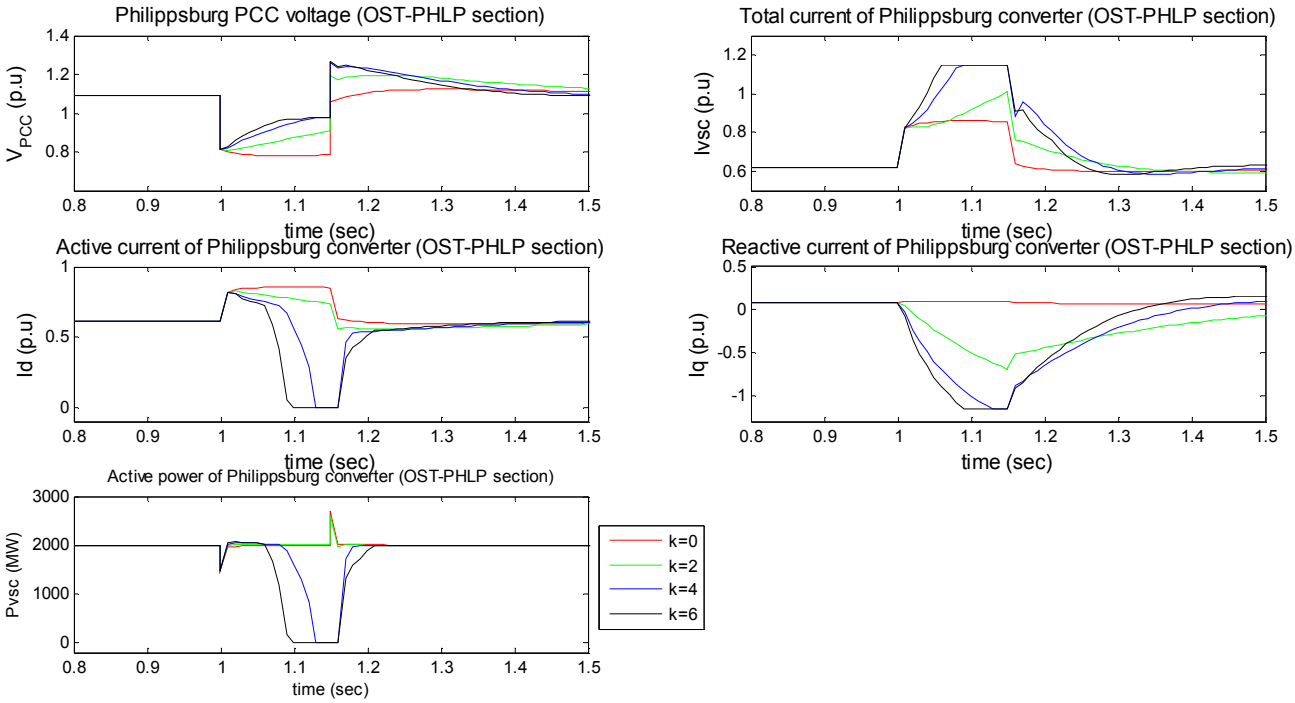

Fig. 4.8 Response of Philippsburg's converter (OST-PHLP section) to a 3-phase bus fault in Hopfingen (Zone 3) for different values of k

The response of Philippsburg's HVDC converter to a fault near it, is similar to the responses of the converters seen previously. No further analysis is needed. Osterath's sending converter response can be found in appendix D.

4.3.1.2 Effect of the k gain on the AC system's bus voltages

For the case of the fault in Dorpen, the voltages of a selected number of buses both in Germany and in the Netherlands are shown in figure 4.9. The selected 380 kV buses in Germany are Diele, Conneforde, Dulken and Rommerskirchen. Diele and Conneforde are located in Zone 1 and Dulken and Rommerskirchen in Zone 2. Bus voltages in Zone 3 will not be presented because the fault location if too far from that zone and therefore the voltage dips and the effect of Philippsburg's converter response are small. The selected buses in the Netherlands are Meeden, Diemen, Maasbracht, and Geertruidenberg. Meeden is close to the border with Germany. It is located close to Emden's HVDC converter and is directly connected to Germany's 380 kV bus in Diele. Maasbracht is located in the south of the Netherlands again close to the border with Germany. It is relatively close to Zone 2. Diemen and Geertruidenberg are located towards the west of the Netherlands far from the border

with Germany and far from Corridor A's HVDC converters. These buses were selected in order to show the effect of the HVDC converters on the voltages of buses located both close and far from them.

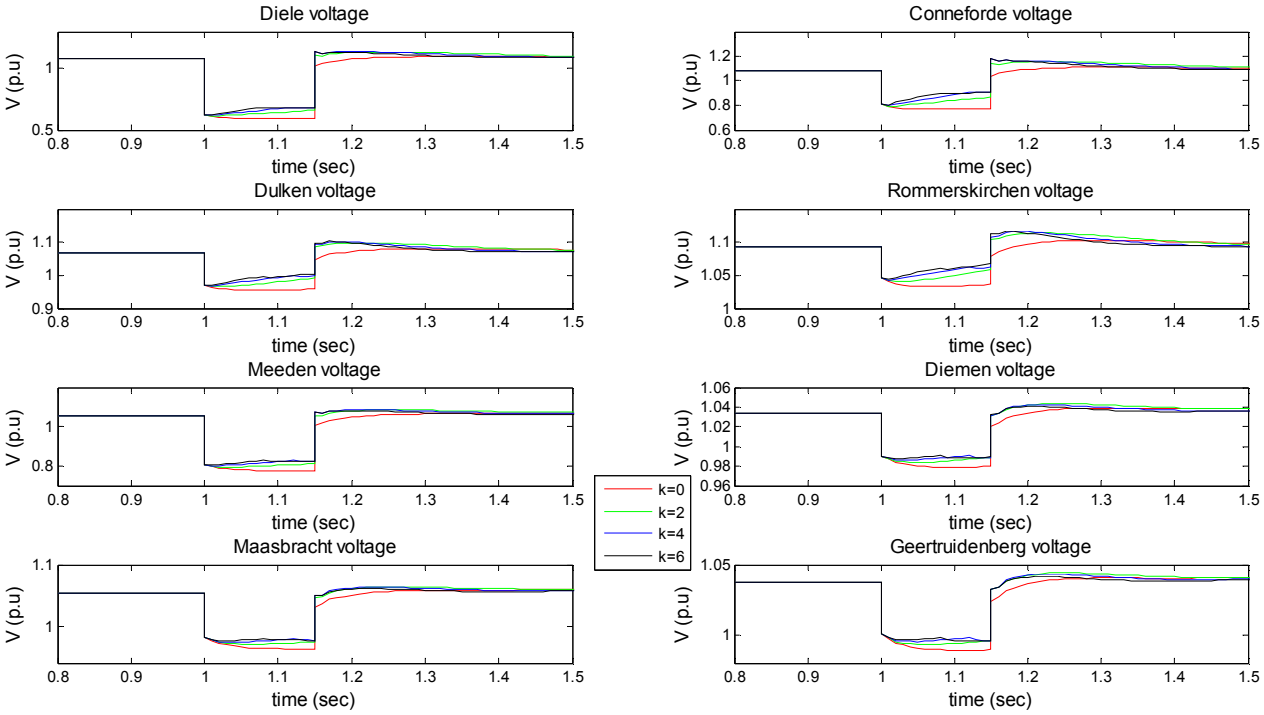

Fig. 4.9 Effect of the k gain on the 380 kV bus voltages for a fault in Dorpen (Zone 1)

Figure 4.9 shows that the bus voltage profile is better when k>0, i.e when additional reactive current support is given by the converter during the fault. As can be seen, the effect of the k gain is more pronounced in the buses close to the HVDC converters. It can also be seen that, as expected, the effect of the fault on the system becomes less and less severe as we move away from the fault's location. The voltage drop during the fault is small in Dulken, Maasbracht and Diemen which are located far from Dorpen. Once again its pointed out that the scale of the graphs is not the same for each bus.

The effect of the k factor on the buses can be better observed by the average voltage dip that was defined in paragraph 3.3.1.2 by equation 3.1. For practical reasons the definition is repeated in this chapter by equation 4.1:

$$\Delta V_{\%} = \frac{V_{prefault} - \overline{V}_{fault}}{V_{prefault}} \cdot 100\% \qquad (4.1)$$

where, $V_{prefault}$ is the prefault value of the bus' voltage and $\overline{V}_{fault}$ is the average value of the bus' voltage during the fault. The average voltage dip for each selected bus is shown in table 4.1.

	Diele (Zone 1)	Conneforde (Zone 1)	Dulken (Zone 2)	Rommerskirchen (Zone 2)	Meeden (NL)	Diemen (NL)	Maasbracht (NL)	Geertruidenberg (NL)
k	**ΔV%**	**ΔV%**	**ΔV%**	**ΔV%**	**ΔV%**	**ΔV%**	**ΔV%**	**ΔV%**
0	44.938	29.048	10.462	5.304	26.3453	8.435	5.239	4.553
2	40.957	23.404	8.518	4.035	24.101	7.757	4.695	4.156
4	38.700	20.048	7.558	3.409	22.761	7.380	4.456	3.966
6	37.801	18.688	7.041	3.075	22.246	7.269	4.389	3.933

Table 4.1 Effect of k gain on the average voltage dip for a fault in Dorpen (Zone 1)

The converter affected most from the fault in Dorpen is the one in Emden. Therefore, as was seen from figures 4.3 and 4.4, it generates higher additional reactive current during the fault and thus affects the system voltages the most. The closer a bus to an HVDC converter and especially the one in Emden, which is affected the most, the higher the effect of increased additional reactive current on its voltage. For example the improvement on Conneforde's voltage when k is 4 instead of 2 is 3.356% (23.404%-20.048%) while on Gertruidenberg is 0.19% (4.156%-3.966%).

It has to be made clear that what plays a role is not the geographical distance but the "electrical" distance. The "electrical" distance between two points in a grid is practically the equivalent impedance between these two points. The equivalent impedance depends on the line lengths connecting the two points (and thus their geographical distance) but also on the grid configuration. Nevertheless, geographical distance can usually give a rough approximation of electrical distance.

The voltage profile of buses close to Zone 1 (Diele, Conneforde, Meeden) for k equal to 4 and 6 is not that big because in both cases the converter reaches its current limit during the fault and thus no extra reactive current is given after the limit has been reached. The only difference is that the increase in reactive current is faster in the case of k=6 than for k=4 and this still helps improve slightly the voltage boost.

From figure 4.9 and table 4.1 it can be observed how the distance of a bus from the HVDC converter affects its voltage boost during a fault. Another interesting thing is the influence of the distance of a bus from the fault location on its voltage boost. In order to see this, a fault will be applied in Conneforde and in Diele. The voltage at the buses of Unterwerser and Rhede will be observed in both cases. Unterweser's 380 kV bus is directly connected to Conneforde's bus, while Rhede is directly connected to Diele's bus. The voltages for the aforementioned cases are shown in figure 4.10 and the respective voltage dips in table 4.2.

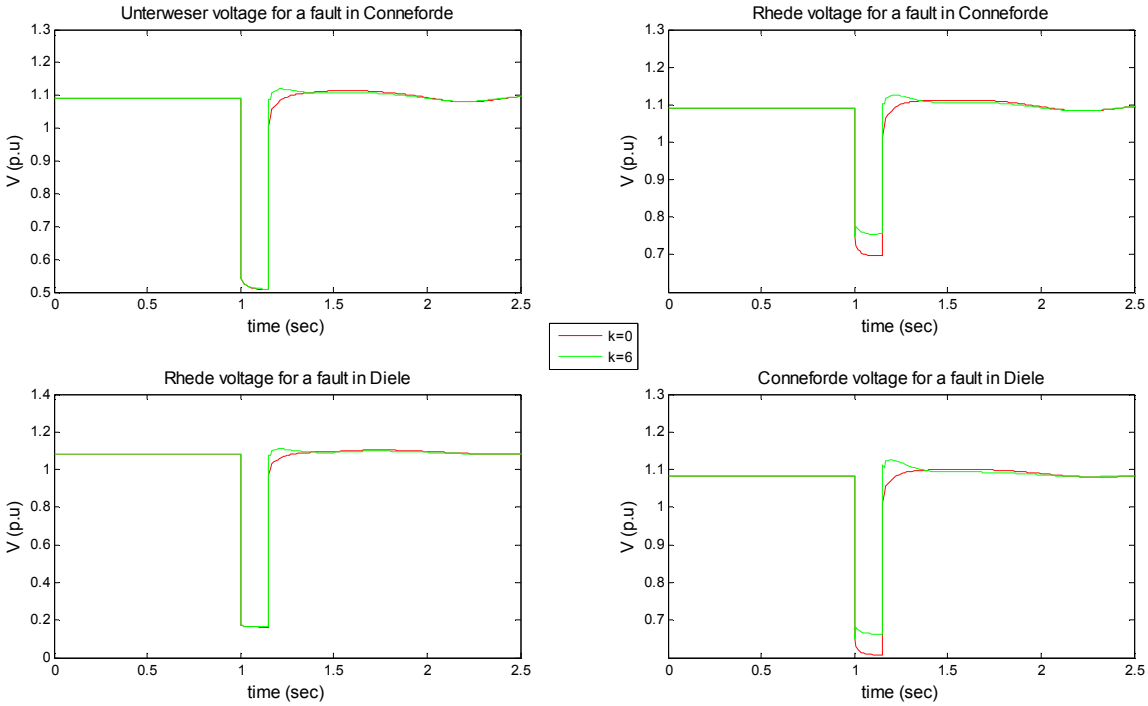

Fig. 4.10 Unterweser and Rhede bus voltages for different fault locations (Conneforde and Diele)

	Fault in Conneforde		Fault in Diele	
k	**Unterweser**	**Rhede**	**Unterweser**	**Rhede**
	ΔV%	**ΔV%**	**ΔV%**	**ΔV%**
0	53.213	35.953	43.695	84.871
6	53.070	30.762	38.587	84.759

Table 4.2 Effect of fault location on the average voltage dip

As can be seen, the effectiveness of the voltage support given by the HVDC converters depends on the bus' distance from the fault. The fault locations, Conneforde and Diele, are located in Zone 1. As explained above Unterweser is located close to Conneforde while Rhede is located close to Diele. When a fault occurs in Conneforde's 380 kV bus, two things can be noticed; first of all, as expected, the voltage dip due to the fault is higher in Unterweser than in Diele and the voltage boost for k=6 on Unterweser is 0.143% (53.213%-53.07%), which is almost unnoticeable. On the other hand, for the same fault location (Conneforde) the voltage boost is 5.191% (35.953%-30.762%) which is much larger than in Unterweser.

When the fault is applied in Diele, the voltage boost in Unterweser and Rhede changes. This time the voltage boost in Unterweser is 5.108% (43.695%-38.587) while in Rhede it's 0.112% (85.871%-84.759%).

From the above results it is clear that the voltage boost at a bus, as a result of the HVDC converter's voltage support during a fault, becomes smaller as the distance of the bus from the fault decreases. The same conclusions have been also drawn in **[14]**, where the effect of wind turbines, on the grid voltage is studied.

Next the effect of the k gain on the system voltages for a fault in Sechtem will be shown. Only the values of the average voltage dips, as defined by equation 4.1, will

be shown in order to save space. The reader can find the respective result plots in the appendix D. Emphasis will be given in the voltages of Zone 2, since this is the area affected most by the fault, and less in Zones 1 and 3. Also some buses in the Netherlands will be shown in order to show the effect of the fault and the HVDC converters there. The selected buses for a fault in Sechtem are Diele from Zone 1, Niederrhein, Neurath and St. Peter from Zone 2, Wiesloch from Zone 3 and finally Meeden, Maasbracht and Krimpen aan den IJssel (KIJ) from the Netherlands.

	Diele (Zone 1)	Niederrhein (Zone 2)	Neurath (Zone 2)	Dulken (Zone 2)	Wiesloch (Zone 3)	Meeden (NL)	Maasbracht (NL)	KIJ (NL)
k	**ΔV%**	**ΔV%**	**ΔV%**	**ΔV%**	**ΔV%**	**ΔV%**	**ΔV%**	**ΔV%**
0	6.240	21.451	49.806	34.022	4.649	6.124	19.268	5.905
2	5.016	17.654	46.294	26.523	4.030	5.156	18.319	5.430
4	3.840	14.963	43.794	21.199	3.514	4.243	17.630	5.034
6	3.473	14.337	43.196	19.939	3.264	3.959	17.465	4.920

Table 4.3 Effect of k gain on the average voltage dip for a fault in Sechtem (Zone 2)

The results from table 4.3 lead to the same observations as the results for a fault in Dorpen. The higher the k gain (higher additional reactive short circuit current) the bigger the improvement of the voltage profiles of the buses. From the voltages of the Dutch buses it is seen that the further the bus from the HVDC converters (and especially Osterath's converters) the smaller the improvement of their voltages due to the voltage support of the converters.

Finally the effect of the k gain on the average voltage dips of the systems buses is shown for the case of a fault in Hopfingen (Zone 3).

	Neurath (Zone 2)	St. Peter (Zone 2)	Wiesloch (Zone 3)	Philippsburg (Zone 3)	Meeden (NL)	Diemen (NL)	Maasbracht (NL)	Geertruidenberg (NL)
k	**ΔV%**	**ΔV%**	**ΔV%**	**ΔV%**	**ΔV%**	**ΔV%**	**ΔV%**	**ΔV%**
0	2.005	1.623	39.900	27.845	0.337	0.274	0.879	0.350
2	1.643	1.403	37.176	23.016	0.258	0.220	0.744	0.290
4	1.227	1.218	34.918	19.035	0.173	0.155	0.618	0.225
6	1.216	1.143	34.302	17.956	0.108	0.094	0.546	0.169

Table 4.4 Effect of k gain on the average voltage dip for a fault in Hopfingen (Zone 3)

Regarding the effect of the HVDC converters on the system voltages for a fault in Hopfingen, no additional analysis is needed. The conclusions that can be drawn are similar to those for the previous two fault locations. It can be seen from the values of table 4.4 that a fault in Zone 3 is bearely noticeable in the Netherlands. Even without voltage support from the converters (k=0) the highest recorded average voltage dip for a bus in the Netherlands is smaller than 1%.

4.3.1.3 Effect of the k gain on the rotor angle response of generators during a fault

Next the effect of the different values of the k gain on the rotor angle responses will be examined. First the case of a three-phase bus fault in Dorpen will be examined. The rotor angles in a selected number of generators in Germany and the Netherlands is monitored. The selected generators are located in Unterweser, Conneforde,

Niederaussem and Neurath in Germany and Eemshaven and Maasbracht in the Netherlands. Unterweser and Conneforde are located in Zone 1, Niederaussem and Neurath are located in Zone 2.

A generator's transient stability and thus its rotor angle response to a fault, depend on many factors. According to **[18]** these factors are the fault location, the fault clearing time, the generator's loading, inertia, reactance and field excitation and the system's voltage magnitude and post-fault reactance.

By examining different values of the HVDC's k gain, the system's voltage magnitude during and after the fault is influenced as was seen in paragraph 4.3.1.2. Additionally the generator loadings are influenced. The influence in the generator's loading can be explained as follows. As was seen in paragraph 4.3.1.1, for k=4 and 6 the HVDC converters reach their current limits. Since the current limitation strategy is set to reactive current priority, only the converter's active current will be reduced once the current limit is reached. The reduction of the HVDC converter active currents concequently leads to the reduction of the power transferred via the HVDC line. One could say that a point-to-point HVDC line embedded in an AC system is perceived by the system as a load in the area of the sending converter of the HVDC line and as a generator in the area of the receiving converter. Therefore when active current reduction takes place, the generation-load balance will be lost in the areas near the sending and receiving HVDC converters. As a result of this generators in the area of the sending converter will accelerate, due to the decrease of the HVDC's power consumption, while generators in the area of the receiving end will decelerate, due to the decrease of the HVDC's power injection. Therefore when the over-current limit is reached, the rotor speed of the generators is simultaneously influenced by the fault and by the active current reduction. This behavior can be seen in figure 4.11.

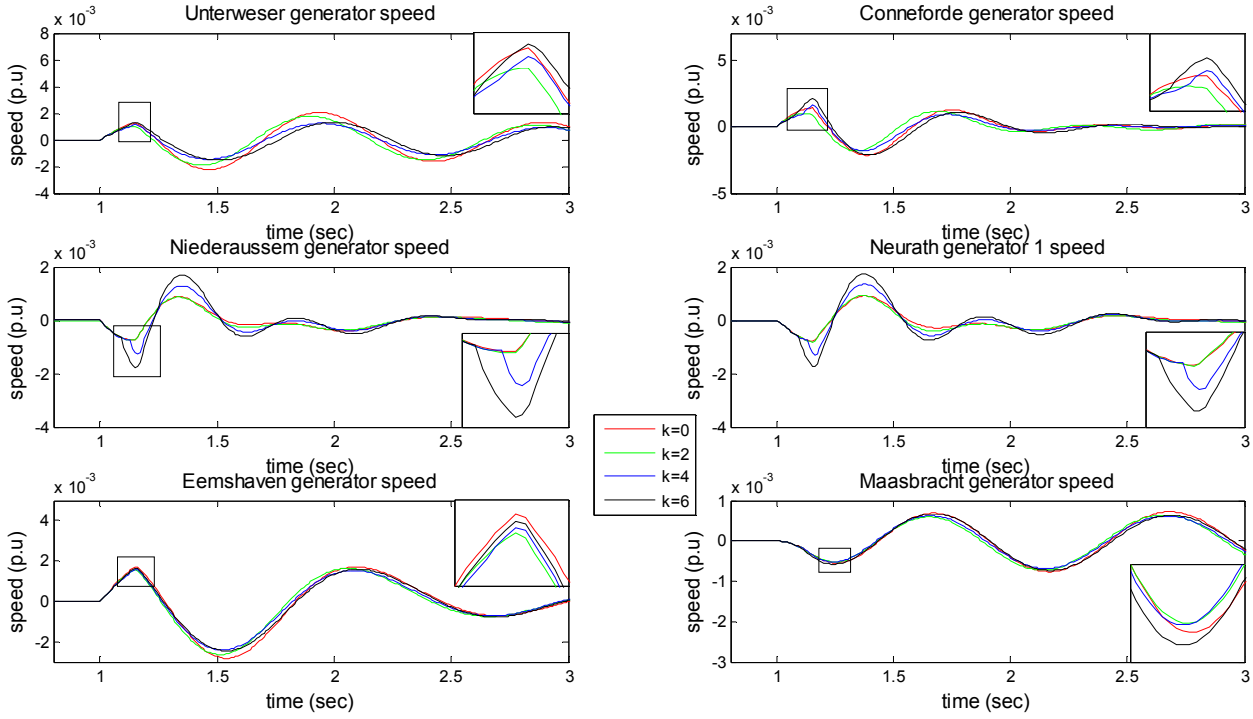

Fig. 4.11 Effect of k gain on generator rotor speeds for a fault in Dorpen (Zone 1)

This thesis focuses on the first swing rotor angle stability, therefore the first peak of the rotor speed oscillation is of interest. As can be seen from figure 4.11 the active current induced acceleration in Zone 1 (sending end) results in a higher peak in Zone 1's generators (Unterweser and Conneforde). This happens because additionally to the initial acceleration of the generators as a response to the fault, the active current reduction in the sending converter acts simultaneously as an accelerating factor and further increases the generator's speed. Similarly the first peak of Zone 2's generators (Niederaussem and Neurath) is higher since the active current reduction-induced deceleration in the receiving end in Zone 2 acts and decreases further the generator speeds which were already decreasing as a response to the fault. The selected generators in the Netherlands are located near Eemshaven and Maasbracht. Eemshaven is located relatively close to Emden's HVDC converter thus it will be affected to some point by the active current reduction. Indeed it can be seen that the first peak of its rotor speed is higher for k=4 and 6 (active current reduction) than for k=2 (no active current reduction). Maasbracht on the other hand is located relatively close to Osterath's converter. A reduction of active current will thus lead to a further deceleration of the generator leading to higher speed peaks for k=4 and 6 than for k=2.

By observing both the rotor angles and speeds of the generators it can be seen that higher speed peaks, or sudden increases in the speed, usually lead to a higher first rotor angle peak.

From the above it is clear that the HVDC converters influence the rotor angles of generators via two factors. First, by affecting the system voltages and secondly by reducing the power transfer when the converter current limits are reached. Higher values of the k gain lead to higher voltages during the fault and a generally improved post-fault voltage profile. The improved voltage profile is beneficiary for the rotor angles since the closer the voltage is kept to the pre-fault voltage the smaller the disturbance as perceived in the generator terminals and concequently the smaller the rotor angle oscillation. The amount by which each factor affects the rotor angle response of the generators depends on many things such as the electrical distance of the generator from the fault location and the HVDC converters, the nature of the HVDC converter (sending or receiving) etc. Howerer it should be expected that the closer a generator to an HVDC converter, the higher the impact active current reduction will have on its rotor angle.

Figure 4.12 shows the rotor angles of the selected generators for various values of the k gain.

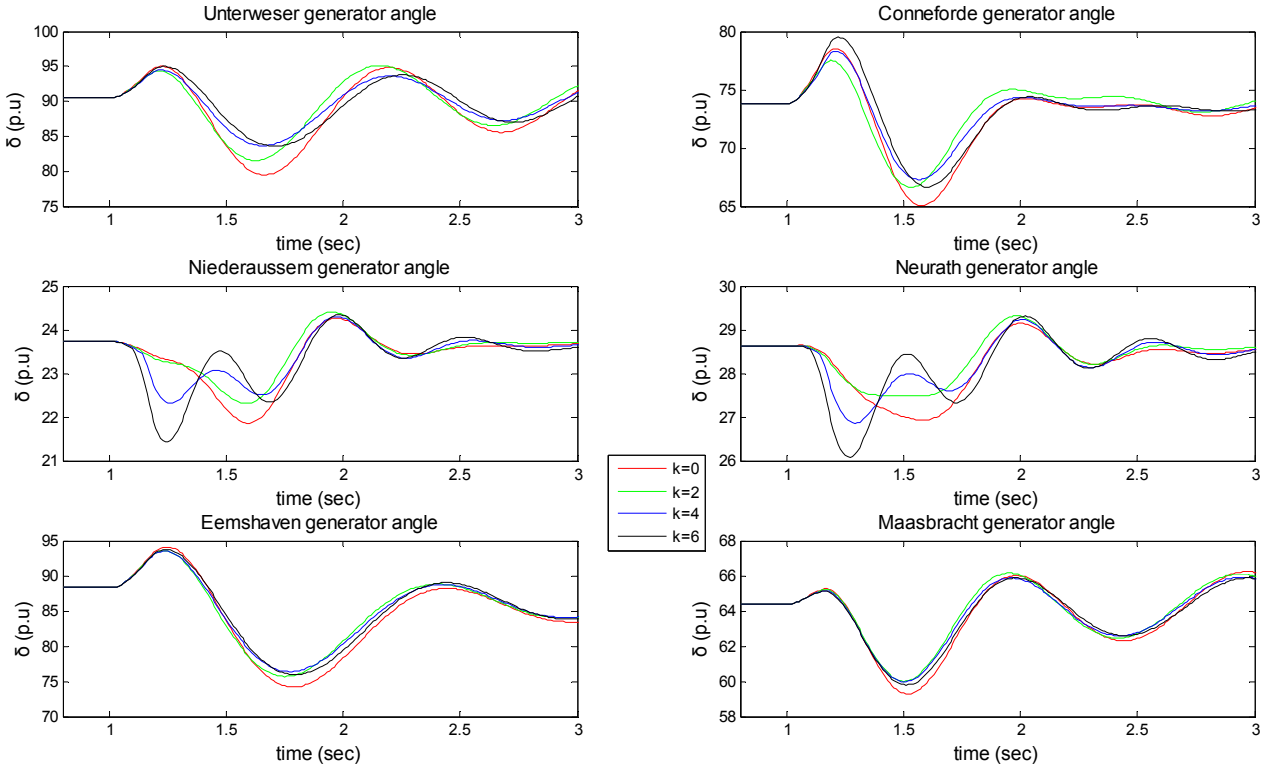

Fig. 4.12 Effect of k gain on generator rotor angles for a fault in Dorpen (Zone 1)

As can be seen from figure 4.12, once again the effect of the k gain is more visible in generators located close to Emden's and Osterath's converter stations, i.e Unterweser Conneforde, Niederaussem and Neurath. In the rest of the generators the effect is smaller. The effect of the k gain on the first peak of the rotor angles can be observed by the values of table 4.5 which provides the rotor angle deviation for the first peak of the angle's oscillation, which was defined in paragraph 3.3.1.3 by equation 3.2.

The definition is repeated below:

$$\Delta\delta_{\max\%} = \frac{|\delta_{prefault} - \delta_{peak}|}{\delta_{prefault}} 100\% \qquad (4.2)$$

where, $\delta_{prefault}$ is the generator's rotor angle before the fault occurs and δ_{peak} is the peak value of the rotor angle's first oscillation after the fault occurs. As explained earlier this thesis focuses on the first swing rotor angle stability and therefore only the first peak of the rotor angles are observed.

	Unterweser (Zone 1)	Conneforde (Zone 1)	Niederaussem (Zone 2)	Neurath (Zone 2)	Eemshaven (Zone 1/NL)	Maasbracht (Zone 2/NL)
k	$\Delta\delta_{max\%}$	$\Delta\delta_{max\%}$	$\Delta\delta_{max\%}$	$\Delta\delta_{max\%}$	$\Delta\delta_{max\%}$	$\Delta\delta_{max\%}$
0	4.940	6.396	7.875	5.902	6.560	1.370
2	4.230	4.993	5.996	3.990	5.944	1.317
4	4.381	6.069	5.923	6.133	5.888	1.217
6	4.933	7.676	9.648	8.851	6.163	1.172

Table 4.5 Effect of k gain on the maximum rotor angle deviation for a fault in Dorpen (Zone 1)

As seen from table 4.5, the first peak of the rotor angle oscillations doesn't necessarily decrease for higher values of k. On one hand, the higher value of the k gain will improve the bus voltages after the fault occurs and this, as mentioned above, should lead to smaller rotor angle oscillations. Indeed for k=2 the first rotor angle peak is smaller than when no short-circuit reactive current support is provided by the HVDC converters (k=0). However for values of k higher than 2 the first rotor angle peak isn't always smaller and the reason for this is the active current reduction. When the k gain is equal to 4 or 6 the HVDC converter in Emden will reach its current limit leading it to reduce its active current. This, as seen in figure 4.11, will lead to higher rotor speeds in all the selected generators. The values of table 4.5 show that the higher first peak of the rotor speed for k=4 and 6 leads also to a higher first peak of the rotor angles in Zone 1 compared to the case where k=2. In Zone 2 the first peak of the rotor angles is higher for k=6 but not for k=4. However by observing figure 4.12 it can be seen that the form of the rotor angle oscillations for k=4 and 6 is quite different than for k=0 and 2. Therefore, the comparison of the first peaks of the rotor angle oscillations in Zone 2 does not lead to clear conclusions. Nevertheless, figure 4.12 shows that the rotor angle oscillations in Zone 2 seem to intensify for k=4 and 6 (from 1-2 sec which is the time period where the first rotor angle swing appears), where active current reduction takes place.

From figure 4.11 it is seen that the first peaks of the rotor speeds of generators in Eemshaven and Maasbracht increase when active current reduction takes place. The increase however is small because the electrical distance between Eemshaven and Emden and between Maasbracht and Osterath is larger than for example between Emden and Conneforde or Osterath and Niederaussem. As seen from table 4.5, the higher rotor speed does not result always in higher rotor angle peaks for Eemshaven and Maasbracht. This happens probably because the effect of active current reduction in these generators in the Netherlands is smaller than the beneficiary effect of the improved voltage profile for higher k gains.

Next the effect of a fault in Sechtem (Zone 2) on the rotor angle stability of generators will be examined. The selected generators are Unterweser and Conneforde from Zone 1, Niederaussem and Neurath from Zone 2 and KKP (Philippsburg) and Neurott from Zone 3. Two generators are selected from the Netherlands and are located in Eemshaven and Maasbracht. The rotor angle plots can be seen in figure 4.13.

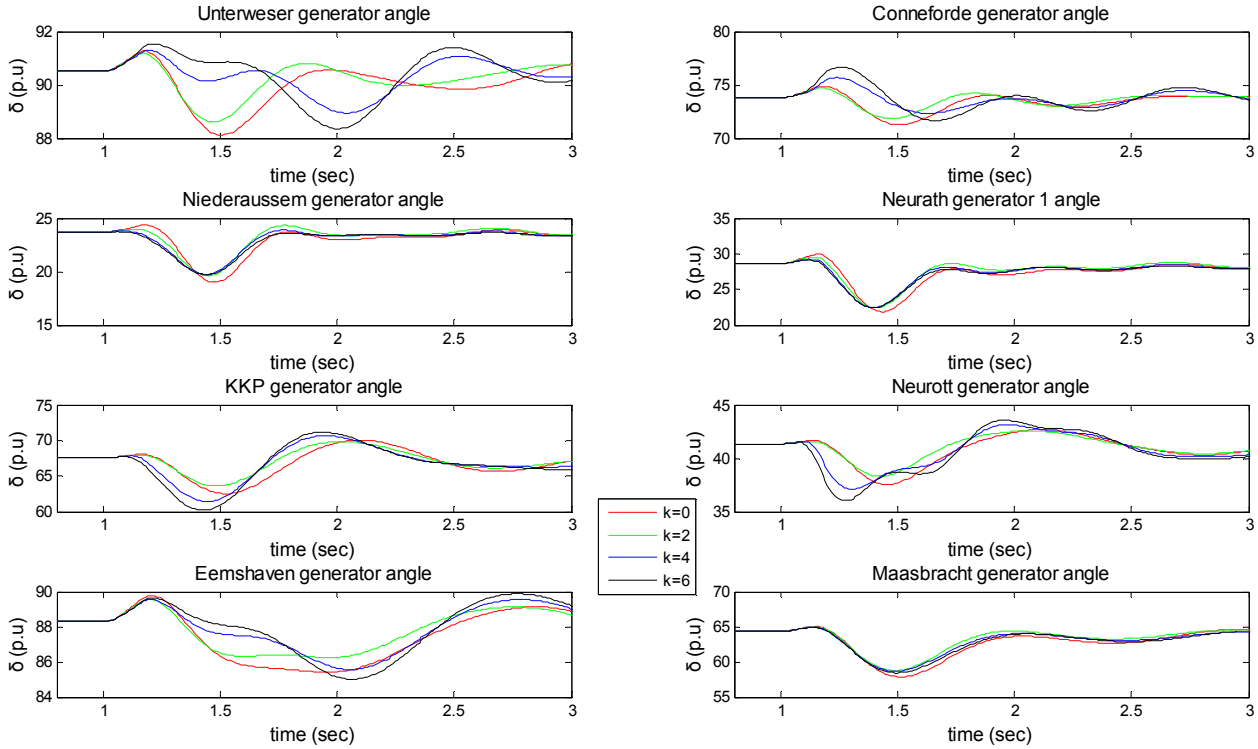

Fig. 4.13 Effect of k gain on generator rotor angles for a fault in Sechtem (Zone 2)

The rotor angle deviations of the first peak of the selected generators for different values of the k gain are shown in table 4.6.

	Unterweser (Zone 1)	**Conneforde (Zone 1)**	**Niederaussem (Zone 2)**	**Neurath (Zone 2)**	**KKP (Zone 3)**	**Neurott (Zone 3)**	**Eemshaven (Zone 1/NL)**	**Maasbracht (Zone 2/NL)**
k	$\Delta\delta_{max\%}$	$\Delta\delta_{max\%}$	$\Delta\delta_{max\%}$	$\Delta\delta_{max\%}$	$\Delta\delta_{max\%}$	$\Delta\delta_{max\%}$	$\Delta\delta_{max\%}$	$\Delta\delta_{max\%}$
0	0.842	1.434	2.662	4.847	0.834	0.646	1.675	0.964
2	0.745	1.196	0.907	3.111	0.716	0.521	1.443	0.890
4	0.876	2.535	0.232	2.089	0.529	0.398	1.416	0.809
6	1.136	3.869	0.096	1.678	0.364	0.324	1.510	0.744

Table 4.6 Effect of k gain on the maximum rotor angle deviation for a fault in Sechtem (Zone 2)

Once again it can be seen that the for k=2, the first rotor angle peak is smaller than for k=0, while for higher values of k that cause the converter to reach its current limit the rotor angle peak is not always smaller.

In order to explain the behavior of the rotor angle peaks the rotor speeds are presented in figure 4.14.

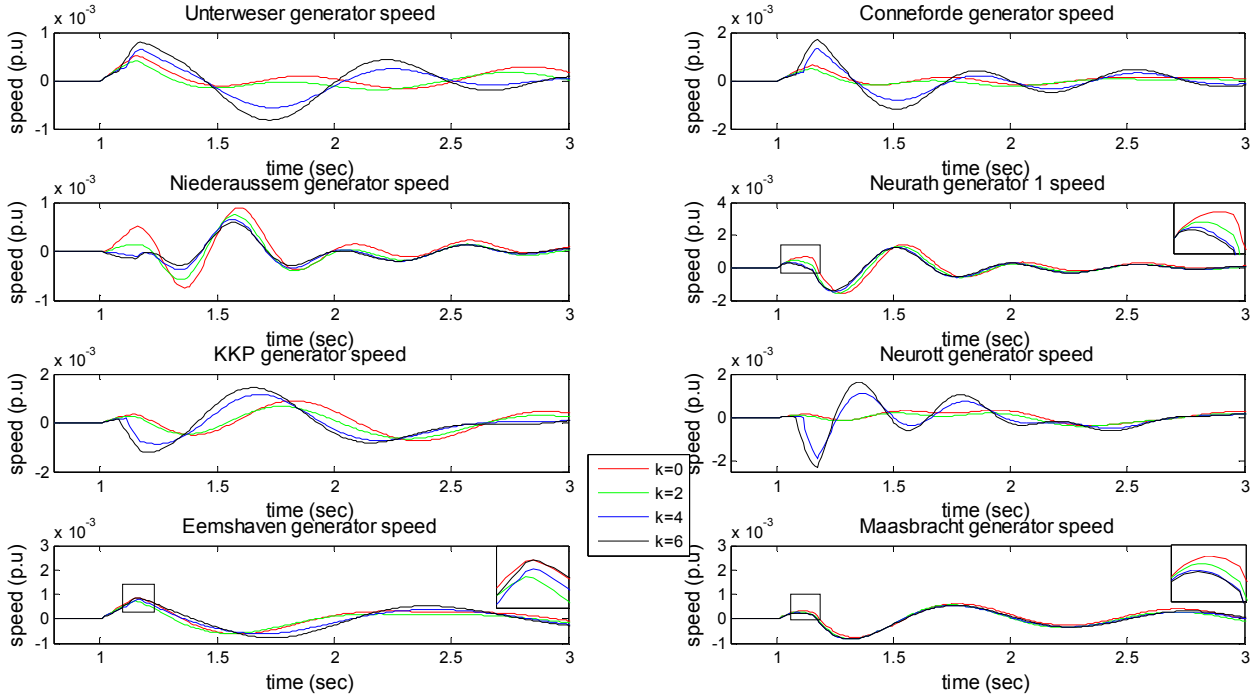

Fig. 4.14 Effect of k gain on generator rotor speeds for a fault in Sechtem (Zone 2)

As is seen from figure 4.14, the generators in Zone 1 (Unterwesser, Conneforde) will accelerate due to the active current reduction leading to a higher first peak of the rotor speed. Therefore a higher first peak will also appear in the rotor angle oscillations of the aforementioned generators. In Zone 3, the active current reduction leads to deceleration since Zone 3 is the receiving end of Corridor A. This decelerating factor acts simultaneously with the accelerating effect the fault has on the generators in Zone 3. These two opposing factors lead to a smaller first peak of the rotor angle for generators in Zone 3. In Zone 2 the situation is more complex. Zone 2 is both a sending and receiving area. It receives power from the Corridor A's EMD-OST section and sends power to Zone 3 via the OST-PHLP section. As was seen in paragraph 4.3.1.1, for k=4 and 6, both converters in Zone 2 will reach their current limits. Therefore active current reduction will take place in both converters and the power transfer of both sections of Corridor A will decrease by the same amount. No significant acceleration or deceleration due to the power transfer reduction in both sections of Corridor A will occur since there is a simultaneous and equal reduction of power injected in Zone 2 by the EMD-OST section and power absorbed from Zone 2 by the OST-PHLP section. The smaller first peak of the rotor speeds for k=4 and 6, seen in figure 4.14, is due to the improved voltage profile thanks to the higher amount of short circuit reactive current provided by a higher value of the k gain. The smaller peak in the rotor speed will result also in a smaller first peak in the rotor angles of the Zone 2 generators.

Regarding the generators in the Netherlands it can be seen that in Eemshaven, which is located close to Zone 1, for k=6 the reduction of active power leads to higher rotor angle deviation just as in Unterweser and Conneforde. However for k=4 the rotor angle stability is improved compared to the case for k=2. This is probably

because for k=4 the active power reduction lasts less and therefore will affect less the rotor angle than the voltage profile improvement.

In Maasbracht, which is located closer to Zone 2, the rotor angle stability improves for higher k gains just as in Niederaussem and Neurath due to the improved voltage offered by the higher k gain.

Finally for the fault in Hopfingen, the rotor angles of selected generators are presented in figure 4.15. The selected generators are Niederaussem and Neurath from Zone 2, KKP and Neurott from Zone 3 and Eemshaven and Maasbracht from the Netherlands.

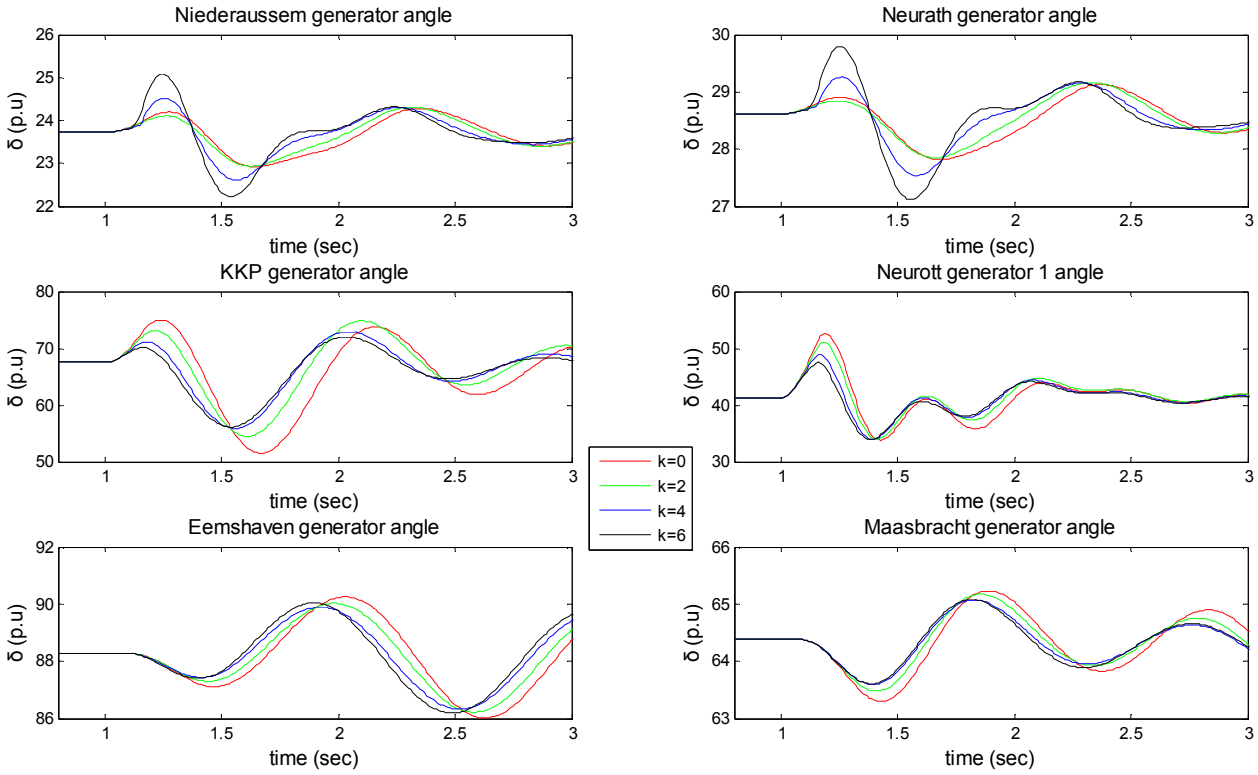

Fig. 4.15 Effect of k gain on generator rotor angles for a fault in Hopfingen (Zone 3)

To make the effect of the HVDC converters clearer, the first peak rotor angle deviations of the aforementioned generators are shown in table 4.7.

	Niederaussem (Zone 2)	**Neurath (Zone 2)**	**KKP (Zone 3)**	**Neurott (Zone 3)**	**Eemshaven (Zone 1/NL)**	**Maasbracht (Zone 2/NL)**
k	$\Delta\delta_{max\%}$	$\Delta\delta_{max\%}$	$\Delta\delta_{max\%}$	$\Delta\delta_{max\%}$	$\Delta\delta_{max\%}$	$\Delta\delta_{max\%}$
0	1.971	1.021	11.061	27.026	1.344	1.681
2	1.596	0.812	8.250	23.409	1.125	1.412
4	3.354	2.247	5.334	18.348	0.975	1.231
6	5.687	4.122	3.940	14.850	1.007	1.212

Table 4.7 Effect of k gain on the maximum rotor angle deviation for a fault in Hopfingen (Zone 3)

Again for k=2, where the Philippsburg's converter doesn't reach its current limit, the rotor angle stability of the generators is improved. For k=4 and 6, when the

current limit is reached, the rotor angle peaks decrease for Zone 3 while they increase in Zone 2.

Figure 4.16 shows the rotor speeds of the generators.

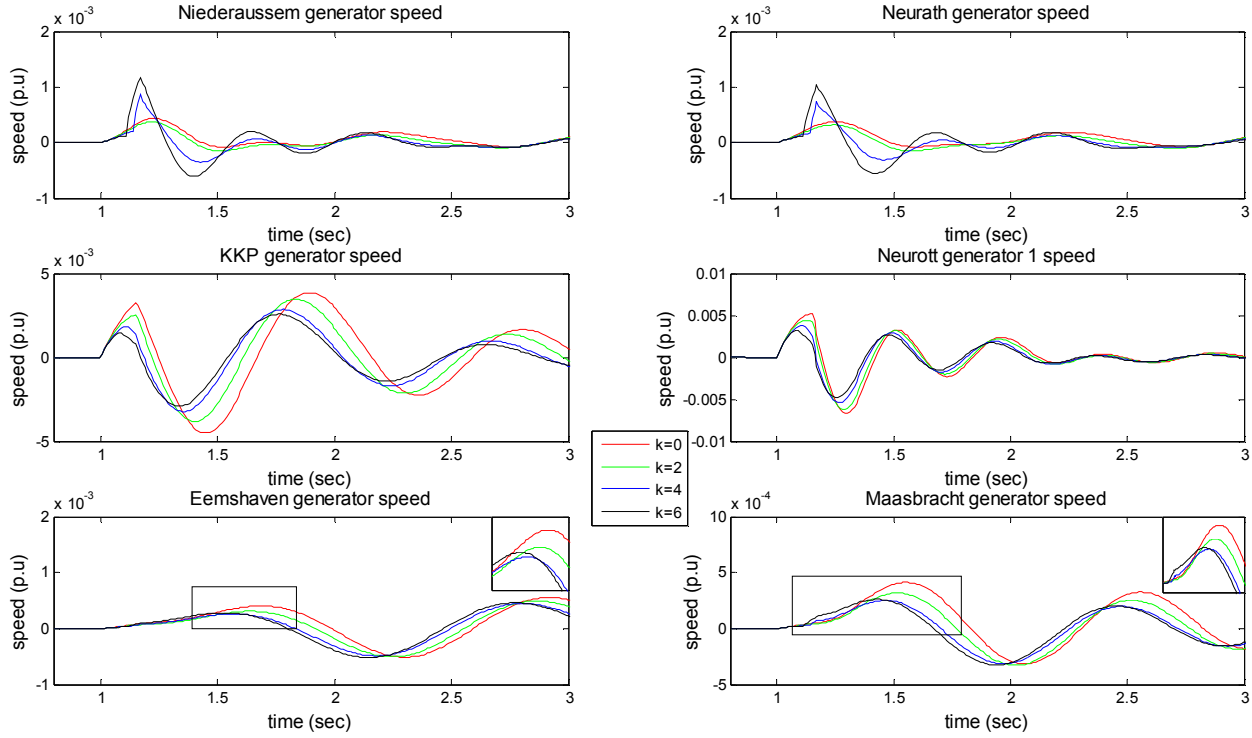

Fig. 4.16 Effect of k gain on generator rotor angles for a fault in Hopfingen (Zone 3)

From figure 4.16 it is seen that a fault in Hopfingen results in the initial acceleration of generators in Zone 2 (Niederaussem and Neurath) as well as of those in Zone 3 (KKP, Neurott). On the other hand, as has already been explained, the reduction of active power transfer in OST-PHLP section will lead to an acceleration of Zone 2 generators and a deceleration of Zone 3 generators. Therefore the rotor speed peak of generators in Zone 2 will increase for k=4 and 6 and for generators in Zone 3 it will decrease. Therefore the increased k gain, which leads to an active power reduction in the OST-PHLP section increases the rotor angle peak in Niederaussem and Neurath (Zone 2) and decreases in KKP and Neurott (Zone 3).

Finally looking at the generators in the Netherlands (Eemshaven and Maasbracht) it seems that they are located quite far from the OST-PHLP section and the rotor angle behavior of their generators is affected mainly by the improvement of the voltage profile thanks to the higher k gains. Therefore their rotor angle stability improves with higher k gains.

Having examined different fault locations and values of the k gain it can be concluded that the response of the rotor angles is influenced by the voltage support the HVDC converters offer to the system and by the active current output of the converters. The active current output plays a more significant role in the rotor angle responses for generators located very close to the converters, while the system voltages become the dominant influencing factor for generators located farther from the converters. Active current reduction can improve or deteriorate the rotor angle stability of generators depending on their location from the fault and the HVDC converters. What is usually seen is that the rotor angle peaks of generators located

electrically close to the sending end of the HVDC line increase for active current reduction. On the other hand, the rotor angle peaks of generators located close to a receiving HVDC converter usually decrease (the only exception is generators in Zone 2 for a fault in Dorpen). For generators that are not located in the vicinity of the converters but not that close (e.g the generators in Eemshaven and Maasbracht) there is not a clear pattern followed by the rotor angle responses because the effect of active current reduction of an HVDC converter is smaller in those generators. Thus the voltage improvement due to a high value of the k gain can become more influencing in those cases.

Nevertheless, what was clearly observed is that as long as no active current reduction takes place in the HVDC converters, a higher value of the k gain always leads to a lower first rotor angle peak which is an indicator of improved first swing rotor angle stability.

4.3.2 The effect of the HVDC converter over-current capability on the AC system for faults in Germany

It was seen in paragraph 3.3.2 that the HVDC voltage-source converters have a current limit which can be reached during a transient situation such as a fault. This current limit cannot be surpassed due to the sensitivity to high currents, solid state switches that the converter comprises. The converter's total current can be maintained within this limit through various methods such as the converter's phase reactor and the current limiting strategies. The over-current capability can affect the response of the converter and thus its effect on the AC grid because it determines the amount of reactive short circuit current injection by the converter during voltage support in the case of a fault.

The examined values of the converter's over-current capability are 1.15 and 1.3 in per unit of the converter's nominal current. The other sensitivity parameters remain unchanged. The k gain is set to be equal to 6, in order to ensure that the converter reaches its current limit during the fault and the current limitation strategy is set to reactive current priority. The fault locations that are examined are the same as shown in figure 4.2.

In the result analysis that follows most of the plots will not be shown in order to save space. The plots can be found in the appendix D.

4.3.2.1 Response of Corridor A's HVDC converters for different current capabilities

The analysis of the results will start for the case of a fault in Dorpen. The fault is located in Zone 1 therefore Corridor A's section that will be affected the most is the EMD-OST section. The responses of Emden's and Osterath's converters for a fault in Dorpen for different current capabilities are shown in figures 4.17 and 4.18 respectively.

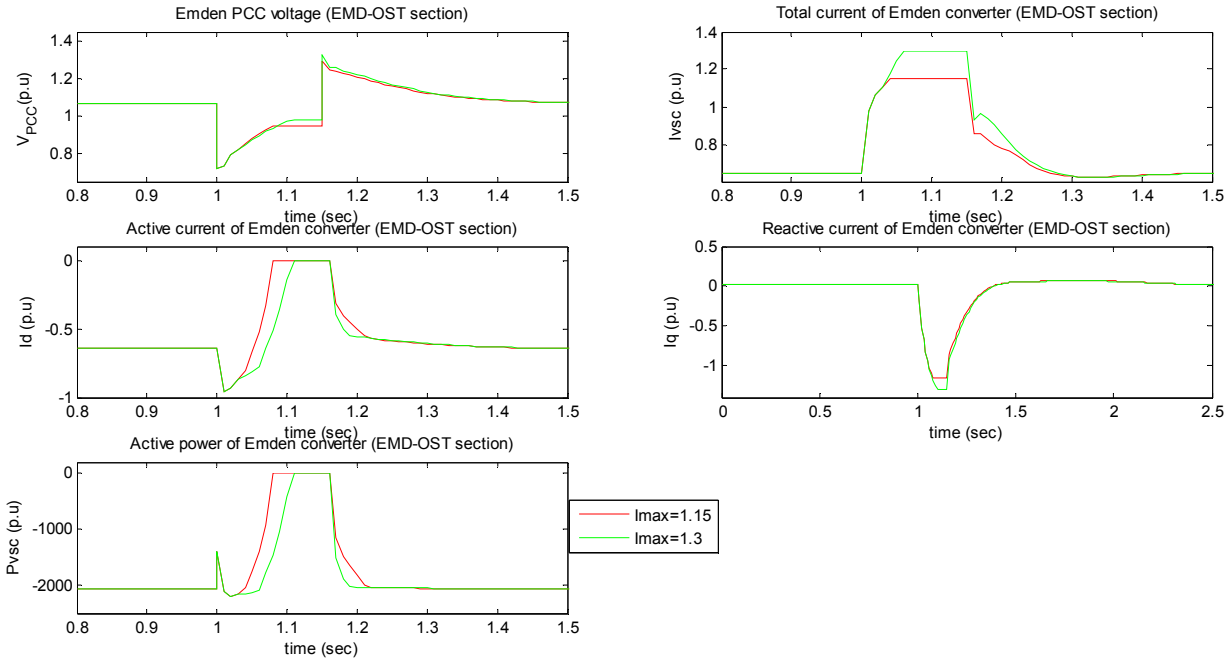

Fig. 4.17 Response of Emden's converter (EMD-OST section) to a 3-phase bus fault in Dorpen (Zone 1) for different current capabilities

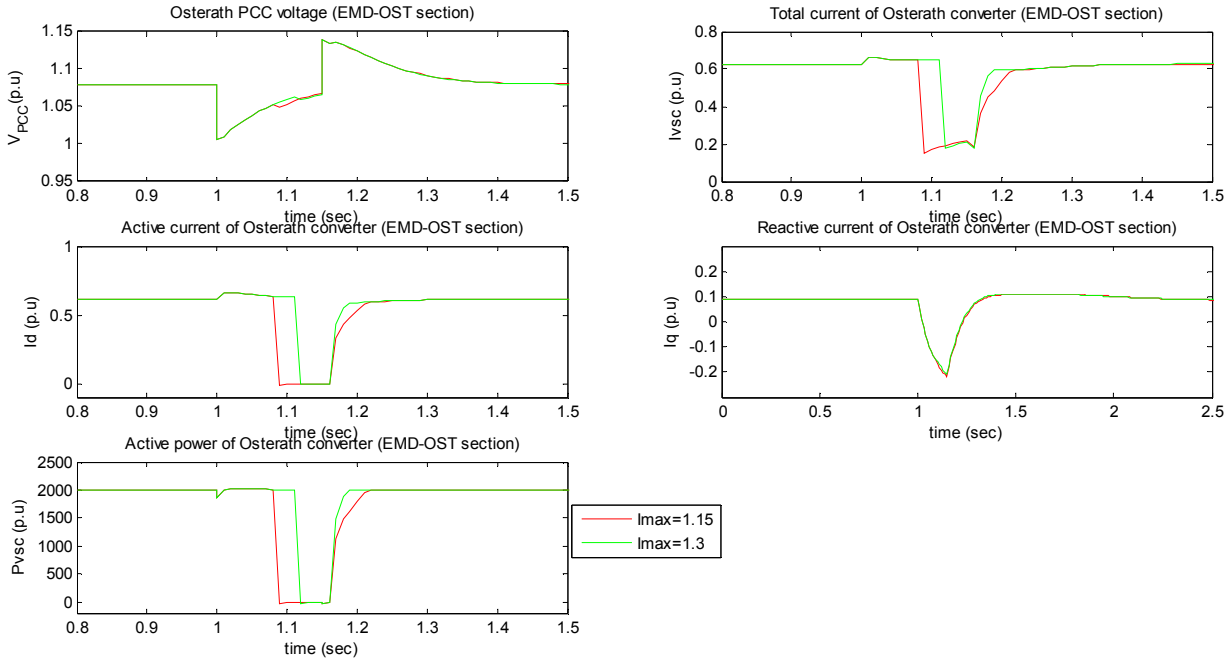

Fig. 4.18 Response of Osterath's converter (EMD-OST section) to a 3-phase bus fault in Dorpen (Zone 1) for different current capabilities

As can be seen from figures 4.17 and 4.18 the increased over-current capability of the converters allows them to provide a greater amount of additional reactive current during the fault and this improves the voltage profile in Emden's filter bus. Osterath's voltage profile on the other hand is almost unaffected by the change because the fault is located far from Osterath and therefore its converter doesn't reach its current limit. It can be seen from figure 4.18 that the reactive current of Osterath's converter is practically the same for both cases of I_{max}. However, there is a small difference in Osterath's filter bus voltage for the two values of I_{max}. As was mentioned in paragraph

4.3.1, when the active current is reduced in one end of the HVDC line, the active current must be reduced in the other end as well in order to maintain the DC voltage. The same happens in this case. However due to the HVDC model's weakness the active power reduction of the non-limit-reaching converter takes place only if the limit-reaching converter's active power is finally reduced to zero (i.e when its reactive current reaches the current limit). Due to this sudden active current change in the non-limit-reaching converter a sudden voltage drop (or boost) occurs in that converter's side. Since the simulations are run for different current limits, Emden's converter will reach its limit sooner for I_{max}=1.15 p.u than for I_{max}=1.3 p.u and this will cause the sudden voltage drop in Osterath's side to take place in different time instances as well, leading to the differences seen in Osterath's filter bus voltage.

Regarding the other faults in Sechtem (Zone 2) and Hopfingen (Zone 3) the response of the converters is similar as in the fault in Dorpen. Therefore no further analysis will be done for them. The only difference is which converter reaches its limit for each fault location. Each time, the converter located closer to the fault is the one that reaches its current limit. Therefore when the fault is applied in Sechtem, Osterath's HVDC converters reach their current limit while when the fault is applied in Hopfingen, the converter in Philippsburg reaches its current limit. The response of the converters can be found in appendix D.

4.3.2.2 Effect of the over-current capability on the AC system's bus voltages

Next the effect of the different current capabilities on the system voltages is presented. Only the voltages in buses inside and near the zone where the fault occurs will be shown. So if for example a fault occurs in Zone 1 only voltages of buses near Zone 1 will be shown. There is no point in examining the voltages in other zones where the respective converters do not reach their current limit.

The average voltage dip in the monitored buses for a fault in Dorpen can be seen in table 4.8.

	Emden	**Conneforde**	**Unterweser**	**Diele**	**Meeden**	**Eemshaven**
$\mathbf{I_{max}}$	**ΔV%**	**ΔV%**	**ΔV%**	**ΔV%**	**ΔV%**	**ΔV%**
1.15	18.622	18.000	10.782	37.367	22.045	16.547
1.3	17.965	17.684	10.643	37.085	21.882	16.436

Table 4.8 Effect of over-current capability on the average voltage dip for a fault in Dorpen (Zone 1)

As can be seen from table 4.8, the higher over-current capability helps improve the voltage profile of the buses, since it gives more room for the reactive current to increase and thus support more the system voltages during the fault. The benefit however is small even for buses located close to Emden's converter (which is the one reaching its current limit for this fault location). Regarding the buses in Meeden and Eemshaven it can be seen that their voltage improvement is even smaller than in Emden. It can be concluded that the voltage improvement for the rest of the buses in the Netherlands, which are located even farther from Emden, will be unnoticeable.

The average voltage dips for the faults in Sechtem and Hopfingen can be seen in tables 4.9 and 4.10 respectively.

	Dulken	Rommerskirchen	Niederrhein	Neurath	St.Peter	Oberzier
I_{max}	ΔV%	ΔV%	ΔV%	ΔV%	ΔV%	ΔV%
1.15	19.938	48.983	14.337	43.197	30.545	28.576
1.3	19.011	48.470	13.862	42.763	30.370	28.333

Table 4.9 Effect of over-current capability on the average voltage dip for a fault in Sechtem (Zone 2)

	Daxlanden	Neurott	Philippsburg	Huffenhardt	Wiesloch	Pulverdingen
I_{max}	ΔV%	ΔV%	ΔV%	ΔV%	ΔV%	ΔV%
1.15	10.710	34.065	17.363	45.038	34.003	21.826
1.3	10.412	33.725	16.748	44.835	33.665	21.531

Table 4.10 Effect of over-current capability on the average voltage dip for a fault in Hopfingen (Zone 3)

Once again it can be noticed that the difference in voltage dips for I_{max}=1.15 p.u and for 1.3 p.u is not that big.

A conclusion that can be drawn is that the improvement of the voltage profile in the system's buses is small even for the buses located close to the HVDC converters. A higher over-current capability than 1.3 p.u could increase slightly the impact on the system's voltage but not by a great amount.

4.3.2.3 Effect of the over-current capability on the rotor angle response of generators during a fault

Finally the effect of different current capabilities on the rotor angles of the system's generators is shown. Tables 4.11, 4.12 and 4.13 show the maximum rotor angle deviation of the first peak of selected generators in Germany and the Netherlands.

	Unterweser (Zone 1)	Conneforde (Zone 1)	Niederaussem (Zone 2)	Neurath (Zone 2)	Eemshaven (NL/Zone 1)	Maasbracht (NL/Zone 2)
I_{max}	$\Delta\delta_{max\%}$	$\Delta\delta_{max\%}$	$\Delta\delta_{max\%}$	$\Delta\delta_{max\%}$	$\Delta\delta_{max\%}$	$\Delta\delta_{max\%}$
1.15	4.932	7.676	9.648	8.851	6.163	1.172
1.3	4.304	6.079	6.716	6.575	5.800	1.192

Table 4.11 Effect of over-current capability on the maximum rotor angle deviation for a fault in Dorpen (Zone 1)

As can be seen the higher over-current capability in the case of a fault in Dorpen improves the rotor angle behavior of all the monitored generators except for the one near Maasbracht. As was seen and explained, in paragraph 4.3.1.3, the rotor angle oscillation peak decreased for the generator near Maasbracht when active current reduction took place. By increasing the over-current capability of the converter the time the converter reaches this new higher limit will be delayed and thus the time period the active current reduction lasts will become smaller (active current returns to its pre-fault value after the fault is cleared). Therefore the beneficiary effect active current reduction has on Maasbracht's generator will decrease. On the contrary, for generators in Zones 1 and 2 it was seen that their rotor angle behavior deteriorated by

active current decrease. Consequently the increase of the converters' over-current capability, and therefore the smaller time period of active current reduction, will have a beneficiary effect on the rotor angle stability of those generators.

	Unterweser (Zone 1)	Conneforde (Zone 1)	Niederaussem (Zone 2)	Neurath (Zone 2)	KKP (Zone 3)	Neurott (Zone 3)	Eemshaven (NL/Zone 1)	Maasbracht (NL/Zone 2)
I_{max}	$\Delta\delta_{max\%}$	$\Delta\delta_{max\%}$	$\Delta\delta_{max\%}$	$\Delta\delta_{max\%}$	$\Delta\delta_{max\%}$	$\Delta\delta_{max\%}$	$\Delta\delta_{max\%}$	$\Delta\delta_{max\%}$
1.15	1.136	3.868	0.096	1.677	0.364	0.324	1.510	0.744
1.3	0.928	2.860	0.088	1.639	0.456	0.337	1.392	0.776

Table 4.12 Effect of over-current capability on the maximum rotor angle deviation for a fault in Sechtem (Zone 2)

	Niederaussem (Zone 2)	Neurath (Zone 2)	KKP (Zone 3)	Neurott (Zone 3)	Eemshaven (NL/Zone 1)	Maasbracht (NL/Zone 2)
I_{max}	$\Delta\delta_{max\%}$	$\Delta\delta_{max\%}$	$\Delta\delta_{max\%}$	$\Delta\delta_{max\%}$	$\Delta\delta_{max\%}$	$\Delta\delta_{max\%}$
1.15	5.687	4.122	3.940	14.850	1.007	1.212
1.3	3.951	2.740	4.601	16.675	0.954	1.193

Table 4.13 Effect of over-current capability on the maximum rotor angle deviation for a fault in Hopfingen (Zone 3)

The same pattern can be seen on the other fault cases shown in tables 4.12 and 4.13. For the generators that were benefited by the active current decrease, the increase of the over-current capability leads to higher rotor angle peaks. On the other hand for generators, the rotor angle response of which deteriorated by the active current decrease, the increase of the current limit has beneficiary effects on the rotor angle oscillations.

For generators located far from the fault location (e.g Eemshaven and Maasbracht for a fault in Hopfingen) or which aren't affected by the active current reduction such as Niederaussem and Neurath for a fault in Sechtem (the active current reduction takes place in both sections and its effects in Zone 2 counteract each other) the higher over-current capability will decrease the first rotor angle peak due to the improved voltage profile that the higher current limit offers.

Having examined all the fault locations it can be concluded that a higher over-current capability can improve or deteriorate the rotor angle response depending on whether the current limit reaching and thus the active current reduction benefits the rotor angle response of a generator or not. Coincidentally it is seen that in most cases the rotor angle response is improved. The results suggest that a high current limit would be beneficiary since the time period the active current reduction lasts will decrease or even become zero, therefore reducing the possible negative effects it can have on the first peaks of the rotor angles.

4.3.3 The effect of the HVDC converter's current limitation strategy (CLS) on the AC system for faults in Germany

As mentioned in paragraph 3.3.3, the current limitation strategy (CLS) is one of the methods an HVDC converter uses in order to keep its total current output below the

current limit. The CLS is practically a series of switching actions the converter performs in order to reduce the total current output. The CLSs examined in this thesis have been introduced and explained in paragraph 3.3.3 and are the active current priority, the equal current priority and the reactive current priority.

The k gain is set equal to 6 in order to ensure that the HVDC converters reach their current limit which is set to 1.15 p.u.

The examined fault locations are the same as in paragraphs 4.3.1 and 4.3.2. The effect of the CLSs on the system's voltages and the rotor angles of the generators are observed.

4.3.3.1 Response of Corridor A's HVDC converters to faults for different current limitation strategies

The response of Emden's converter, located in the same area as the fault, is presented in figure 4.19.

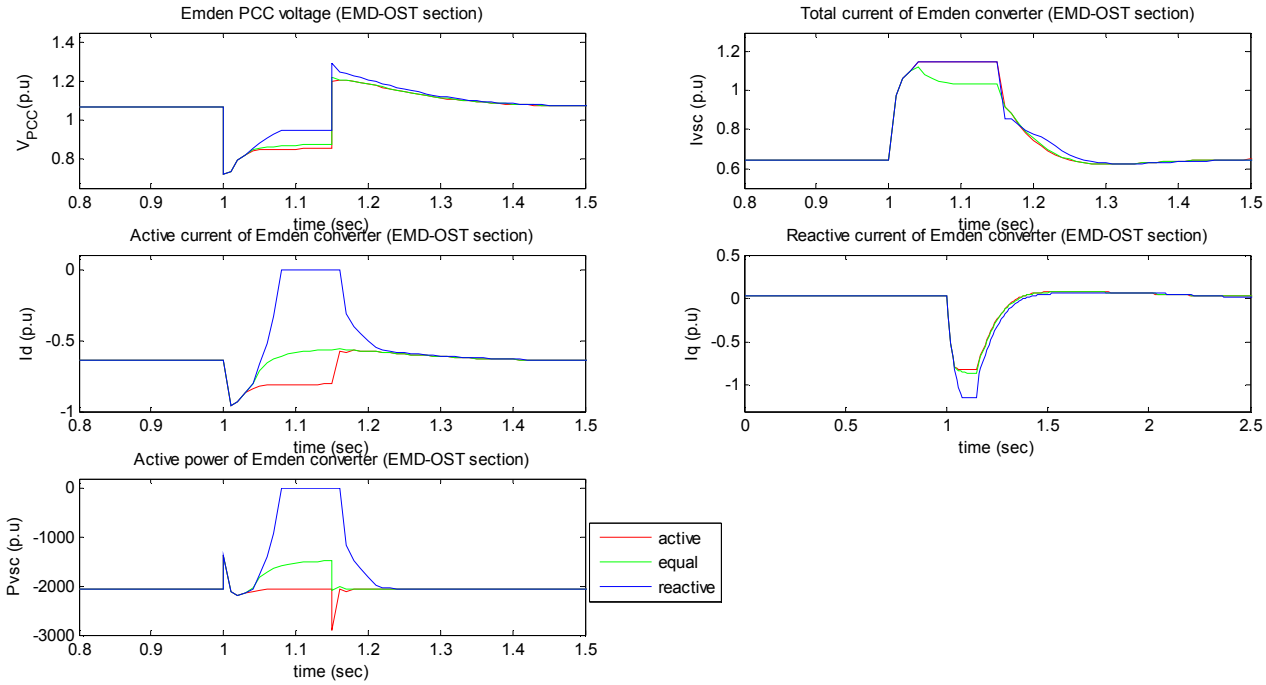

Fig. 4.19 Response of Emden's converter (EMD-OST section) to a 3-phase bus fault in Dorpen (Zone 1) for different CLSs

As can be seen from figure 4.19 the worst voltage support in Emden's filter bus appears when the converter's CLS is set to active current priority. This makes sense because when the converter reaches its current limit the current component that will be reduced is the reactive current. This means that this CLS results in the lowest reactive current component of all three cases, resulting in the poorest voltage support. Equal current priority results in a slightly better voltage profile than active current priority. When the converter reaches its limits both active and reactive current components will be reduced. Therefore the reduction of the reactive current component this time will be smaller than in the case of active current priority. However the improvement, as compared to active current priority, is not that big.

The best result regarding voltage support during a fault is accomplished through reactive current priority. When in reactive current priority the converter's first priority

during a fault is to maintain the AC system voltage and not the active power flow. This CLS allows only active current to be reduced when the converter's current limit is reached. This leaves more "space" for the converter's reactive current to control the voltage. This can be verified also by the converter's reactive current output shown in figure 4.19.

The highest active current is reached for active current priority since for this CLS, the converter's priority is to maintain the active power flow to its scheduled value. When looking at the active power output of the converter one can see that the active power is maintained in its scheduled value, during the fault, only for active current priority. This is expected because, as explained above, in this CLS the active current is not reduced at all when the converter reaches its current limit. Equal current priority results in a small reduction of active power, whereas reactive current priority leads to a temporary reduction of active power to zero in order to give all of the converter's current capability to the reactive current component.

4.3.3.2 Effect of the current limitation strategy on the AC system's bus voltages

In tables 4.14, 4.15 and 4.16 the average voltage dips of the system's buses for the fault locations of Dorpen, Sechtem and Hopfingen are presented. Only the voltages in buses inside and near the zone where the fault occurs will be shown. This is done because the effect of a converter's CLS on the transmission system can be seen only when the converter reaches its current limit. Only faults located close to the converter (in the same zone) are capable of making the HVDC converter reach its current limit.

	Emden	Conneforde	Diele	Unterweser	Meeden	Eemshaven
CLS	**ΔV%**	**ΔV%**	**ΔV%**	**ΔV%**	**ΔV%**	**ΔV%**
active	24.822	21.875	39.860	12.905	23.409	17.555
equal	23.657	21.077	39.340	12.436	23.077	17.291
reactive	19.759	18.688	37.801	11.129	22.246	16.670

Table 4.14 Effect of CLS on the average voltage dip for a fault in Dorpen (Zone 1)

	Dulken	Rommerskirchen	Niederrhein	Neurath	St. Peter	Oberzier
CLS	**ΔV%**	**ΔV%**	**ΔV%**	**ΔV%**	**ΔV%**	**ΔV%**
active	23.193	50.777	15.928	44.715	31.105	29.387
equal	22.626	50.466	15.639	44.450	31.000	29.240
reactive	19.939	48.983	14.337	43.197	30.545	28.576

Table 4.15 Effect of CLS on the average voltage dip for a fault in Sechtem (Zone 2)

	Philippsburg	Wiesloch	Daxlanden	Neurott	Huffenhardt	Pulverdingen
CLS	**ΔV%**	**ΔV%**	**ΔV%**	**ΔV%**	**ΔV%**	**ΔV%**
active	19.097	34.957	11.431	35.027	45.562	22.647
equal	19.036	34.914	11.402	34.982	45.538	22.606
reactive	17.956	34.302	10.940	34.368	45.192	22.071

Table 4.16 Effect of CLS on the average voltage dip for a fault in Hopfingen (Zone 3)

As can be seen from the results above the worst voltage profile of all three cases appears when the HVDC converters are set to active current priority. This is expected because as explained above, when the converter reaches its current limit and its CLS is set to active current priority, the only current component that will be reduced is the reactive component, leaving the active current component unchanged. The best voltage support appears for the reactive current priority CLS just as in the case of Emden's filter bus in paragraph 4.3.3.1. In general it can be seen that the higher the reactive current supplied by the HVDC converter the better the voltage support during the fault.

4.3.3.3 Effect of the current limitation strategy on the rotor angle response of generators during a fault

Next the effect of the CLS on the rotor angle deviations, for different fault locations, will be shown in tables 4.17, 4.18 and 4.19. Only generators in the affected areas will be shown. It has been seen in paragraphs 4.3.1.3 and 4.3.2.3 that when a fault occurs near an HVDC converter and active current reduction takes place, generators in both ends of the embedded HVDC line are affected. So, for a fault in Zone 1 generators in Zones 1 and 2 will be monitored. For a fault in Zone 2 generators in Zones 1, 2 and 3 will be shown and finally for a fault in Zone 3 generators in Zones 2 and 3 will be examined.

	Unterweser (Zone 1)	**Conneforde (Zone 1)**	**Niederaussem (Zone 2)**	**Neurath (Zone 2)**	**Eemshaven (Zone 1/NL)**	**Maasbracht (Zone 2/NL)**
CLS	$\Delta\delta_{max\%}$	$\Delta\delta_{max\%}$	$\Delta\delta_{max\%}$	$\Delta\delta_{max\%}$	$\Delta\delta_{max\%}$	$\Delta\delta_{max\%}$
active	3.857	4.216	3.893	3.077	5.642	1.289
equal	4.084	5.082	4.288	3.207	5.710	1.229
reactive	4.933	7.676	9.648	8.851	6.163	1.172

Table 4.17 Effect of CLS on the maximum rotor angle deviation for a fault in Dorpen (Zone 1)

The analysis will start with the case of the fault located in Dorpen. It has been shown that rotor angle stability in Zone 1 for a fault in Dorpen deteriorates when active current reduction takes place because the power transfer reduction of the HVDC line causes generators in the sending converter's area to accelerate. As can be seen from the values of table 4.17, the first rotor angle peak in Zone 1 increases as the amount of active current reduction increases. Therefore the highest rotor angle peak occurs for reactive current priority, the next worse occurs for equal current priority and finally the smallest rotor angle peak for generators in Zone 1 occurs for active current priority where no active current reduction takes place. Both active current reduction and the fault in Dorpen cause generators in Niederaussem and Neurath in Zone 2 to decelerate. These two decelerating factors lead to a higher rotor speed peak and therefore to a higher deviation of the first rotor angle peaks. Concequently, the smaller the active current reduction the smaller the first peak of the rotor angle oscillation of generators in Niederaussem and Neurath. The active current reduction benefits Maasbracht's rotor angle stability.

The equal priority results for the generators in Zone 2 should be disregarded. As has already been explained the VSCDCT model has a weakness in coordinating the active current reduction of both HVDC converters. The active current component of the non-limit reaching converter does not reduce unless the active current of the limit-

reaching converter is reduced to zero. As seen in figure 4.16, equal current priority results in an active current reduction in the limit-reaching converter's active current but this reduction is small and doesn't result in the active current reducing to zero. Therefore there will be no active current reduction in the non-limit-reaching converter and thus the effects of the equal current priority cannot be seen in the generators of Zone 2. In reality the rotor angle deviation of generators in Zone 2, for equal current priority and for a fault in Dorpen, is expected be worse than for active priority and better than for reactive priority due to the active current reduction which is smaller than in reactive current priority.

	Unterweser (Zone 1)	**Conneforde (Zone 1)**	**Niederaussem (Zone 2)**	**Neurath (Zone 2)**	**KKP (Zone 3)**	**Neurott (Zone 3)**	**Eemshaven (Zone 1/NL)**	**Maasbracht (Zone 2/NL)**
CLS	**$\Delta\delta_{max\%}$**	**$\Delta\delta_{max\%}$**	**$\Delta\delta_{max\%}$**	**$\Delta\delta_{max\%}$**	**$\Delta\delta_{max\%}$**	**$\Delta\delta_{max\%}$**	**$\Delta\delta_{max\%}$**	**$\Delta\delta_{max\%}$**
active	0.659	1.004	0.094	2.037	0.525	0.341	1.308	0.844
equal	0.649	0.991	0.118	2.070	0.518	0.338	1.289	0.835
reactive	1.136	3.869	0.096	1.677	0.364	0.324	1.510	0.744

Table 4.18 Effect of CLS on the maximum rotor angle deviation for a fault in Sechtem (Zone 2)

As has been seen in paragraphs 4.3.1.3 and 4.3.2.3, for a fault in Sechtem, the rotor angle deviation of generators in Zones 1 and 3 deteriorates with active current reduction. The situation in Zone 2 is more complicated because a reduction of power transfer in both sections of Corridor A leads to a simultaneous decrease of power injected in and out of Zone 2. It is seen that Niederaussem's rotor angle deviation increases by the active current reduction while Neurath's rotor angle deviation becomes smaller.

Regarding the equal current priority in Zones 1 and 3, as explained above, it should lead to the same results as reactive current priority, but less severe. For example, the rotor angle deviation for the equal current priority in reality should be higher than for active current priority and lower than for reactive current priority.

	Niederaussem (Zone 2)	**Neurath (Zone 2)**	**KKP (Zone 3)**	**Neurott (Zone 3)**	**Eemshaven (Zone 1/NL)**	**Maasbracht (Zone 2/NL)**
CLS	**$\Delta\delta_{max\%}$**	**$\Delta\delta_{max\%}$**	**$\Delta\delta_{max\%}$**	**$\Delta\delta_{max\%}$**	**$\Delta\delta_{max\%}$**	**$\Delta\delta_{max\%}$**
active	1.343	0.671	6.418	20.411	1.002	1.266
equal	1.157	0.544	5.873	19.147	0.941	1.235
reactive	5.687	4.122	3.940	14.850	1.007	1.212

Table 4.19 Effect of CLS on the maximum rotor angle deviation for a fault in Hopfingen (Zone 3)

The case for a fault located in Hopfingen is more straightforward than the case for Sechtem. The analysis is similar to that of for a fault in Dorpen. Additionally, what has been explained above for the equal current priority is valid for this fault location as well.

A general observation about the values of tables 4.17-4.19 is that the faults in Germany do not affect much the rotor angle stability of the Dutch generators. The fault that affects most Dutch generators is the fault in Dorpen (Zone 1) which affects most generators in Eemshaven. However, even in this case the maximum deviation of the rotor angle there is rather small, close to 6%.

In general it can be said that active current reduction has mixed effects on the rotor angle response of the generators depending on the location of the fault and the generators

4.4 Sensitivity analysis: Three-phase bus faults in the Netherlands

In this paragraph simulations will be run for scenarios where a three-phase bus fault occurs in the Netherlands. A separate paragraph is done in order to show the effect of faults in the Netherlands on Corrido A's converters and how their response affects the Dutch transmission system's dynamic behavior.

The selected fault locations in the Netherlands have been shown in figure 4.1 and are Meeden, Maasbracht and Zwolle. Meeden is located close to Emden's HVDC converter, while Maasbracht is located close to Osterath's HVDC converter. Zwolle is not located close to any converter of Corridor A and the location was selected in order to show if a fault in the general area of the Netherlands, not so close to any converter, will have a considerable effect on the HVDC converters of Corridor A.

4.4.1 The effect of the k gain on the AC system for faults in the Netherlands

The response of the system for different values of the k gain will be examined in this paragraph. The current limit of the converter is set to 1.15 p.u and the CLS is set to reactive current priority.

4.4.1.1 Response of Corridor A's HVDC converters to faults for different values of k

The response of Emden's and Osterath's converters to a fault in Meeden can be seen in figures 4.20 and 4.21 respectively.

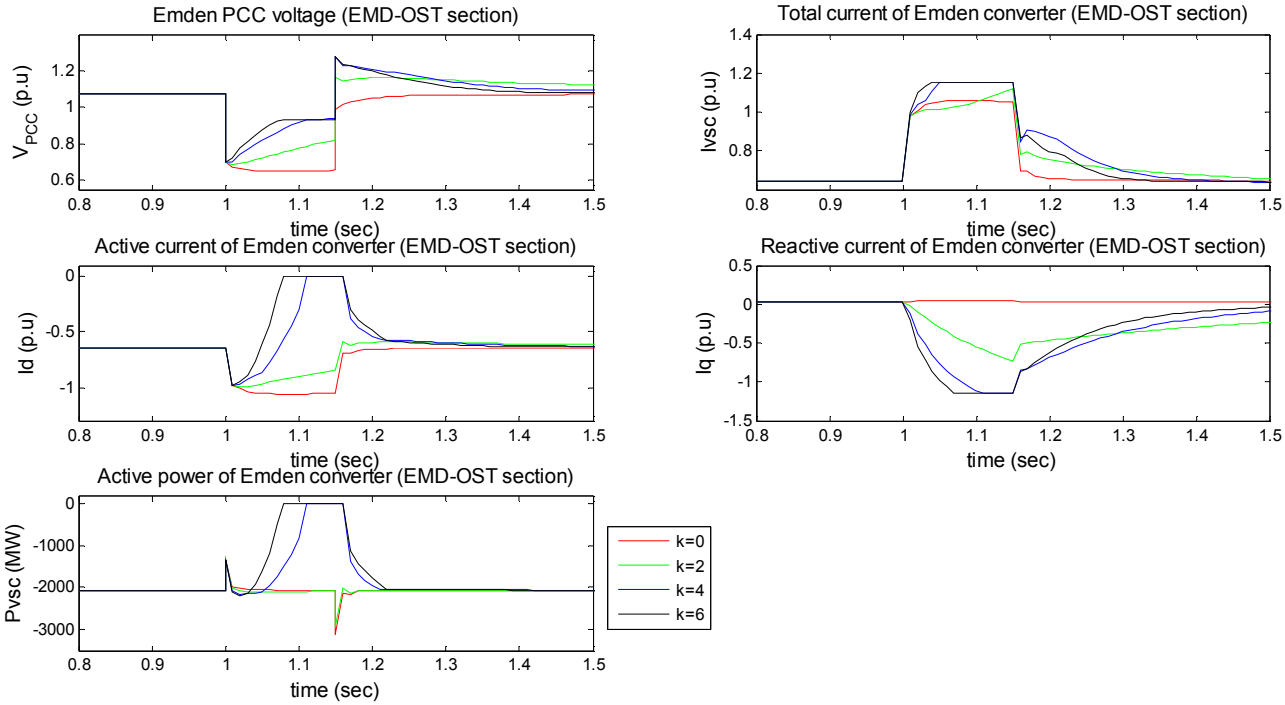

Fig. 4.20 Response of Emden's converter (EMD-OST section) to a 3-phase bus fault in Meeden for different values of k

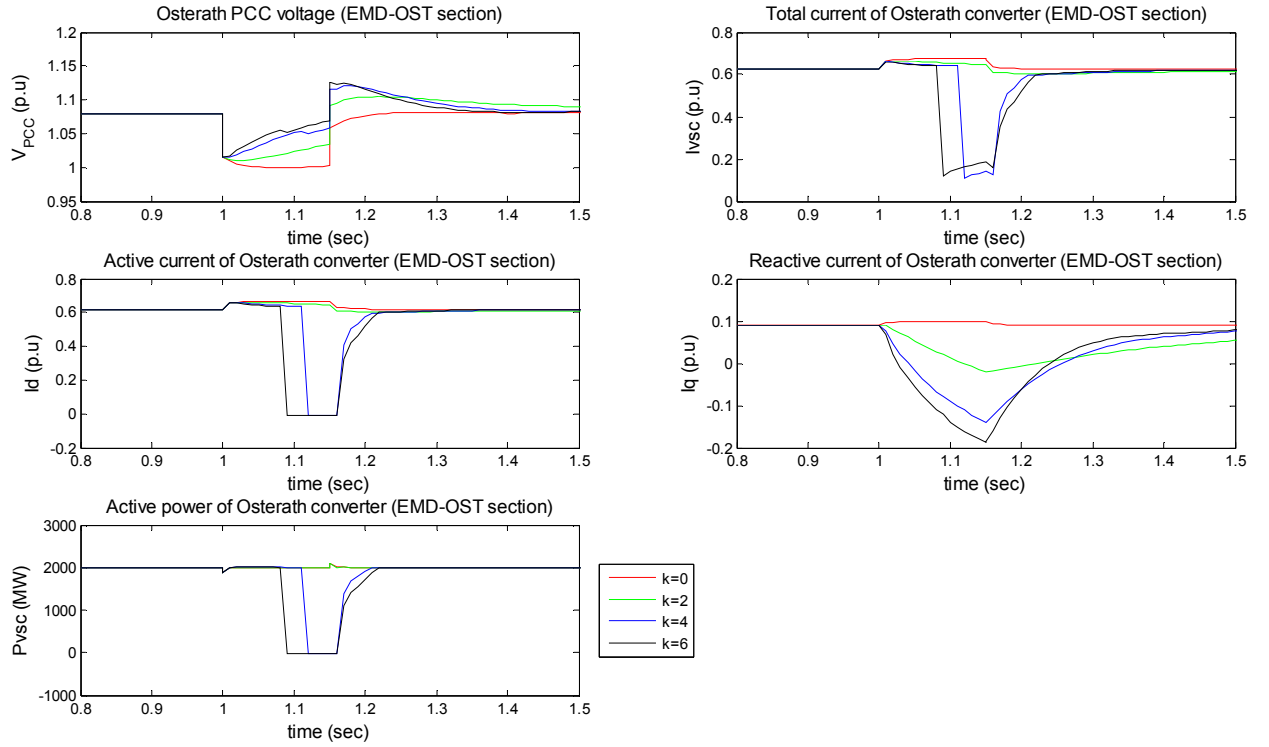

Fig. 4.21 Response of Osterath's converter (EMD-OST section) to a 3-phase bus fault in Meeden for different values of k

Figure 4.20 shows that a fault in Meeden is severe enough to lead Emden's converter to its current limit when the k gain is equal to 4 and 6. In fact for these

values of the k gain, the reactive current component of Emden's converter becomes equal to the current limit while the active current component becomes zero. Emden's converter response is similar to that for a fault in Dorpen and thus no further analysis will be done.

On the other hand it is seen that for a fault in Meeden, the voltage drop in Osterath's filter bus is small and therefore the response of Osterath's converter to the fault will also be small.

Next the response of Emden's and Osterath's converters for a fault in Zwolle is presented. Zwolle is not located close to any of Corridor A's converters and therefore it is interesting to see how such a fault will affect Corridor A.

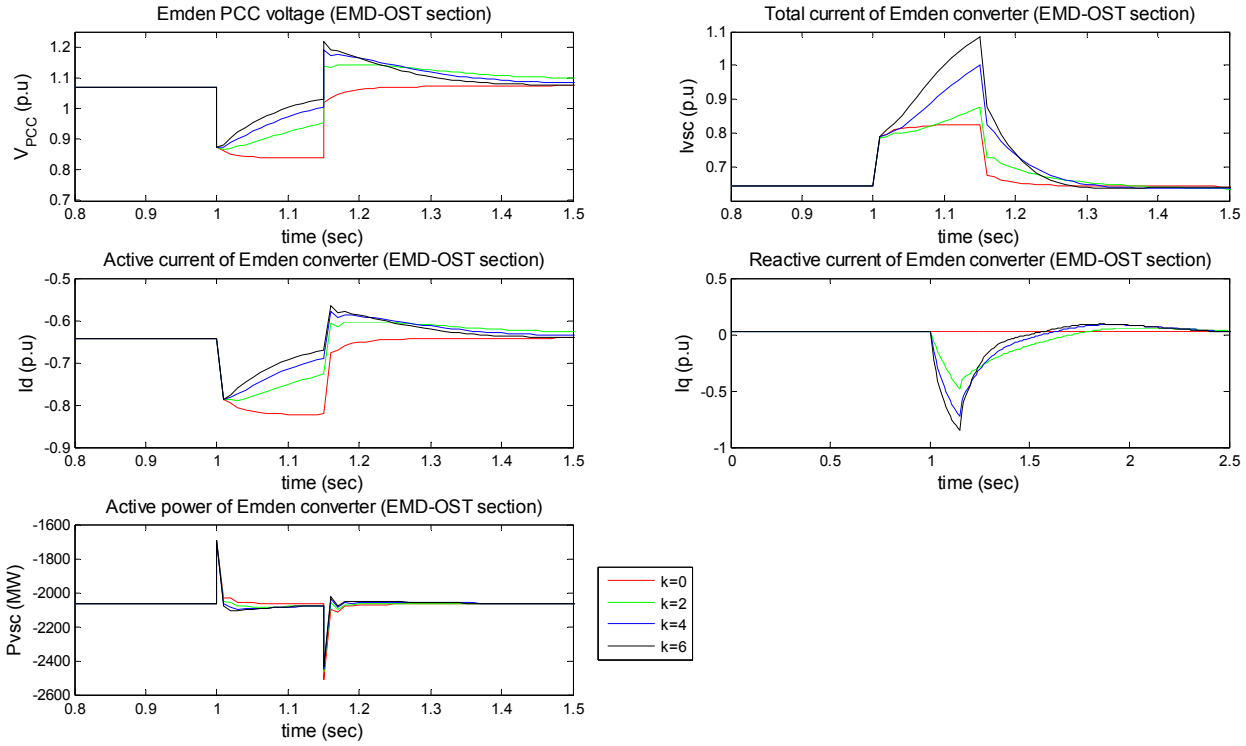

Fig. 4.22 Response of Emden's converter (EMD-OST section) to a 3-phase bus fault in Zwolle for different values of k

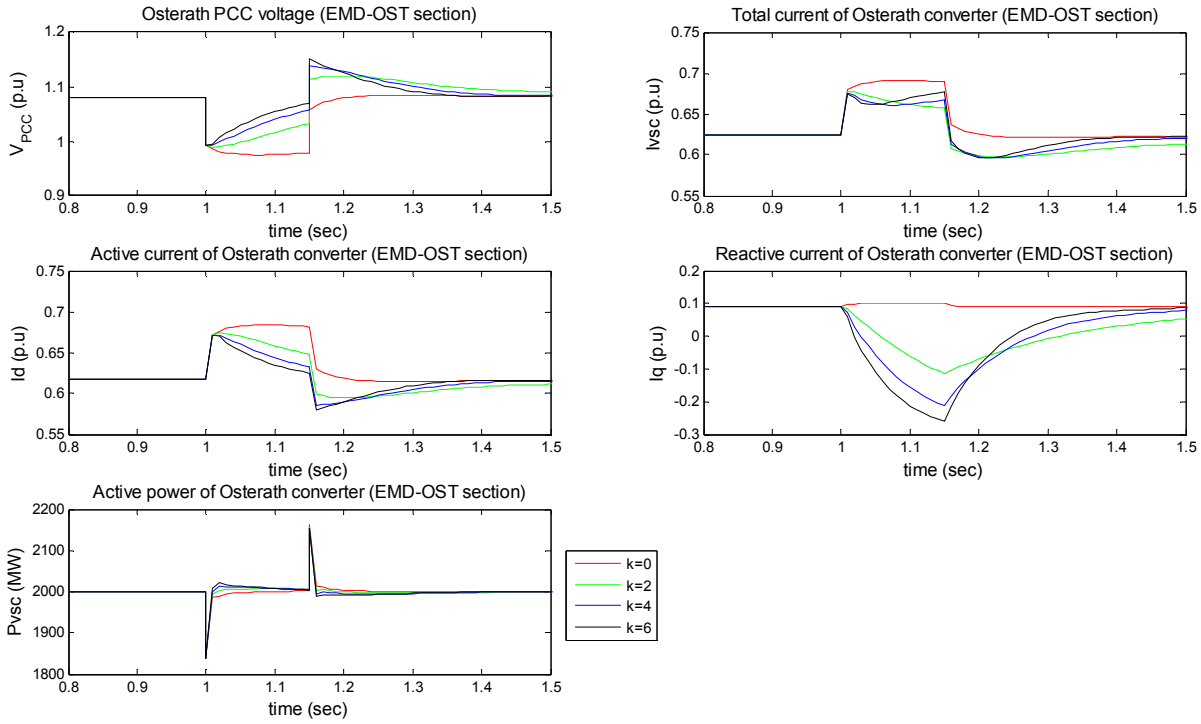

Fig. 4.23 Response of Osterath's converter (EMD-OST section) to a 3-phase bus fault in Zwolle for different values of k

Figures 4.22 and 4.23 show that a fault in Zwolle is not severe enough, to cause any of Corridor A's converters, to reach their current limit.

Finally the fault in Maasbracht is examined. As seen in figure 4.1, Maasbracht is located geographically close to Osterath. It is also located far from Emden and thus it will not affect its HVDC converter much. The response of Osterath's converter for this fault location is shown in figure 4.24.

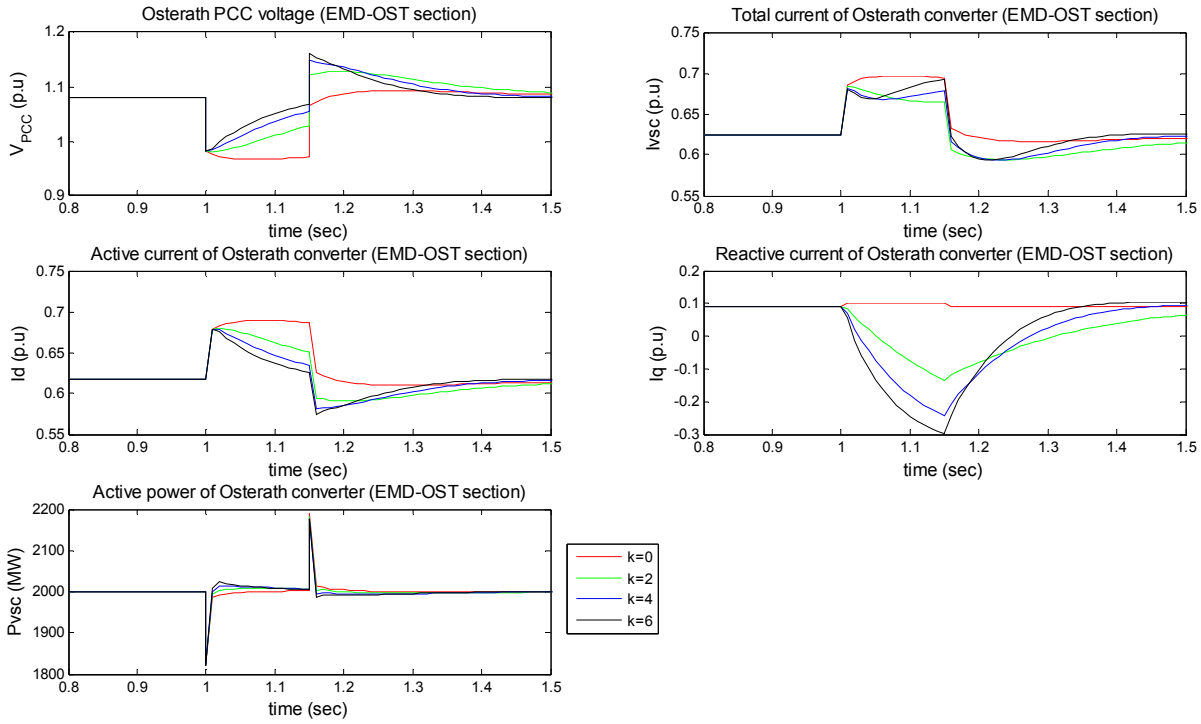

Fig. 4.24 Response of Osterath's converter (EMD-OST section) to a 3-phase bus fault in Maasbracht for different values of k

Figure 4.24 shows that despite the geographical proximity of Maasbracht to Osterath, the electrical distance between them is big. The voltage drop in Osterath's filter bus is rather small (around 0.1 p.u) and thus the HVDC converter doesn't reach its current limit.

4.4.1.2 Effect of the k gain on the AC system's bus voltages

In this paragraph the effect of different values of the k gain on the voltages of the Dutch grid, for faults in the Netherlands, will be shown. The selected buses, the voltage of which will be shown are Eemshaven, Doetichem, Maasbracht, Lelystad, Tilburg and Krimpen aan den IJssel (KIJ). For a fault in Maasbracht, Eindhoven's voltage is monitored instead of Maasbracht's. Eemshaven, Doetinchem and Maasbracht are located close to the borders with Germany and thus closer to Corridor A. Lelystad and Tilburg are located more towards the west and approximately in the center of the country, while KIJ is located far from Corridor A, in the western part of the Netherlands.

The average voltage dips of the aforementioned buses, for different fault locations, are presented in tables 4.20, 4.21 and 4.22.

	Eemshaven	Doetinchem	Maasbracht	Lelystad	Tilburg	KIJ
k	ΔV%	ΔV%	ΔV%	ΔV%	ΔV%	ΔV%
0	74.165	18.367	8.697	42.288	10.871	15.953
2	74.127	17.537	8.285	42.053	10.650	15.791
4	74.108	17.202	8.137	41.965	10.589	15.747
6	74.106	17.051	8.075	41.944	10.580	15.748

Table 4.20 Effect of k gain on the average voltage dip for a fault in Meeden

	Eemshaven	Doetinchem	Maasbracht	Lelystad	Tilburg	KIJ
k	ΔV%	ΔV%	ΔV%	ΔV%	ΔV%	ΔV%
0	46.250	28.806	13.141	62.649	16.337	23.735
2	45.537	28.064	12.724	62.477	16.127	23.597
4	45.120	27.624	12.477	62.376	16.002	23.514
6	44.846	27.342	12.318	62.310	15.921	23.460

Table 4.21 Effect of k gain on the average voltage dip for a fault in Zwolle

	Eemshaven	Doetinchem	Eindhoven	Lelystad	Tilburg	KIJ
k	ΔV%	ΔV%	ΔV%	ΔV%	ΔV%	ΔV%
0	6.353	20.137	45.653	12.559	32.320	18.156
2	6.026	19.464	45.532	12.268	32.213	18.037
4	5.824	19.058	45.459	12.090	32.148	17.964
6	5.693	18.797	45.412	11.974	32.106	17.917

Table 4.22 Effect of k gain on the average voltage dip for a fault in Maasbracht

As can be seen from the values of the tables above, higher values of the k gain result in lower voltage dips during the fault. However the improvement in voltage support is very small even for buses located rather close to Emden's or Osterath's converters (such as Eemshaven and Maasbracht). The difference in voltage support in Eemshaven for a fault in Meeden is extremely low because it is located very close to the fault location. These results confirm that the effect of the HVDC converters on voltage support is quite regional. The majority of the 380 kV buses in the Netherlands are located electrically far from any of Corridor A's converters and therefore the voltage support they receive is very small. Even for buses located close to Corridor A's converters, such as Eemshaven, the voltage improvement is not that big.

4.4.1.3 Effect of the k gain on the rotor angles of generators

Finally in this paragraph the effect of Corridor A on the rotor angle stability of the generators in the Netherlands will be shown. The rotor angles of large generating units are monitored. The selected generators are located in the areas of Eemshaven, Maasbracht, Diemen, Geertruidenberg and Maasvlakte.

The rotor angle deviations of the generators for different fault locations are presented in tables 4.23, 4.24 and 4.25.

	Eemshaven	Maasbracht	Diemen	Geertruidenberg	Maasvlakte
k	$\Delta\delta_{max\%}$	$\Delta\delta_{max\%}$	$\Delta\delta_{max\%}$	$\Delta\delta_{max\%}$	$\Delta\delta_{max\%}$
0	26.490	0.970	9.049	5.668	11.043
2	25.544	0.898	8.697	5.345	10.621
4	25.541	0.783	8.543	5.073	10.457
6	25.753	0.703	8.542	4.988	10.431

Table 4.23 Effect of k gain on the maximum rotor angle deviation for a fault in Meeden

	Eemshaven	Maasbracht	Diemen	Geertruidenberg	Maasvlakte
k	$\Delta\delta_{max\%}$	$\Delta\delta_{max\%}$	$\Delta\delta_{max\%}$	$\Delta\delta_{max\%}$	$\Delta\delta_{max\%}$
0	18.514	0.804	15.774	9.064	16.039
2	17.784	0.750	15.517	8.798	15.748
4	17.516	0.718	15.445	8.707	15.704
6	17.401	0.697	15.433	8.681	15.691

Table 4.24 Effect of k gain on the maximum rotor angle deviation for a fault in Zwolle

	Eemshaven	Maasbracht	Diemen	Geertruidenberg	Maasvlakte
k	$\Delta\delta_{max\%}$	$\Delta\delta_{max\%}$	$\Delta\delta_{max\%}$	$\Delta\delta_{max\%}$	$\Delta\delta_{max\%}$
0	3.049	5.519	6.836	16.168	14.266
2	2.907	5.491	6.741	16.057	14.165
4	2.852	5.488	6.721	16.024	14.189
6	2.831	5.486	6.720	16.018	14.166

Table 4.25 Effect of k gain on the maximum rotor angle deviation for a fault in Maasbracht

As is seen in table 4.23, Eemshaven's rotor angle stability deteriorates for k=6 when a fault occurs in Meeden. This happens because for a fault in Meeden and k=6, Emden's converter reaches its current limit and its active current reduces to zero. Eemshaven's generators are close enough to Zone 1, as defined in paragraph 4.3. The generator in Eemshaven is therefore affected by the active power reduction in the sending end of Corridor A. This can be seen in figure 4.25 where the generator speeds are shown. Observing Eemshaven's generators speed it can be seen that the active current reduction-induced accelerarion is superimposed to the generator's acceleration due to the fault and thus the first peak of the rotor speed for k=4 and 6 is higher than for k=2. This results also in a higher peak for the rotor angle.

From figure 4.25 it can also be seen that the rotors of Maasbracht's generators are also influenced by the active current reduction for k=4 and 6 and are additionally decelerated. However the rotor angle peaks decrease as the k gain increases. This happens because the influence of active current reduction on Maasbrachts generator is smaller than for Eemshaven's generator. It seems that the influence of the improved voltage profile due to the higher k gain is greater than that of active current reduction.

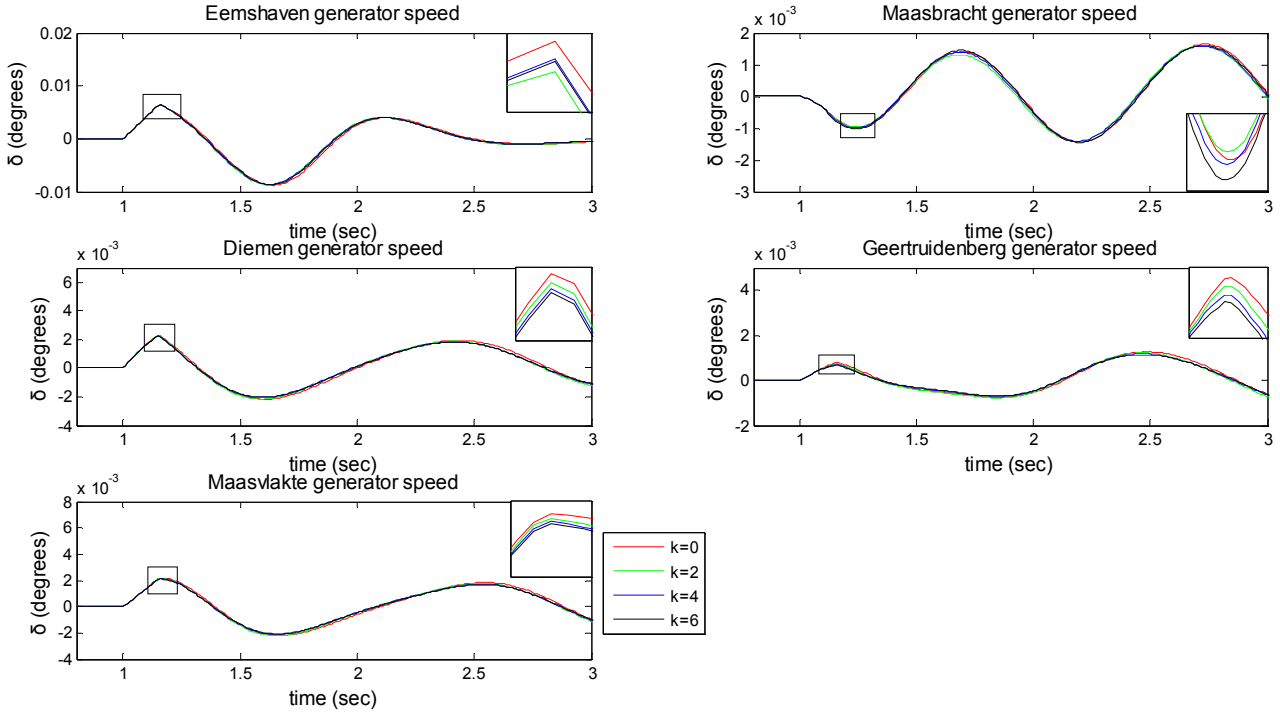

Fig. 4.25 Effect of k gain on generator rotor speeds for a fault in Meeden

Setting aside the case of Eemshaven's generator for a fault in Meeden, the first peak of the rotor angle of the other generators for different fault locations improve for higher values of the k gain. This happens for two reasons. First of all, no other fault location is capable of leading Corridor A's converters to their current limit and thus to reduce their active power output. Secondly most of the generators in the Netherlands are located far from the HVDC converters and aren't affected in the case that Corridor A's transferred active power reduces. The improved rotor angle stability for higher values of k, is due to the improved voltage profile. The system voltages are held to a higher value during the fault and the generators perceive the fault as less severe, leading to a smaller rotor angle oscillation.

However, it has to be pointed out that, once again the improvement is very small compared to what has been seen in similar situations in Germany.

From the results of this paragraph two main conclusions can be drawn. First of all, the majority of the Dutch transmission system buses are located electrically far from the HVDC converters of Corridor A. This means that the effect of a fault in a Dutch bus, on the converters of Corridor A will be rather small and thus they won't reach their current limit. This was seen for the cases of faults in Zwolle and Maasbracht.

Secondly, even for the limited cases where a fault in the Netherlands is capable of leading one of Corridor A's converters to its limit (such as a fault in Meeden) it has been seen that the impact of the HVDC converters is quite regional. This means that any improvement or deterioration of the voltage profile and rotor angle stability is marginal for buses and generators that are not located close to the affected HVDC converters.

The examination of the over-current capability and CLS sensitivities is impossible for most of the faults in the Netherlands because they are located electrically far from Corridor A's converters and are thus incapable of leading them to reach their current limit. Even for the limited fault locations that can lead any of Corridor A's converters

to their limit (such as a fault Meeden), the examination of the over-current capability and the CLS sensitivities will offer no further information about the effect of Corridor A on the transmission system. As has already been seen in paragraph 4.3 the effect of the different current capabilities and CLSs of the converters is considerable only close to the limit-reaching converters. Therefore the effect of these sensitivities on the Dutch transmission system will be very small.

4.5 Loss of Corridor A and the impact on the transmission system

As the title indicates, this paragraph will examine the effect that a trip of Corridor A will have on the transient stability of the grid. In order to do this a sudden and permanent disconnection of one or both sections of Corridor A will be simulated. This scenario could represent the failure of one HVDC converter which leads to the disconnection of the converter at the other point of the HVDC line resulting in the loss of DC power transferred.

Initially, the loss of Corridor A will be examined for the planned DC power transmission of 2000 MW. For this power transfer three scenarios will be examined. First, the loss of only the EMD-OST section, next the loss of only the OST-PHLP section and finally the loss of both sections of Corridor A.

Finally the effect of losing Corridor A for increased loadings will be examined. The examined cases will be for an HVDC power transmission of 3000, 4000, 5000 and 6000 MW. Only the scenario where both sections of Corridor A are lost will be examined. The goal of this series of simulations is to figure out if there is a maximum DC power transfer which if lost, will lead the system to instability.

4.5.1 Loss of one or both sections of Corridor A for scheduled DC power transfer (2000 MW)

As mentioned earlier, three scenarios will be examined in this paragraph:

1. Loss of the EMD-OST section
2. Loss of the OST-PHLP section
3. Both sections of Corridor A lost

The analysis will start by showing how the interconnection power between the Netherlands and Germany is affected by a sudden loss of one or both sections of Corridor A. The Dutch and German 380 kV transmission systems are interconnected using AC lines. The interconnection points are Meeden-Diele (double circuit), Hengelo-Gronau (double circuit), Doetinchem-Niederrhein (double circuit), Maasbracht-Siersdorf and Maasbracht-Oberzier. The location of the connection points can be seen in figure 4.26. It can be seen that the Meeden-Diele interconnection is close to Emden's HVDC converter, while the Doetinchem-Niederrhein, Maasbracht-Siersdorf and Maasbracht-Oberzier interconnections are close to Osterath's HVDC converter.

Fig.4.26 Interconnection buses between the Netherlands and Germany

The behavior of the power flow between these connection points are shown in figures 4.27-4.29 for the three loss cases.

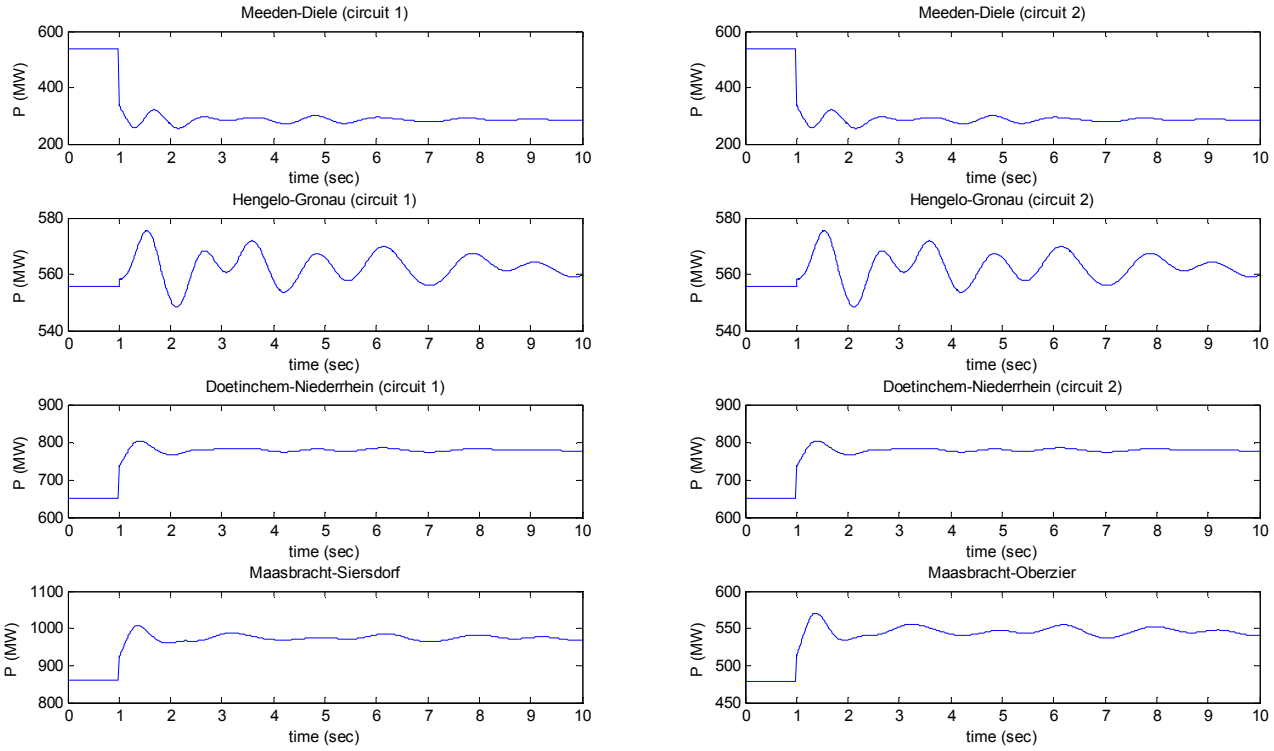

Fig.4.27 NL-DE interconnection power for loss of the EMD-OST section

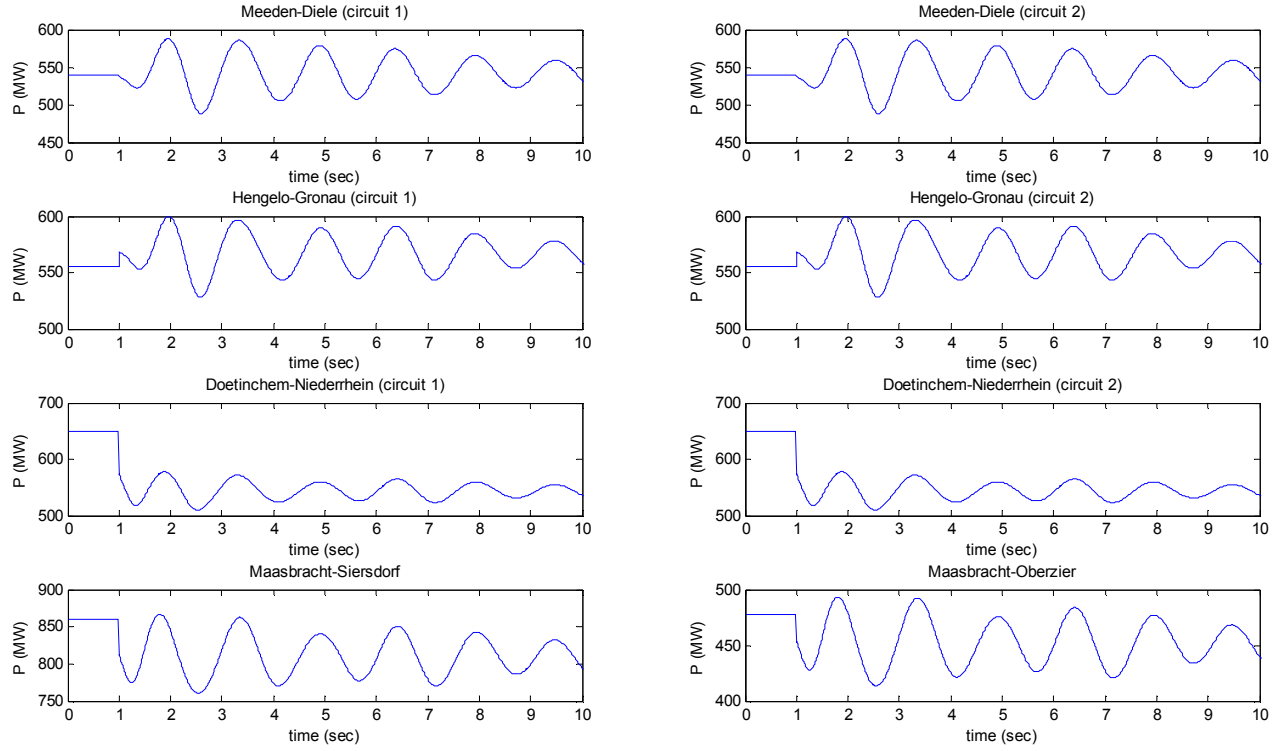

Fig.4.28 NL-DE interconnection power for loss of the OST-PHLP section

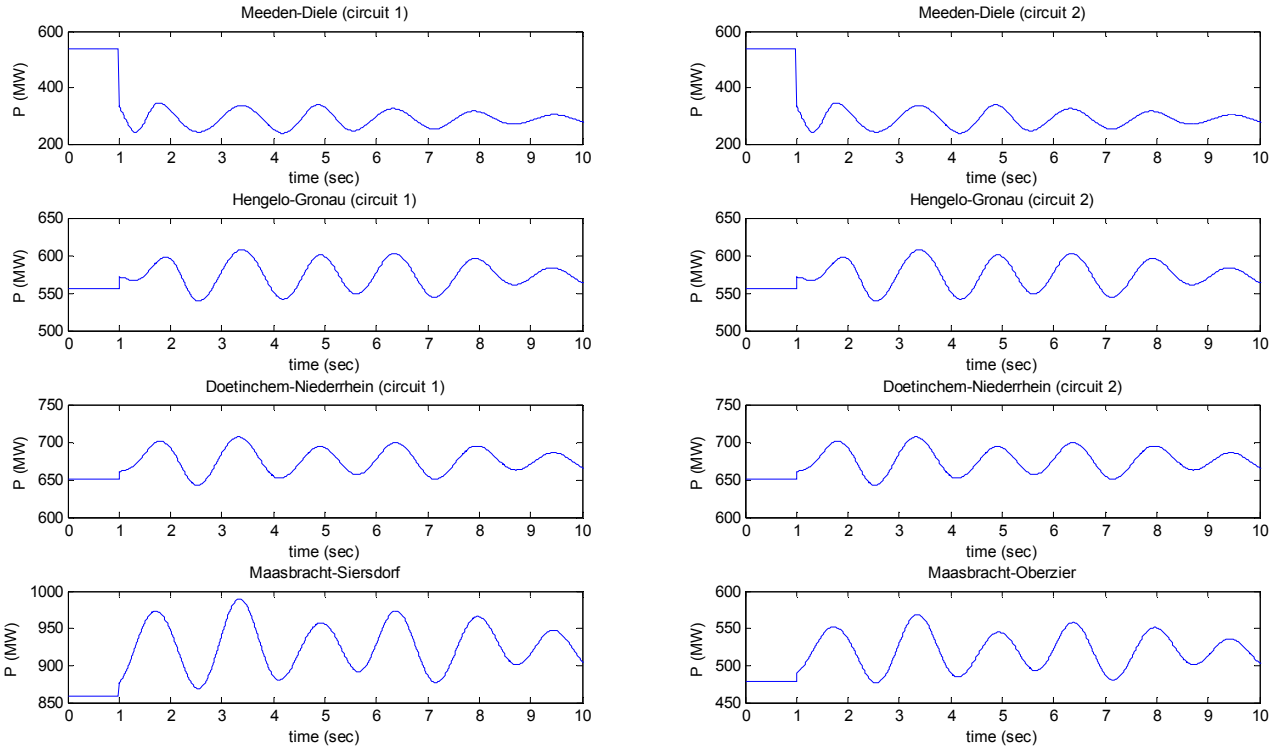

Fig.4.29 NL-DE interconnection power for loss of both sections

From figures 4.27, 4.28 and 4.29 it can be seen that in the scenario studied in this thesis, the Netherlands export active power to Germany and evidently a part of that power is absorbed by Corridor A.

When Emden's converter is tripped (loss of EMD-OST section and loss of both sections) the active power transfer from Meeden to Diele reduces because Corridor A no longer absorbs power from the grid near Emden.

In the case that only the EMD-OST section is lost, the power transfer from the Netherlands to Germany between the connection points near Osterath increases as seen in figure 4.27. This happens because the loss of the EMD-OST section reduces the power infeed in the grid near Osterath which is needed to supply the regional loads and the OST-PHLP section's sending converter. This lack of active power is replenished partly by an increase in the Netherland's export to Germany near Osterath. The active power transfer between Hengelo and Gronau oscillates after the loss of Corridor A's section but its power transfer doesn't actually change since it is located relatively far from Emden's and Osterath's converters and is thus unaffected by the change in the power flow.

On the other hand when the OST-PHLP section is out of order the active power flowing in the the Doetinchem-Niederrhein, Maasbracht-Siersdorf and Maasbracht-Oberzier interconnections is reduced. Power no longer is sent from Osterath to Philippsburg and thus Osterath ends up with an excess of active power. In order to bring balance to the active power infeed and consumption in Osterath's region the active power export from the Netherlands to Germany, near Osterath is reduced. Setting aside the disturbance-induced oscillation, the active power transfer in the interconnection of Meeden-Diele and Hengelo-Gronau remains more or less constant

since these interconnection points are located far from Osterath's region and apparently are unaffected by the change in the power flow.

In the case where both of Corridor A's sections are lost, the power flow in the Meeden-Diele interconnection decreases as explained above. The power flow in the Hengelo-Gronau interconnection remains relatively unchanged while the power flow in the rest of the interconnections near Osterath slightly increases. It appears that since Osterath is both a sending and receiving region for Corridor A, when a simultaneous loss of both sections occurs, the effects of an HVDC line loss are nullified in the region. The small increase in the power transfer in the Doetincem-Niederrhein, Maasbracht-Sierdsdorf and Maasbracht-Oberzier interconnections probably occurs in order to satisfy the consumption of Osterath's regional loads that were previously accommodated partly by the EMD-OST section of Corridor A.

In figure 4.30 the apparent power (MVA) of the interconnecting lines for the loss of the EMD-OST section can be seen.

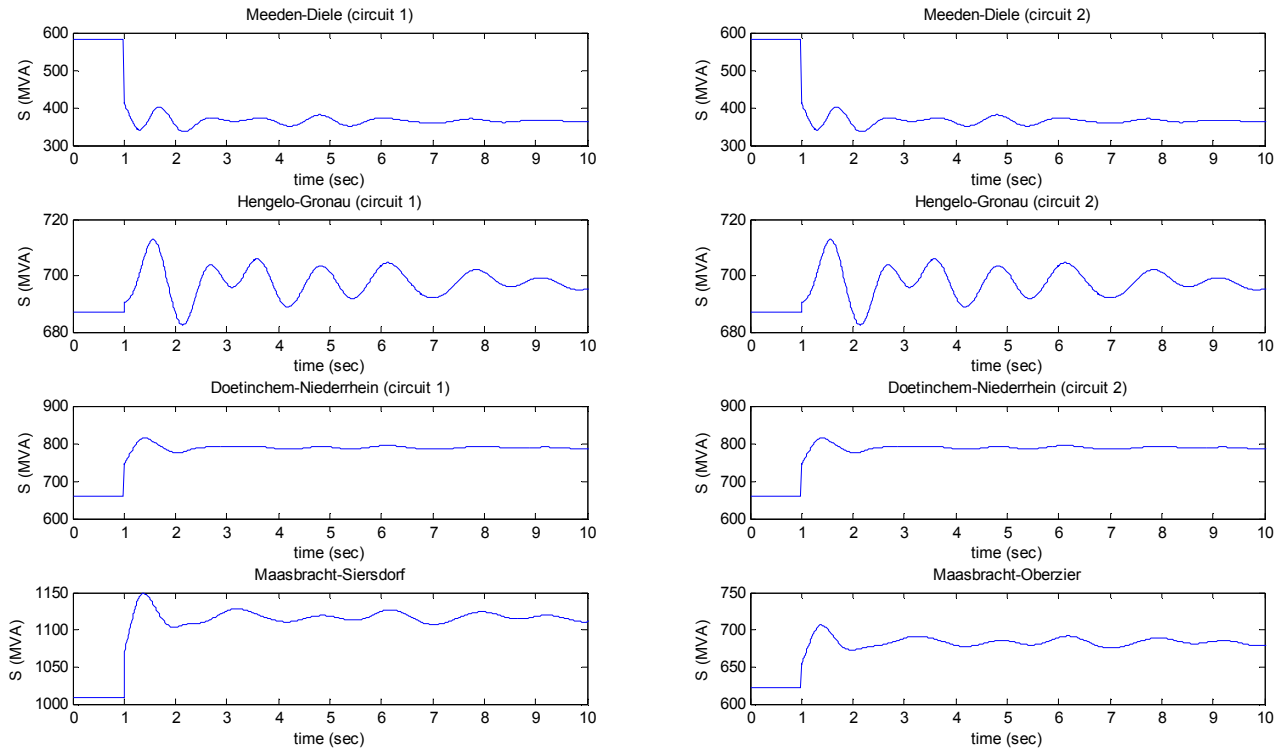

Fig.4.30 NL-DE interconnection apparent power for loss of the EMD-OST section

An important observation from the above figure is that the loading limits of the lines are not violated in any case. The same is true for the other two loss cases (loss of OST-PHLP section and loss of both sections). Therefore, for the examined generation-load scenario, the lines interconnecting the Netherlands and Germany are safe from over-loadings in the case where Corridor A is lost. A more extensive study must be done in order to examine other generation-load scenarios that result in different export power between the Netherlands and Germany.

In order to determine the stability of the system after a partial or total loss of Corridor A, the rotor angle behavior of a selected number of generators in Germany and the Netherlands will be examined. The selected generators in Germany are located in Unterweser, Conneforde, Niederaussem, Neurath, Philippsburg (KKP) and

Neurott and are located in the areas near the HVDC converters (Zones 1, 2 and 3) where the impact of the loss of a section or the whole Corridor A will be the highest. The selected generators in the Netherlands are located in Eemshaven, Maasbracht, Diemen, Geertruidenberg and Maasvlakte. Although most of these generators are located far from Zones 1, 2 and 3 their behavior is monitored in order to show how severe the loss of Corridor A will be on the stability of neighboring countries such as the Netherlands.

The rotor angles of the aforementioned generators will be shown for the most severe case, which is the simultaneous loss of both sections of Corridor A. The reader can find the plots of the rotor angles for the other two cases (loss of the EMD-OST section and loss of the OST-PHLP section) in appendix D.

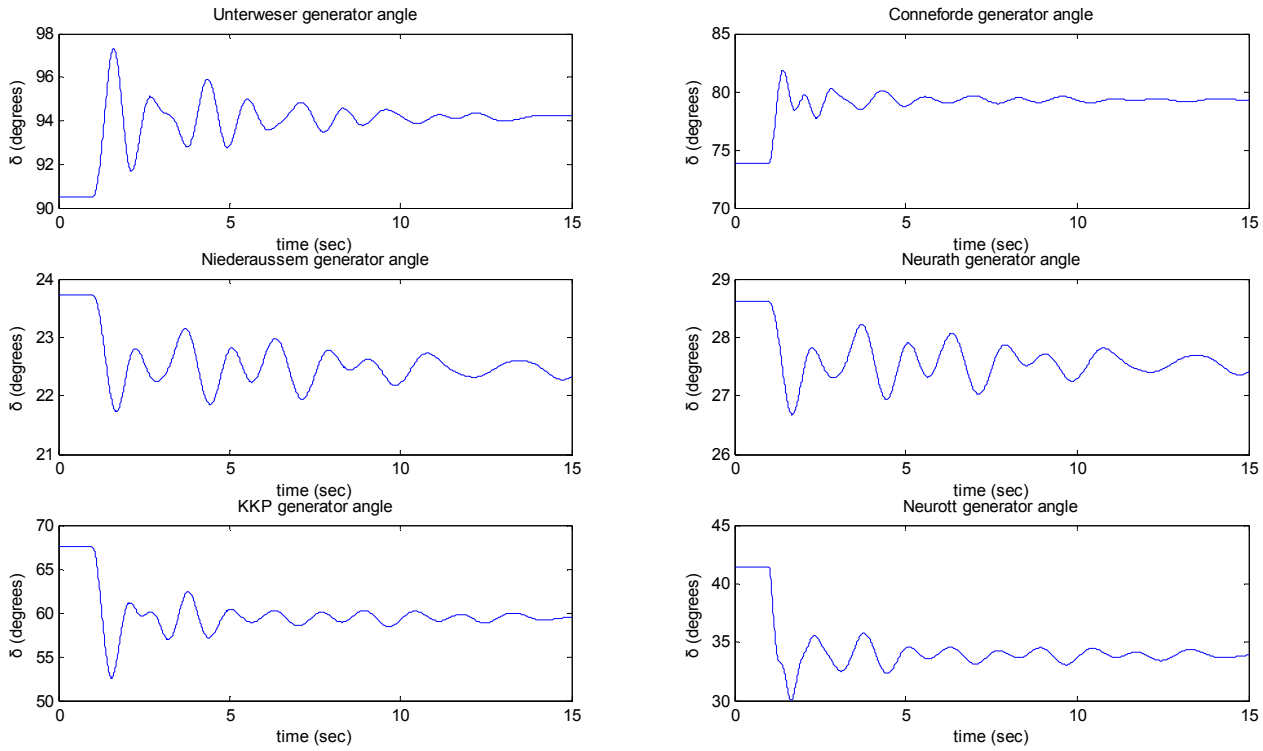

Fig.4.31 Effect of loss of both sections of Corridor A on the rotor angles in Germany

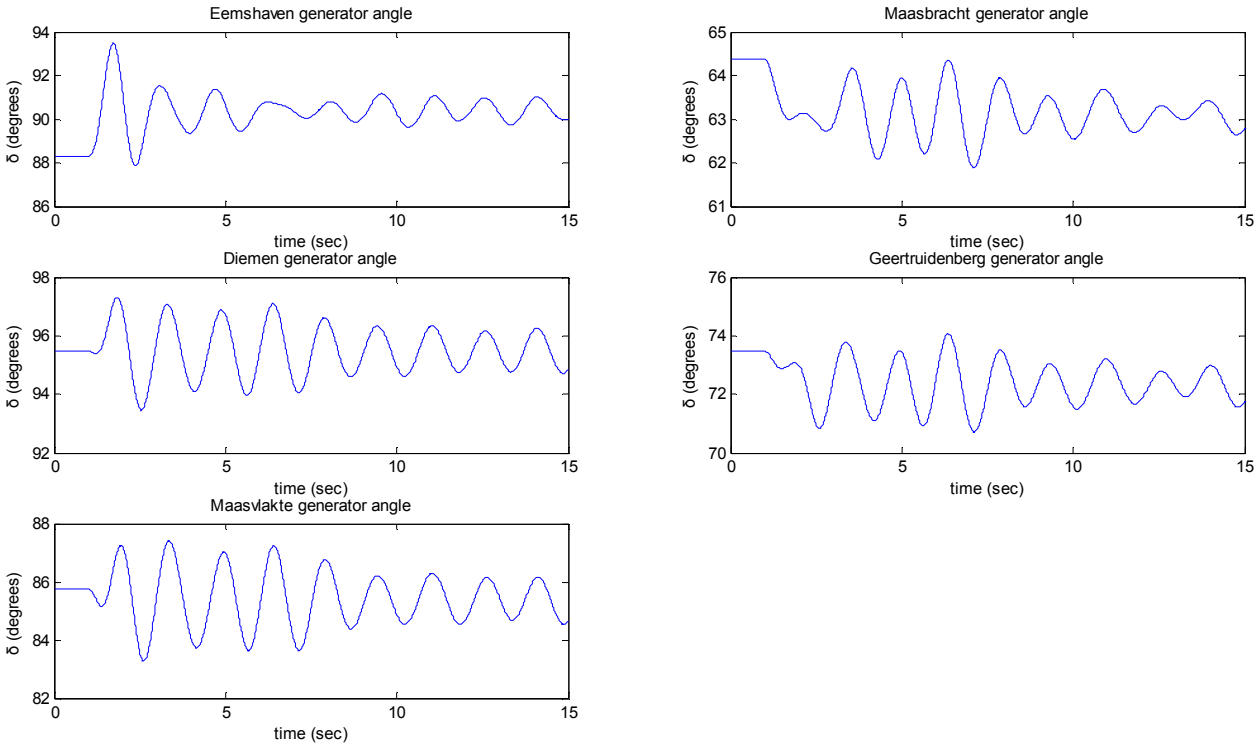

Fig.4.32 Effect of loss of both sections of Corridor A on the rotor angles in the Netherlands

As can be seen from figures 4.31 and 4.32, after the total loss of Corridor A, the rotor angles of the generators oscillate but their value does not increase unlimitedly. This means that the disturbance is not severe enough to lead the system to instability. However the oscillations that occur after the loss of Corridor A appear to be poorly damped. After the disturbance, the rotor angles of the generators in Zones 1, 2 and 3 (close to Corridor A's converters) will reach new values since a new flow of active power has been established after the permanent loss of Corridor A. Generators far from the affected areas near Corridor A's converters (such as Maasvlakte) will also oscillate after the HVDC line loss. However once the oscillations damp out, the rotor angles will have the same or almost the same value as the pre-fault situation, since the power flows in that part of the grid are not affected a lot.

From the results above it appears that a sudden and permanent loss of 2000 MW transferred through Corridor A is not enough to drive the system to an unstable situation. The system is well into stability since, as can be seen in figure 4.31, the largest observed oscillation has a peak-to-peak value of less than 10^{o} degrees, which is not that severe.

It has to be pointed out that a permanent loss of both sections of Corridor A will probably result in the over-loading of some transmission lines in Germany and probably its neighboring countries and might cause over and under-voltage problems in some areas due to the resulting excess and lack of active power in those areas. These conditions might not represent a realistic operation of the system. However such a study is beyond the scope of the present thesis. Clearly from a rotor angle stability point of view, a sudden loss of Corridor A does not result in a problematic situation.

4.5.2 Maximum loading of Corridor A

Having seen that the sudden loss of 2000 MW transmitted through the HVDC lines of Corridor A does not result in an unstable situation, for the specific generation-load scenario examined, the question that emerges is if there is a maximum transmitted power through Corridor A, the loss of which will cause rotor angle stability problems to the system.

In order to answer this question a study similar to that of the previous paragraph will be performed, but this time for higher loadings of the HVDC corridor. Only the case where both sections of Corridor A are lost simultaneously, which is the most severe, will be examined. The rotor angle of the most affected generators will be shown. As mentioned above the generators affected most by the loss of Corridor A are the ones located near the HVDC converters. The selected generators are located in Unterweser, Conneforde (Zone 1), Niederaussem, Neurath (Zone 2), Philippsburg and Neurott (Zone 3).

Initially the case where 3000 MW are transferred through Corridor A is examined. The rotor angles are presented in figure 4.33.

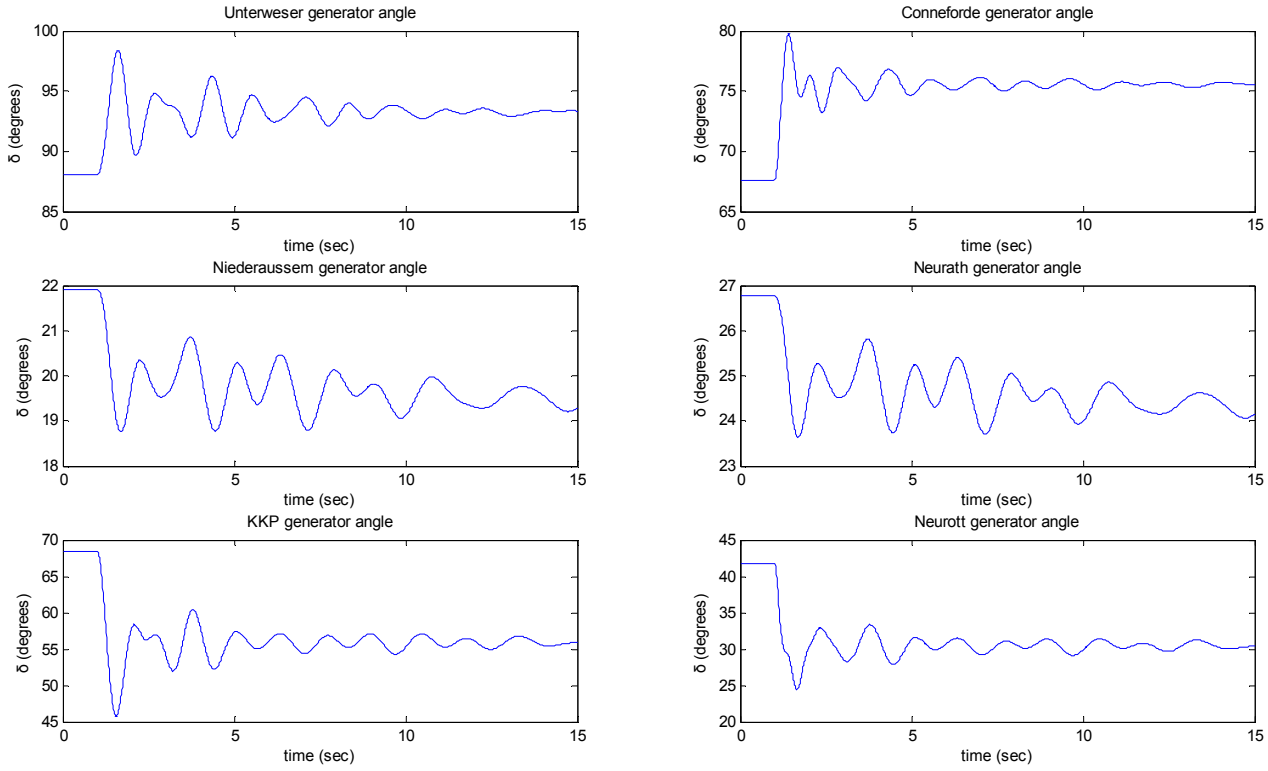

Fig. 4.33 Effect of loss of both sections of Corridor A (3000 MW) on the rotor angles in Germany

As can be seen from figure 4.33 the generators in Zones 1, 2 and 3 remain in a stable operation point even after the loss of 3000 MW of HVDC transferred power through Corridor A. This is also the case for 4000, 5000 and 6000 MW.

The plots of the rotor angles for the cases of 4000 MW, 5000 MW and 6000 MW of HVDC power transfer can be found in appendix D.

In order to compare the different cases of HVDC power transfer, the maximum rotor angle divergences, as defined by equation 4.2, for the generators of figure 4.34 are shown in table 4.26.

	Unterweser (Zone 1)	**Conneforde (Zone 1)**	**Niederaussem (Zone 2)**	**Neurath (Zone 2)**	**KKP (Zone 3)**	**Neurott (Zone 3)**
DC power (MW)	$\Delta\delta_{max\%}$	$\Delta\delta_{max\%}$	$\Delta\delta_{max\%}$	$\Delta\delta_{max\%}$	$\Delta\delta_{max\%}$	$\Delta\delta_{max\%}$
3000	11.722	17.902	14.392	11.741	33.134	41.452
4000	16.667	27.111	22.331	18.037	44.647	56.462
5000	22.688	39.578	34.015	26.587	56.760	72.765
6000	29.997	54.812	50.240	37.167	68.073	87.140

Table 4.26 Effect of different HVDC power transfer loss on the maximum rotor angle deviation

As seen from table 4.26 the higher the HVDC power transfer through Corridor A, the bigger the first peak of the rotor angle oscillation of the generators. Despite this fact, none of the examined cases results in rotor angle instability.

4.6 Synopsis

In this chapter the results of the simulations were presented. The analysis emphasized in two subjects. First an analysis was performed on the sensitivity of the AC system on parameters of the VSC-HVDC converters such as the k gain, the converter's over-current capability and its control limitation strategy. The effect of these parameters on the AC system's voltages and rotor angle stability was examined for faults located in the Netherlands and Germany. The results and analysis of these simulations were shown in paragraphs 4.3 and 4.4.

Finally the second part of the study focused on the effect of the loss of one or both sections of Corridor A could have on the rotor angle stability of the transmission system. The effect of the loss of higher than the scheduled DC transmitted power was also examined. The results and analysis of these simulations were shown in paragraph 4.5.

The conclusions drawn from the result analysis in this chapter will be presented in chapter 5.

5. Conclusions and Future research

5.1 Conclusions

The present thesis has stressed out two main topics. First, a sensitivity analysis on important control parameters related to the short circuit reactive current injection of the VSC-HVDC link is performed. The boundary condition for this study is the compliance of the VSC-HVDC link with typical grid code requirements. As introduced in chapter 3, the parameters of the AC voltage controllers, the over-current capability of the converters and the current limitation strategy applied are examined. The effect of these parameters on the Dutch and German system's voltages and the rotor angle response of the Dutch and German generators after the occurrence of a symmetrical three phase fault was examined.

In addition, the outage of Corridor A (i.e due to a failure of the HVDC converters or as a result of a fault at the connection point of the converters) is examined. The study focuses on the impact from an outage of Corridor A on the rotor angle stability of large conventional generators in the Netherlands and Germany. Additionally the effect of this outage on the power flows of the AC interconnectors between the Dutch and German system was observed. The loss of Corridor A was examined for various loading cases including the scheduled loading (2000 MW) but also higher ones (3000, 4000, 5000 and 6000 MW).

The main conclusions of the aforementioned studies are presented in this paragraph.

Conclusions on sensitivity analysis

Regarding the AC voltage control parameters, it was observed that the higher the amount of reactive current injection, the better is the voltage support by means of keeping the system's voltages during a fault at values closer to the pre-fault values. A high value of short circuit reactive current can be accomplished through high values of the k gain and the over-current capability and by a current limitation strategy set to reactive current priority. The high value of the k gain will ensure a high amount of short circuit reactive current injection for a given voltage drop during a fault. A high value of the over-current capability gives more space for the short circuit reactive current component to increase and therefore attain a higher value. Finally the reactive current priority maintains the reactive current component of the converter constant once the over-current capability is reached and reduces only the active current component.

An important conclusion regarding the voltage support during AC system faulted conditions is that it is regional to the area electrically close to the converters. The voltage support at buses that are not located close to the HVDC converters is marginal to moderate, even for high values of the k gain. Therefore, the voltage response at the majority of the buses in the Dutch transmission system is not sensitive to the control parameters applied at VSC-HVDC link.

Concerning the influence of the control parameters on the rotor angle response of generators the situation is more complex. In general the rotor angle response depends on many parameters, however the examined parameters influence it through the effect they have on the system's voltage and the generation-load balance in the area near the HVDC converters.

First it was observed that the deviation of the first peek of the rotor angle's response becomes smaller as the voltage support of the system's voltages becomes more effective. This happens because the smaller voltage dip at the generator terminals results in a smaller disturbance of the generator leading to a smaller rotor angle deviation. On the other hand it was seen that the generation-load balance in an area can affect the speed of the generators. HVDC lines can affect the generation-load balance depending on the active current output of its converters since the sending HVDC converter is perceived by the power system as a load while the receiving HVDC converter is perceived as a generator.

If the current limitation strategy is set to equal or reactive current priority and an active current reduction takes place, as a result of reaching of the over-current capability limit during faulted condtions, there will be an acceleration of the generators located close to the sending converter and a deceleration of generators located close to the receiving converter. This acceleration/deceleration is strongly related to the rotor angle response of the generators. The amount by which each factor affects the rotor angle response depends on the distance of the generators from the fault and the HVDC converters as well as the operating point of the HVDC converter (whether it is in sending or receiving mode).

Generators that are located near the HVDC converters are mainly influenced by the active current reduction in the converters while generators located far from the converters are mainly influenced by the voltage profile of the system's buses. Therefore the majority of generators in the Netherlands, with the exception of the generators in the area of Eemshaven, are mainly affected by the voltage improvement. Active current reduction takes place in both the sending and receiving converter in order to maintain the DC voltage in the HVDC line, therefore generators in both ends of the HVDC line will be affected by it. In general it is expected that when active current reduction takes place in the HVDC converters, as a result of the total current output reaching the over-current capability limit, the first peak of the rotor angles will increase in generators located close to the sending converter and it will decrease for generators located close to the receiving converter. This pattern however is not always followed because depending on the location of the generator from the HVDC converters, the rotor angle influencing factors (voltage profile and generation-load balance) affect each generator by a different amount.

The results indicate that in most monitored generators (including the generators in Eemshaven) the rotor angle peaks increased due to active current reduction. Therefore following a conservative approach it is recommended to avoid if possible the reaching of the converter over-current limit and if that is not possible (as a result of a fault) then it is recommended to reduce the amount of active current reduction. Taking into account only the rotor angle stability, a small value of the k gain and a large value of the over-current limit is preferred in order to avoid or delay the reaching of the over-current limit. Additionally, the current limitation strategy should be set to active current priority in order to avoid active current reduction in case the over-current limit reaching cannot be avoided.

Observing the recommendations from both the voltage profile point of view and from the rotor angle stability point of view it can be seen that they are conflicting. It appears that a high short circuit reactive current and the subsequent active current reduction cannot achieve the best results for both the voltage profile and the rotor angle stability simultaneously. For this reason a compromise should be done. Taking this into account, the final recommendation for the sensitivity parameters is:

- A moderate value of the k gain (2-4)
- A high value of the converter's over-current capability
- A current limitation strategy set to equal current priority

A moderate value of the k gain can reduce the chance of reaching the converter's over-current capability and still offer an adequate voltage support during a fault. A high over-current capability is beneficiary for both the voltage profile and the rotor angle stability since it provides a higher margin for the reactive current to increase during voltage support and it can delay or even prevent in some cases the current limit reaching.

The technological and financial restrictions of increasing the over-current capability of converters above the current typical value of 1.15 p.u should be compared to the benefit on the voltage and rotor angle stability. Hence, a cost benefit analysis could be an option. Finally, the equal current priority is a compromise between the active and reactive current priorities. On one hand the reactive current component will be reduced, but in this case by a smaller amount than in active priority leading to an adequate voltage support. On the other hand the active current reduction will be smaller than in reactive current priority leading to a smaller acceleration of the sending end generators and consequently to a smaller rotor angle peak than in the case of reactive current priority.

The above recommendations have been decided mainly observing the response of the German transmission system and the area of Eemshaven in the Netherlands. A general observation from the results is that the effect of the VSC-HVDC converters is quite regional in the sense that the effect of the voltage support is more pronounced in the buses located electrically close to the HVDC converters. The effect for example of the voltage support of Corridor A's converters, during a fault, is very small in e.g the Krimpen aan den IJssel 380 KV bus in the Netherlands. Even in the event of faults located near an HVDC converter that will cause the converter to generate a greater amount of additional reactive current for voltage support, the effect of the voltage support fades away as the distance from the converter increases. The influence of the examined sensitivities is small also in the rotor angle response of the majority of Dutch generators since as already mentioned, their response is mainly influenced by the voltage support which is small regardless of the selected sensitivity parameters.

This leads to the conclusion that Corridor A's effects on the voltage profile and rotor angle response of the Dutch transmission system is rather small.

Conclusions on loss of Corridor A

Concerning the loss of Corridor A, it is observed that in the case of an exporting scenario for the Netherlands, it cannot jeopardize the rotor angle stability of the Dutch system even in the case that both sections are lost simultaneously. As a matter of fact, it was seen that the grid can cope with the sudden outage of both sections of Corridor A, even if it were to transfer power higher than the planned value of 2000 MW.

Additionally it was seen that the loss of Corridor A impacts the loading of the lines interconnecting the Dutch and German transmission system. However no reversal of the power flow was witnessed (the Netherlands keep exporting power to Germany in all cases) and the maximum transfer capacities of the lines were not violated. At least for the snapshot studied.

On the other hands the electro-mechanical oscillations which are triggered as a result of corridor A outage on the interconnection lines demonstrates poor damping.

The later in situations where the AC interconnector is heavily loaded may trigger the protection schemes and outage of the lines. Further investigation should be done in order to determine if this is caused by the modeling of the transmission system or due to issues in the actual system.

The above conclusions, on the effects of the loss of Corridor A, regard the specific "snapshot" of the system, i.e the specific generation-load scenario. For another scenario, where for example the Netherlands are importing and not exporting power from Germany, the above conclusions might not be valid. A thorough analysis of the effects of the loss of Corridor A on the system's transient stability should be done in order to draw safer conclusions.

5.2 Recommendations for future research

In this paragraph some recommendations for continuing the present study are done.

- As mentioned in previous chapters, PSS®E's point-to-point VSC-HVDC line model has a weakness in coordinating the active current reduction of the converters when one of them reaches its current limit. This can lead to a small voltage jump in the area of the non-limit-reaching converter. A recommendation for future work is therefore to validate the results of this study by using a user-written VSC-HVDC line model that overcomes this weakness. This can be done by modeling the DC side dynamics of the HVDC line.
- As mentioned in chapter 1, Corridor A is only one of the four planned HVDC corridors in Germany. It would be interesting to add the rest of these HVDC corridors in the German transmission system model. This would give a more realistic representation of the situation of the future transmission system and also would allow the examination of the interactions of the VSC-HVDC lines and their total effect on the interconnected transmission systems of Germany and its neighboring countries.
- In this present study, three current limitation strategies where examined, namely, active, equal and reactive current priority. This study could be extended by examining also other current limitation strategies such as blocking the converter's active current component during the fault **[37]**. Additionally the effect of a deadband on the voltage support during a fault could be examined **[47]**.
- Finally the effects of the loss of Corridor A on the systems transient stability could be studied for other generation-load scenarios of the system. Different generation-load scenarios will change the operating point of the system and thus a loss of Corridor A could compromise the secure operation of the system and lead it to instability.

APPENDIX A: Power system stability

A general definition of power system stability is the ability of the power system to remain in a state of operating equilibrium under normal operating conditions and to regain an acceptable state of equilibrium after being subjected to a disturbance **[18]**. This definition gives a generalized and holistic definition of power system stability and indeed power system is a single problem. However instability problems can manifest themselves in various ways. Therefore a categorization of stability based on the nature of the resulting instability, the size of the disturbance and the time-frame that should be taken into consideration, can help the analysis of power system stability. A categorization of power system stability can be seen in figure A.1.

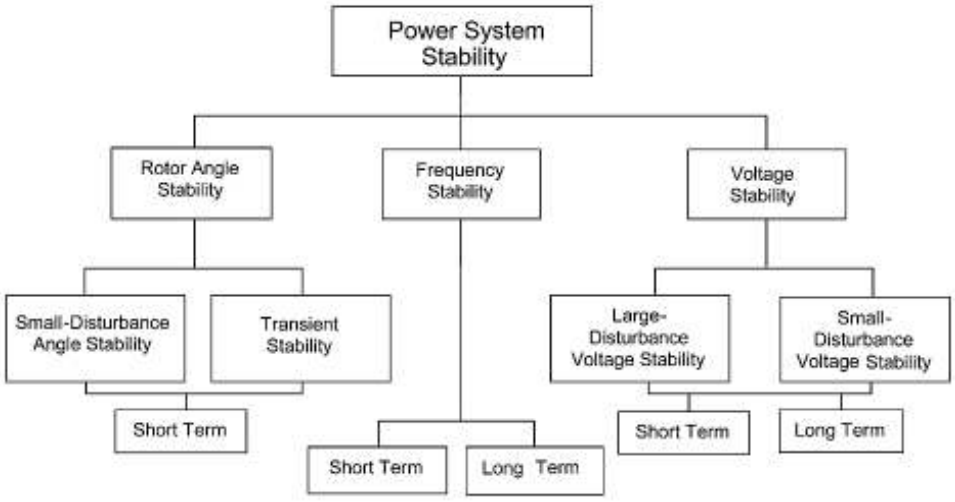

Fig. A.1 Categorization of power system stability [39]

Rotor angle stability

Rotor angle stability is the ability of interconnected synchronous machines to remain in synchronism after a disturbance. **[18]** When the equilibrium between electromagnetic and mechanical torque is lost, some generators will accelerate while others decelerate. The change of speed will not be the same for each generator and thus the angular separation of the rotor angles between some generators will increase. If the angular separation increases beyond a point, some generators will not be able to create a sufficient amount of restoring torque and some generators will lose synchronism.

Rotor angle stability can be categorized as small-signal stability and transient stability. Small signal rotor angle stability is the ability of the system to maintain synchronism after a small disturbance occurs. Small disturbances can be a small variation in the generation or the load.

Transient rotor angle stability is the ability of the system to maintain synchronization after a large disturbance. Large disturbances can be one, two or three phase faults (bus or line faults), loss of a generation unit etc. The time frame of interest for transient stability studies is usually a few seconds.

Figure A.2 presents some cases of instability. Case 1 represents a stable situation, while cases 2 and 3 represent unstable situations occurring after a transient disturbance.

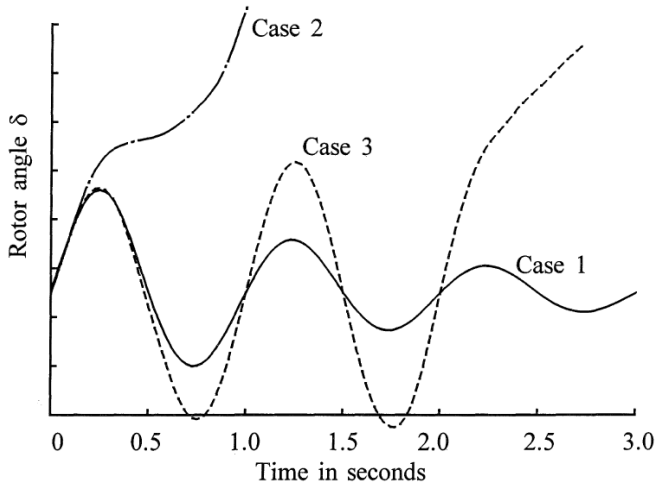

Figure A.2 Rotor angle response as a result of a transient disturbance [18]

In Case 2 the rotor angle of a generator increasessteadily after the occurance of a transient disturbance until synchronism is lost. This type of instability is referred to as first swing instability and is the subject of focus of this thesis.
Case 3 is stable regarding the first swing but reaches instability after some time due to a continuously increasing amplitude of the rotor oscillation. This type of instability is a result of small signal instability issues. **[18]**

Voltage stability

Voltage stability is the ability of the power system to maintain steady acceptable voltages at all buses in the system during steady state and after disturbances **[18]**. Voltage instability practically means that due to a change in the load demand or system conditions the system voltages drop uncontrollably. According to **[40]** voltage instability occurs due to the attempt of dynamic loads to restore their power consumption beyond the capability of the transmission and generation system.
Voltage instability is mainly a local phenomenon but its effects can spread to the whole system. Such a situation can be voltage collapse where a series of events can lead to an unacceptably low voltage profile in a wide area of the grid. Reasons that may lead to voltage collapse are the attempt of dynamic loads, such as induction motors that adjust their slip and thermostatic loads, to restore their consumption but also tap changing transformers that attempt to raise the distribution voltage.
Just like rotor angle stability, voltage stability can be categorized as large disturbance or small disturbance voltage stability. Additionally voltage stability can be categorized according to the time frame of interest. **[39]**

Frequency stability

Frequency stability describes the ability of the system to maintain its frequency stable after a disturbance that leads to an imbalance between generation and load. Frequency stability issues emerge due to inadequacies in equipment responses, poor coordination of protection and control devices, or deficiency of active/reactive power reserves. Frequency stability can be categorised in short term and long term stability.

APPENDIX B: Alternative HVDC technologies

B.1 VSC converter types

The modular multi-level VSC converter introduced in paragraph 2.1.2 is a relatively new concept. Other older, but well tested converter types, are the two-level and three-level converters. A presentation of these converter types will be done in this paragraph.

Two-level converters

In paragraph 2.1, it was explained that the main module of a two-level VSC is the Graetz bridge. The bridge for a VSC is shown in fig. B.1.

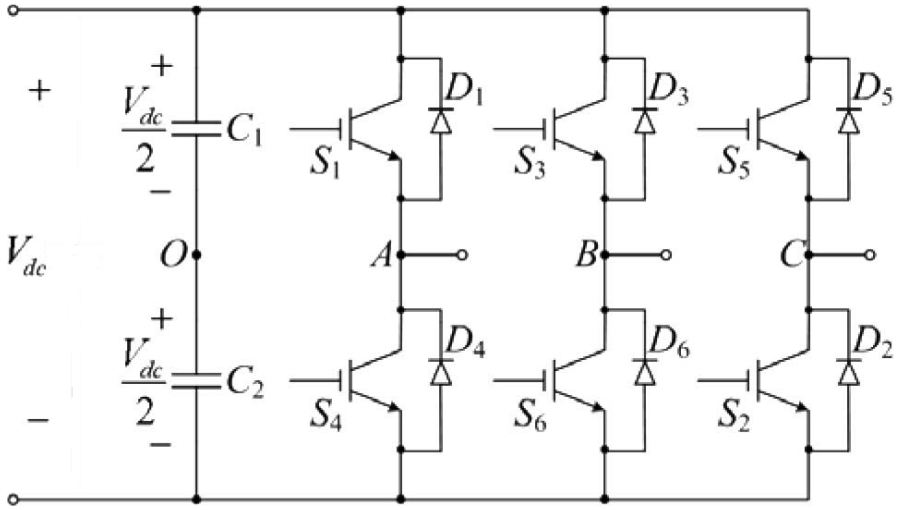

Fig. B.1 VSC-HVDC bridge [22]

The switches can conduct only in one direction, therefore anti-parallel diodes are connected to each switch in order to allow flow of the current in both directions, while the bridge voltage has one polarity. This ensures the four quadrant operation of the converter. The DC capacitor stores energy in order to allow control of the power flow and also filter DC harmonics. There are only four possible states of conduction for each phase as can be seen in fig. B.2 (a).

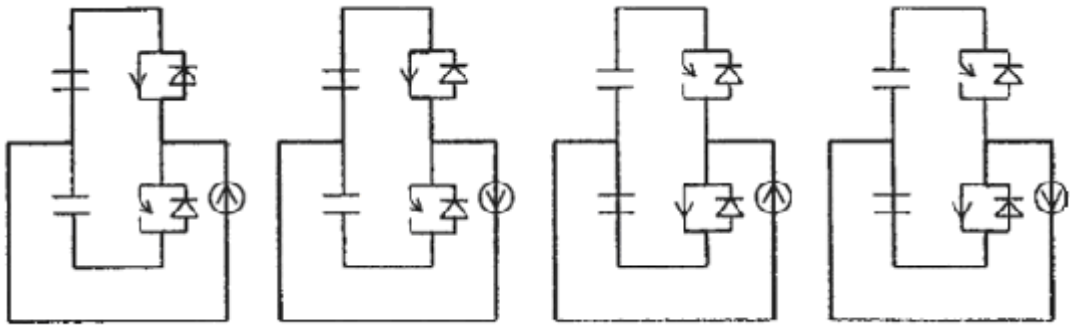

(a)

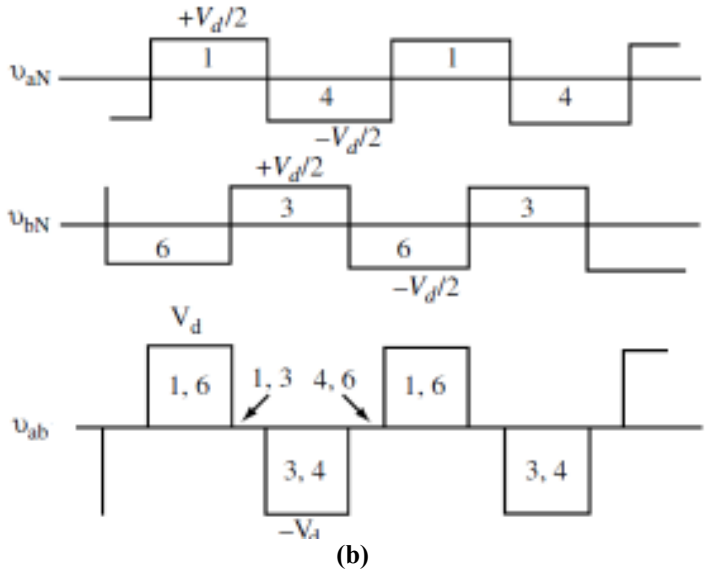

Fig. B.2 One phase of two-level converter: (a) Conduction states, (b) Output voltages

Two switches in the same phase of the bridge must not be closed at the same time since then the DC side capacitor will be short-circuited and this will create a high discharge current which is dangerous for the switches. In order to avoid this a blanking time of a few microseconds is introduced between the switching of the switches. **[17]**

When the upper switch is closed and the lower is open, the AC output is connected to the positive DC capacitor voltage $V_{dc}/2$ while for the opposite switch state the output voltage is connected to $-V_{dc}/2$. The resulting AC voltage can be seen in fig. B.2 (b). Depending on the current direction, it will flow through the switch or the anti-parallel diode.

A drawback of anti-parallel diodes is that during a DC fault they create a current path. This current has to be cleared by the AC circuit breakers, since no reliable DC circuit breakers technology exists yet. This fault current can be hazardous for the switches which have a limited current tolerance. **[17]**

The waveforms shown in figure B.2 represent a simple switching scheme that results in square waveforms. In order to improve the harmonic content the PWM switching technique is used. In this switching technique a control signal is compared with a triangular waveform, known as carrier signal, in order to generate switching signals for the switches. In order to accomplish a sinusoidal fundamental frequency component of the output, the control signal must also be sinusoidal **[34]**. The principle of PWM can be explained through figure B.3 and equations B.1.

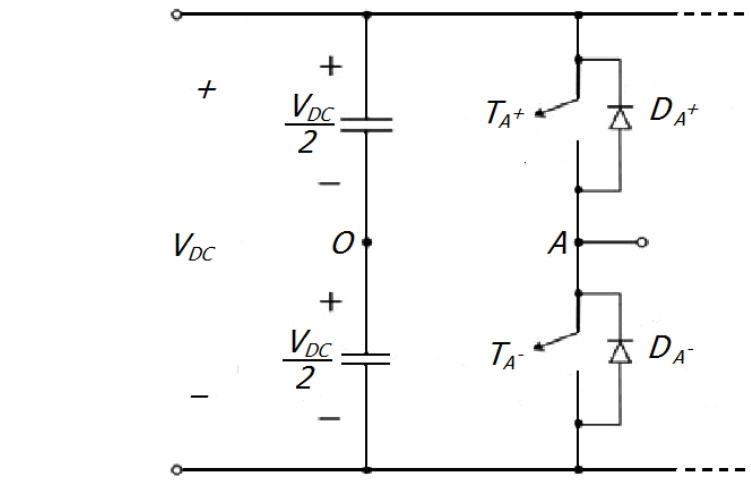

(a)

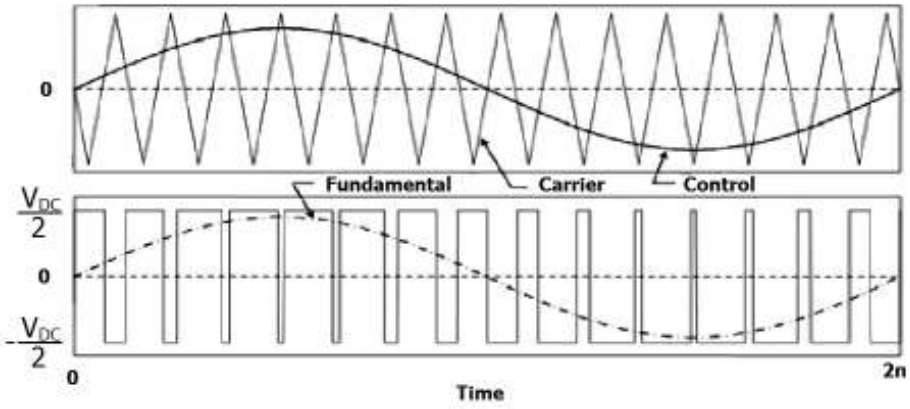

(b)

Fig. B.3 (a) One leg of VSC converter, (b) Carrier and Control signals and phase to neutral voltage output

$$v_{control} > v_{triangular}\ ,\ T_{A+}\ is\ on\ \Rightarrow v_{Ao} = \frac{V_{DC}}{2}$$
$$v_{control} < v_{triangular}\ ,\ T_{A-}\ is\ on\ \Rightarrow v_{Ao} = -\frac{V_{DC}}{2} \qquad \text{(B.1)}$$

Switching frequencies used in this technique are usually around 1-2 KHz and the resulting harmonics are multiples of this frequency **[21]**. This is an important feature of PWM since harmonics of high frequency are in general easier to filter. Also by appropriate selection of the switching frequency harmonics of even order disappear completely from the output, leading to less harmonic content **[34]**. On the other hand high switching frequencies result in higher switching losses. Since high switching frequencies are used, the use of IGBTs is favoured. In order to withstand the high voltages used in HVDC transmission each switch consists of a series connection of many IGBTs. For instance in the original HVDC light (a VSC-HVDC transmission system developed by ABB) 300 series connected IGBTs per switch where used for a 150 kV scheme. **[8]**

The main advantage of the two-level VSC-converter is its simplicity. However it has some serious disadvantages such as high blocking voltage of semiconductor switches and highly non-sinusoidal output AC voltage. **[21]**

Three-level converters

The high blocking voltage and dv/dt applied to the switches of a two-level converter as well as the highly non-sinusoidal AC output waveform of two-level converters can be improved by increasing the number of voltage levels of the converter's output. Three-voltage level converters are a solution towards this direction. There is a number of available circuits used for three level VSC converters. The most used ones are the Neutral point clamped (NPC) converter and the flying capacitor converter **[22]**. The output of three-level converters approaches that of a sinusoid more than the output of a two level converter, however the harmonic content is still high, therefore PWM is still needed in lower switching frequencies however, than in two-level schemes. Therefore switching losses are reduced **[8]**.

The topology of one phase leg of a three level diode clamped converter is shown in fig. B.4 (a).

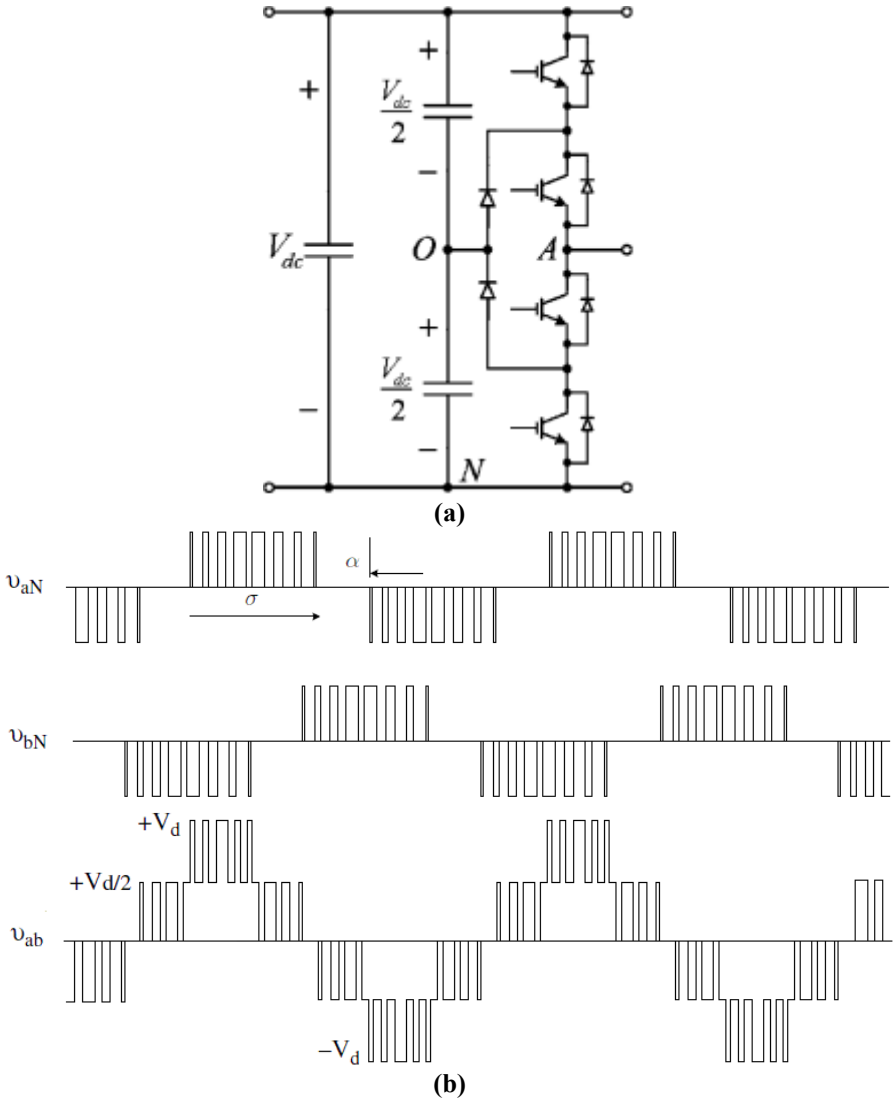

Fig. B.4 One phase of three-level diode clamped converter: (a) Conduction states, (b) Output voltages

The phase voltage consists of a positive, negative and zero level. The positive level is accomplished when the two upper switches are switched on, while the negative

voltage level is accomplished by switching on the two lower switches. By switching on the upper and lower middle valves the zero level is achieved.

The RMS value of the fundamental voltage component depends on the conducting time of the top upper and bottom lower switches (represented by σ). Specific harmonics of the output can be eliminated by selecting appropriate values for the zero-voltage time (represented by α). **[8]**, **[23]**

A problem of the diode clamped converter is the uneven distribution of losses across its devices. This can be solved by replacing each center tap diode by a switch-antiparallel diode set. This converter is known as an actively clamped neutral point clamped converter (ANPC) **[22]**.

The other topology for three-level VSC converters is the flying capacitor converter. One phase leg of this converter is presented in fig. B.5.

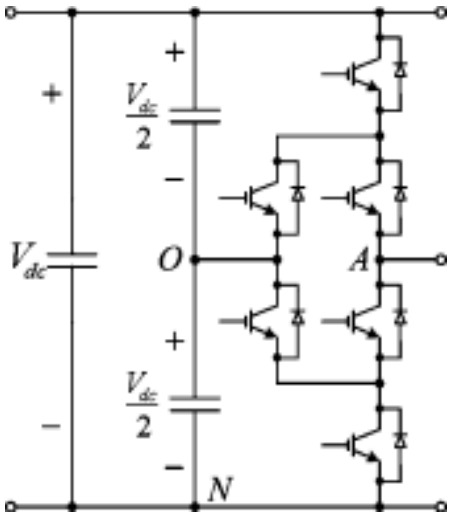

Fig. B.5 One phase of three level flying capacitor converter

The AC voltage waveforms of this topology are exactly the same as for the NPC. No diodes are used to clamp the voltage. In order to achieve the intermediate voltage level an extra capacitor per phase leg is used which is charged at half the DC voltage level. To achieve the $+V_{dc}/2$ voltage level, the top switches of the upper and lower switch pairs must be turned on. The negative voltage level $-V_{dc}/2$ is reached when the bottom switches of the upper and lower switch pairs must be turned on. The zero voltage level is achieved when the top switch of the upper pair and the bottom switch of the lower pair are turned on or when the bottom switch of the upper pair and the top switch of the lower pair are turned on. Due to the extra capacitor per phase leg the capacitive rating of this converter is considerably higher than that of the NPC. **[8]**, **[23]**

B.2 Comparison of LCC and VSC HVDC

Due to the different converter technologies used in LCC and VSC HVDC transmission systems, they exhibit substantial differences in their operation.

The main reason that causes these differences is that the commutation of the thyristor valves used in LCC depends on the AC system's voltage while the valves of VSCs can commute independently of the AC voltage. This characteristic leads LCC HVDC converters to always consume reactive power. As a matter of fact the

consumption of reactive power of the LCC converter is proportional to the transferred active power.

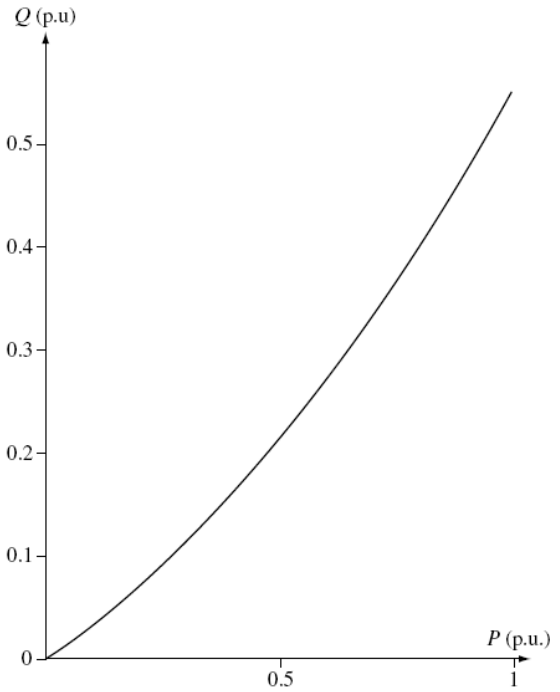

Fig. B.6 LCC HVDC link reactive power consumption over active power [8]

VSC HVDC links on the other hand have the inherent ability of controlling active and reactive power independently. This means that VSCs can not only absorb but can also generate reactive power if needed and any change in reactive power can be done without affecting the active power conversion.

The dependency of reactive power consumption and active power conversion in LCC HVDC links is the reason why they cannot be connected to weak AC systems with a low Short Circuit Ratio (SCR). The SCR is defined as the ratio of the system's short circuit power and the HVDC converter's power rating. The voltage of systems with a low SCR (lower than 2) are more sensitive changes in reactive power. When a LCC HVDC link connected to a low SCR system changes its active power conversion then its reactive power consumption will change according to fig. B.6 and this will lead to voltage fluctuations; these voltage drops cause additional reactive power consumption leading to further reduction of voltage and finally voltage instability. VSC HVDC links have solved the commutation problems that LCC-HVDC systems face when connecting to low SCR systems. Despite this fact weak AC systems can affect negatively in other ways the VSC-HVDC. One of the major advantages of VSC-HVDC systems is the independent control of active and reactive power, however according to **[36]** weak AC systems can result in interactions between active and reactive power controllers. Also, weak AC systems are characterized by a high system impedance at the connection point, which can limit the active power transfer.

Due to the high harmonic content and low switching frequencies the AC output of LCC HVDC systems needs heavy harmonic filtering. The capacity of the needed filters may reach 20% to 30% of the converter's rating. Thanks to PWM the AC output of VSC HVDC systems is filtered easier than that of LCC HVDC and in case a MMC converter is used the filtering might be completely eliminated.

The heavy filtering required for LCC HVDC in combination with the shunt capacitors that compensate the reactive power absorption of the converters increase the footprint of LCC HVDC converter stations in comparison to that of VSC HVDC stations. Actually the converter station size of the LCC HVDC can be up to four times bigger than that of a VSC HVDC **[29]**.

Another difference in the operation of LCC and VSC HVDC systems is that during a short circuit on the AC system commutation failure can occur in the valves of the LCC. The VSC on the contrary can continue operating but with limited output due to the reduced voltage.

From the above it seems that LCCs are inferior to VSC HVDC systems, however LCCs have some advantages over VSCs. First of all the current and blocking voltage ratings of thyristors are currently higher than those of IGBTs. As a concequence higher power transfer at higher voltage levels can be accomplished by using LCC HVDC systems. At present the maximum rating for LCC HVDC is 6400 MW at 800 kV while for VSC HVDC (two-level) it is 1200 MW at 320 kV. **[29]**

Another advantage of LCC HVDC is that it has lower switching losses than VSC HVDC due to low switching frequencies.

A comparison of LCC and VSC HVDC regarding system compatibility, environmental impact, cost effectiveness and technical characteristics is done in **[30]**. The system compatibility criterion involves elements such as reactive power behaviour, behaviour in the event of failure, effect of short circuit level, load flow controllability and impact on system reliability. The environmental impact criterion focuses on issues such as land use, ecological impact during normal operation and in the event of failure. The cost effectivness criterion focuses on investment, operating and loss costs for a period of 40 years. Finally the technical characteristics criterion, examines elements such as civil engineering, construction time, life expectancy, operational experience and fault clearance costs.The comparison is done regarding a general onshore transmission scenario of 4000 MW transmission capacity and 400 kV voltage level.

Regarding system compatibility VSC-HVDC is considered a better solution especially when it is based on underground cables. Regarding the environmental impact LCC HVDC combined with overhead lines scores higher, meaning that it affects the environment the most while on the other hand VSC HVDC with underground cables has the least environmental impact. However LCC HVDC using overhead lines is the most cost effective alternative and has at the same time the best technical characteristics.

APPENDIX C: Control of VSC-HVDC links

The control of the VSC-HVDC systems is one of its most important aspects since its control affects the way it influences the AC system in steady state but also in transient situations.

There are more than one control strategies available for VSC-HVDC systems:

- Power-angle control
- Vector control

From the above methods, vector control is traditionally used in VSC-HVDC applications and thus will be explained in detail in paragraph C.1.1.

The power-angle control is the simplest method to control a VSC-HVDC system. The main idea behind this control method comes from the equations describing the power transfer across a transmission line **[41]**:

$$P = \frac{V_1 V_2 \sin\theta}{X} \tag{C.1}$$

$$Q = \frac{V_1^2 - V_1 V_2 \cos\theta}{X} \tag{C.2}$$

where V_1 and V_2 are the voltages in the sending and receiving end of the transmission line, θ is the phase difference between the two voltages and X is the reactance of the line. The resistance of the line R, is neglected because in most cases its value is very small compared to that of its reactance X for transmission systems. Equations (C.1) and (C.2) can be applied on the phase reactor of the VSC-HVDC system and then V_1 will represent the voltage at the PCC, V_2 the converter voltage and X the reactance of the phase reactor.

If the derivatives $\frac{\partial P}{\partial \theta}, \frac{\partial P}{\partial V_2}, \frac{\partial Q}{\partial \theta}, \frac{\partial Q}{\partial V_2}$ are computed it can be seen that the active power P, is more sensitive to the phase angle θ and that the reactive power is more sensitive to the voltage magnitude. Therefore active power can be controlled through the phase angle of the converter voltage and reactive power through the magnitude of the converter voltage using Proportional-Integral (PI) controllers. In fact, in order to create 3-phase alternating voltages the converter needs three variables, voltage magnitude, voltage angle and frequency. The voltage amplitude is given by a voltage or reactive power controller, voltage phase is given by an active power controller and frequency is calculated by a Phase-Locked Loop (PLL).

Although Power-angle control is simple to implement it has some important drawbacks. First of all, this control method has no means of damping resonances in the AC system which makes the bandwidth of the controller very limited. Additionally there is no way in limiting the valve current in the converter. This can be dangerous for the converter during disturbances. For the aforementioned reasons Power-angle control has never been implemented for VSC-HVDC transmission schemes.

Besides the traditional control strategies mentioned above, a variety of novel control schemes can be found in literature. Some of these are the *Non-linear Lyapunov based control* **[42],** H_∞ *control* **[43]** and *Power-synchronization control* **[41]**. Although these

methods can theoretically enhance the behavior of the VSC-HVDC system, e.g overcome difficulties the vector control has when connected to weak systems, they haven't been applied in any HVDC system yet.

C.1.1 Vector control

The control scheme of a VSC-HVDC system is cascaded. This means that it consists of various control levels connected in series. The output of each level acts as an input to the next one. The lower the level the faster its response. Vector control consists of four control levels which are presented from higher to lower level [32]:

- Supplementary controls
- Outer control
- Inner current control
- Firing pulse control

The firing pulse control is the lowest level and acts in a time scale of a few micro seconds (μs). This control level is responsible for supplying the converter with the correct firing pulse in order to create the voltage according to the reference value. The inner current control level is slower than the firing pulse level. It acts in a time scale of a few milliseconds. It creates the voltage reference value needed for the firing pulses. The outer control level's time response is less than a second but slower than the inner current control. It creates the current references needed by the inner current loop. Finally the VSC-HVDC system's control can have a supplementary control level which can implement frequency control, oscillation damping etc. Its time response is of a few seconds.

The whole control system can be seen in fig. C.1.

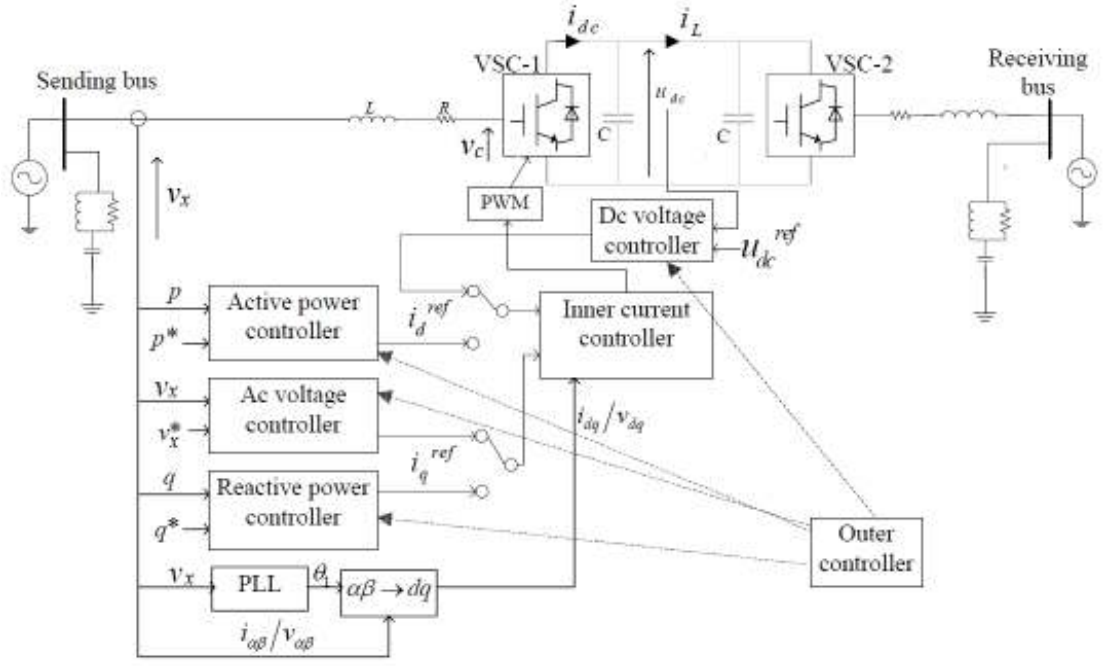

Fig. C.1 Control system of VSC-HVDC [44]

The vector control technique was initially applied in variable speed drive applications, where a VSC controlled an AC machine. The use of vector control to

VSC-HVDC transmission is a dual application to that of the variable speed drive application. Through vector control active and reactive power can be controlled independently from each other through the inner current control loop. This will be explained further in the following analysis.

The basic idea behind vector control is the d-q reference frame. A 3-phase quantity can be represented through Clarke's transformation as an equivalent 2-phase quantity in a stationary reference frame α-β. The conversion can be done according to equation C.3:

$$X_{\alpha\beta} = X_\alpha + jX_\beta = k(X_a + X_b e^{j\frac{2\pi}{3}} + X_c e^{\frac{4\pi}{3}}) \qquad \text{(C.3)}$$

where X represents a general 3-phase and 2-phase quantity and the subscripts denote the reference frame. k is a real number that can be equal to either $\frac{2}{3}$ or $\frac{\sqrt{2}}{3}$. When k is equal to $\frac{2}{3}$ the transformation is voltage invariant, while in the other case it is power invariant. The following analysis is done using the voltage invariant transformation.

Equation (C.3) can be expressed in matrix form:

$$\begin{bmatrix} X_\alpha \\ X_\beta \end{bmatrix} = k \begin{bmatrix} 1 & -\frac{1}{2} & -\frac{1}{2} \\ 0 & \frac{\sqrt{3}}{2} & -\frac{\sqrt{3}}{2} \end{bmatrix} \begin{bmatrix} X_a \\ X_b \\ X_c \end{bmatrix} \qquad \text{(C.4)}$$

The next step is to convert the quantities into a rotating d-q reference frame through Park's transformation. The converter creates a rotating d-q reference frame which rotates in a speed equal to the synchronous speed and its phase is adjusted in such a way that the d-axis is always aligned with the filter bus voltage. The synchronization of the converter's d-q reference frame is accomplished via a PLL. The reason this reference frame is chosen will become clear in the analysis to follow.

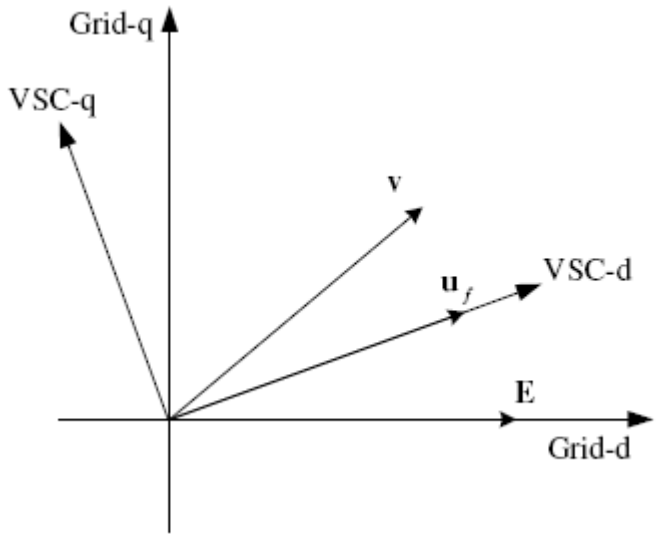

Fig. C.2 Converter d-q reference frame

The conversion from the α-β to the d-q reference frame is done by Park's transformation, which is presented in equation (C.5):

$$\begin{bmatrix} X_d \\ X_q \end{bmatrix} = \begin{bmatrix} \cos\theta & \sin\theta \\ -\sin\theta & \cos\theta \end{bmatrix} \begin{bmatrix} X_\alpha \\ X_\beta \end{bmatrix} \tag{C.5}$$

where θ is the angle between the α-β and d-q reference frames. θ=ωt and ω is the rotation speed of the d-q frame.

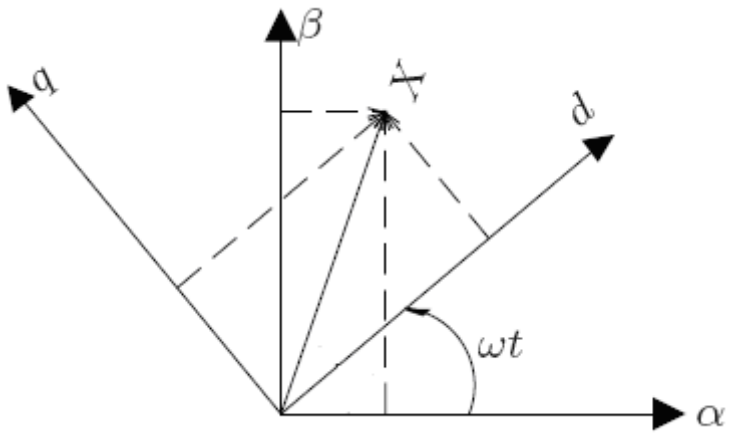

Fig. C.3 Relative position between α-β and d-q reference frames

Equation (C.5) can be easily written in complex phasor form as:

$$X_d + jX_q = (X_\alpha + jX_\beta)(\cos\theta - j\sin\theta) \Rightarrow$$
$$\vec{X}_{dq} = \vec{X}_{\alpha\beta} \cdot e^{-j\theta} \tag{C.6}$$

In order to find the equations that characterize the VSC-HVDC's vector control **[45]**, **[46]** let us focus on the phase reactor which is located between the converter and the PCC.

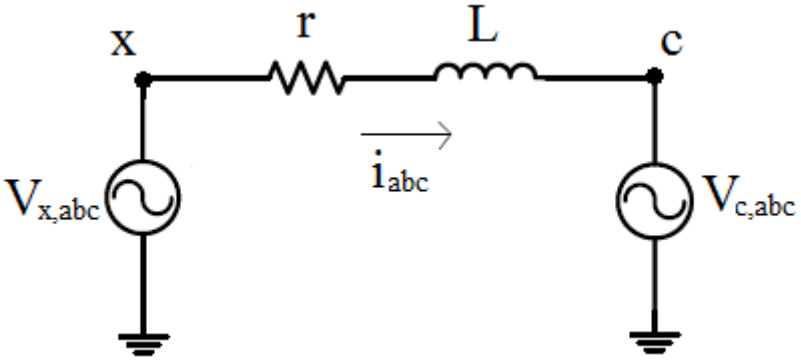

Fig. C.4 VSC-HVDC AC side

In fig. C.4, x represents the PCC and c the AC terminal of the VSC. L and r are the resistance and reactance resulting from the series connection of the phase reactor and the converter transformer's inductance.

Applying Kirchhoff's voltage law in the above circuit, equation (C.7) occurs:

$$V_{x,abc} - V_{c,abc} = ri_{abc} + L\frac{di_{abc}}{dt} \tag{C.7}$$

where the subscript abc means that the quantities are expressed in the 3-phase reference system.

By applying Clarke's transformation in equation (C.7) we get:

$$V_{x,\alpha\beta} - V_{c,\alpha\beta} = ri_{\alpha\beta} + L\frac{di_{\alpha\beta}}{dt} \tag{C.8}$$

Using equation (C.6) on equation (C.8) we get:

$$V_{x,dq}e^{j\omega t} - V_{c,dq}e^{j\omega t} = ri_{dq}e^{j\omega t} + L\frac{d(i_{dq}e^{j\omega t})}{dt} \Rightarrow$$

$$V_{x,dq}e^{j\omega t} - V_{c,dq}e^{j\omega t} = ri_{dq}e^{j\omega t} + j\omega tLi_{dq}e^{j\omega t} + e^{j\omega t}L\frac{di_{dq}}{dt} \Rightarrow \tag{C.9}$$

Finally by dividing equation (C.9) by $e^{j\omega t}$ we get:

$$V_{x,dq} - V_{c,dq} = ri_{dq} + j\omega tLi_{dq} + L\frac{di_{dq}}{dt} \tag{C.10}$$

Equation (C.10) can be written in matrix form:

$$L\frac{d}{dt}\begin{bmatrix} i_d \\ i_q \end{bmatrix} = \begin{bmatrix} V_{x,d} \\ V_{x,q} \end{bmatrix} - \begin{bmatrix} V_{c,d} \\ V_{c,q} \end{bmatrix} - r\begin{bmatrix} i_d \\ i_q \end{bmatrix} - \omega L\begin{bmatrix} 0 & 1 \\ -1 & 0 \end{bmatrix}\begin{bmatrix} i_d \\ i_q \end{bmatrix} \tag{C.11}$$

Now, the apparent power is given by equation (C.12):

$$S = \frac{3}{2}V_{x,dq}i_{dq}^{*} = \frac{3}{2}(V_{x,d} + jV_{x,q})(i_d - ji_q) \tag{C.12}$$

The factor 3/2 is present because the voltage invariant transformation is used and not the power invriant.

It is therefore concluded that the active and reactive power are given by the following equations:

$$P = \frac{3}{2}(V_{x,d}i_d + V_{x,q}i_q) \tag{C.13}$$

$$Q = \frac{3}{2}(V_{x,q}i_d - V_{x,d}i_q) \tag{C.14}$$

By choosing the d-axis of the d-q reference frame to coincide with the PCC voltage vector ($V_{x,d}=V_x$, $V_{x,q}=0$) we finally get:

$$P = \frac{3}{2} V_{x,d} i_d \qquad \text{(C.15)}$$

$$Q = -\frac{3}{2} V_{x,d} i_q \qquad \text{(C.16)}$$

From equations (C.15) and (C.16) it is clear that the active and reactive power can be controlled separately through the d and q components of the phase reactor current respectively. For this reason the d-component of the current is usually called the active current and the q-component is the reactive current.

C.1.1.1 Inner current loop

The inner current controller is based on equations (C.11), (C.15) and (C.16).
The inner current control loop has as inputs the current references in the d-q frame ($i_{d,ref}$ and $i_{q,ref}$) and creates the converter reference voltage ($v^*_{c,d}$ and $v^*_{c,q}$).

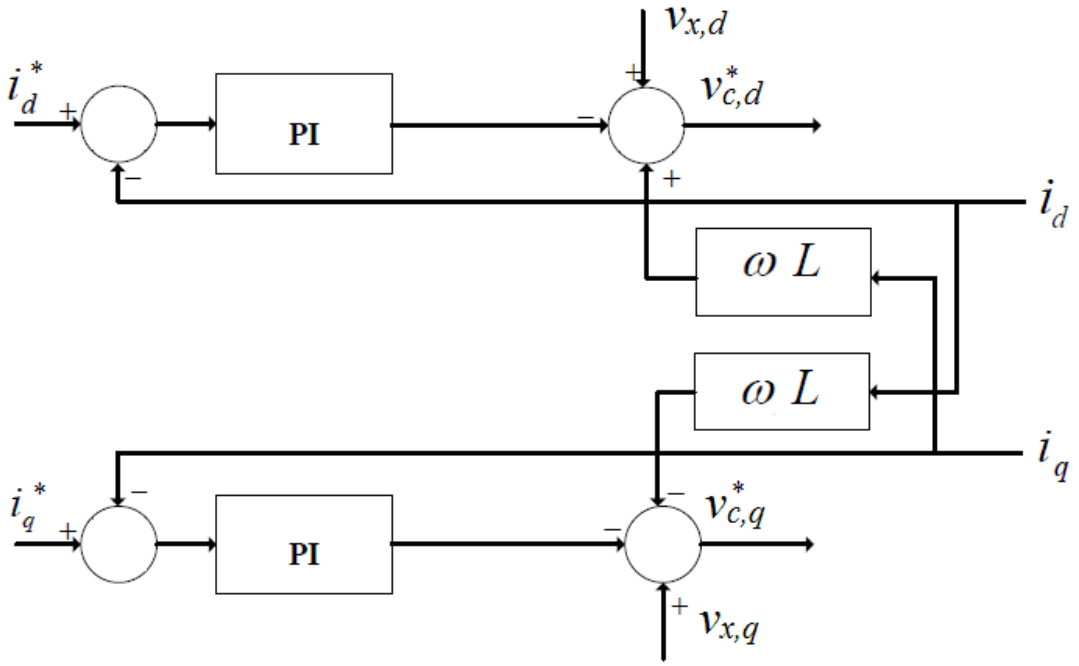

Fig. C.5 Inner current control loop

As can be seen from fig. C.5 the first stage of the inner current loop is a PI controller. In order to create the converter reference voltage, according to equation (C.11), the cross coupling terms $-\omega L i_q$ and $\omega L i_d$ and the PCC voltages $v_{x,d}$ and $v_{x,q}$ are added to the output of the PI controller.

The output of the inner current loop is fed into the firing pulse controller of the converter which creates the needed switching pulses.

C.1.1.2 Outer controllers

As mentioned earlier, the reference currents which act as an input to the inner current loop are created by the outer controllers. The outer controllers can control the converter's active power, DC voltage, AC voltage and reactive power. The active power and DC voltage are related to the active current reference while the reactive power and the AC voltage are related to the reactive current reference. Therefore each converter can control either the active power exchanged with the AC system or the DC voltage of the DC link but not both at the same time. Similarly each converter can control either the reactive power exchange with the AC system or the AC voltage at the PCC.

Active power control

As can be seen in equation (C.15) the active power is related to the active component of current. The simplest way to control active power is through an open loop controller. The equation describing the active power controller is given below:

$$i_d^* = \frac{P^*}{v_{x,d}} + (K_{p,d} + \frac{K_{i,d}}{s})(P^* - P) \qquad \text{(C.17)}$$

The block diagram of the active power open loop control is presented in figure C.6.

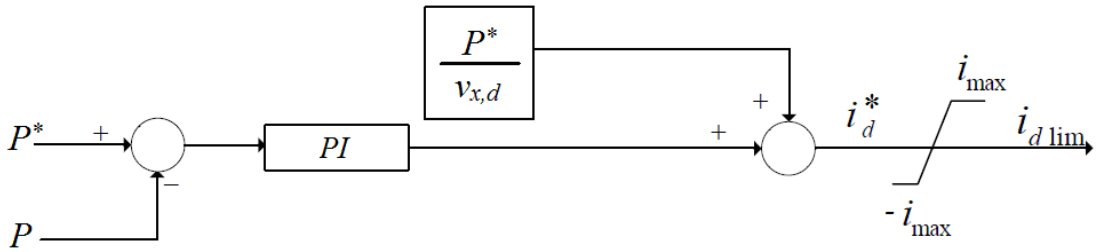

Fig C.6 Active power controller

A limiter is added in the output of the active power controller in order to avoid current in the switches of the converter.

DC voltage controller

Neglecting the converter losses, the losses in the phase reactor and the losses in the DC line the following equation is valid:

$$P_{AC} = P_{DC} \Rightarrow$$
$$\frac{3}{2} V_{x,d} i_d = V_{DC} I_{DC} \Rightarrow$$
$$I_{DC} = \frac{3V_{x,d}}{2V_{DC}} i_d \qquad \text{(C.18)}$$

The differential equation that describes the DC side capacitor's behaviour is given by equation (C.19):

$$C\frac{dV_{DC}}{dt} = I_{DC} - I_L \qquad \text{(C.19)}$$

Where I_{DC} is the current injected by the converter in the DC side and I_L is the current flowing in the DC line as can be seen in fig. C.1.

By integrating equation (C.19) over one switching period of the converter (Ts) and dividing by Ts we get **[46]**:

$$\frac{C}{T_s}[V_{DC}(k+1) - V_{DC}(k)] = \langle I_{DC} \rangle - \langle I_L \rangle \qquad \text{(C.20)}$$

Where $<I_{DC}>$ and $<I_L>$ are the mean values of I_{DC} and I_L respectively.
Assuming the system is in steady state $<I_{DC}>=I_{DC}$ and $<I_L>=I_L$.

Assuming there is one sample time delay in the controller the following is true:

$$V_{DC}(k+1) = V_{DC}^*(k) \qquad \text{(C.21)}$$

Combining equations (C.20) and (C.21) and assuming the system is in steady state equation (C.22) is formulated:

$$\frac{C}{T_s}[V_{DC}^*(k) - V_{DC}(k)] = I_{DC} - I_L \qquad \text{(C.22)}$$

Substituting equation (C.18) into (C.22) and solving for i_d we get:

$$i_d^* = K_{DC}(V_{DC}^* - V_{DC}) + K_L I_L \qquad \text{(C.23)}$$

Where $K_{DC} = \frac{2V_{DC}^* C}{3V_{x,d}T_s}$ and $K_L = \frac{2V_{DC}^*}{3V_{x,d}}$

From equation (C.23) the DC voltage controller of fig.C.7 is deducted.

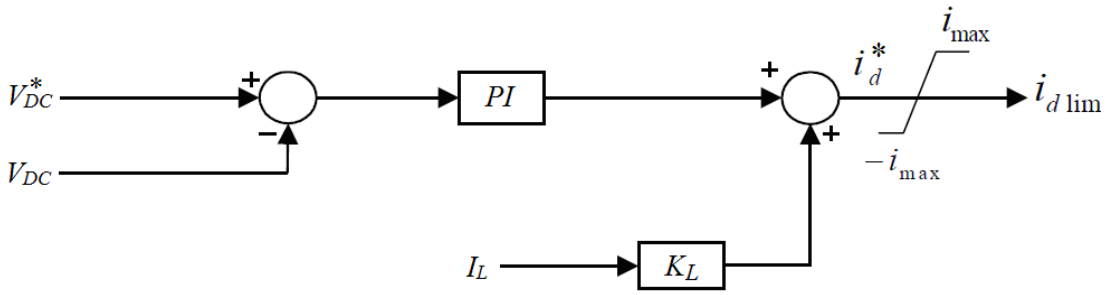

Fig C.7 DC voltage controller

Again as can be seen a current limiter should be used in the output of the controller.

Reactive power controller

From equation (C.16) it is clear that the reactive power the converter exchanges with the AC system is dependent on the reactive current component. In a similar way with the active power controller an open loop controller can be used to implement the reactive power controller.

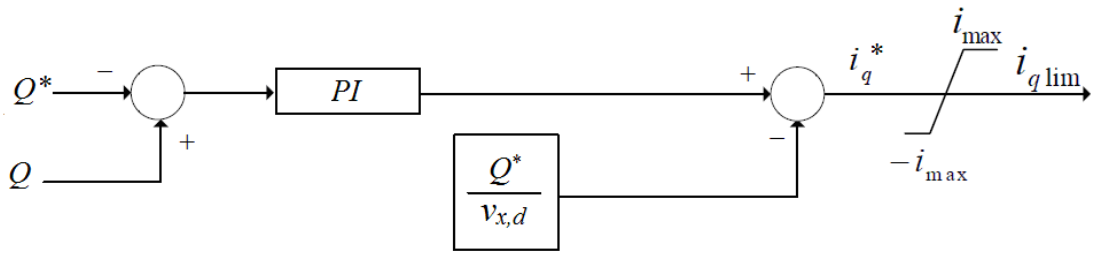

Fig. C.8 Reactive power controller

AC voltage controller

Applying the Kirchhoff's voltage law across the phase reactor, shown in fig. C.4 we get the following equation:

$$\tilde{V}_x - \tilde{V}_c = (r + j\omega L)\tilde{I} \qquad \text{(C.24)}$$

The current flowing across the phase reactor is given by the following equation:

$$\tilde{I} = \left(\frac{P + jQ}{V_x}\right)^* = \frac{P - jQ}{V_x} \qquad \text{(C.25)}$$

where P and Q are the active and reactive power respectively at the PCC.

Substituting equation (C.25) into (C.24) results in equation (C.26):

$$\tilde{V}_x - \tilde{V}_c = \frac{rP + \omega LQ}{V_x} + j\frac{\omega LP - rQ}{V_x} \qquad \text{(C.26)}$$

The imaginary part of equation (C.26) is negligible therefore the voltage drop across the phase reactor is approximately:

$$\tilde{V}_x - \tilde{V}_c = \frac{rP + \omega LQ}{V_x} \qquad \text{(C.27)}$$

Since usually in transmission systems the resistance X/R ration is large, i.e the resistance r is considerably smaller than the reactance X=ωL, equation (C.27) leads to the conclusion that the voltage drop is dependant on the reactive power, which according to equation (C.16) depends on the reactive current component i_q. Even for cases where the X/R ratio is small, the active power is already separately controlled as seen above, therefore it cannot be used to control the AC voltage **[45]**.

The controller shown in fig. C.9 can be used to control the AC voltage in the PCC.

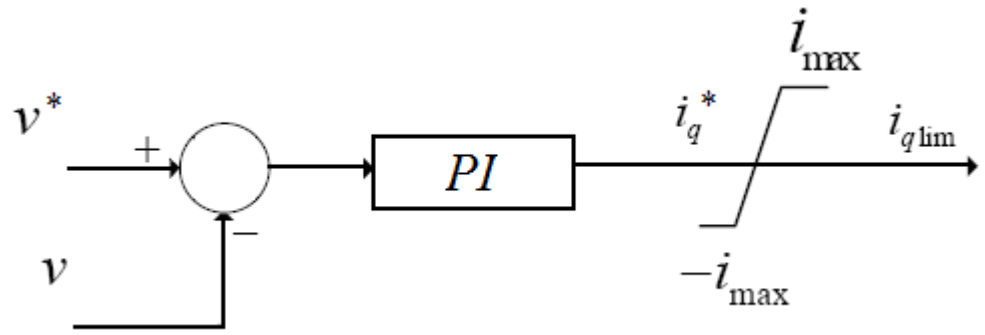

Fig. C.9 AC voltage controller

C.1.2 Selection of control modes

Each converter can operate either in active power or DC voltage. At the same time each converter can control either reactive power or AC voltage both not both at the same time. Regarding the active current control one converter must regulate the DC voltage and the other the power exchanged with the AC grid. If both converters control DC voltage or active power exchange then a stable operation mode during steady state is not guaranteed. On the other hand regarding the reactive current control there is more freedom in choosing the control mode. One converter may control the AC voltage at a bus while the other controls the reactive power exchange, both can control reactive power exchange or both can control the AC voltage at AC system buses. When the HVDC system is connected to a weak AC system it is preferable for the converter connected to the AC system to control the AC voltage. This is because weak AC systems are characterized by a high equivalent impedance as seen from the connection point, this means that voltage drop varies greatly with active power flow variation.

The selection of which converter controls DC voltage and which active power exchange is not of great importance for the stability of the HVDC system's steady state operation. However it is recommended that the sending end (i.e the rectifier) controls the DC voltage while the receiving end (i.e the inverter) controls the active power exchange **[45]**; this can be explained as follows. Assume that the rectifier controls the active power while the inverter controls the DC voltage. If for example the inverter itself fails then it will be unable to receive the power sent by the power controlling rectifier, this will lead to DC overvoltage which can be hazardous for the HVDC equipment.

APPENDIX D: Results

Results of paragraph 4.3.1.1

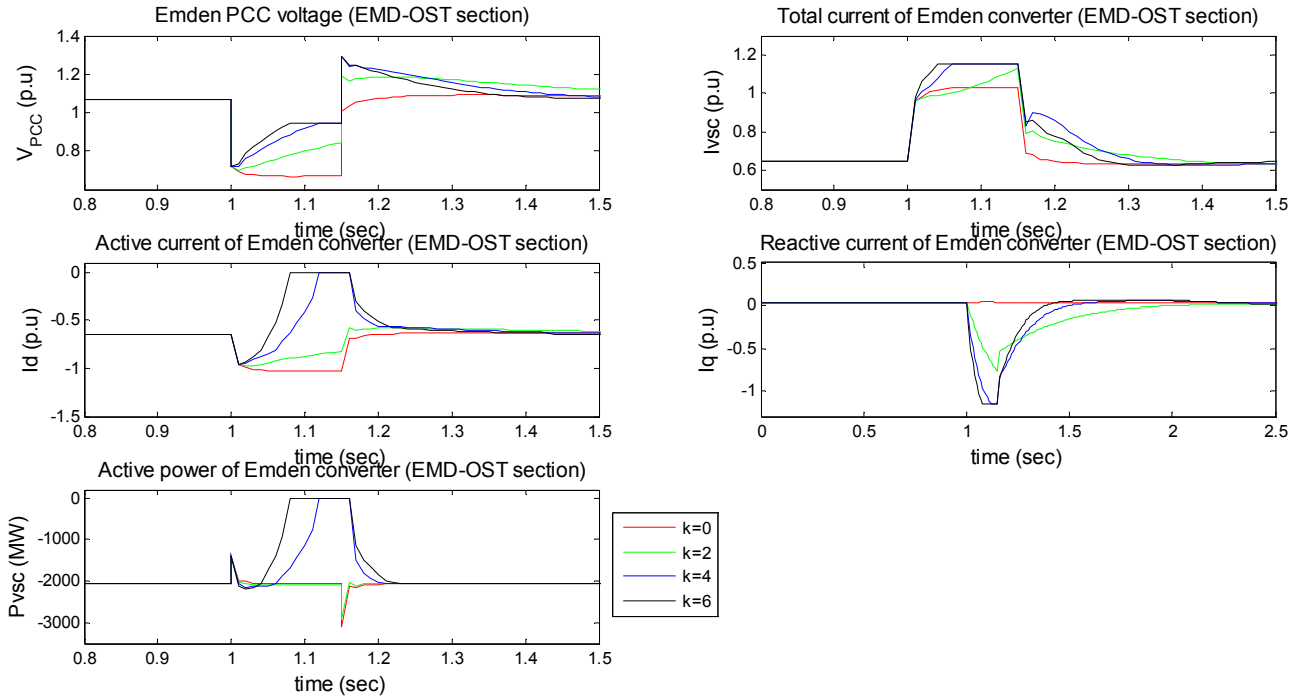

Fig.E.1 Response of Emden's converter (EMD-OST section) to a 3-phase bus fault in Dorpen (Zone 1) for different values of k

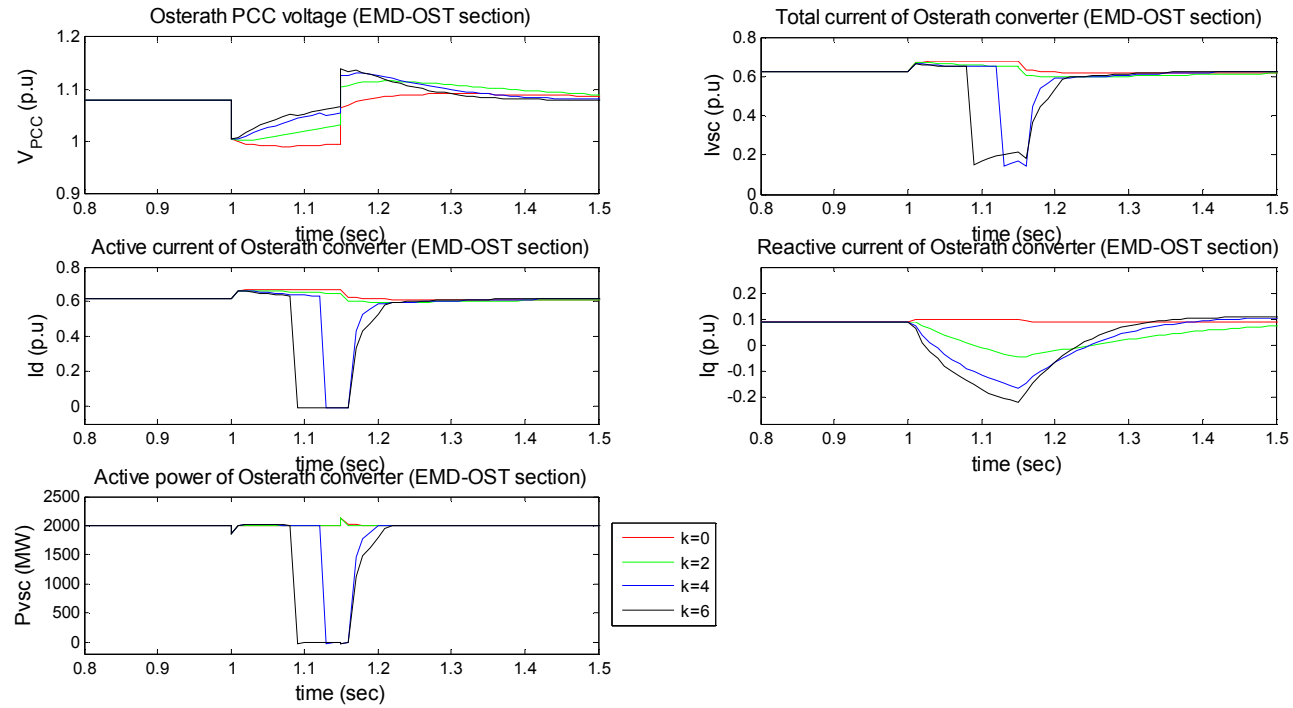

Fig.E.2 Response of Osterath's converter (EMD-OST section) to a 3-phase bus fault in Dorpen (Zone 1) for different values of k

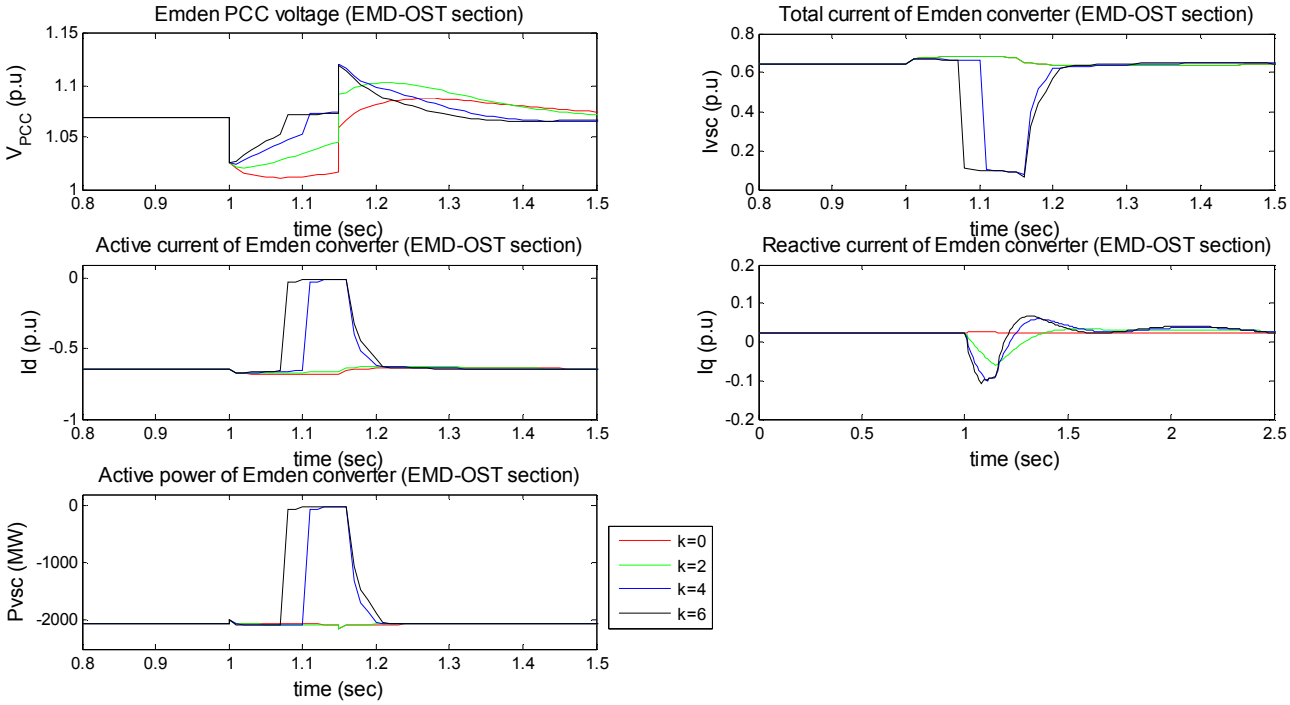

Fig.E.3 Response of Emden's converter (EMD-OST section) to a 3-phase bus fault in Sechtem (Zone 2) for different values of k

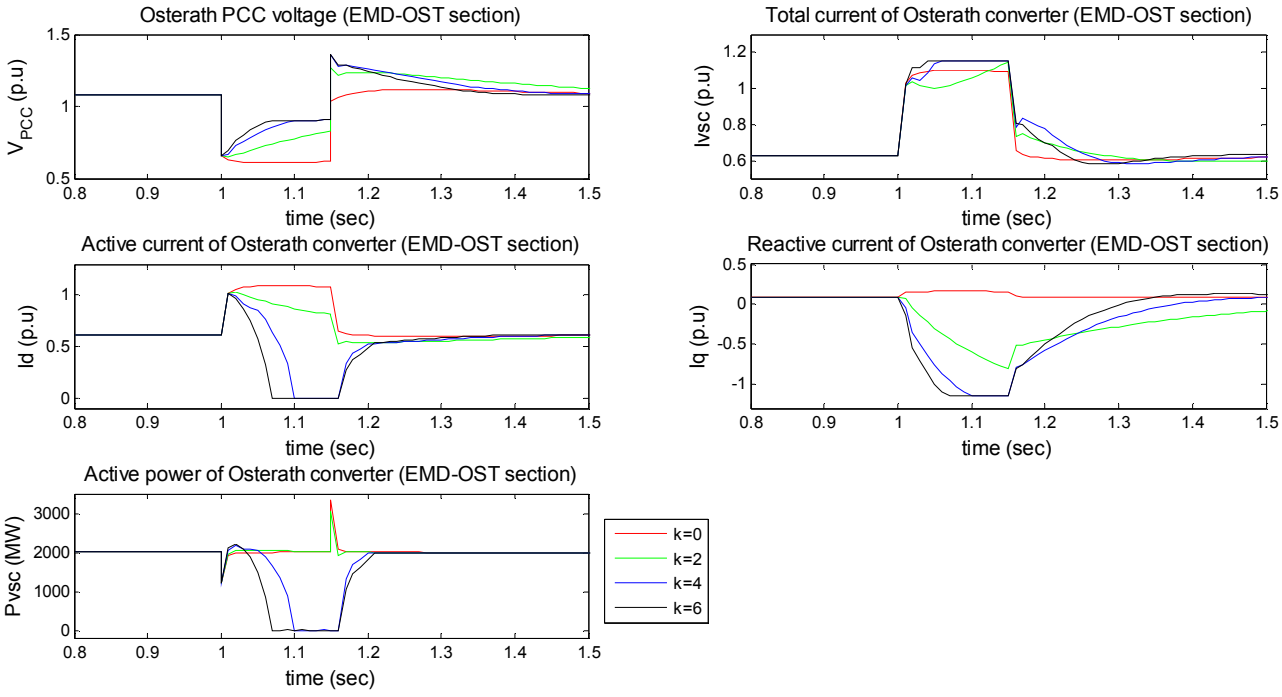

Fig.E.4 Response of Osterath's converter (EMD-OST section) to a 3-phase bus fault in Sechtem (Zone 2) for different values of k

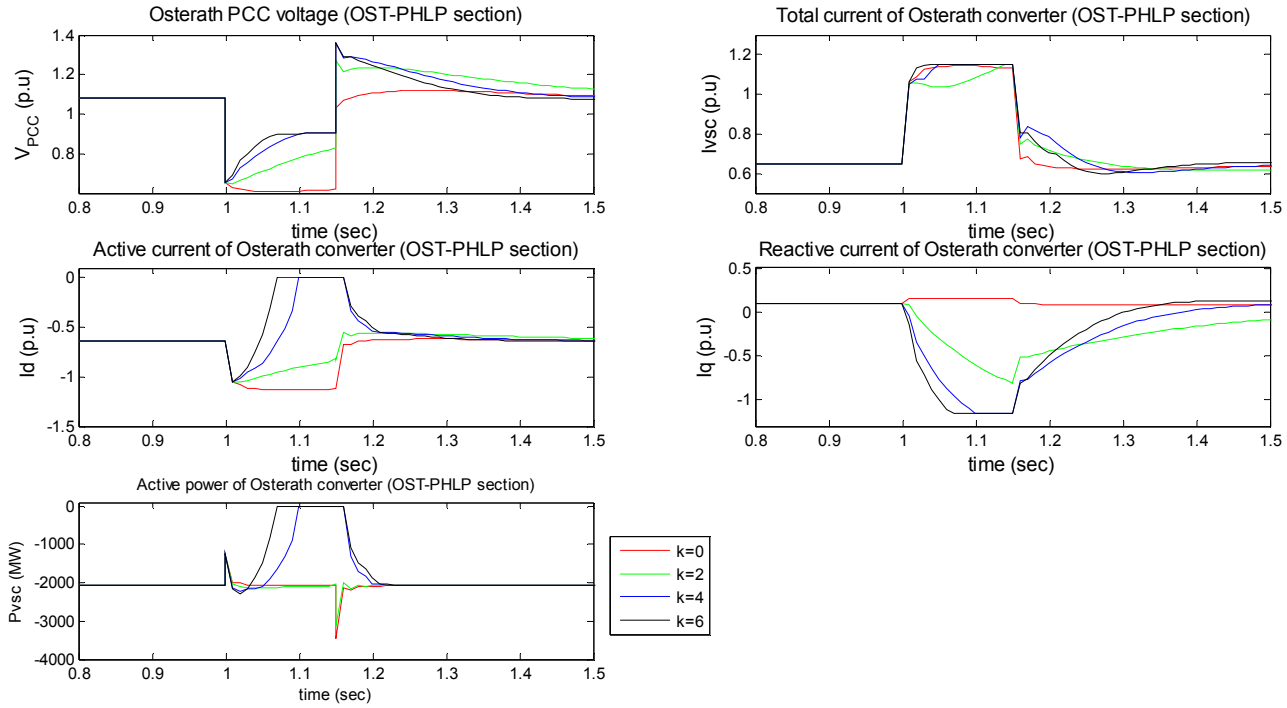

Fig.E.5 Response of Osterath's converter (OST-PHLP section) to a 3-phase bus fault in Sechtem (Zone 2) for different values of k

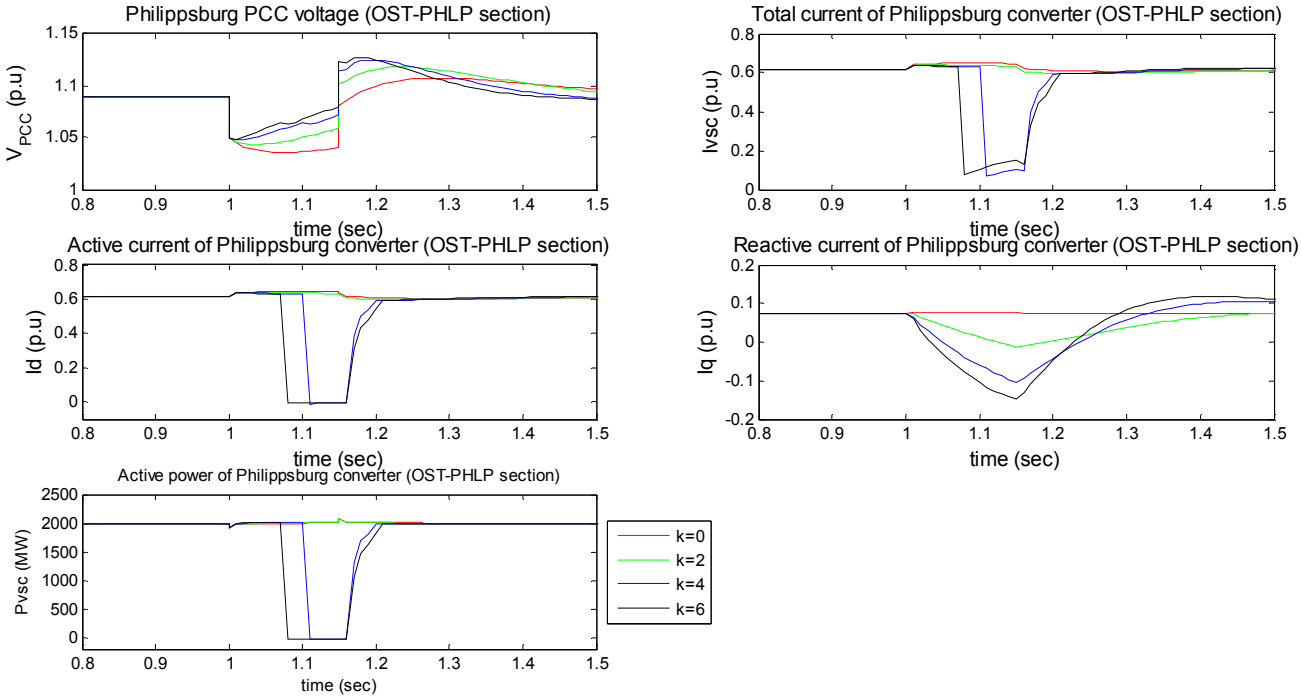

Fig.E.6 Response of Philippsburg's converter (OST-PHLP section) to a 3-phase bus fault in Sechtem (Zone 2) for different values of k

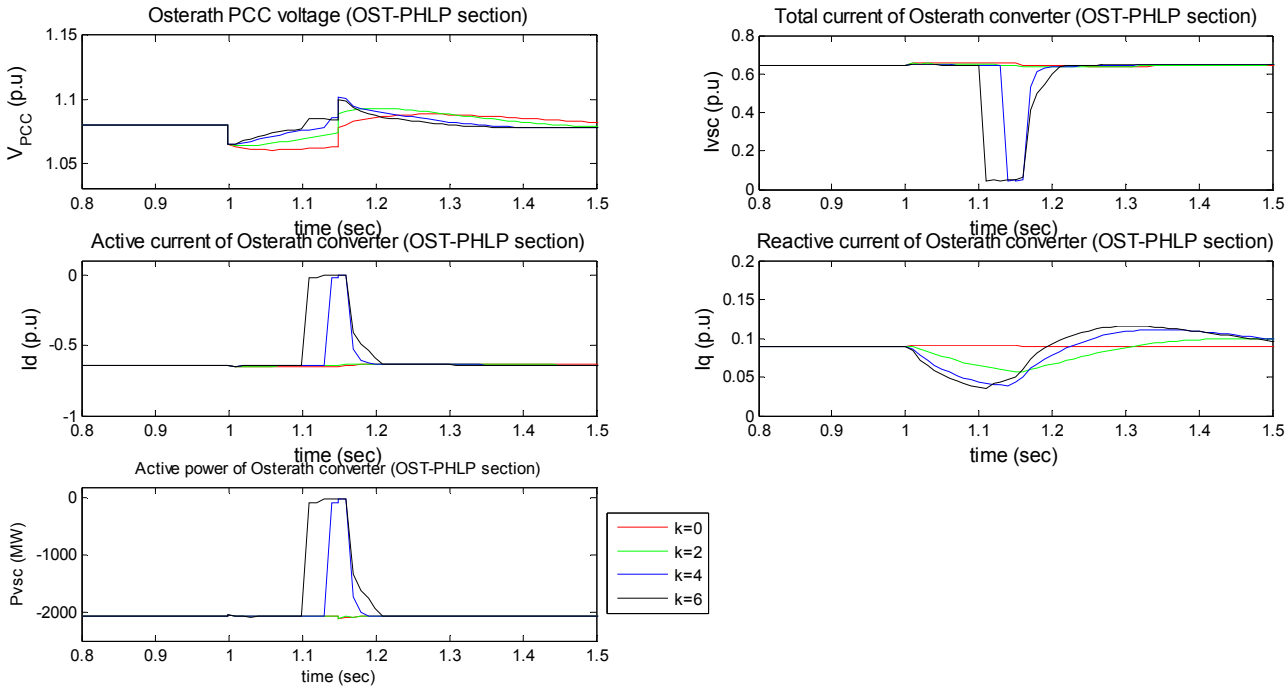

Fig.E.7 Response of Osterath's converter (OST-PHLP section) to a 3-phase bus fault in Hopfingen (Zone 3) for different values of k

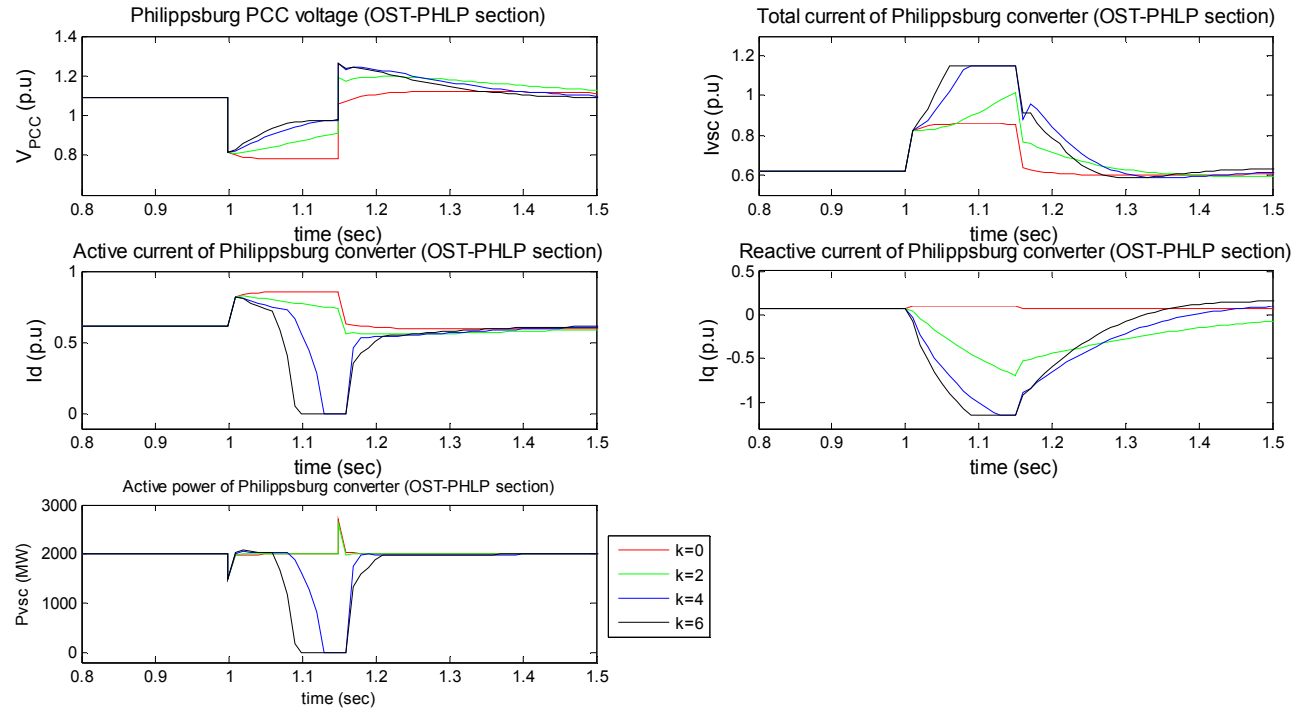

Fig.E.8 Response of Philippsburg's converter (OST-PHLP section) to a 3-phase bus fault in Hopfingen (Zone 3) for different values of k

Results of paragraph 4.3.1.2

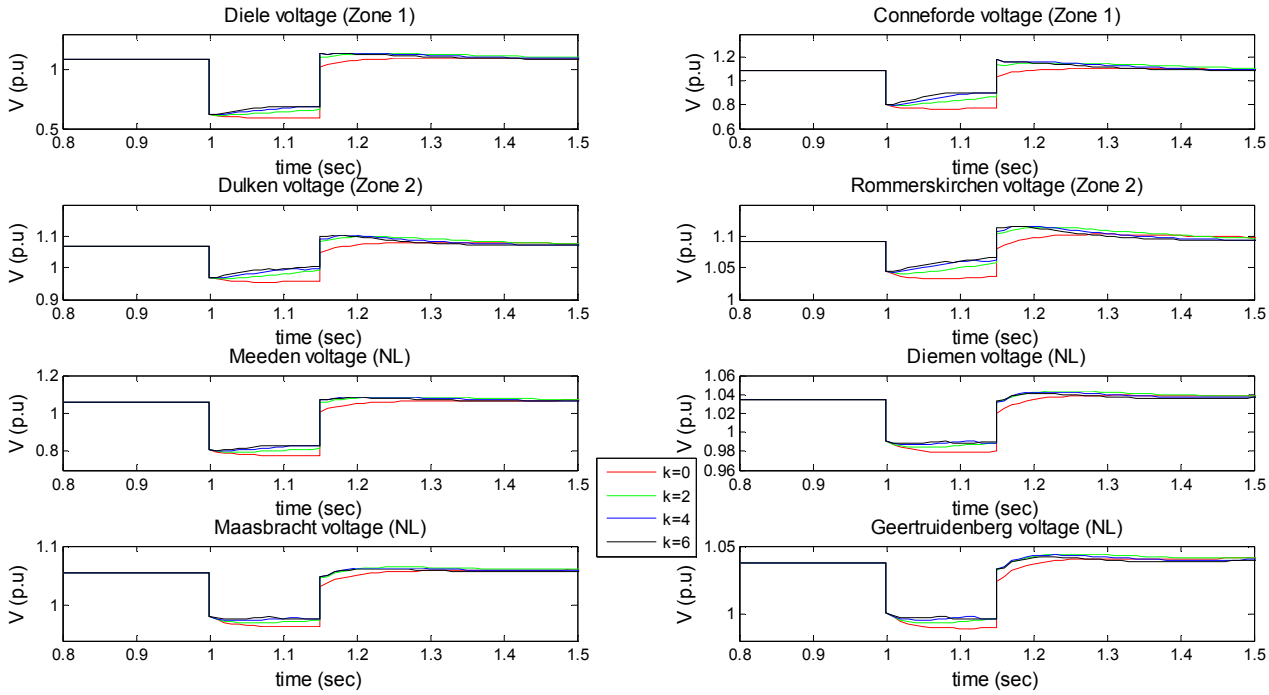

Fig. E.9 Effect of the k gain on the 380 kV bus voltages for a fault in Dorpen (Zone 1)

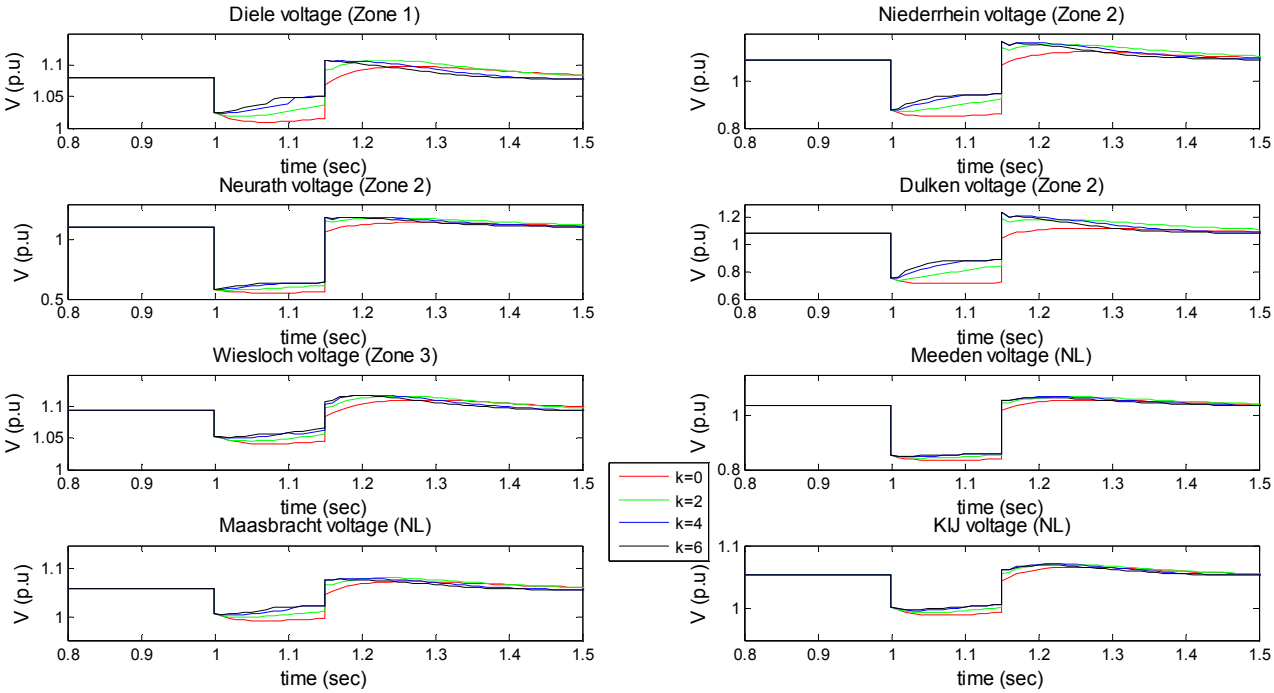

Fig. E.10 Effect of the k gain on the 380 kV bus voltages for a fault in Sechtem (Zone 2)

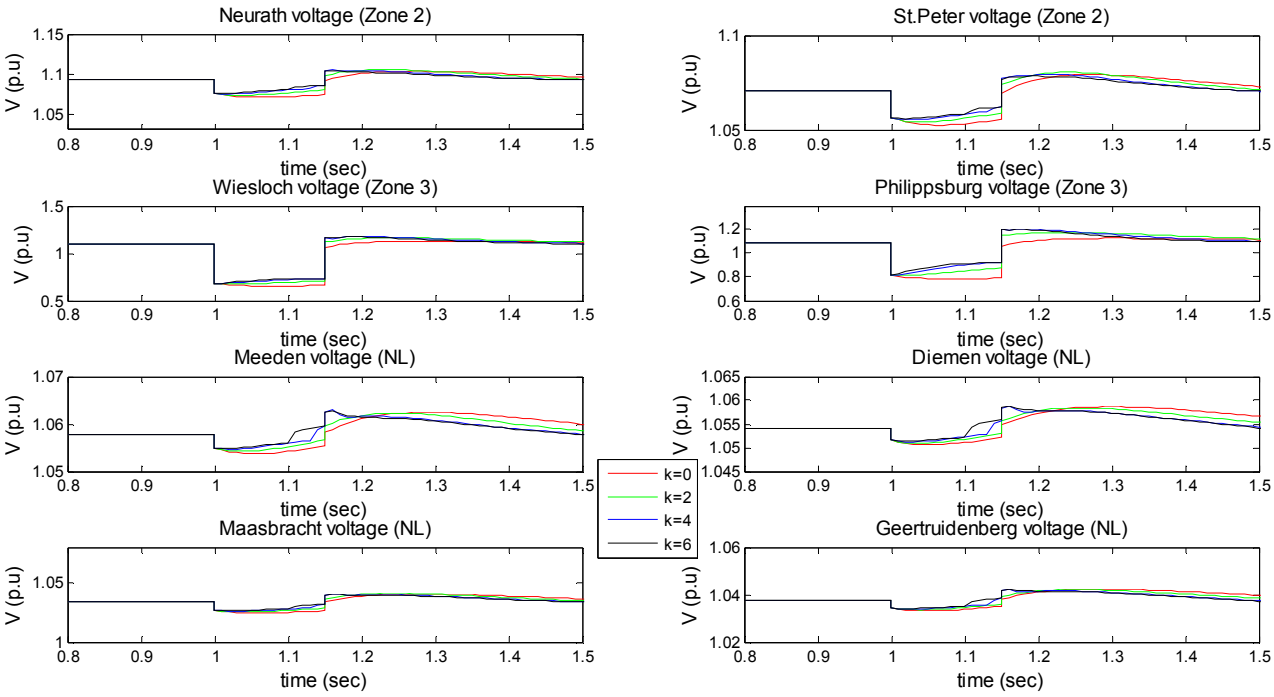

Fig. E.11 Effect of the k gain on the 380 kV bus voltages for a fault in Hopfingen (Zone 3)

Results of paragraph 4.3.1.3

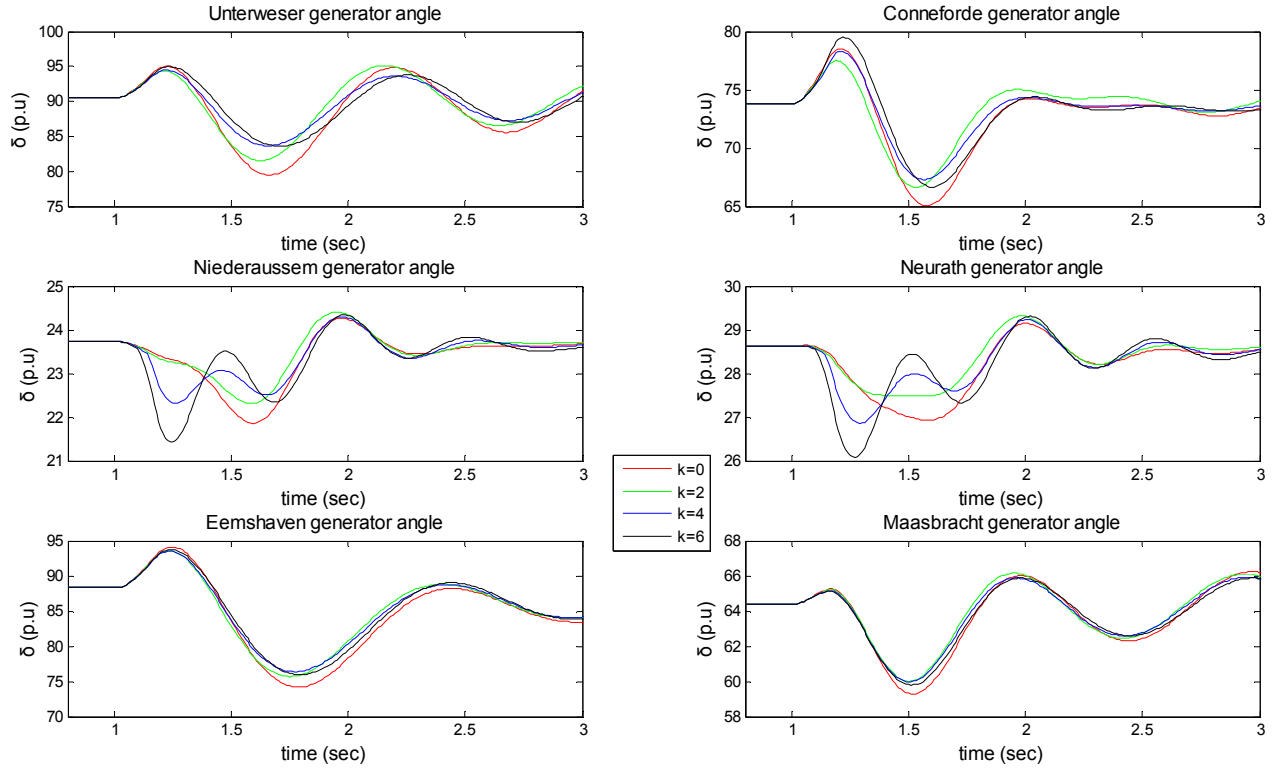

Fig. E.12 Effect of k gain on generator rotor angles for a fault in Dorpen (Zone 1)

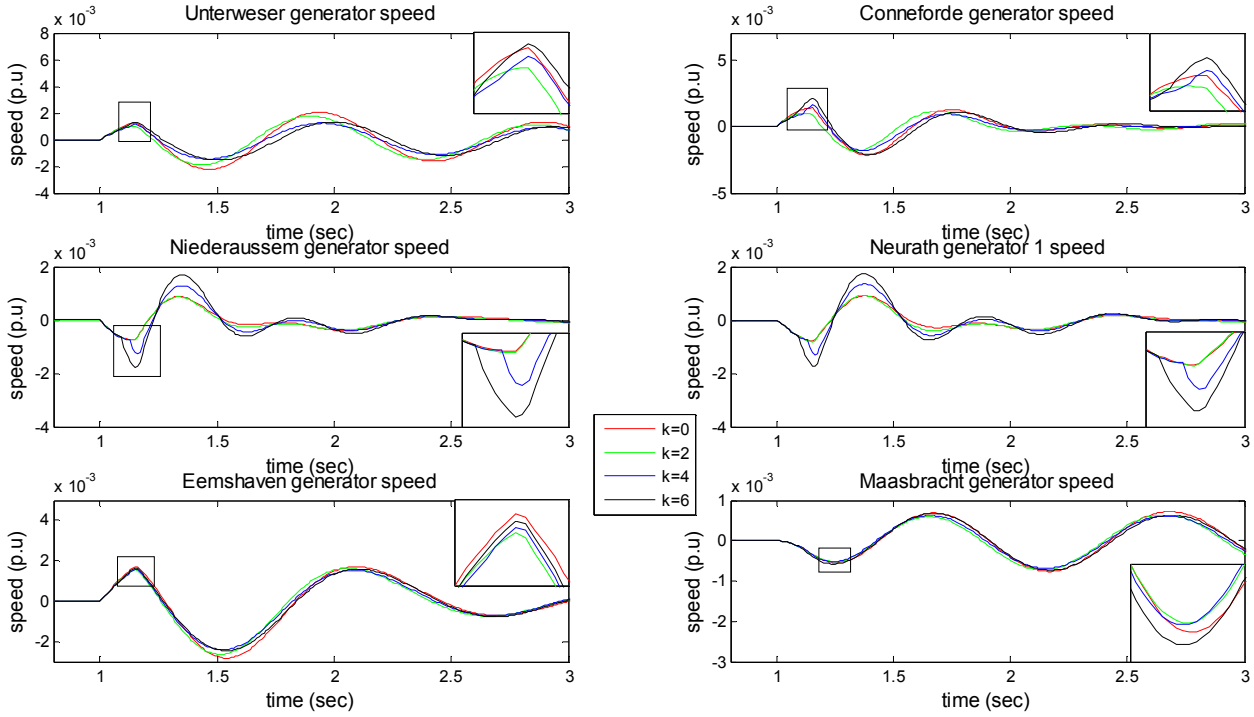

Fig. E.13 Effect of k gain on generator rotor speeds for a fault in Dorpen (Zone 1)

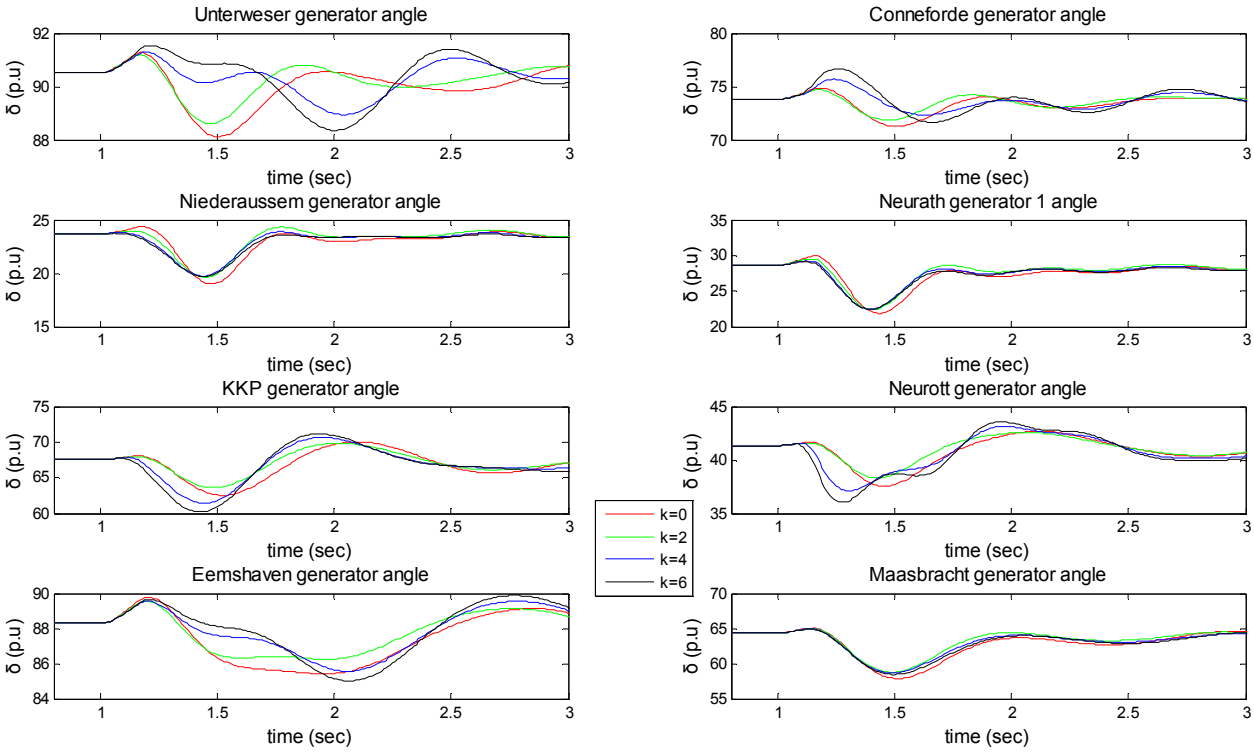

Fig. E.14 Effect of k gain on generator rotor angles for a fault in Sechtem (Zone 2)

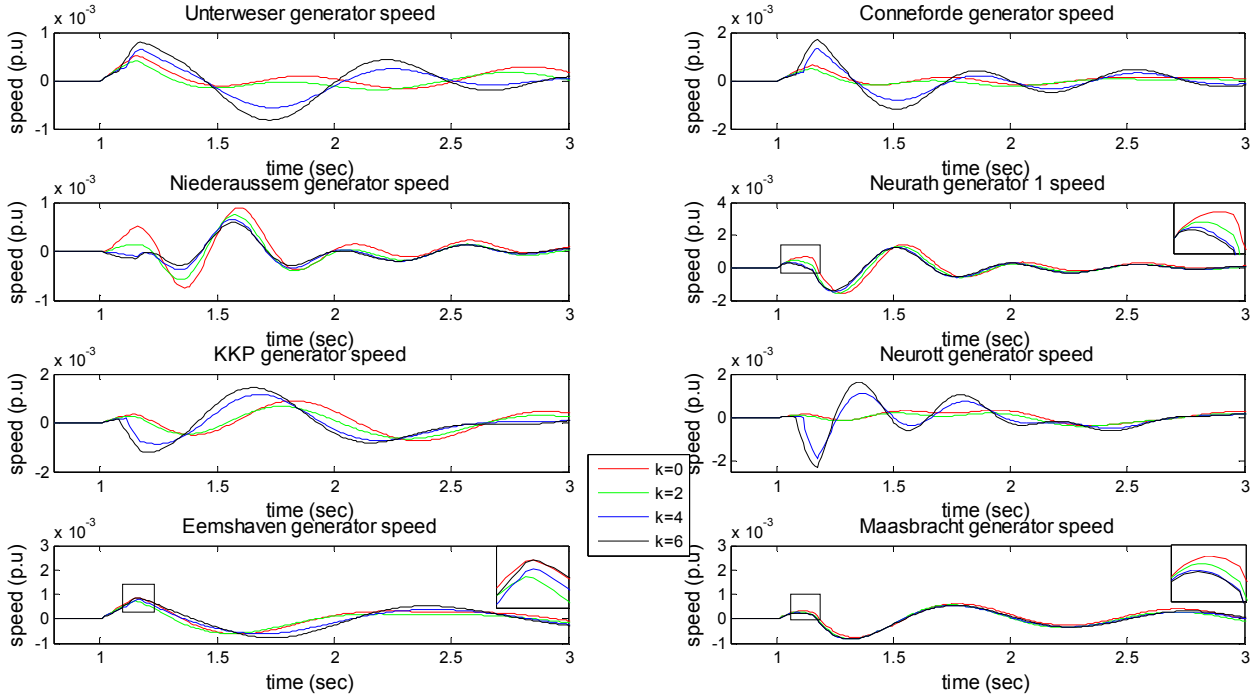

Fig. E.15 Effect of k gain on generator rotor speeds for a fault in Sechtem (Zone 2)

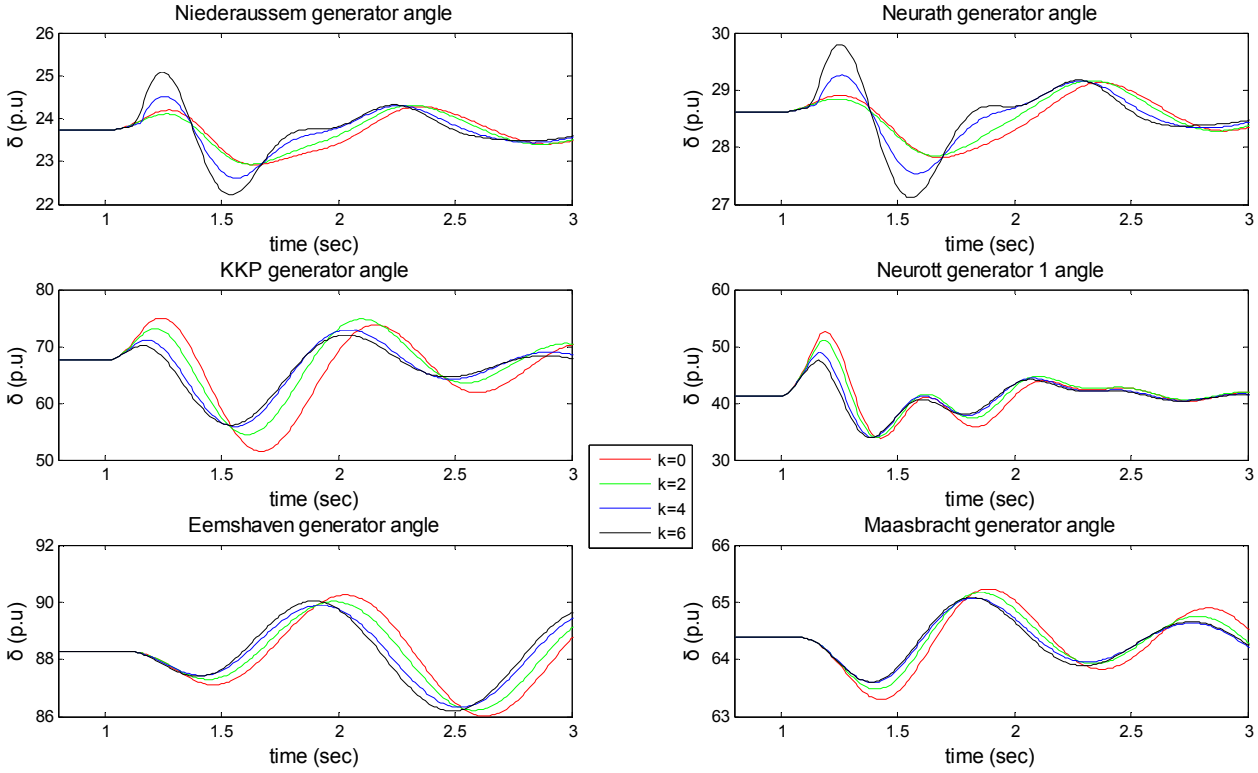

Fig. E.16 Effect of k gain on generator rotor angles for a fault in Hopfingen (Zone 3)

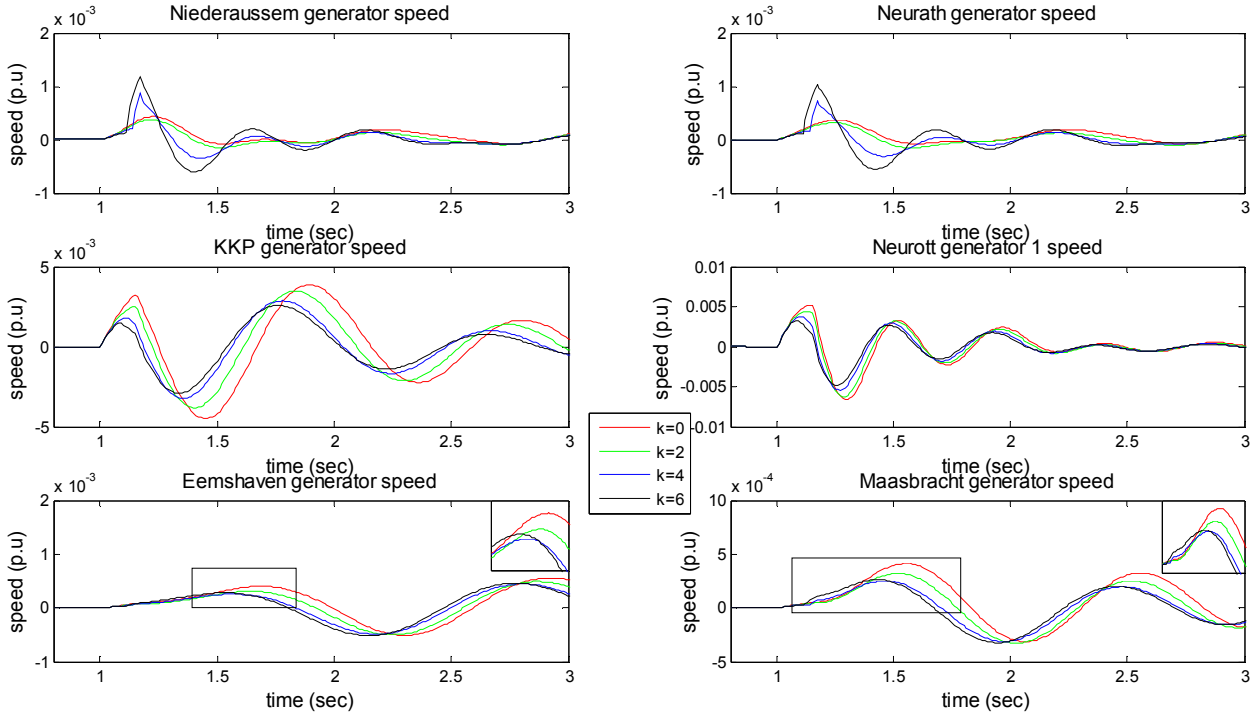

Fig. E.17 Effect of k gain on generator rotor speeds for a fault in Hopfingen (Zone 3)

Results of paragraph 4.3.2.1

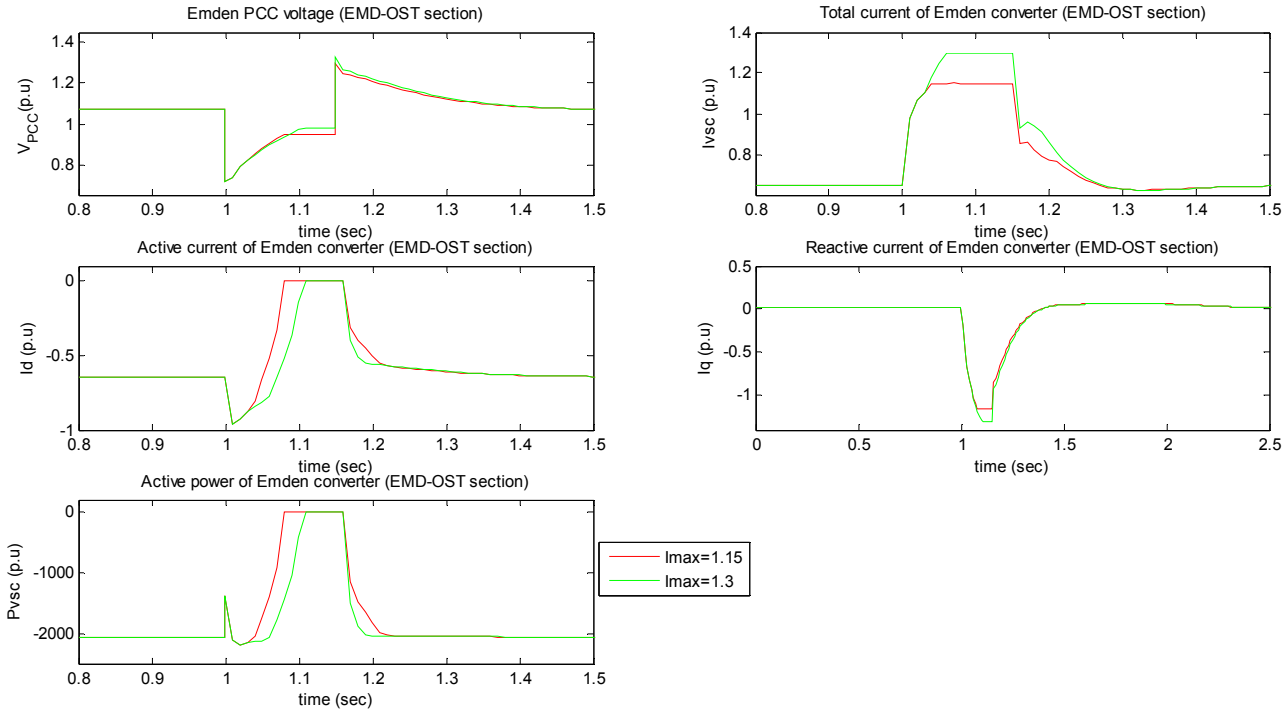

Fig.E.18 Response of Emden's converter (EMD-OST section) to a 3-phase bus fault in Dorpen (Zone 1) for different current capabilities

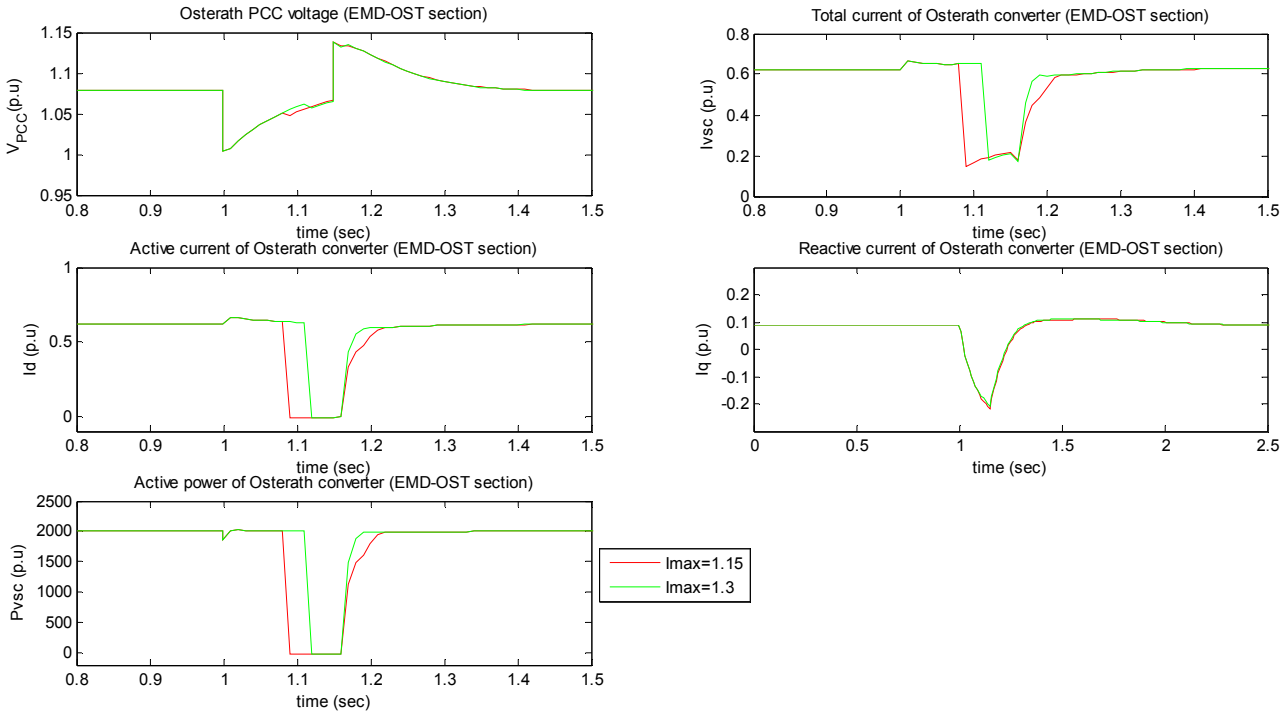

Fig.E.19 Response of Osterath's converter (EMD-OST section) to a 3-phase bus fault in Dorpen (Zone 1) for different current capabilities

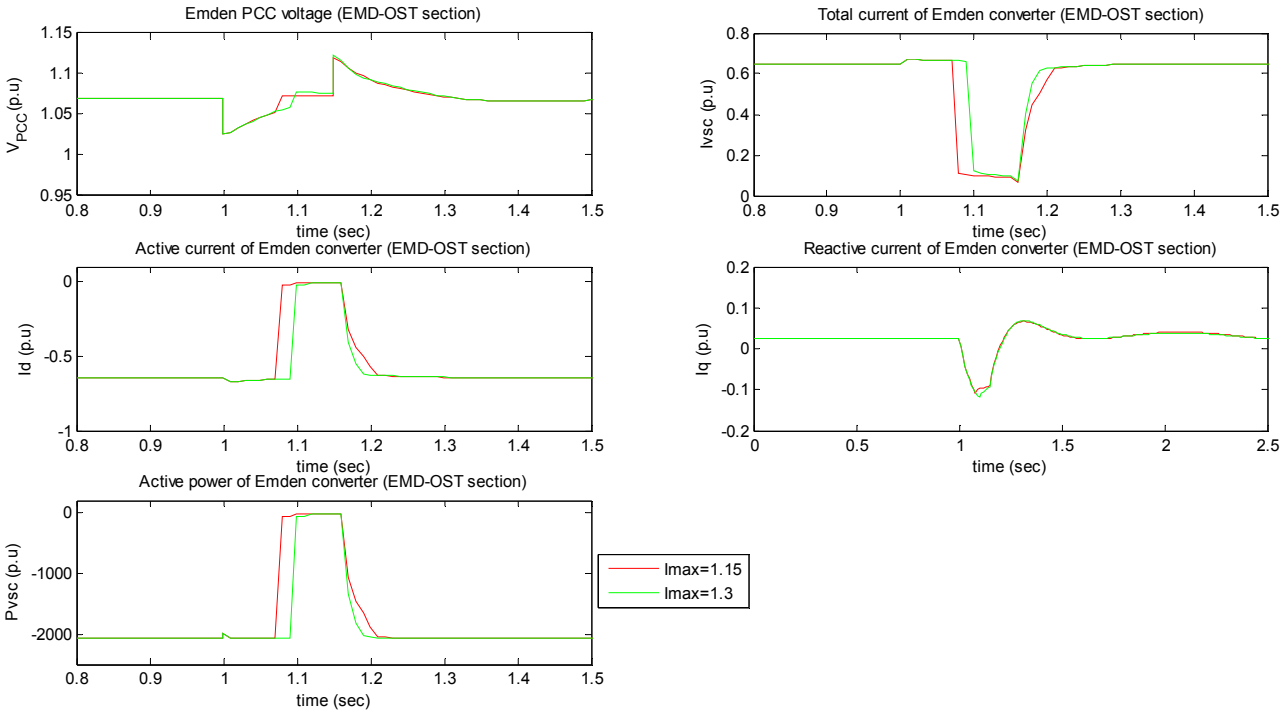

Fig.E.20 Response of Emden's converter (EMD-OST section) to a 3-phase bus fault in Sechtem (Zone 2) for different current capabilities

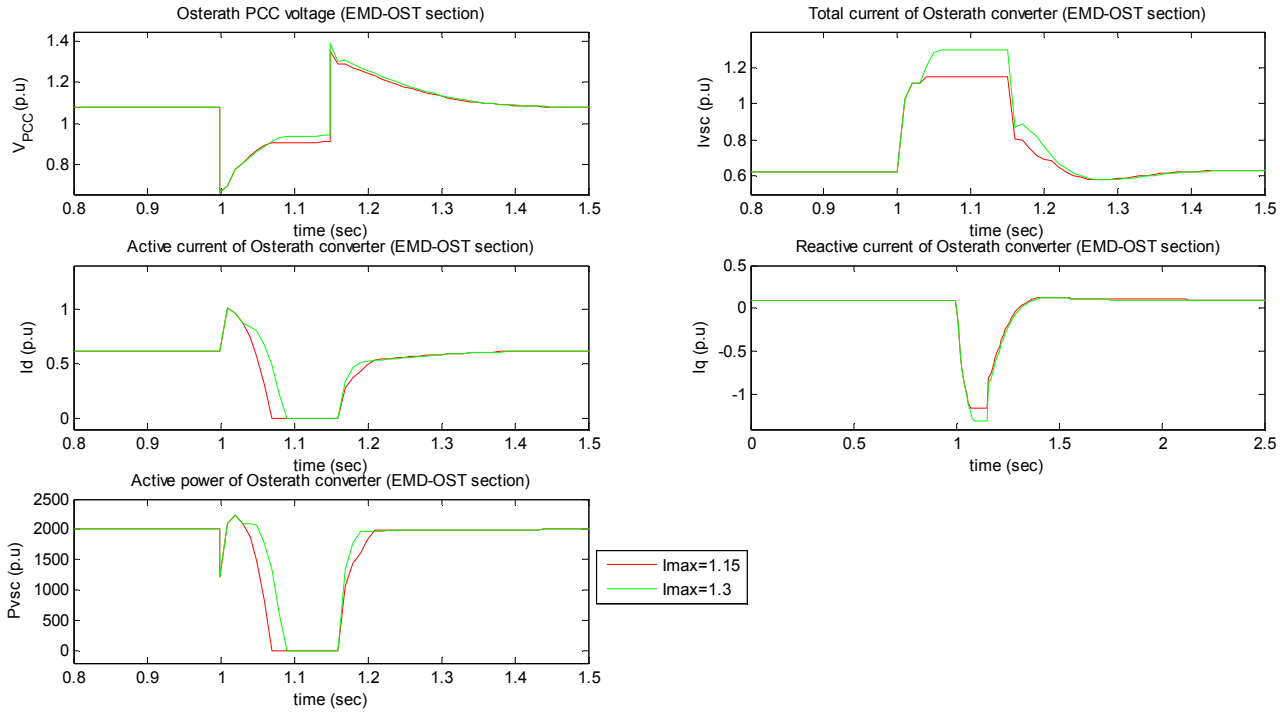

Fig.E.21 Response of Osterath's converter (EMD-OST section) to a 3-phase bus fault in Sechtem (Zone 2) for different current capabilities

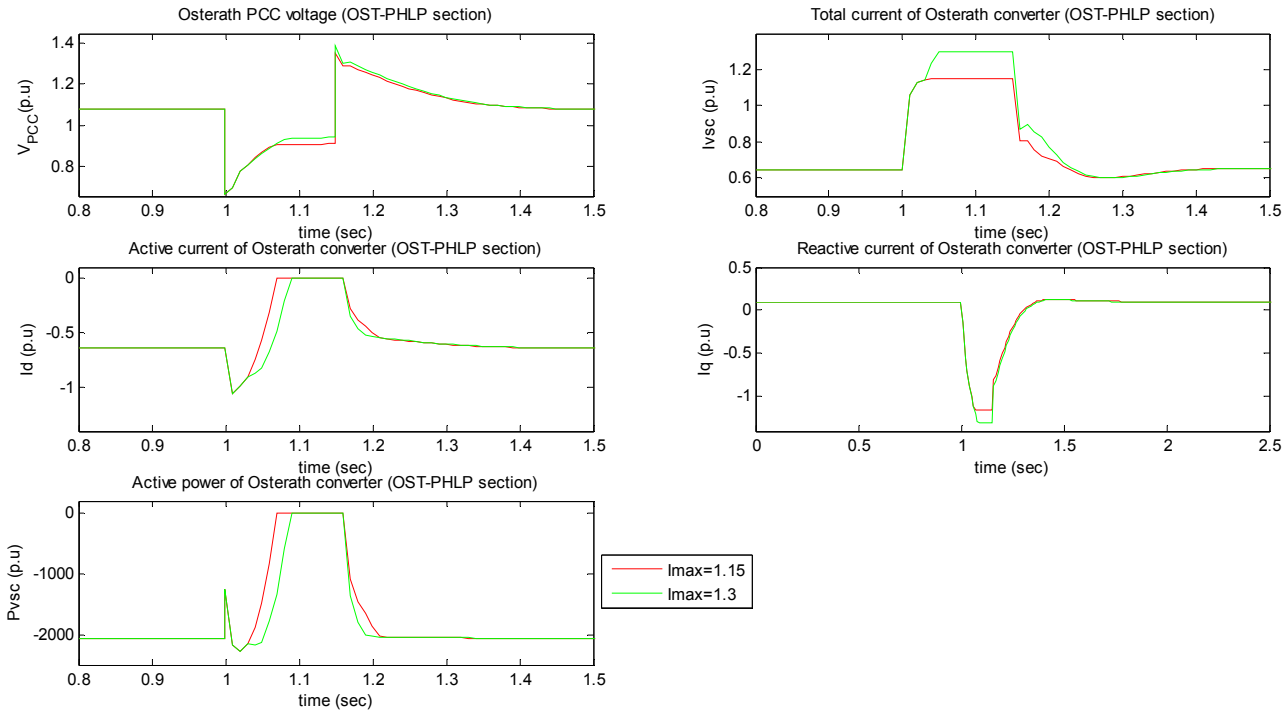

Fig.E.22 Response of Osterath's converter (OST-PHLP section) to a 3-phase bus fault in Sechtem (Zone 2) for different current capabilities

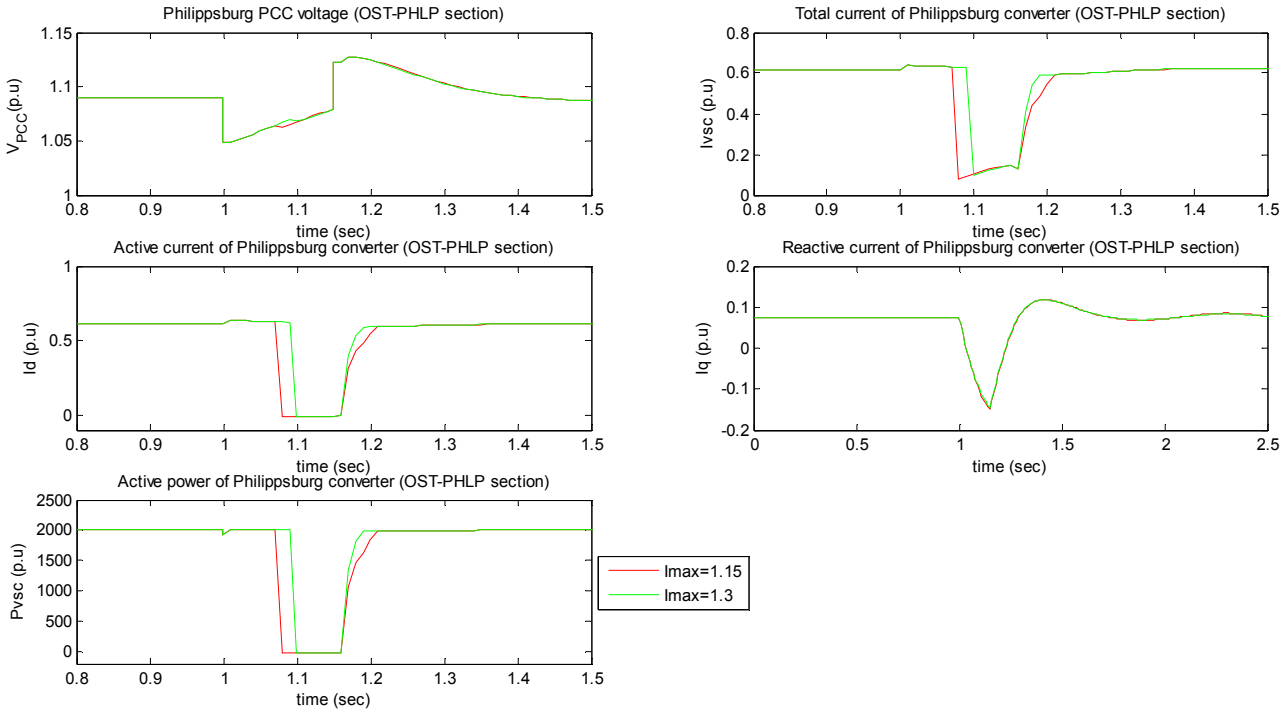

Fig.E.23 Response of Philippsburg's converter (OST-PHLP section) to a 3-phase bus fault in Sechtem (Zone 2) for different current capabilities

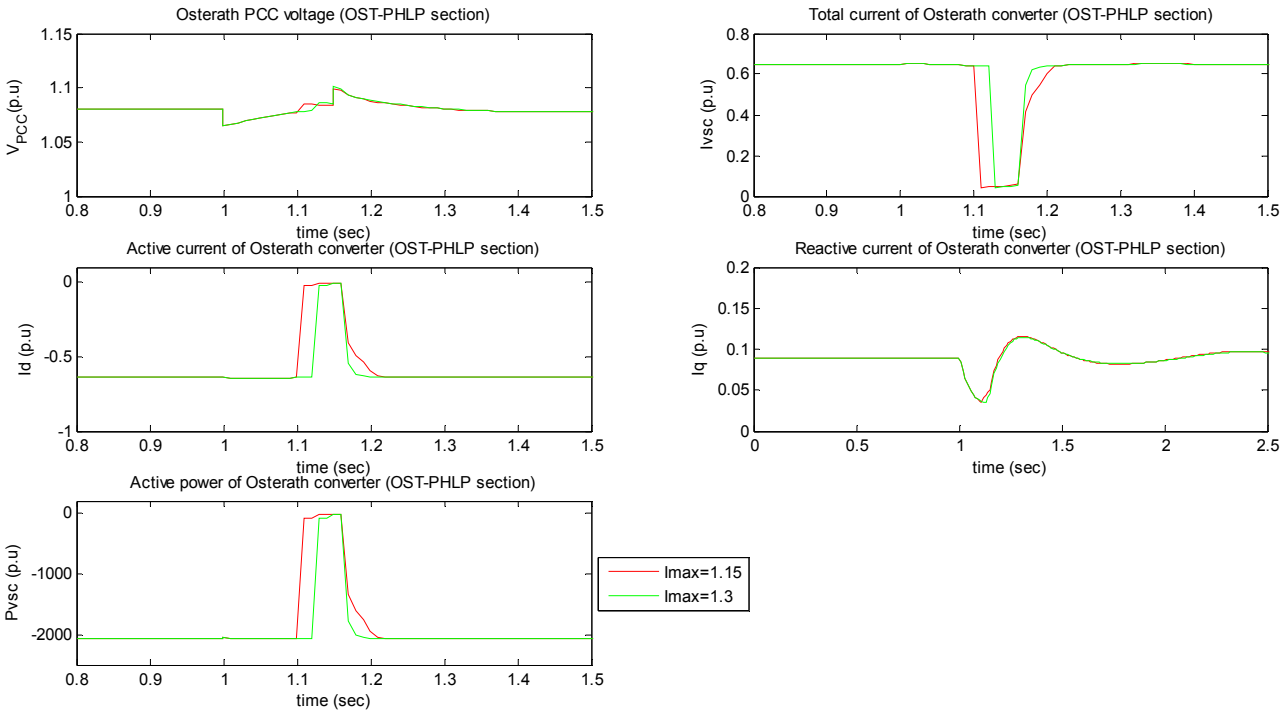

Fig.E.24 Response of Osteraht's converter (OST-PHLP section) to a 3-phase bus fault in Hopfingen (Zone 3) for different current capabilities

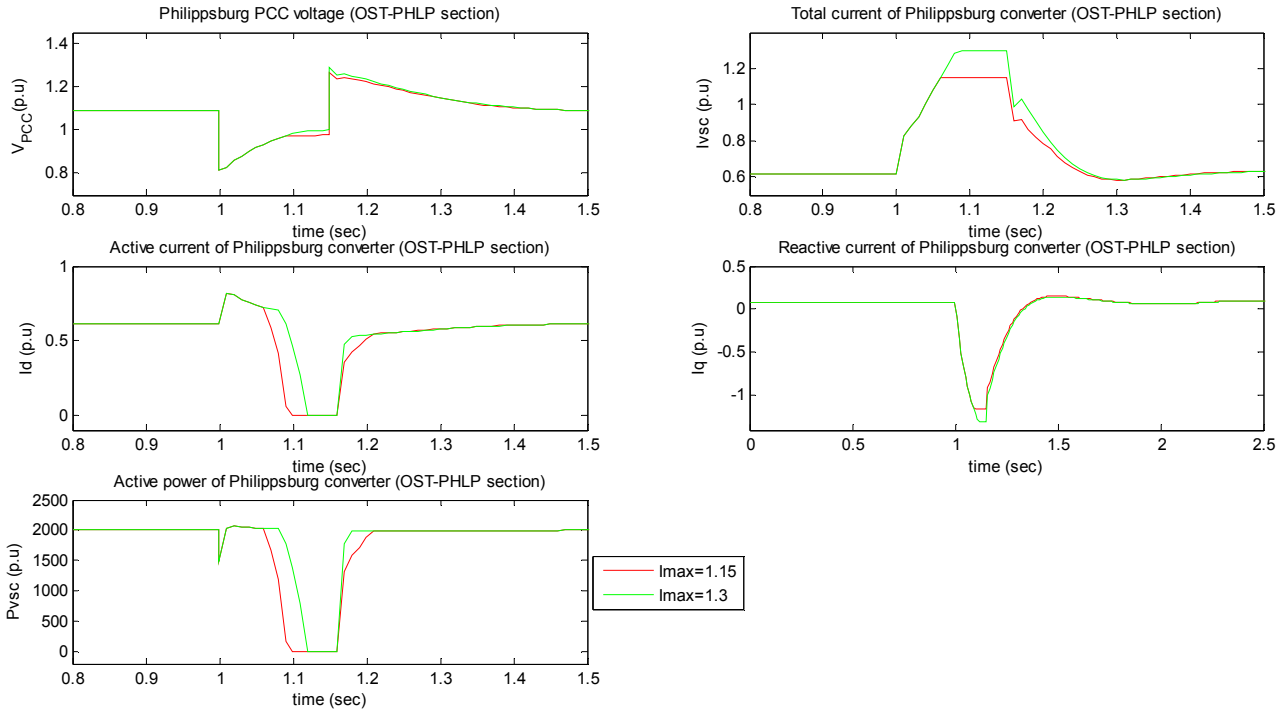

Fig.E.25 Response of Philippsburg's converter (OST-PHLP section) to a 3-phase bus fault in Hopfingen (Zone 3) for different current capabilities

Results of paragraph 4.3.2.2

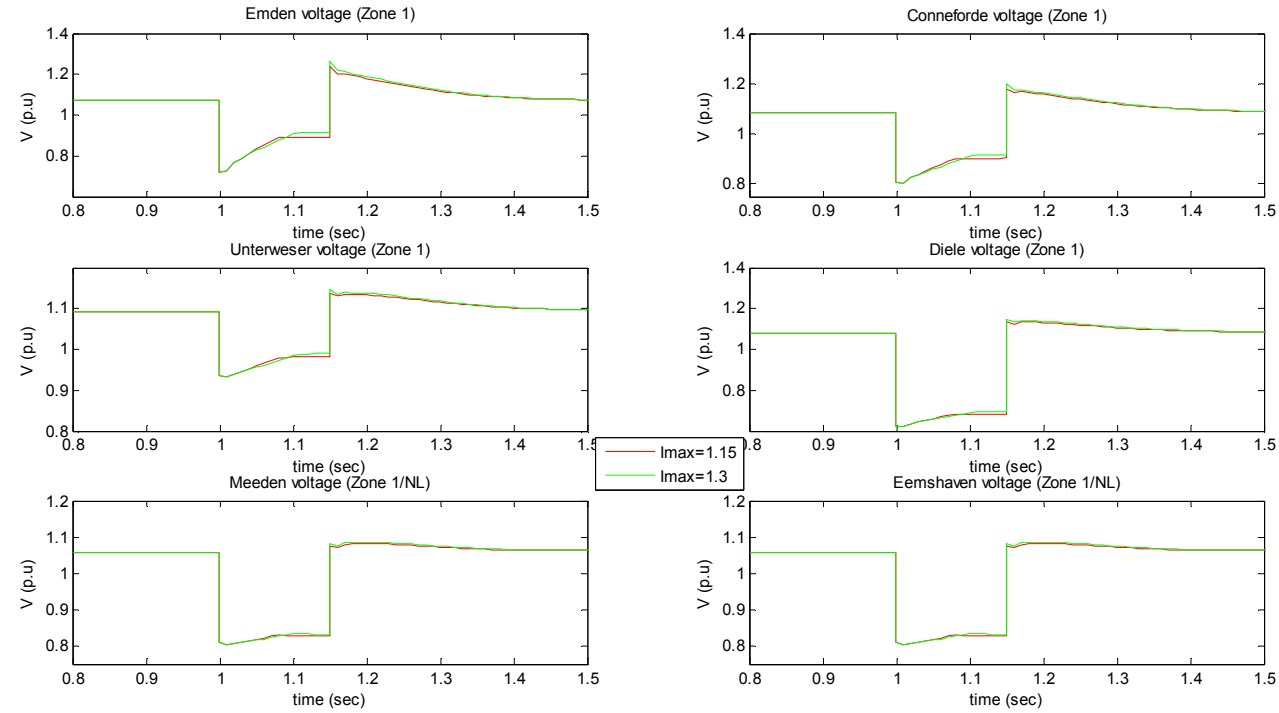

Fig. E.26 Effect of the over-current capability on the 380 kV bus voltages for a fault in Dorpen (Zone 1)

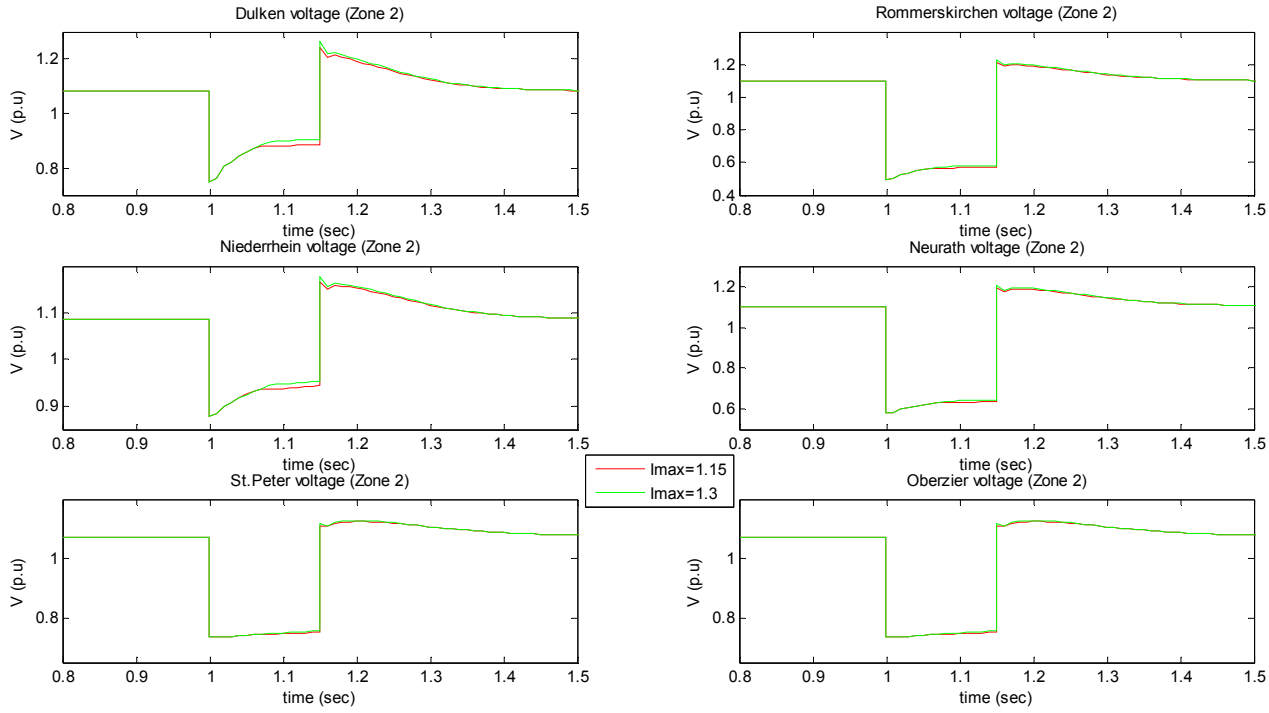

Fig. E.27 Effect of the over-current capability on the 380 kV bus voltages for a fault in Sechtem (Zone 2)

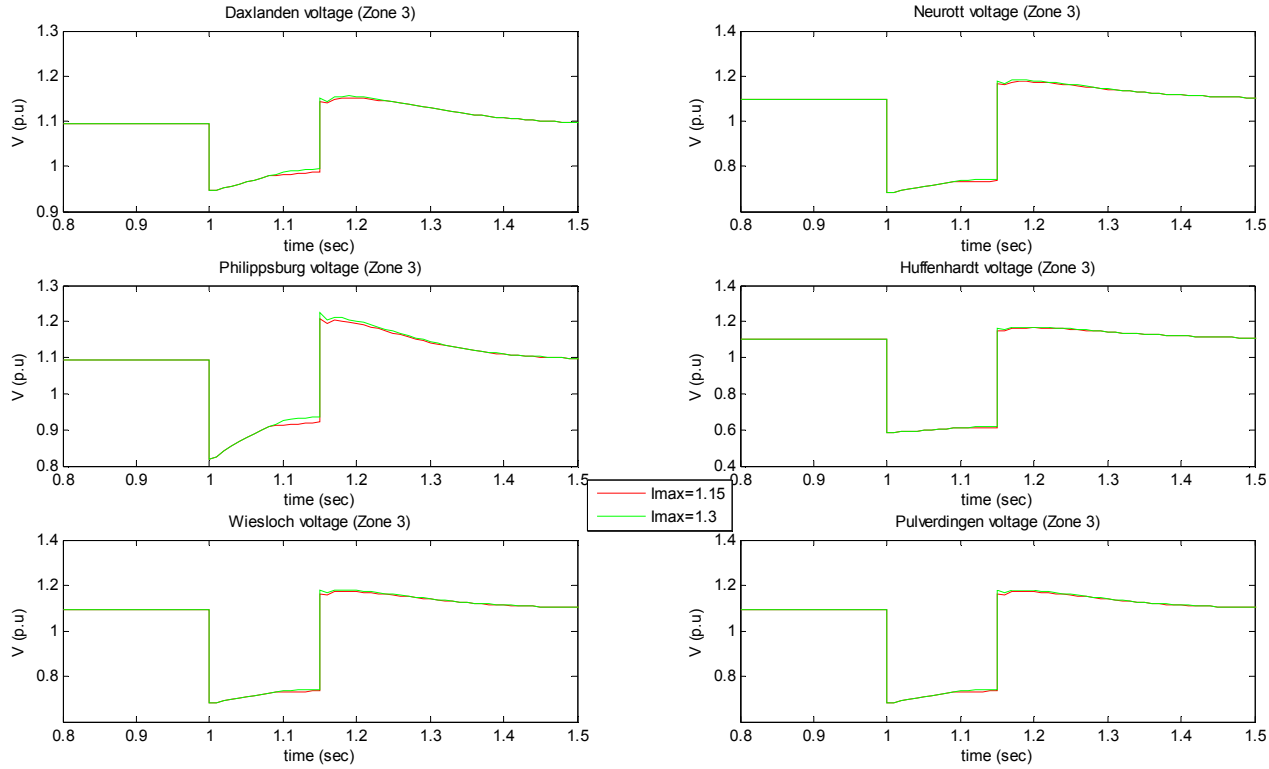

Fig. E.28 Effect of the over-current capability on the 380 kV bus voltages for a fault in Hopfingen (Zone 3)

Results of paragraph 4.3.2.3

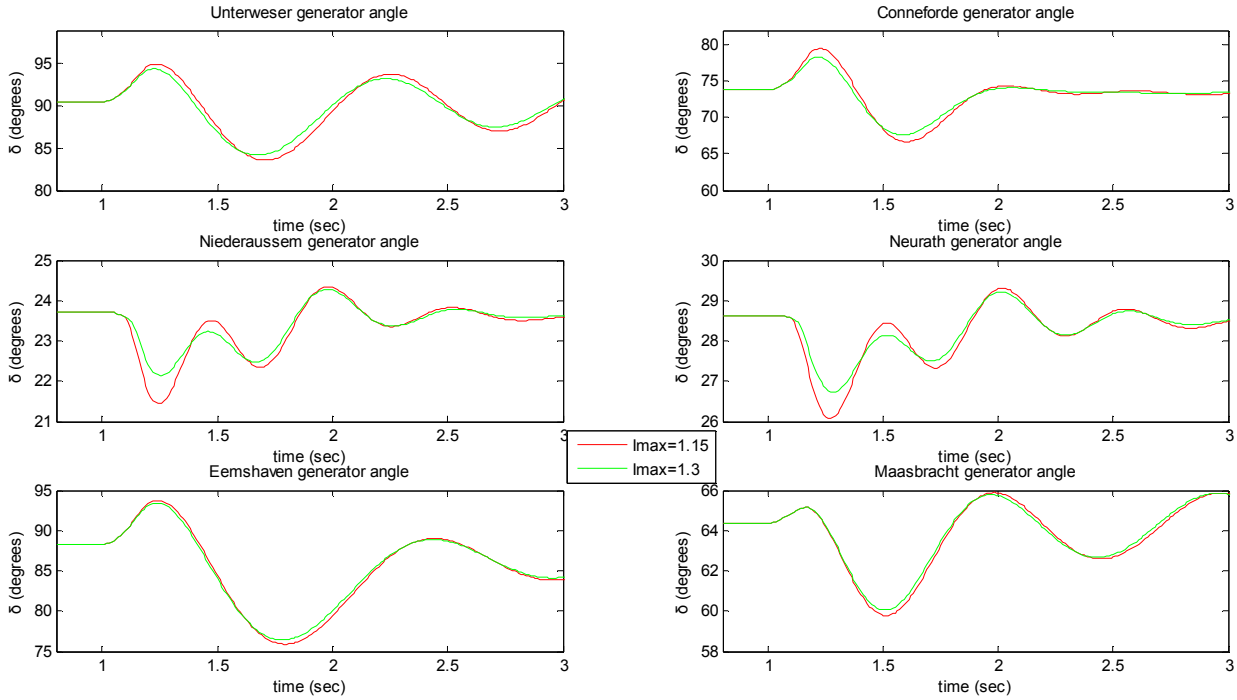

Fig. E.29 Effect of the over-current capability on generator rotor angles for a fault in Dorpen (Zone 1)

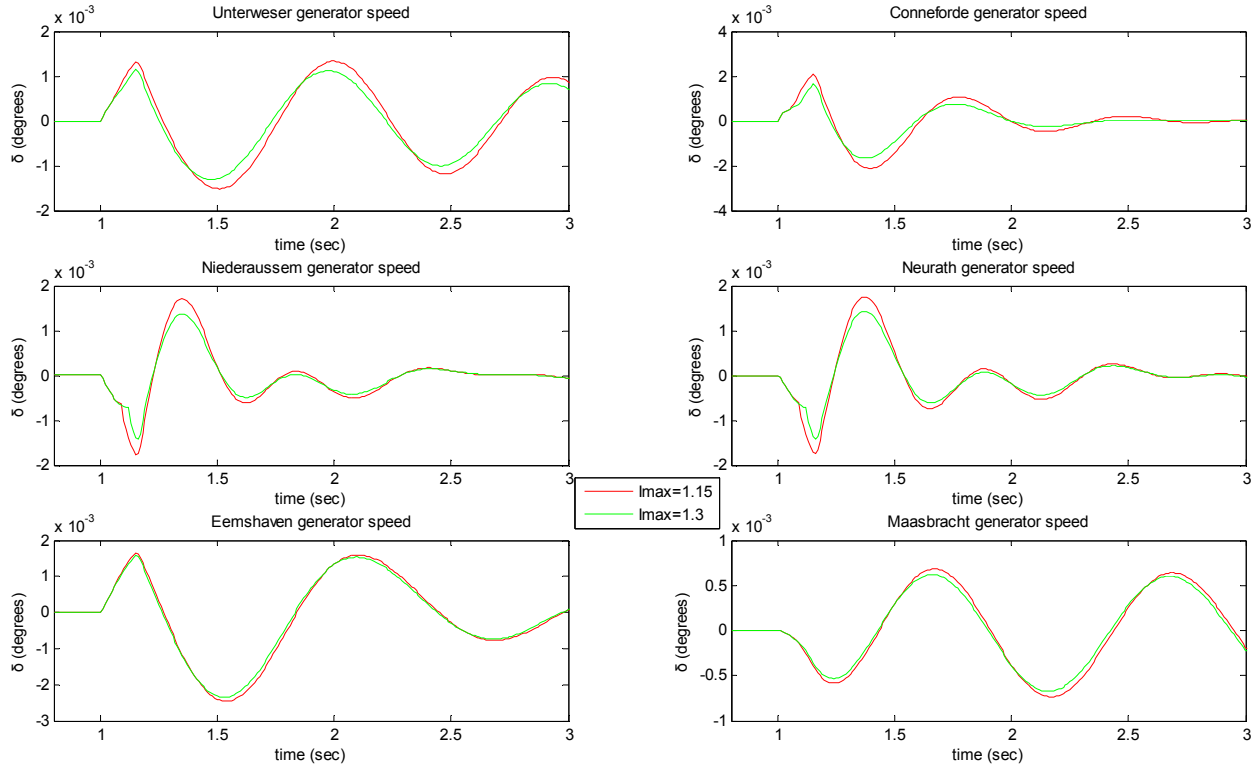

Fig. E.30 Effect of the over-current capability on generator rotor speeds for a fault in Dorpen (Zone 1)

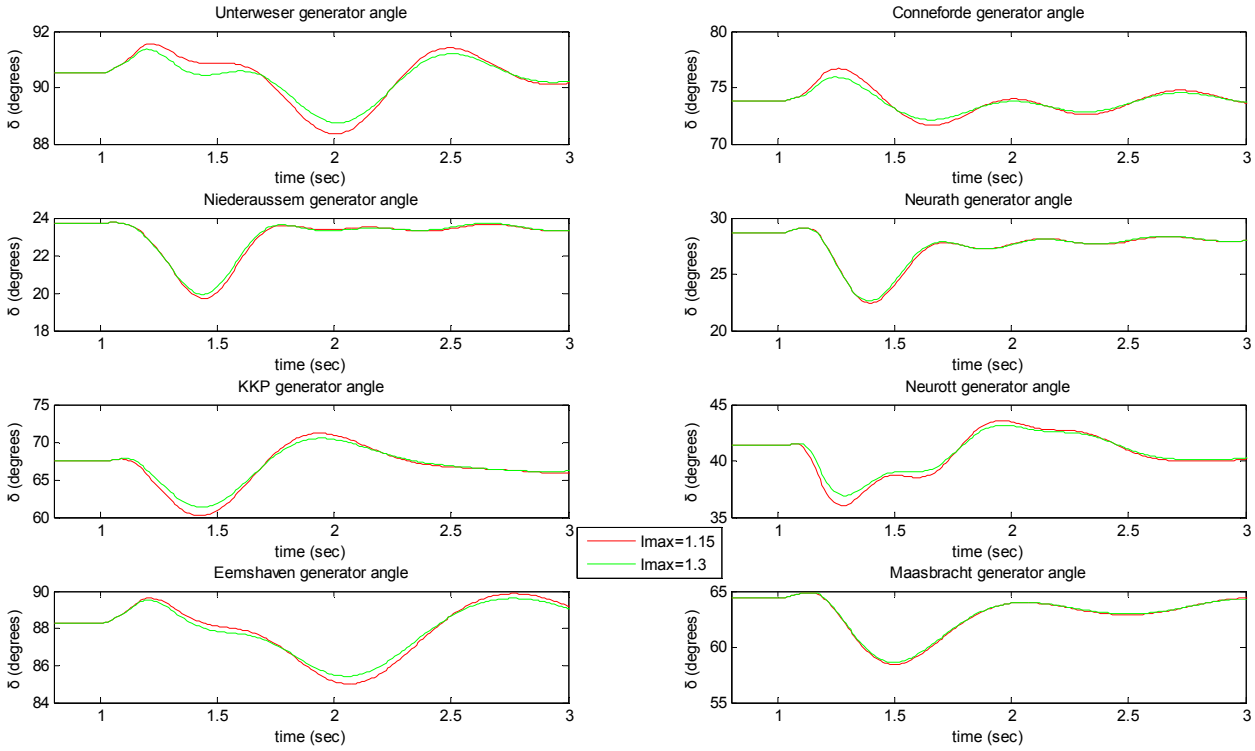

Fig. E.31 Effect of the over-current capability on generator rotor angles for a fault in Sechtem (Zone 2)

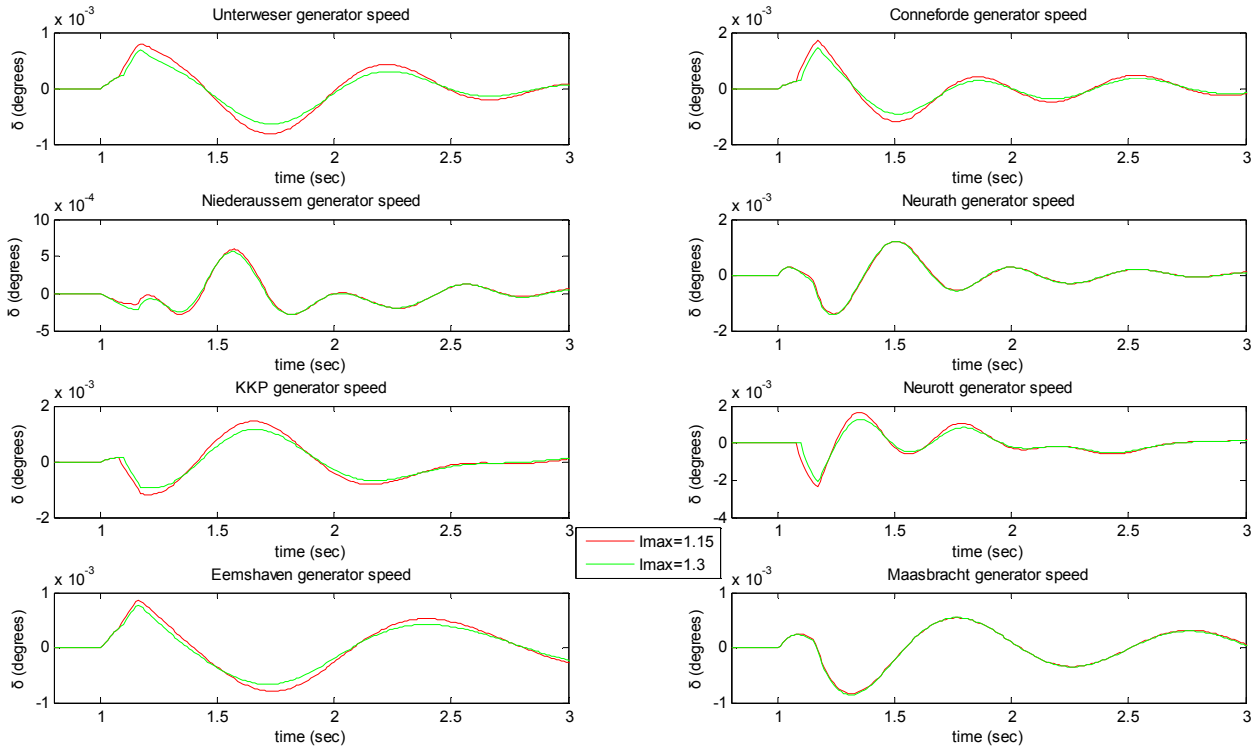

Fig. E.32 Effect of the over-current capability on generator rotor speeds for a fault in Sechtem (Zone 2)

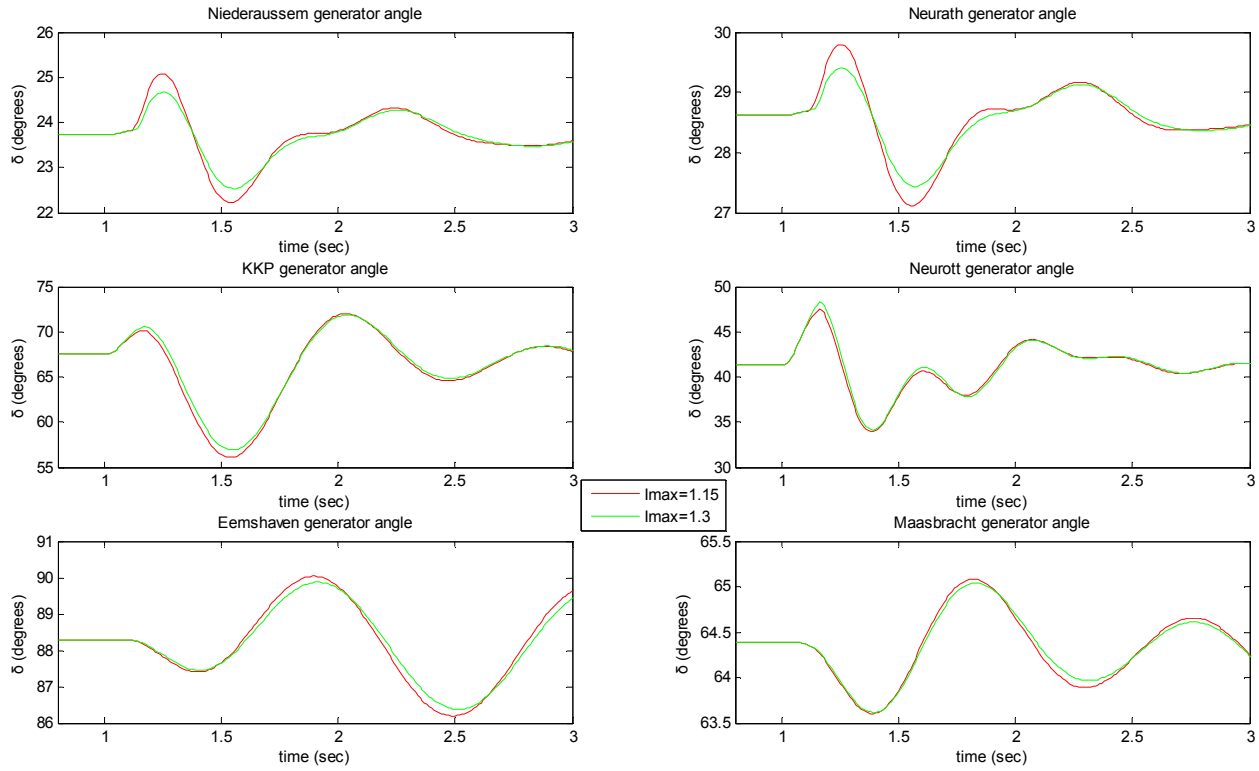

Fig. E.33 Effect of the over-current capability on generator rotor angles for a fault in Hopfingen (Zone 3)

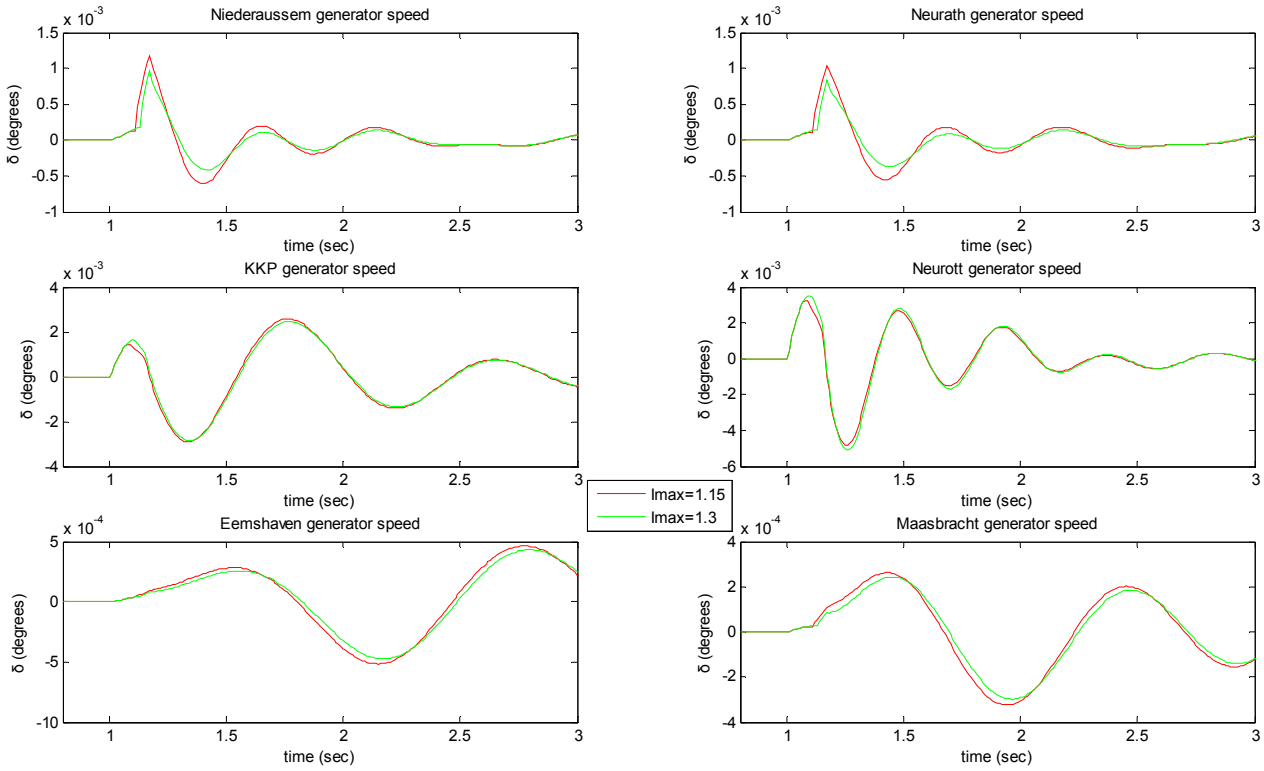

Fig. E.34 Effect of the over-current capability on generator rotor speeds for a fault in Hopfingen (Zone 3)

Results of paragraph 4.3.3.1

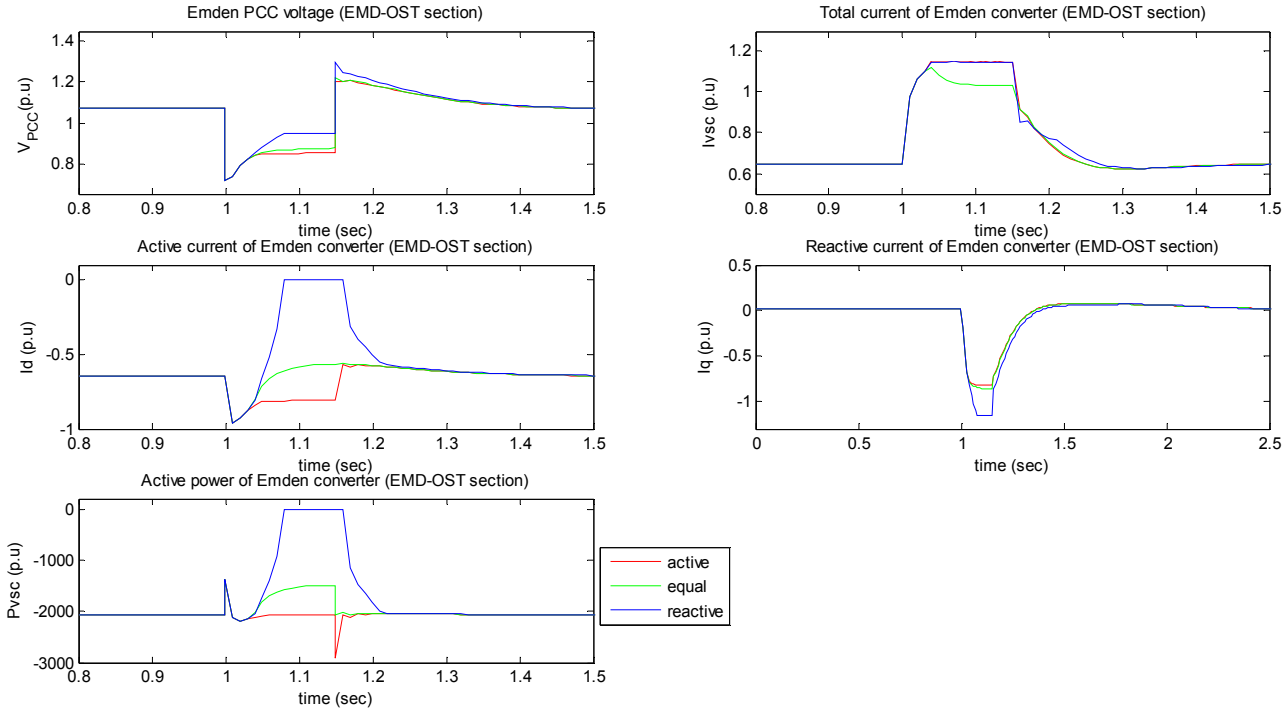

Fig. E.35 Response of Emden's converter (EMD-OST section) to a 3-phase bus fault in Dorpen (Zone 1) for different CLSs

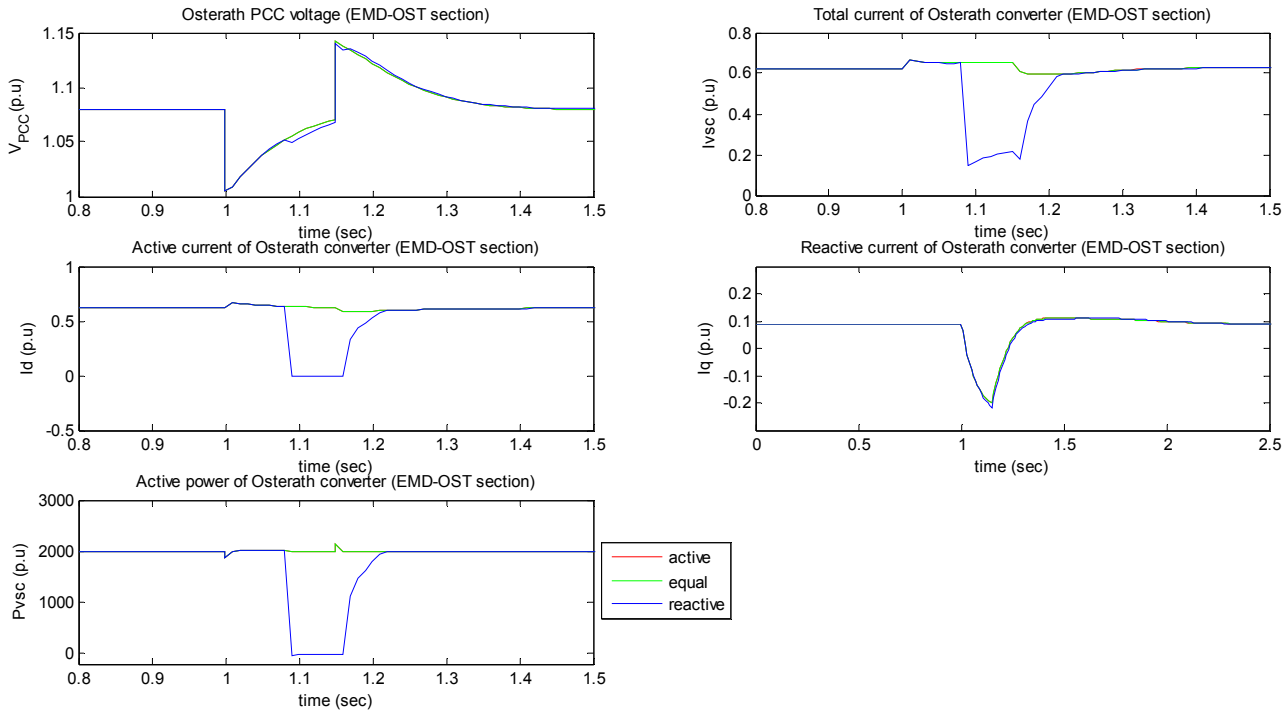

Fig. E.36 Response of Osterath's converter (EMD-OST section) to a 3-phase bus fault in Dorpen (Zone 1) for different CLSs

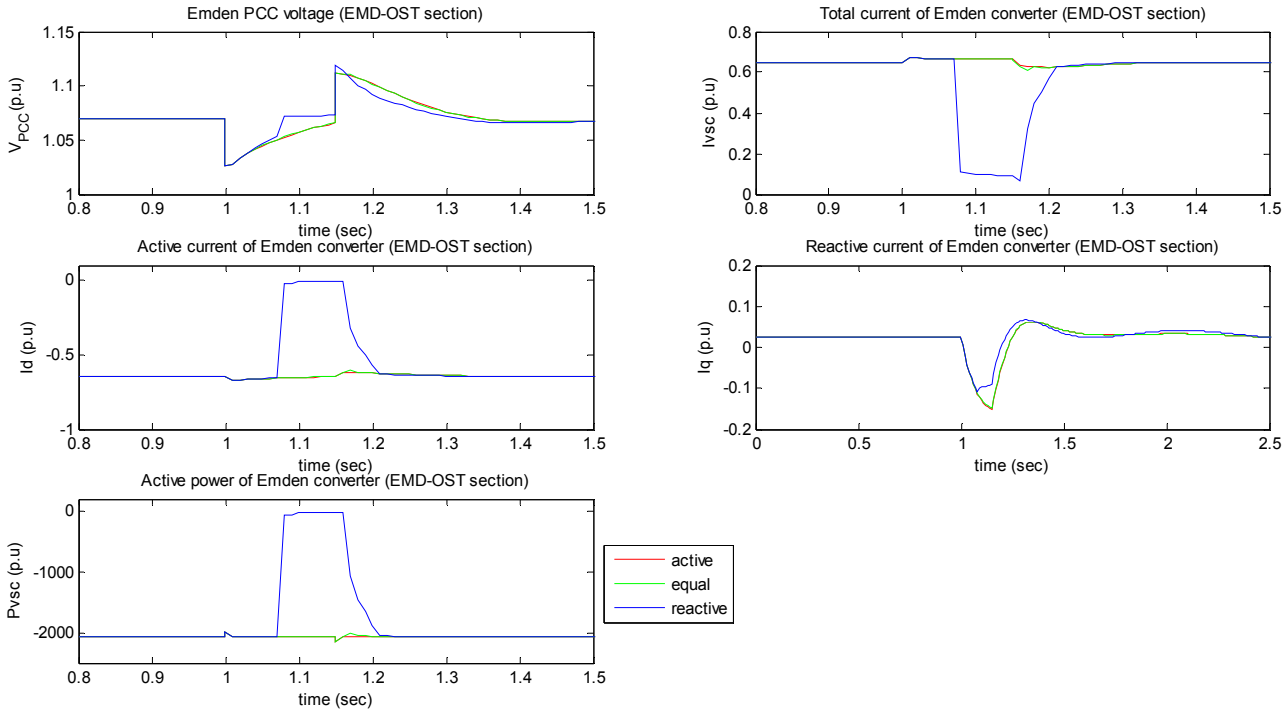

Fig. E.37 Response of Emden's converter (EMD-OST section) to a 3-phase bus fault in Sechtem (Zone 2) for different CLSs

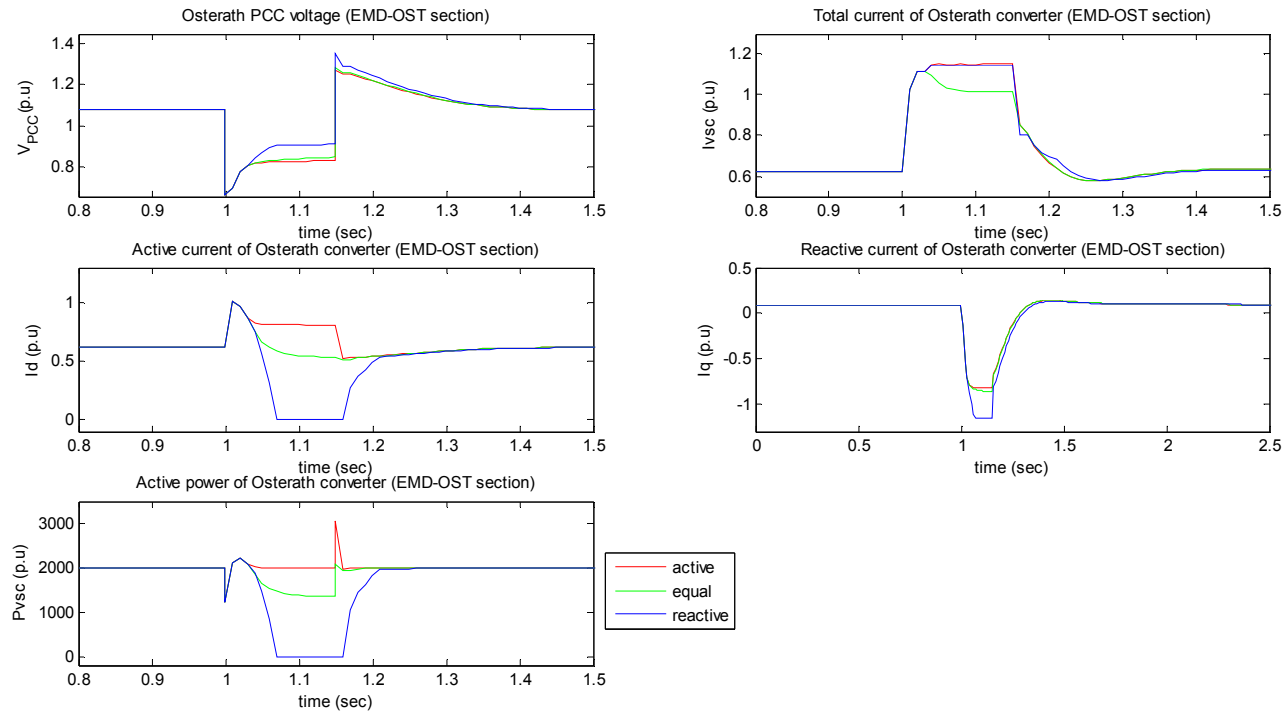

Fig. E.38 Response of Osterath's converter (EMD-OST section) to a 3-phase bus fault in Sechtem (Zone 2) for different CLSs

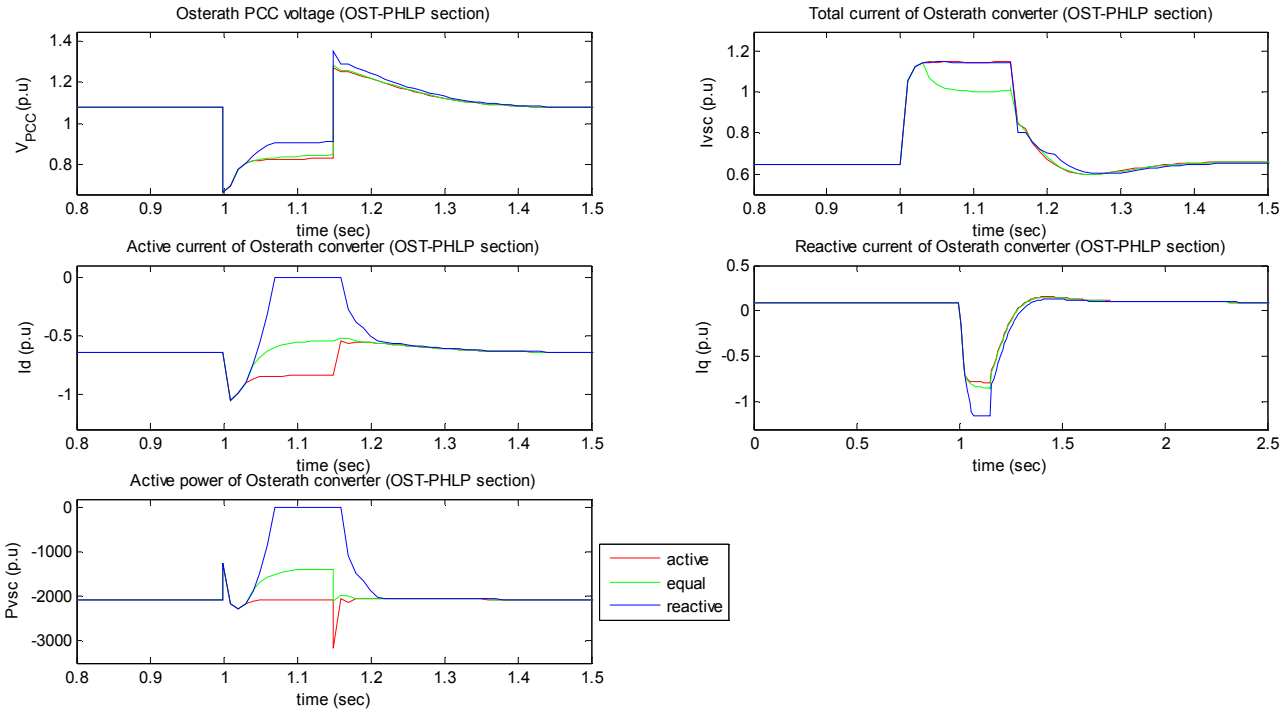

Fig. E.39 Response of Osterath's converter (OST-PHLP section) to a 3-phase bus fault in Sechtem (Zone 2) for different CLSs

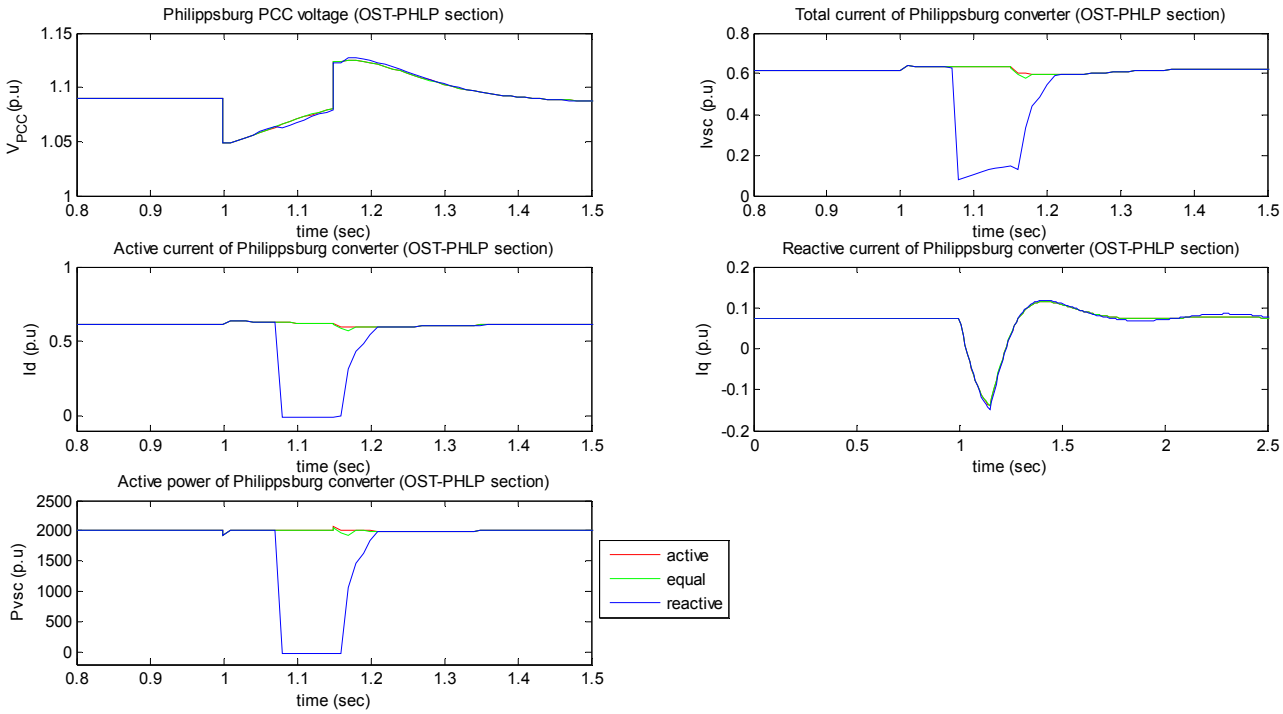

Fig. E.40 Response of Philippsburg's converter (OST-PHLP section) to a 3-phase bus fault in Sechtem (Zone 2) for different CLSs

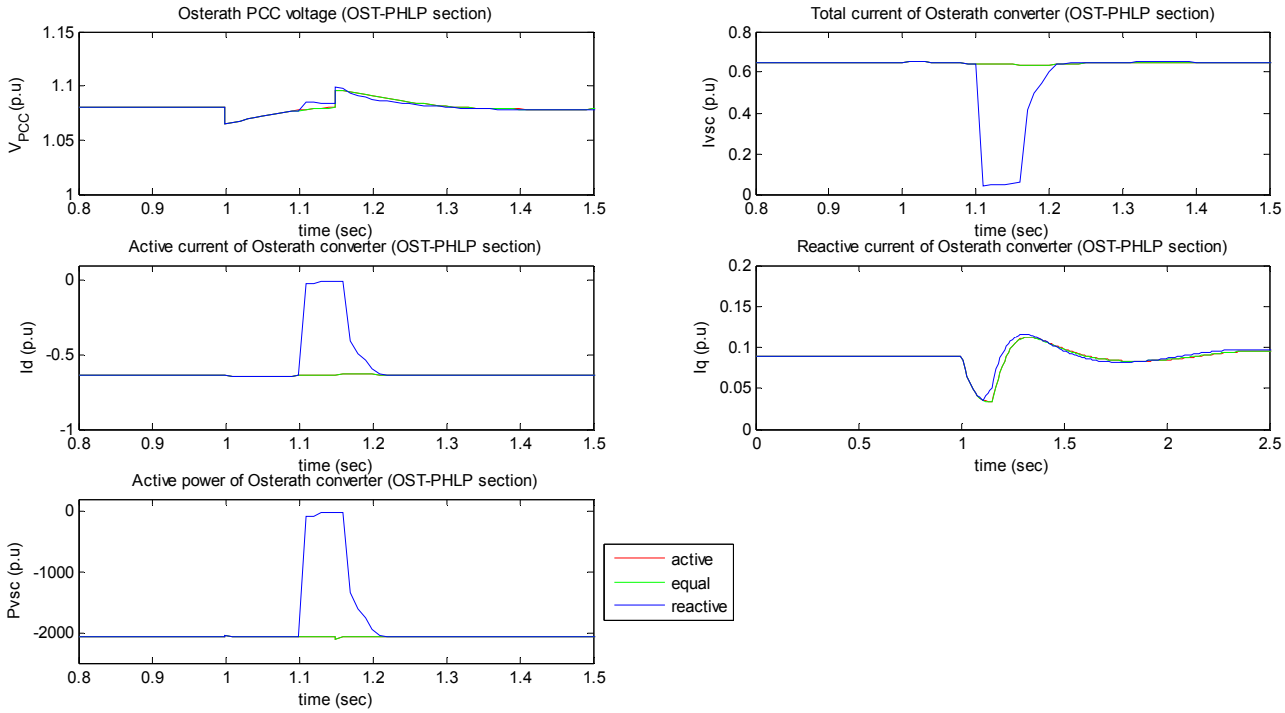

Fig. E.41 Response of Osterath's converter (OST-PHLP section) to a 3-phase bus fault in Hopfingen (Zone 3) for different CLSs

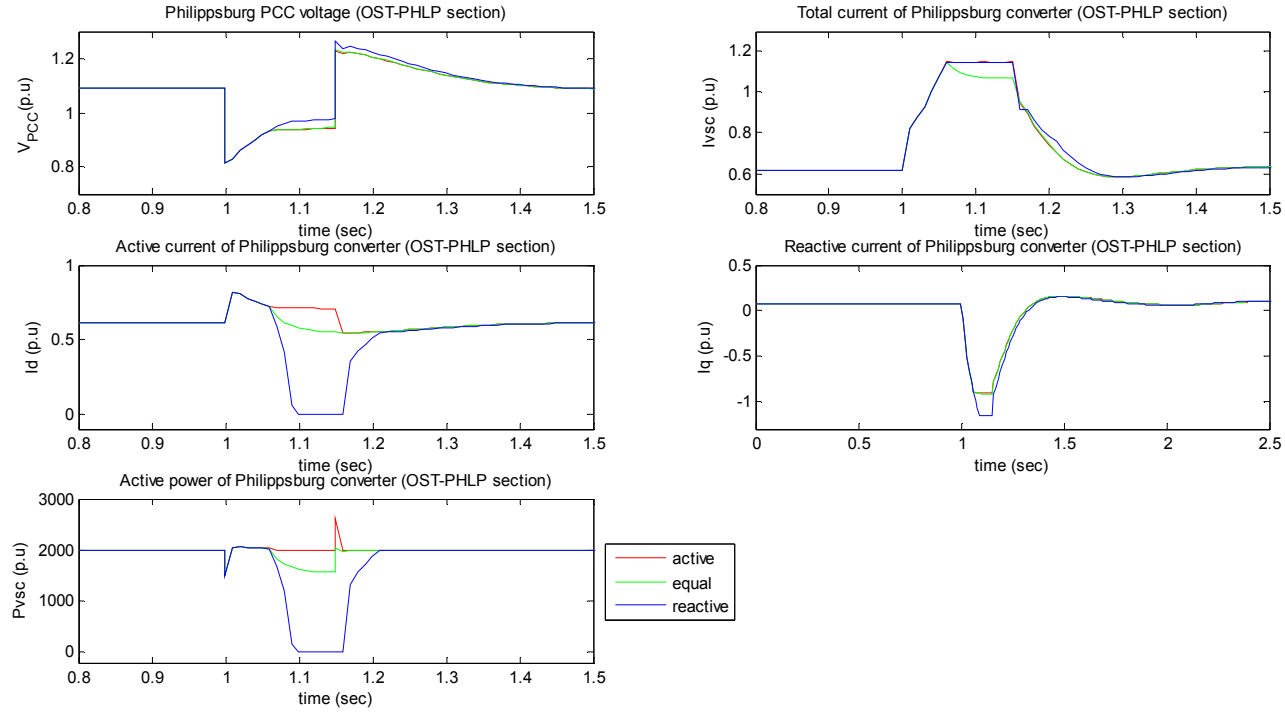

Fig. E.42 Response of Philippsburg's converter (OST-PHLP section) to a 3-phase bus fault in Hopfingen (Zone 3) for different CLSs

Results of paragraph 4.3.3.2

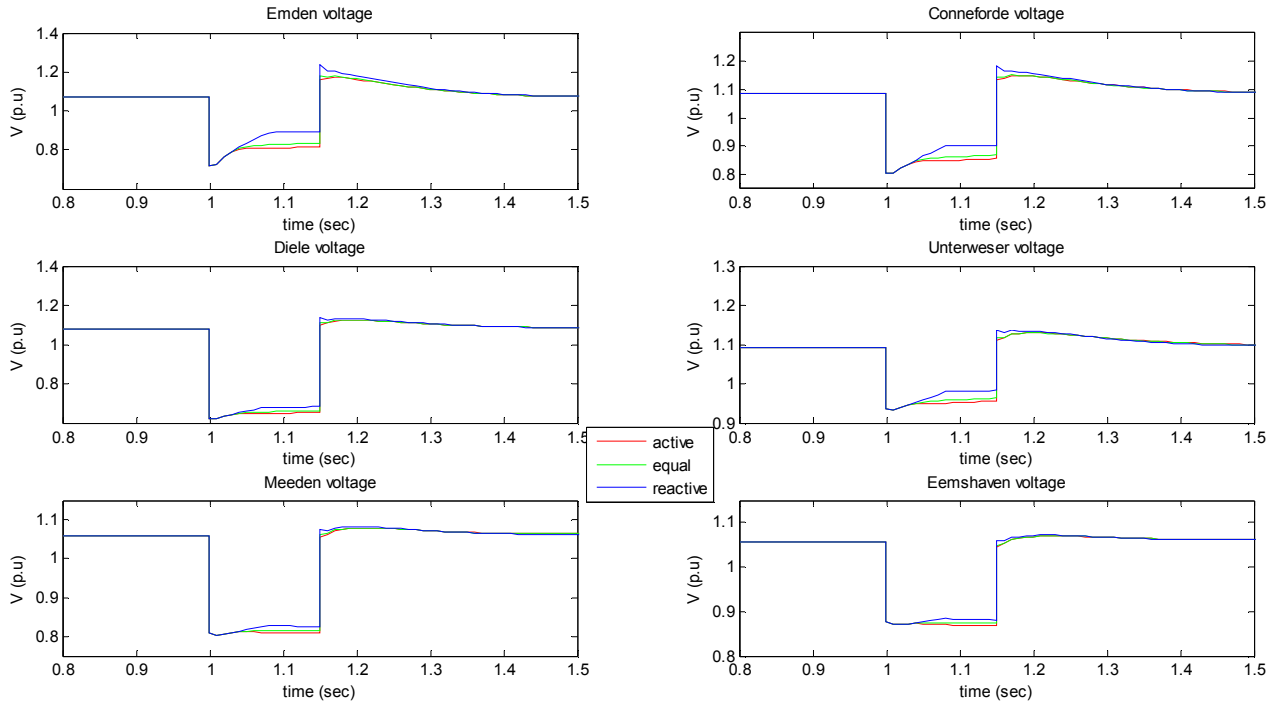

Fig. E.43 Effect of the CLS on the 380 kV bus voltages for a fault in Dorpen (Zone 1)

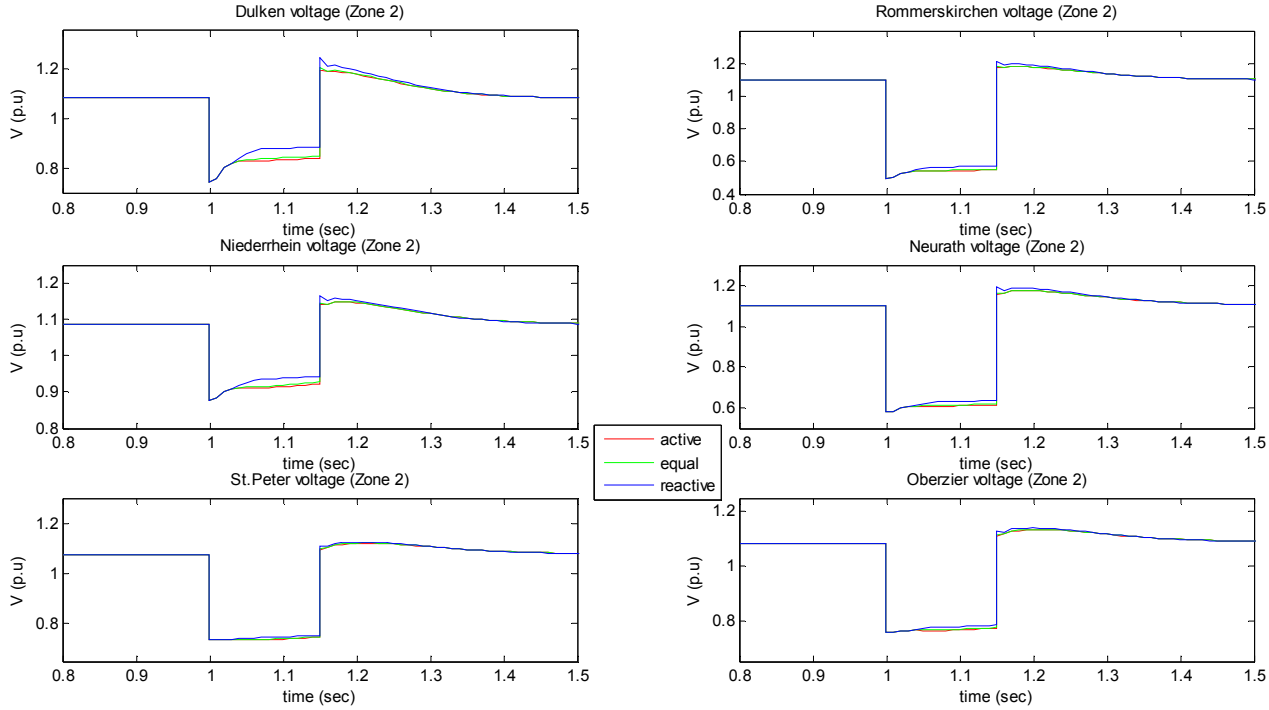

Fig. E.44 Effect of the CLS on the 380 kV bus voltages for a fault in Sechtem (Zone 2)

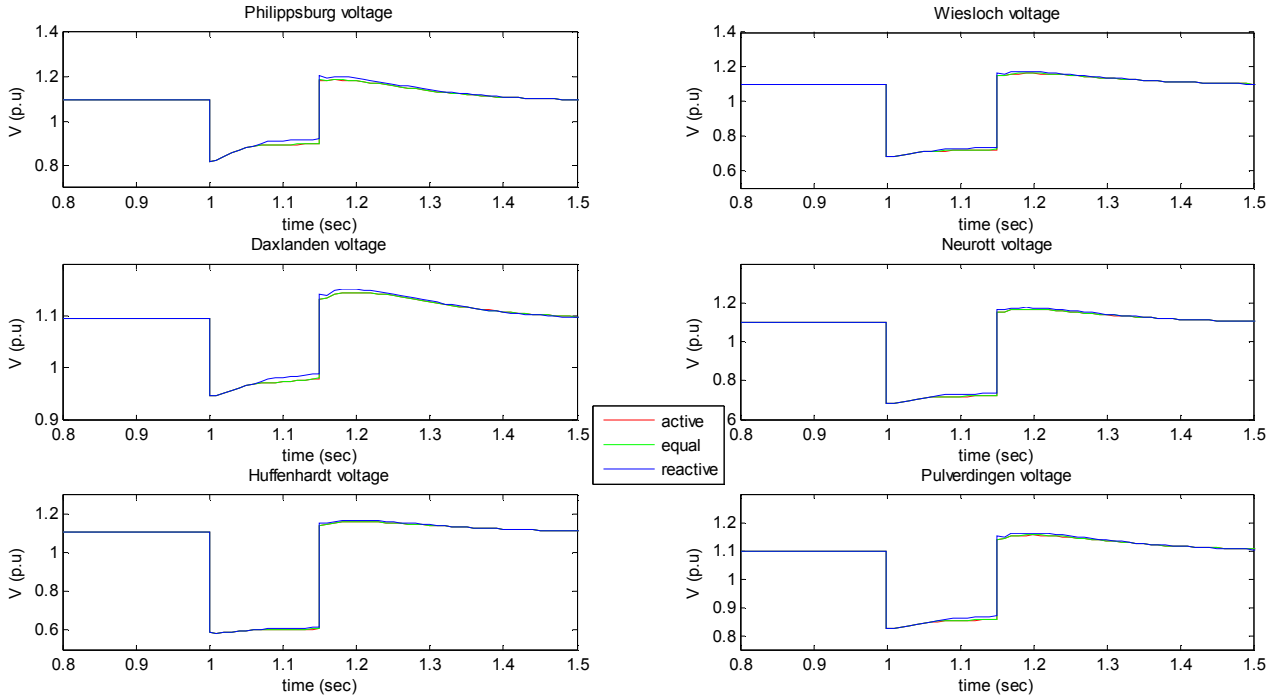

Fig. E.45 Effect of the CLS on the 380 kV bus voltages for a fault in Hopfingen (Zone 3)

Results of paragraph 4.3.3.3

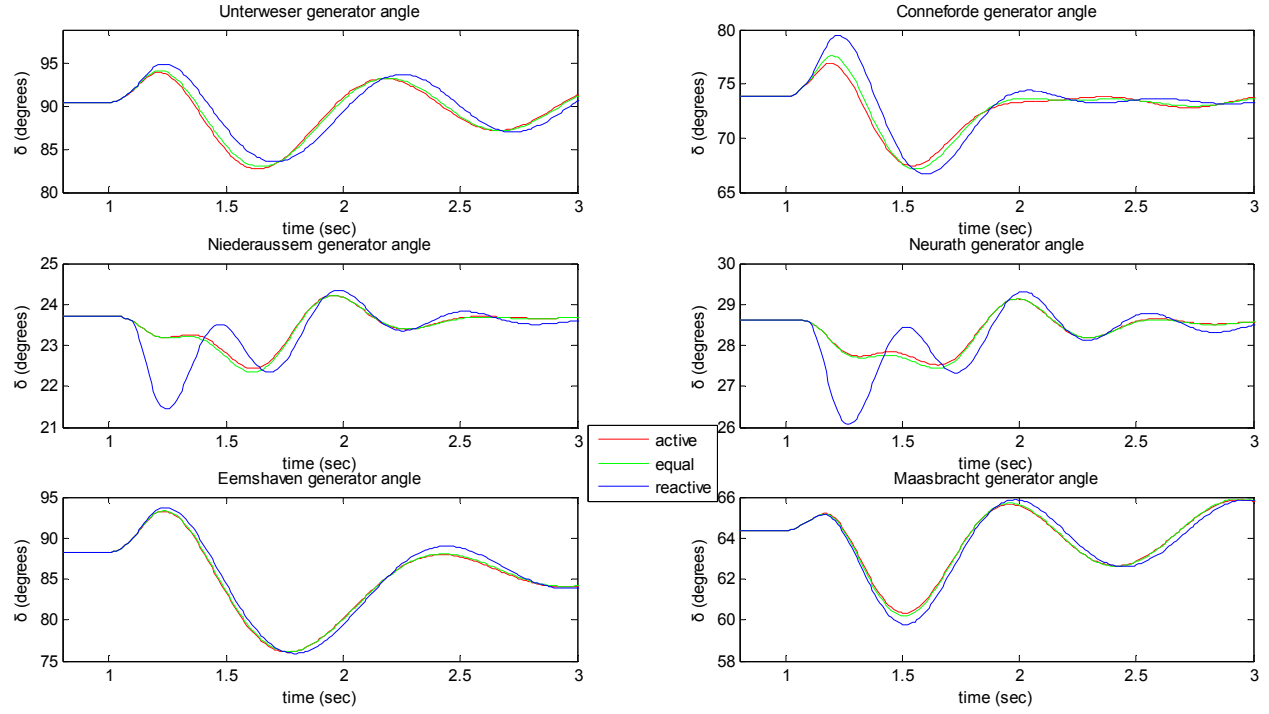

Fig. E.46 Effect of the CLS on generator rotor angles for a fault in Dorpen (Zone 1)

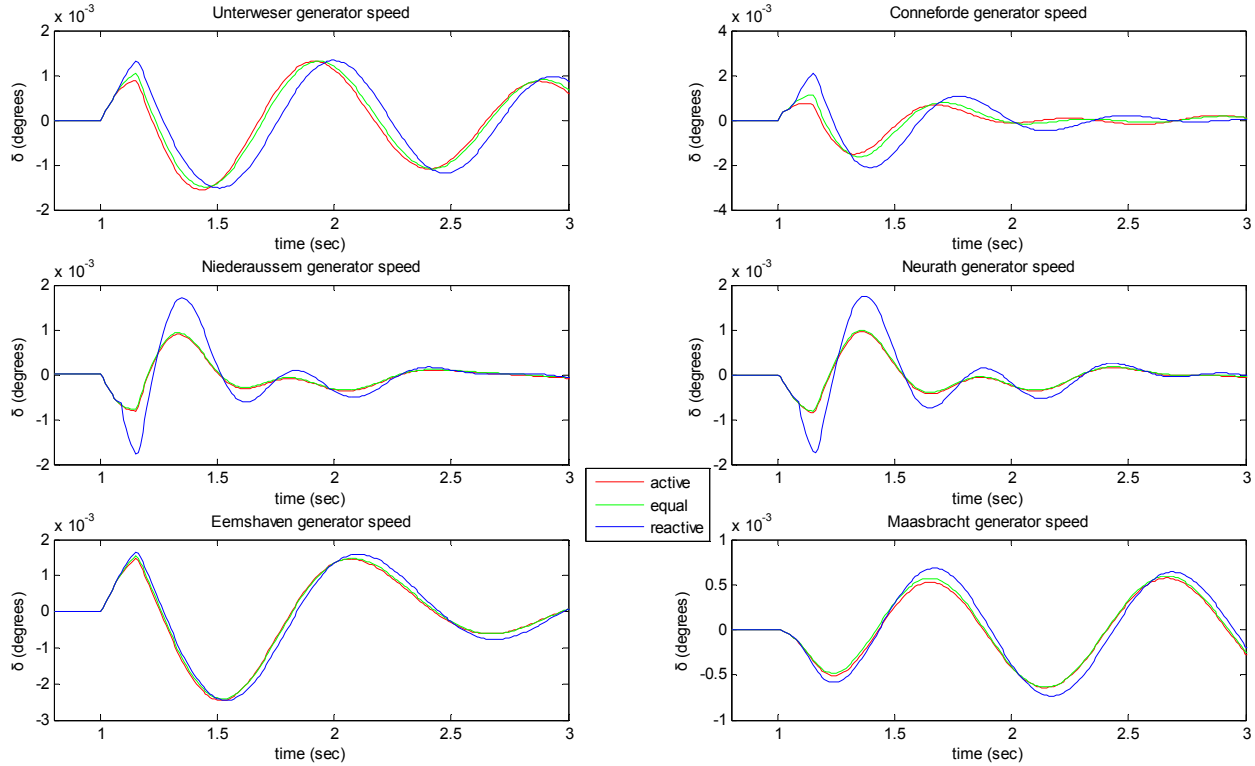

Fig. E.47 Effect of the CLS on generator rotor speeds for a fault in Dorpen (Zone 1)

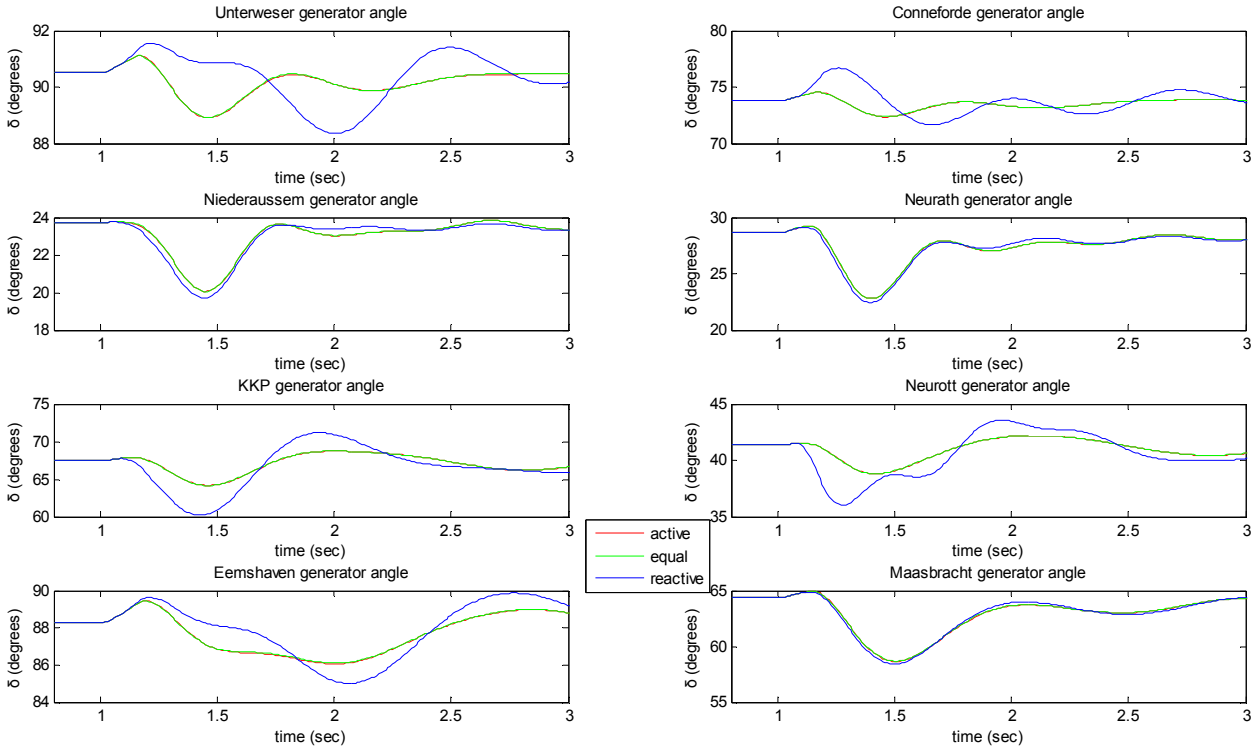

Fig. E.48 Effect of the CLS on generator rotor angles for a fault in Sechtem (Zone 2)

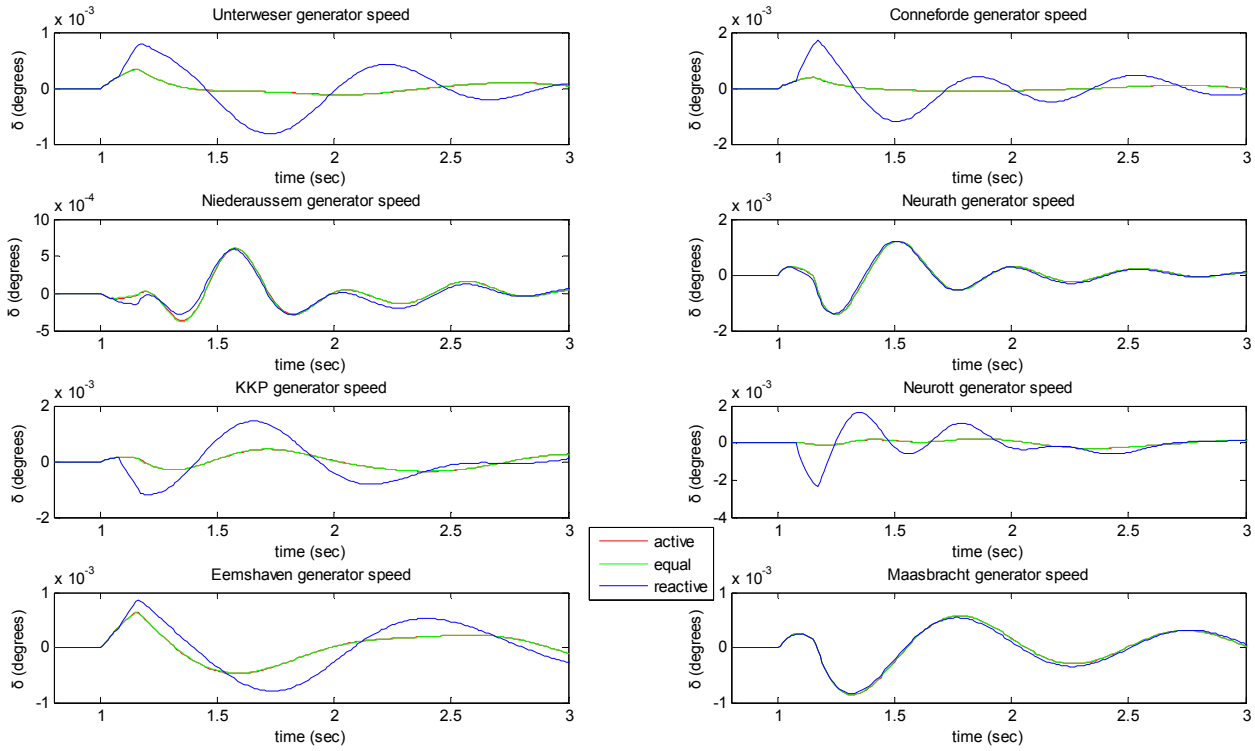

Fig. E.49 Effect of the CLS on generator rotor speeds for a fault in Sechtem (Zone 2)

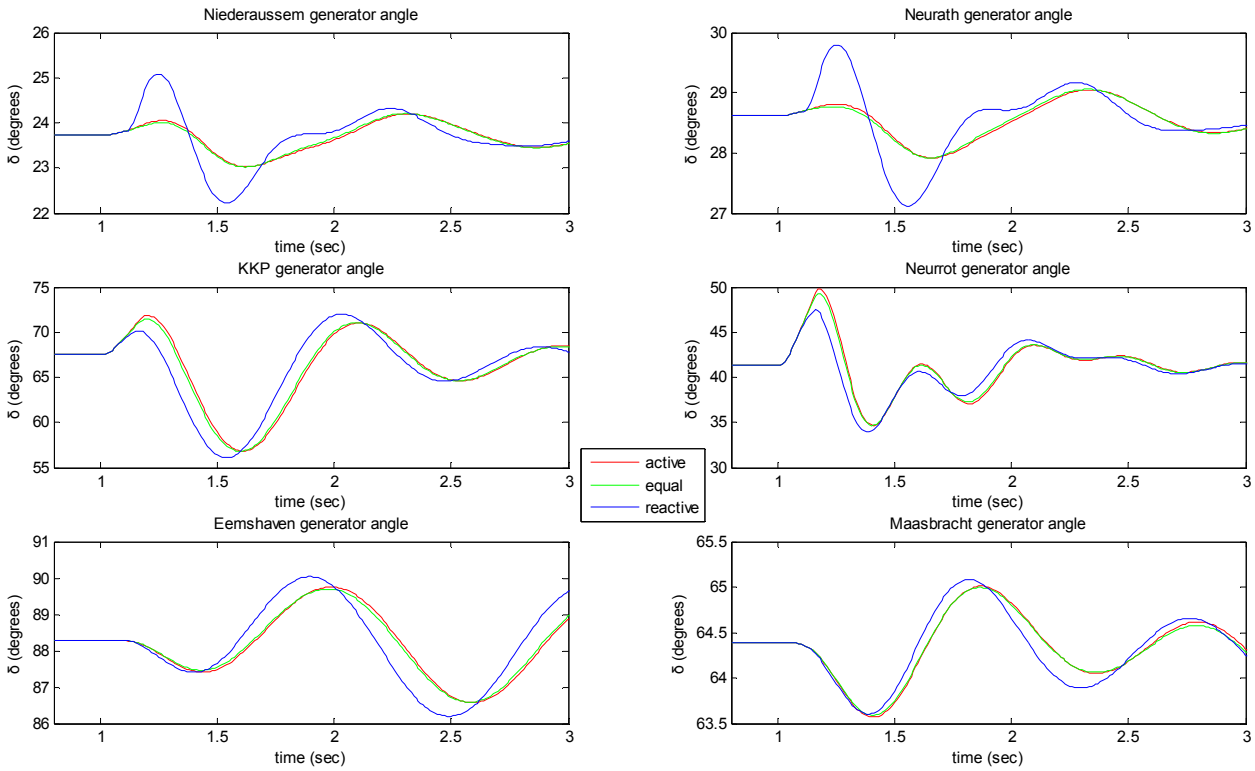

Fig. E.50 Effect of the CLS on generator rotor angles for a fault in Hopfingen (Zone 3)

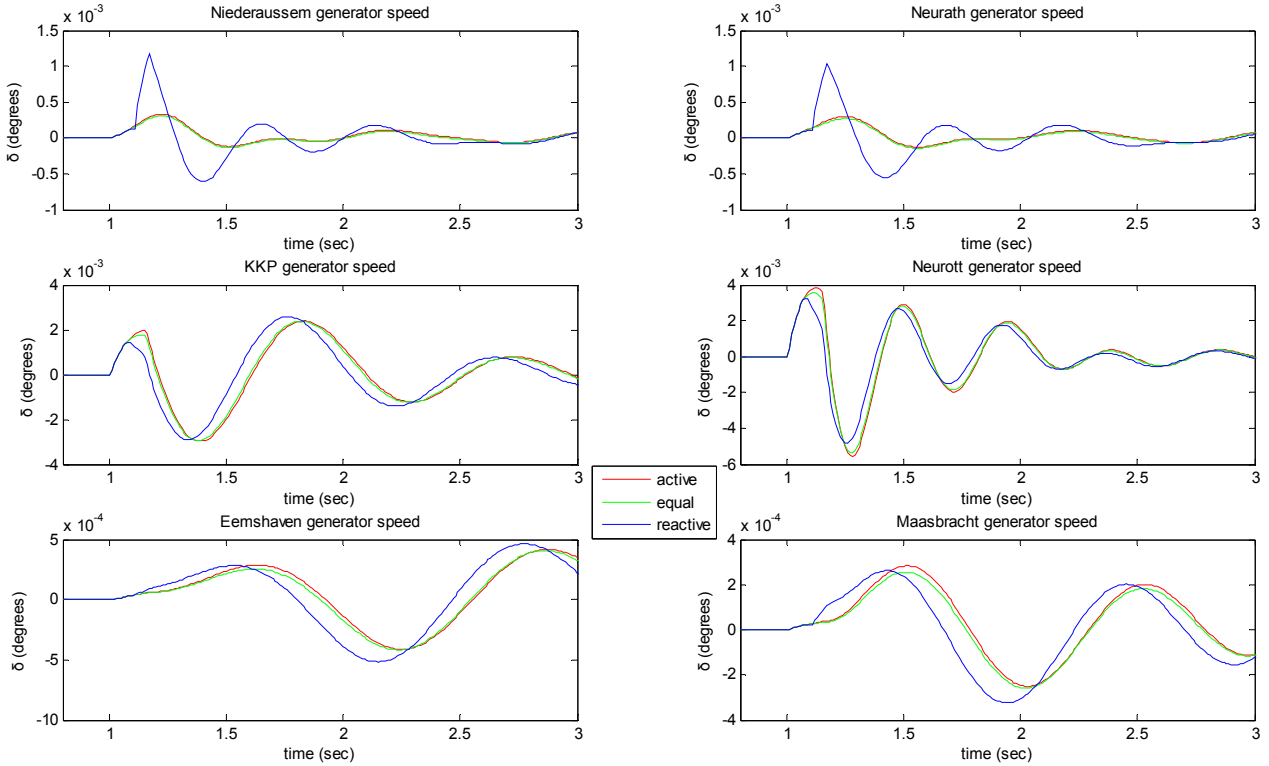

Fig. E.51 Effect of the CLS on generator rotor speeds for a fault in Hopfingen (Zone 3)

Results of paragraph 4.4.1.1

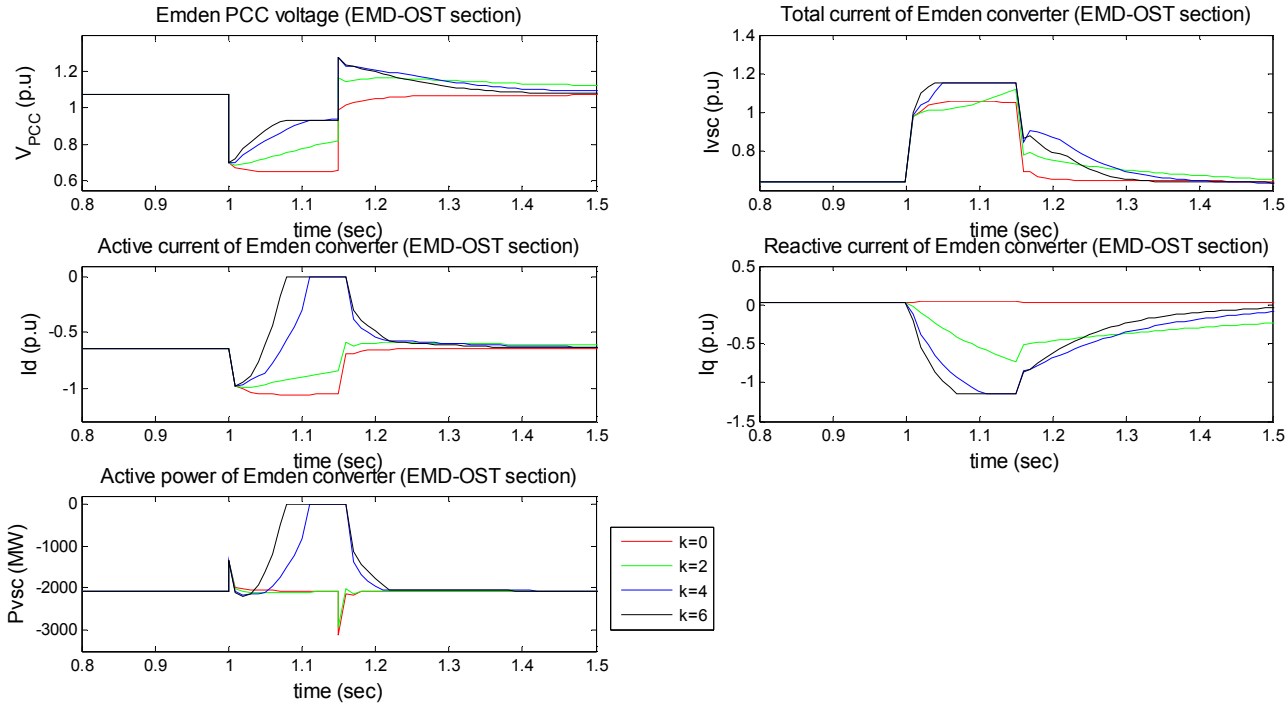

Fig. E.52 Response of Emden's converter (EMD-OST section) to a 3-phase bus fault in Meeden for different values of k

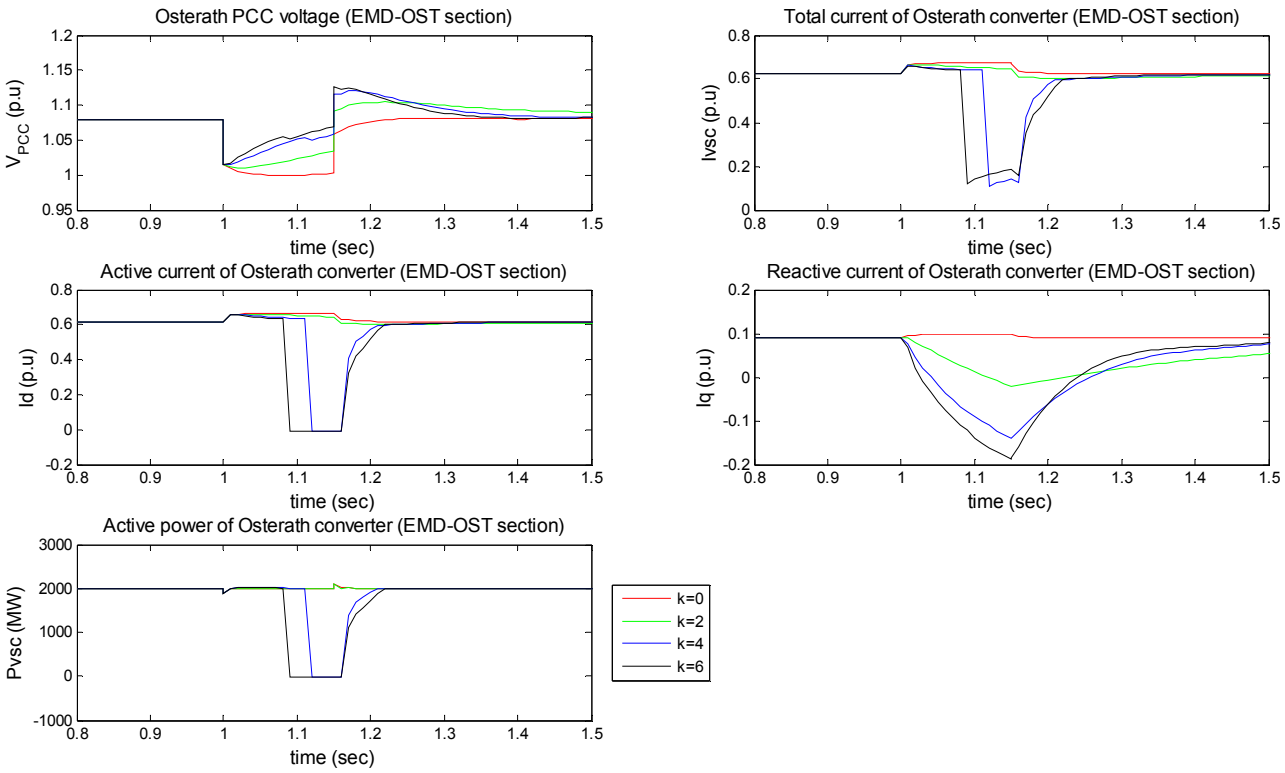

Fig. E.53 Response of Osterath's converter (EMD-OST section) to a 3-phase bus fault in Meeden for different values of k

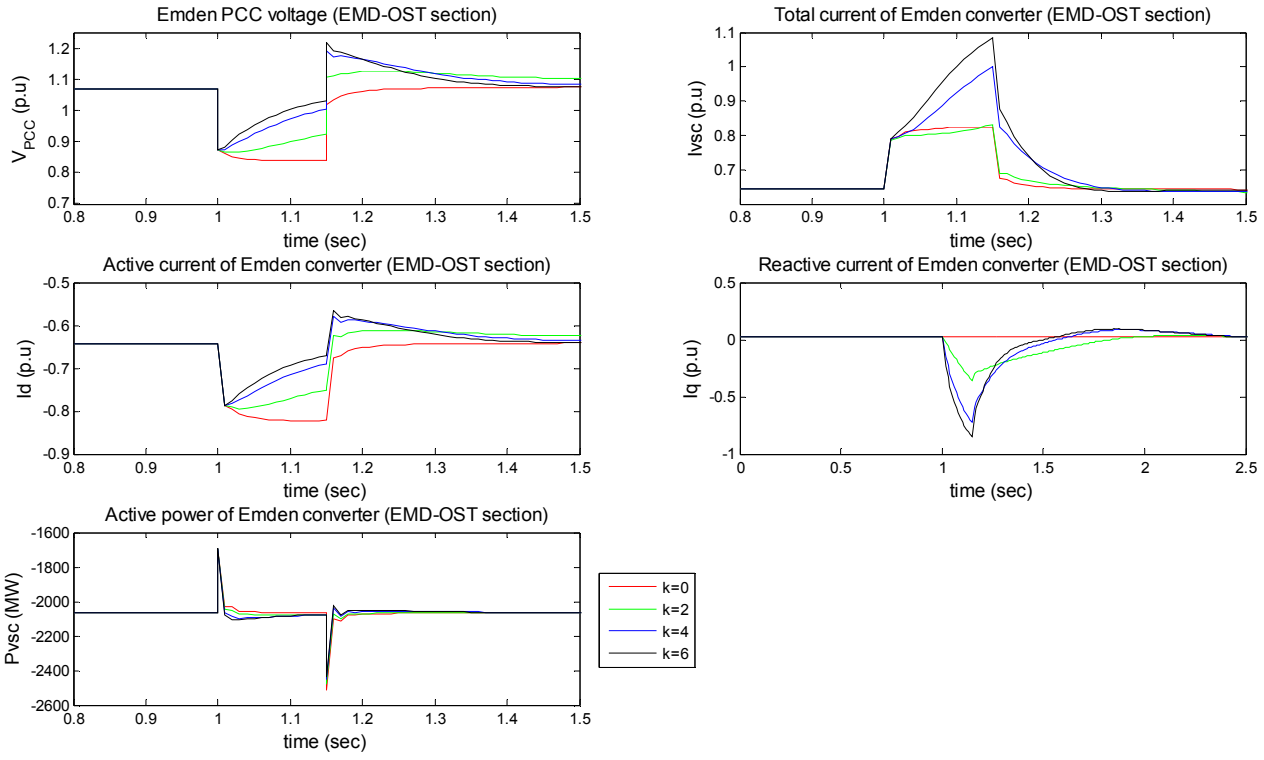

Fig. E.54 Response of Emden's converter (EMD-OST section) to a 3-phase bus fault in Zwolle for different values of k

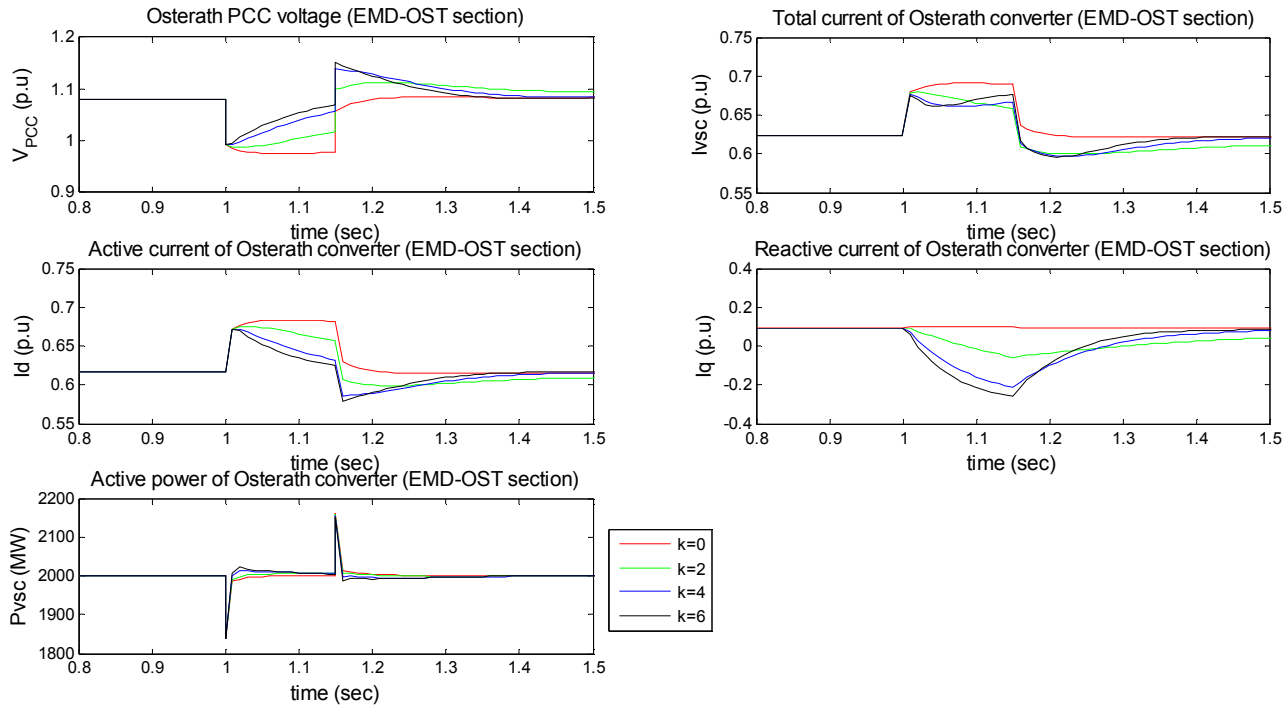

Fig. E.55 Response of Osterath's converter (EMD-OST section) to a 3-phase bus fault in Zwolle for different values of k

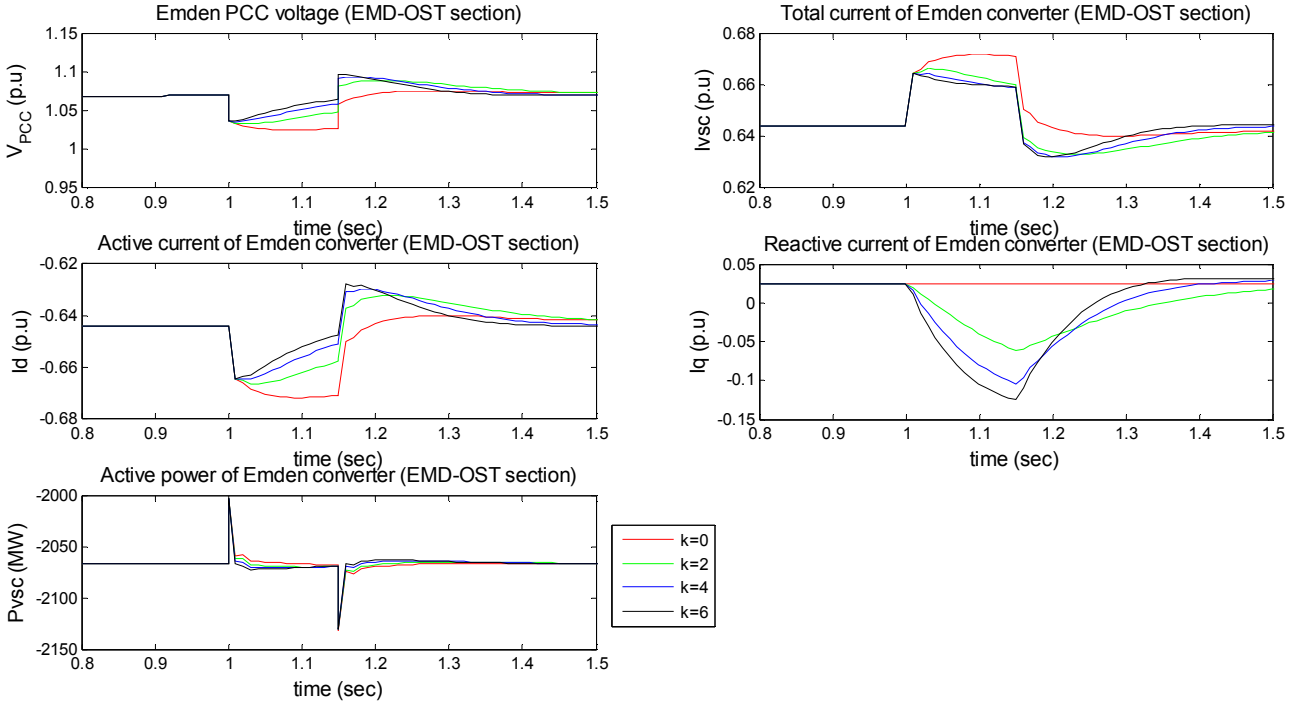

Fig. E.56 Response of Emden's converter (EMD-OST section) to a 3-phase bus fault in Maasbracht for different values of k

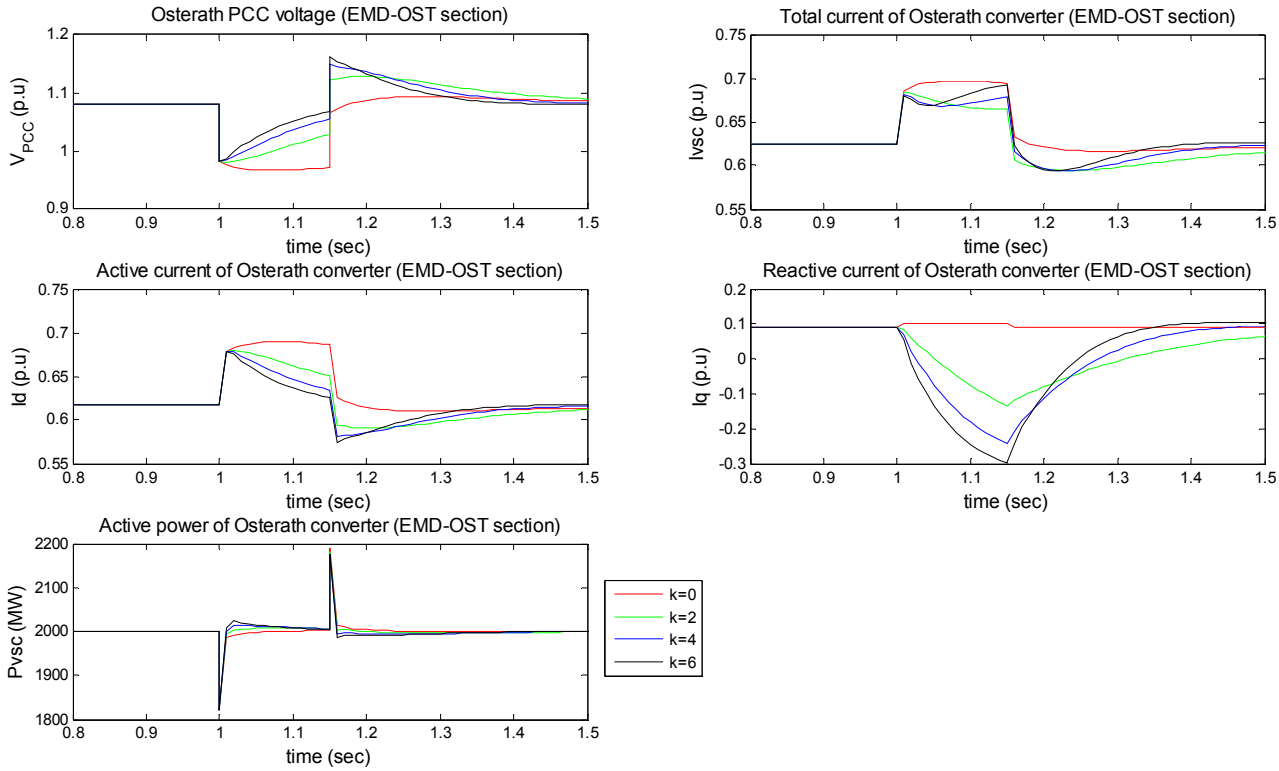

Fig. E.57 Response of Osterath's converter (EMD-OST section) to a 3-phase bus fault in Maasbracht for different values of k

Results of paragraph 4.4.1.2

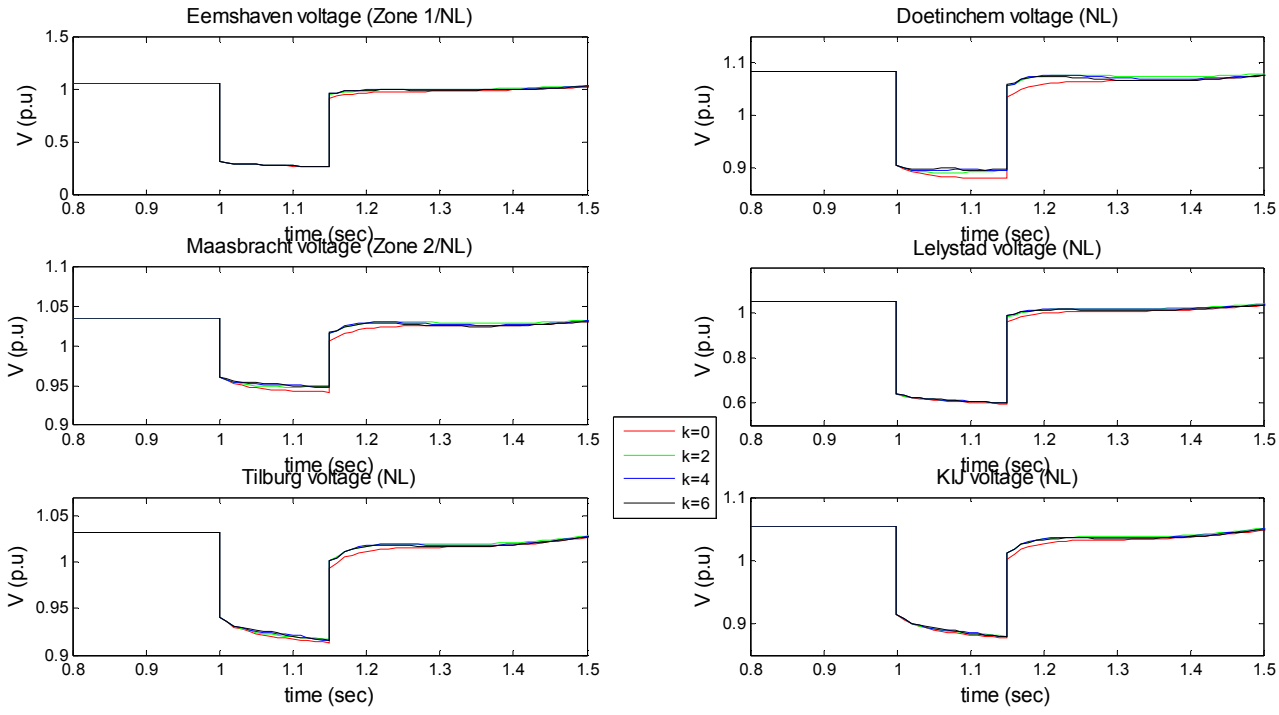

Fig. E.58 Effect of the k gain on the 380 kV bus voltages for a fault in Meeden

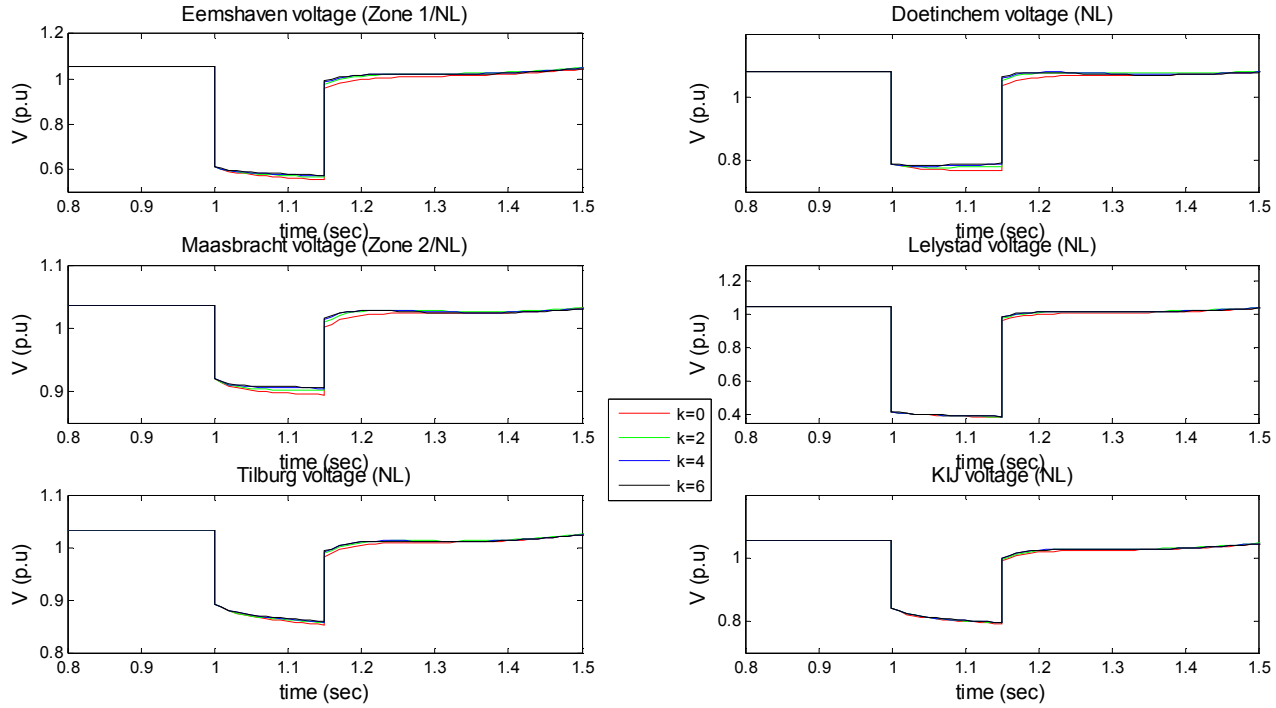

Fig. E.59 Effect of the k gain on the 380 kV bus voltages for a fault in Zwolle

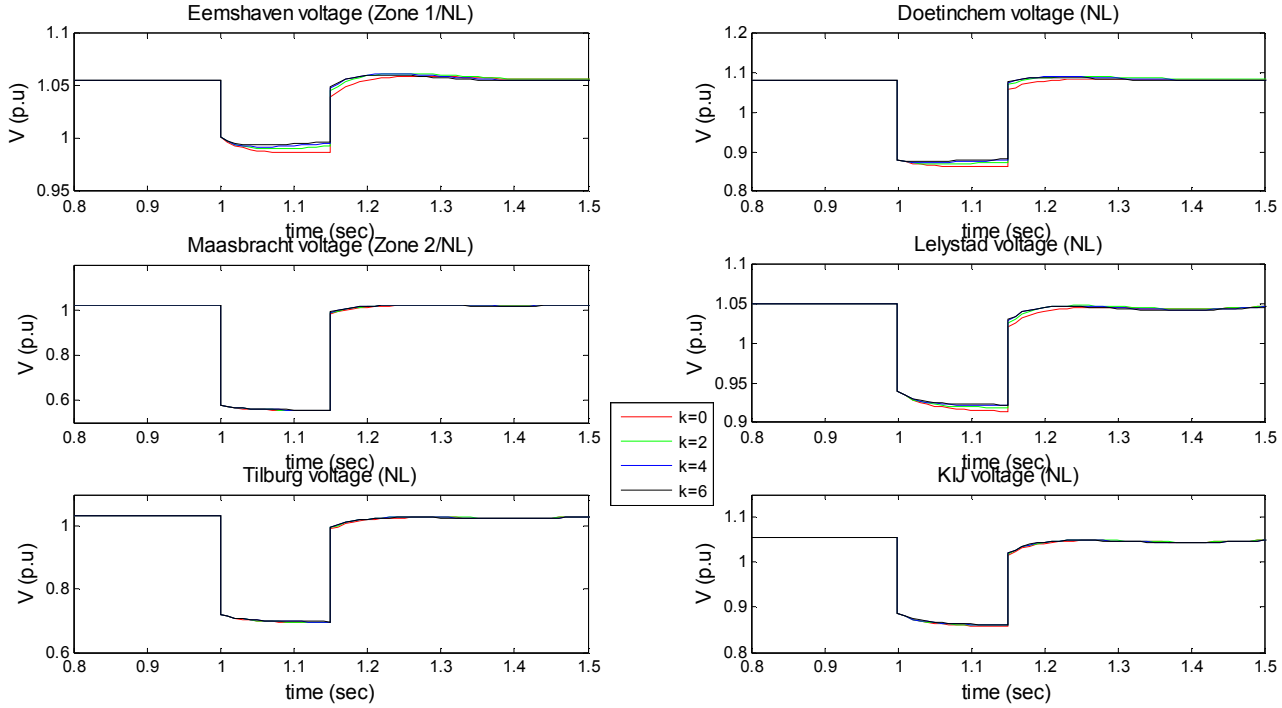

Fig. E.60 Effect of the k gain on the 380 kV bus voltages for a fault in Maasbracht

Results of paragraph 4.4.1.3

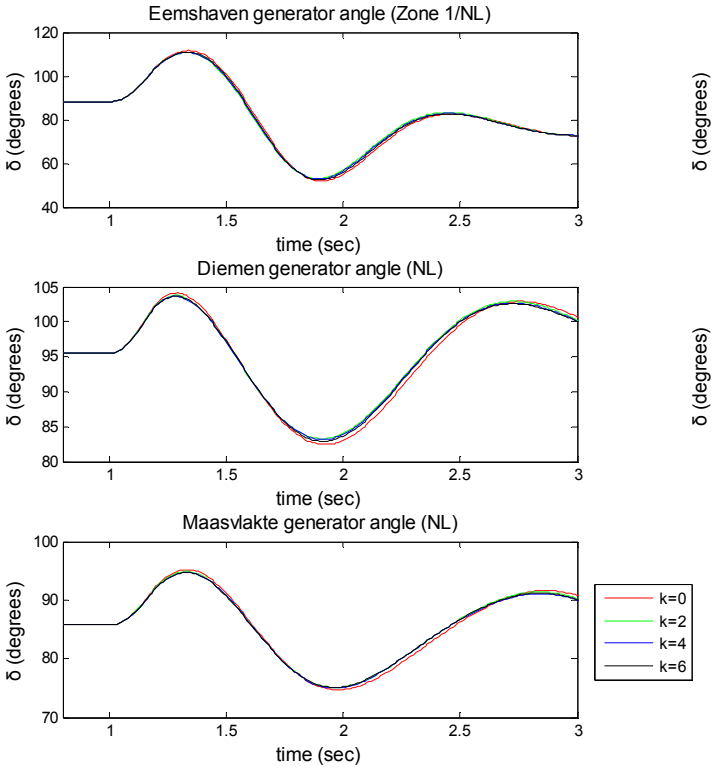

Fig. E.61 Effect of k gain on generator rotor angles for a fault in Meeden

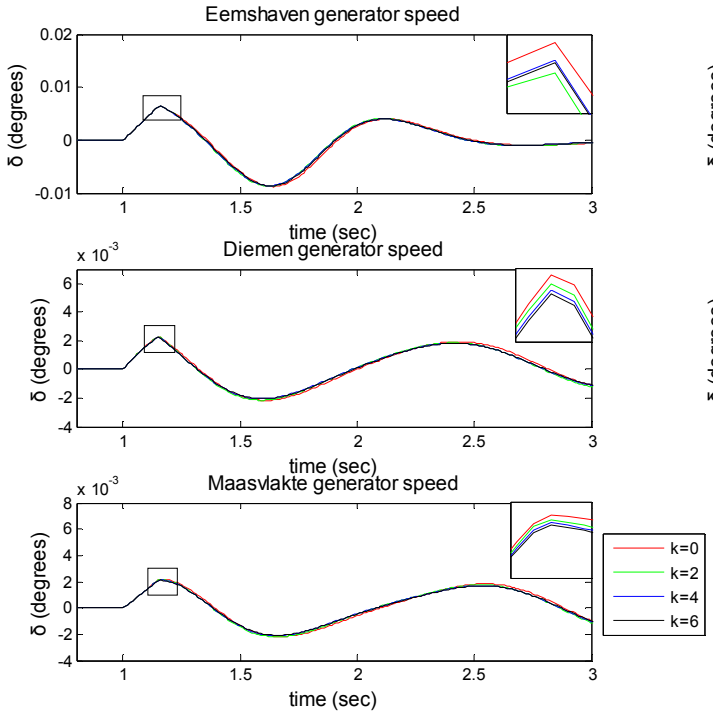

Fig. E.62 Effect of k gain on generator rotor speeds for a fault in Meeden

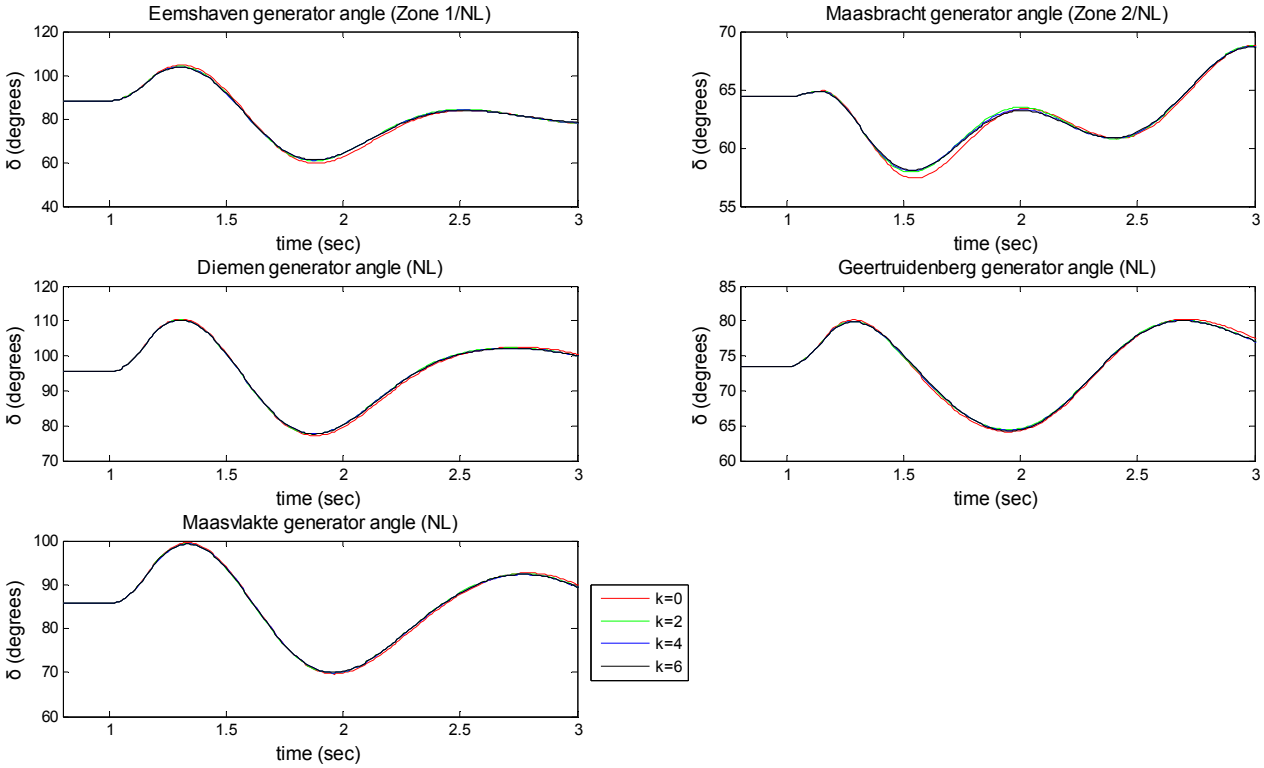

Fig. E.63 Effect of k gain on generator rotor angles for a fault in Zwolle

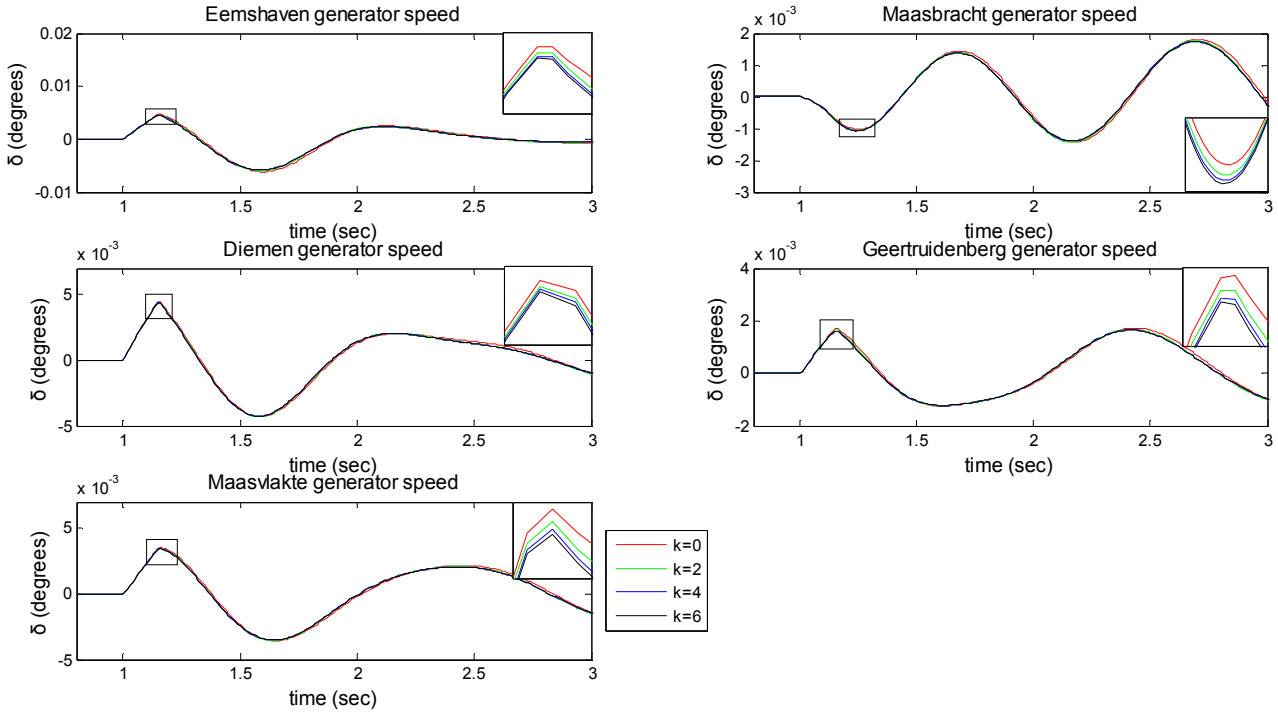

Fig. E.64 Effect of k gain on generator rotor speeds for a fault in Zwolle

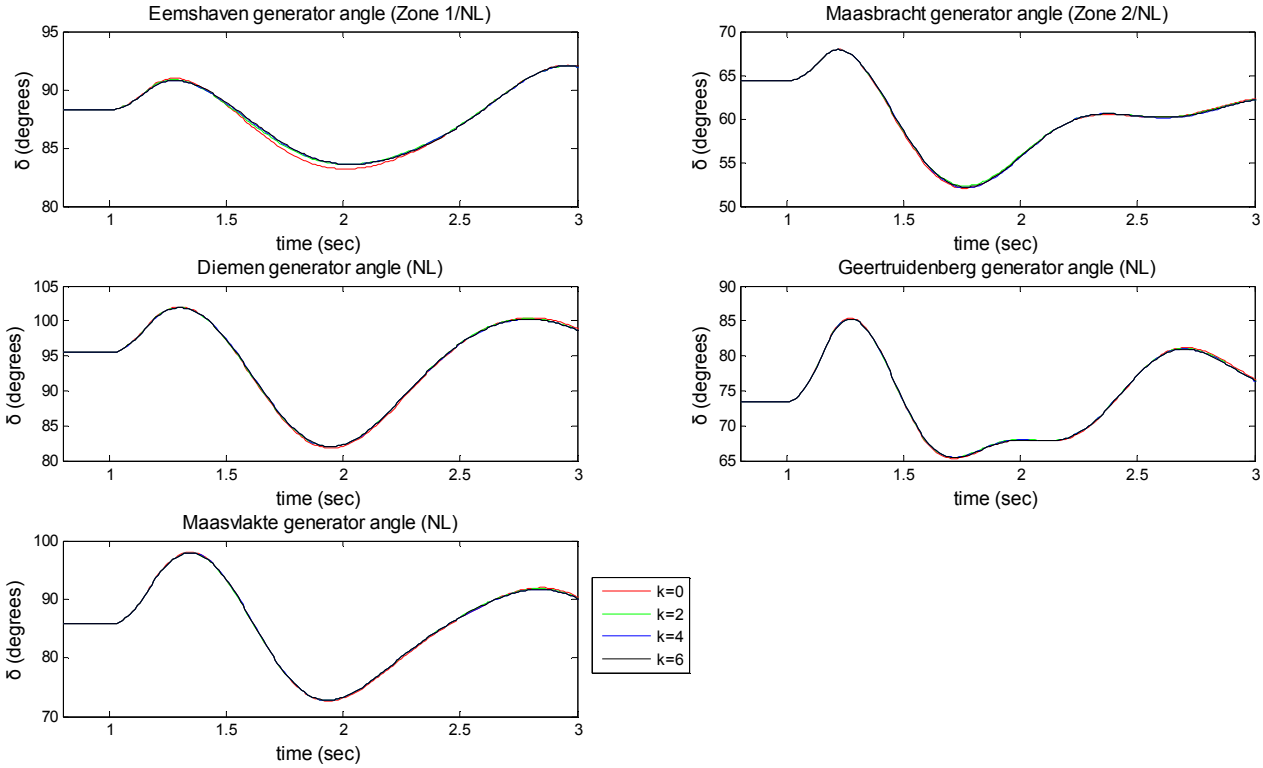

Fig. E.65 Effect of k gain on generator rotor angles for a fault in Maasbracht

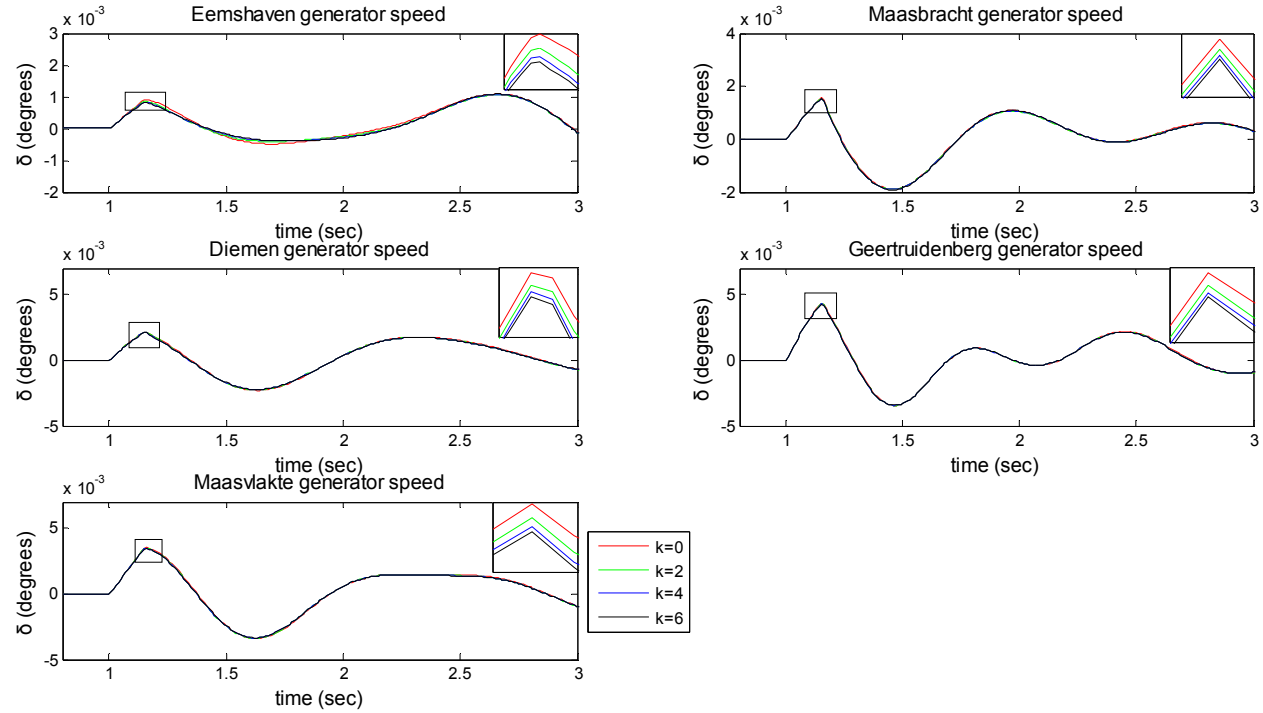

Fig. E.66 Effect of k gain on generator rotor speeds for a fault in Maasbracht

Results of paragraph 4.5.1

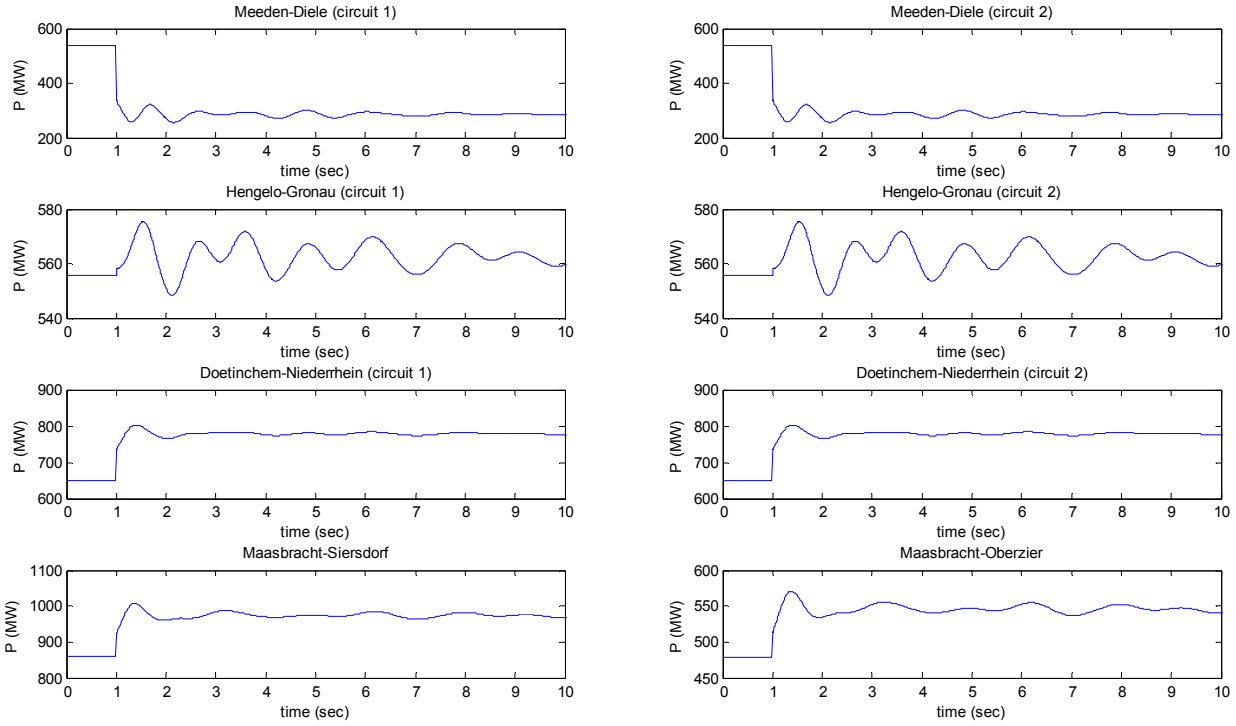

Fig.E.67 NL-DE interconnection power for loss of the EMD-OST section

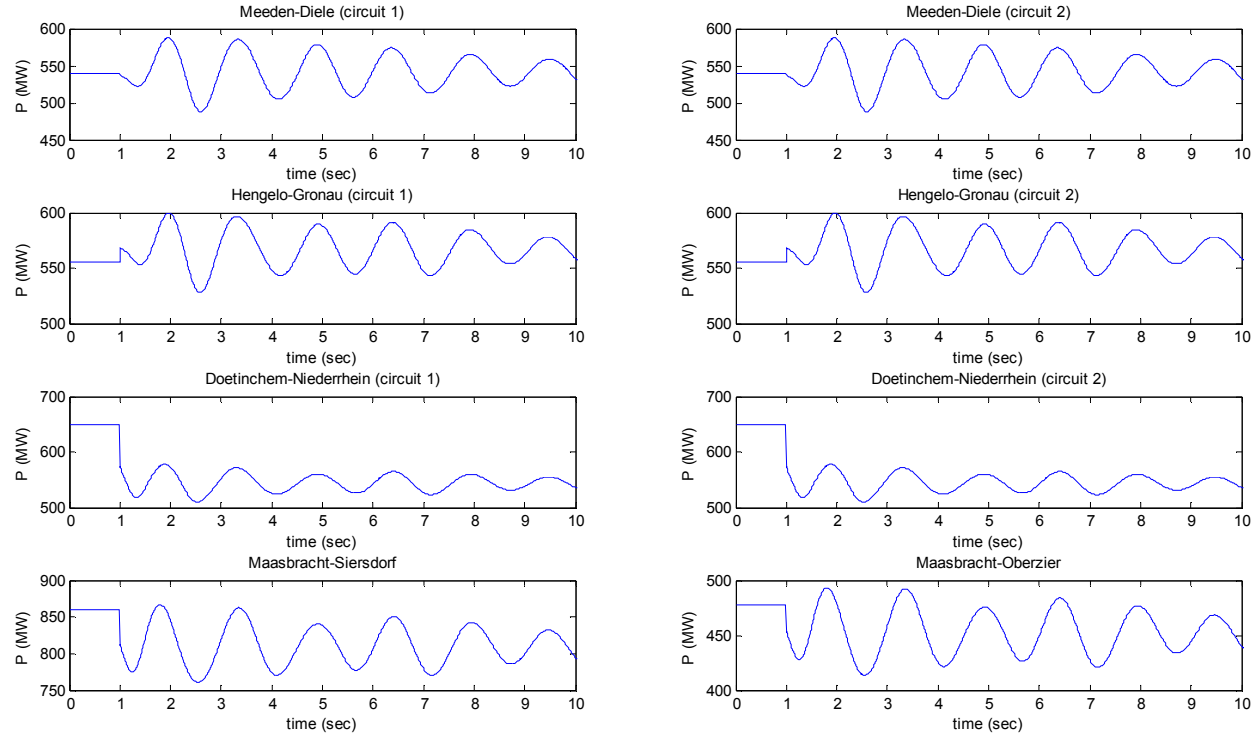

Fig.E.68 NL-DE interconnection power for loss of the OST-PHLP section

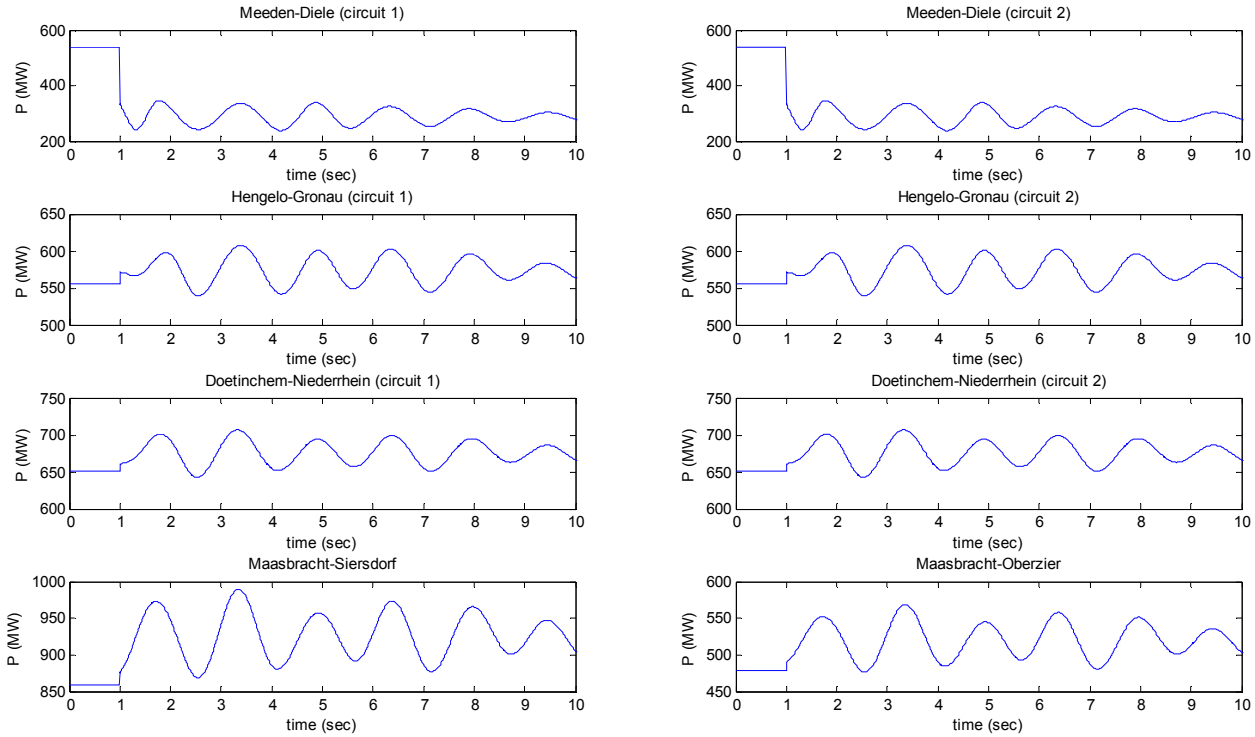

Fig.E.69 NL-DE interconnection power for both section lost

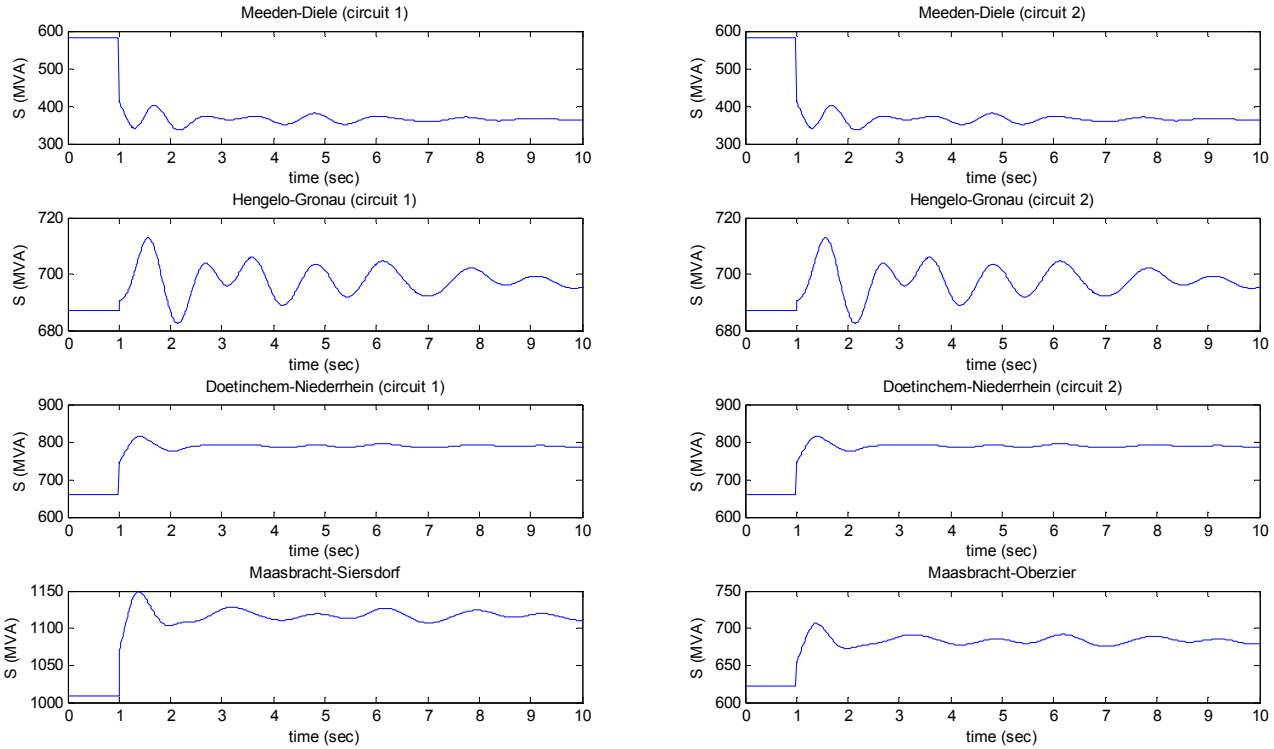

Fig.E.70 NL-DE interconnection apparent power for loss of the EMD-OST section

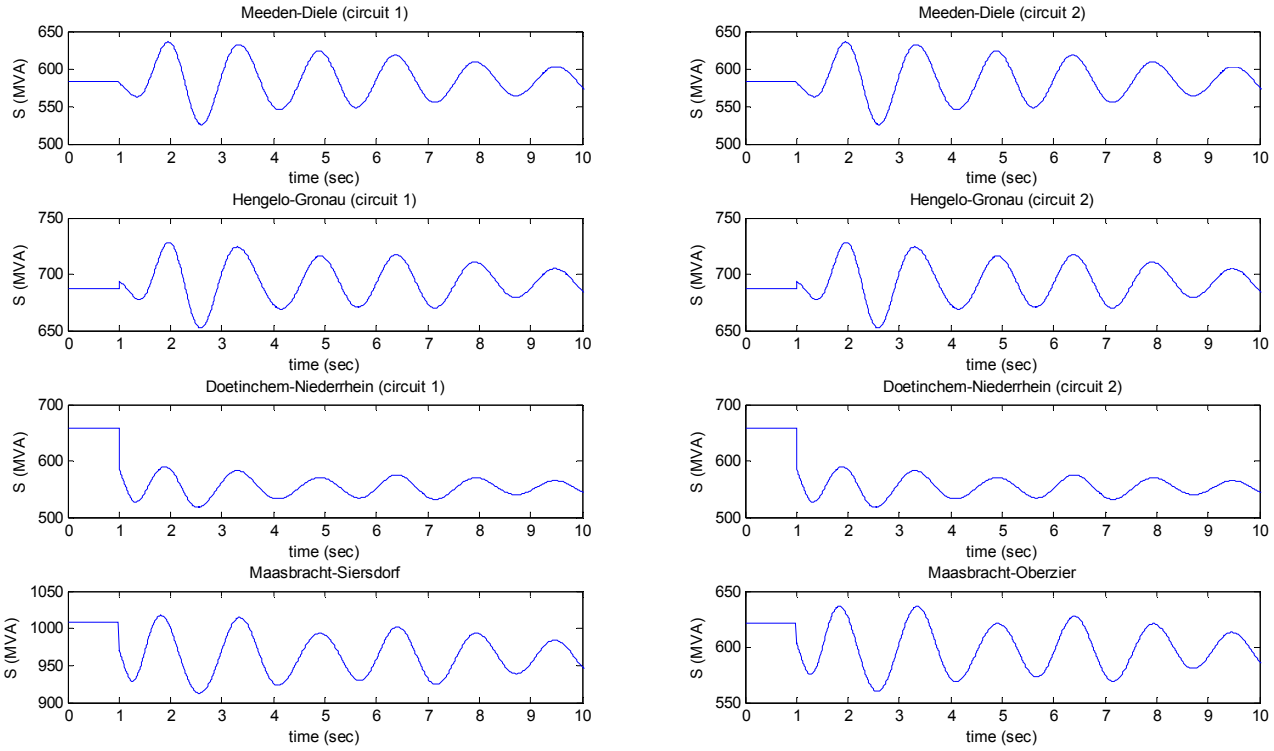

Fig.E.71 NL-DE interconnection apparent power for loss of the OST-PHLP section

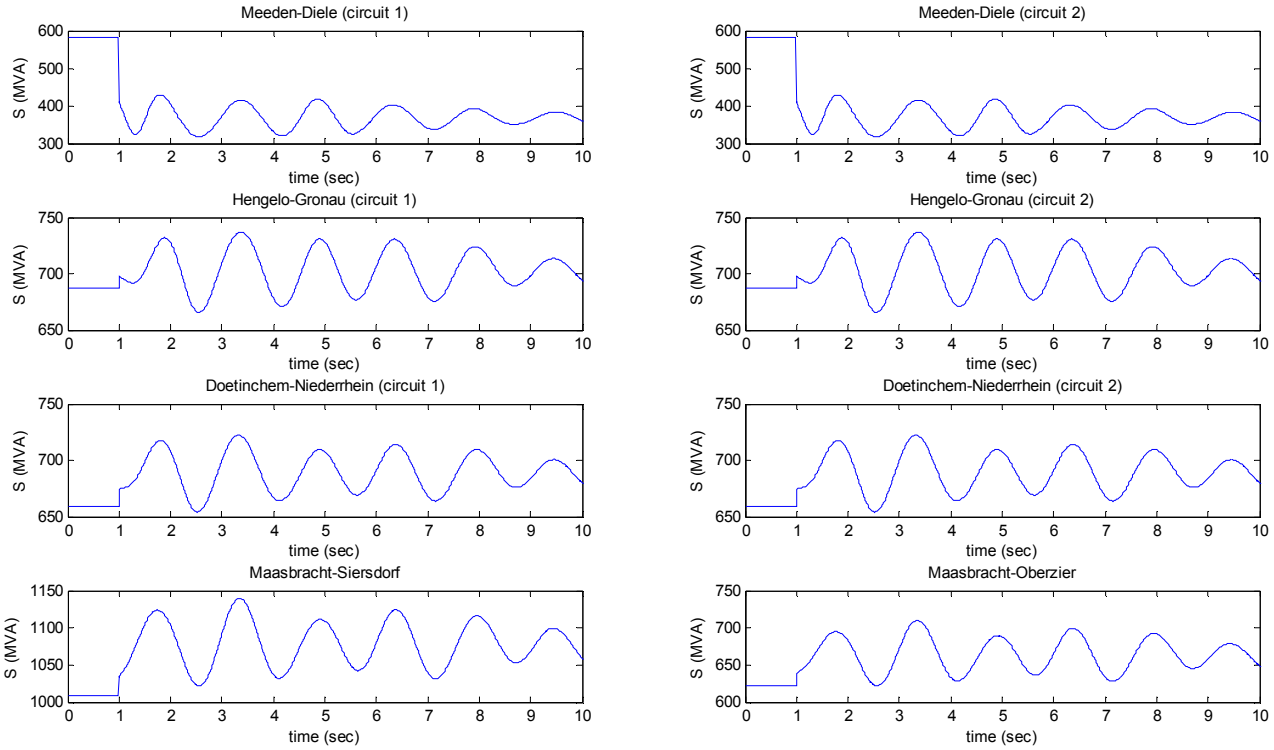

Fig.E.72 NL-DE interconnection apparent power for both sections lost

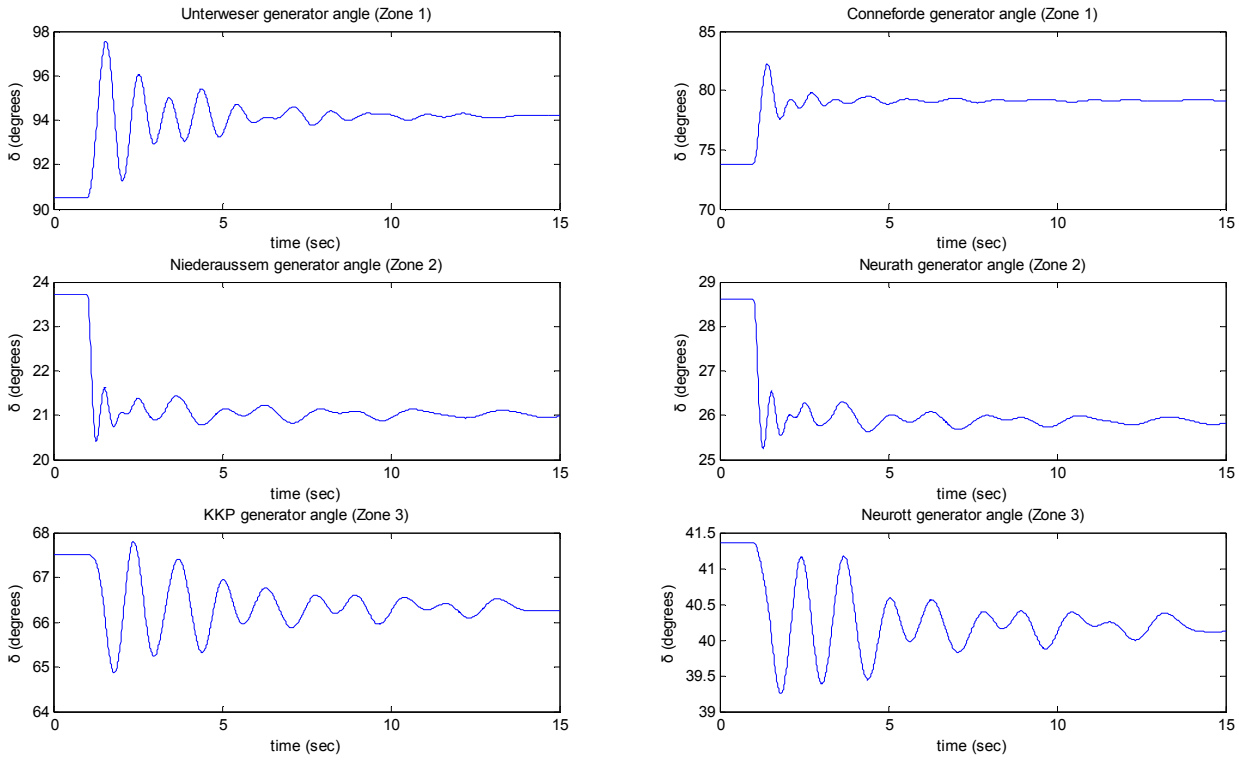

Fig. E.73 Effect of Corridor A's EMD-OST section loss on the rotor angles in Germany

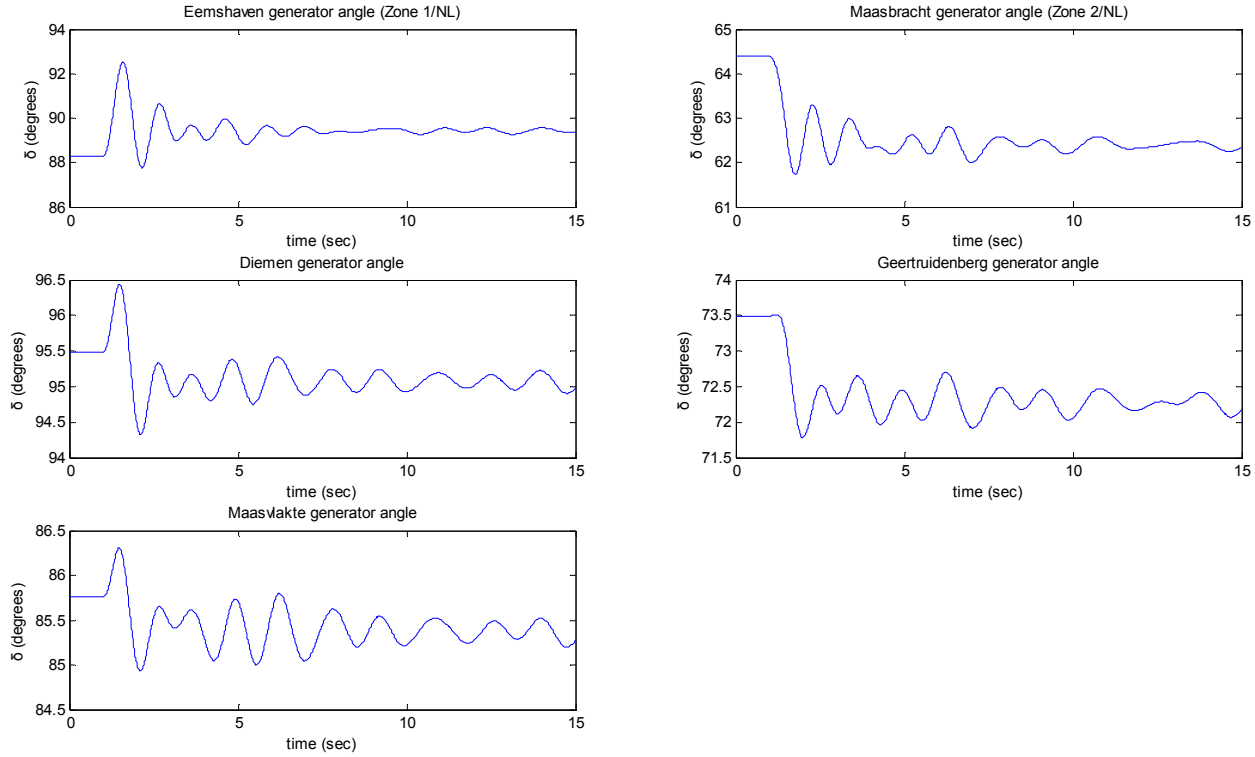

Fig. E.74 Effect of Corridor A's EMD-OST section loss on the rotor angles in the Netherlands

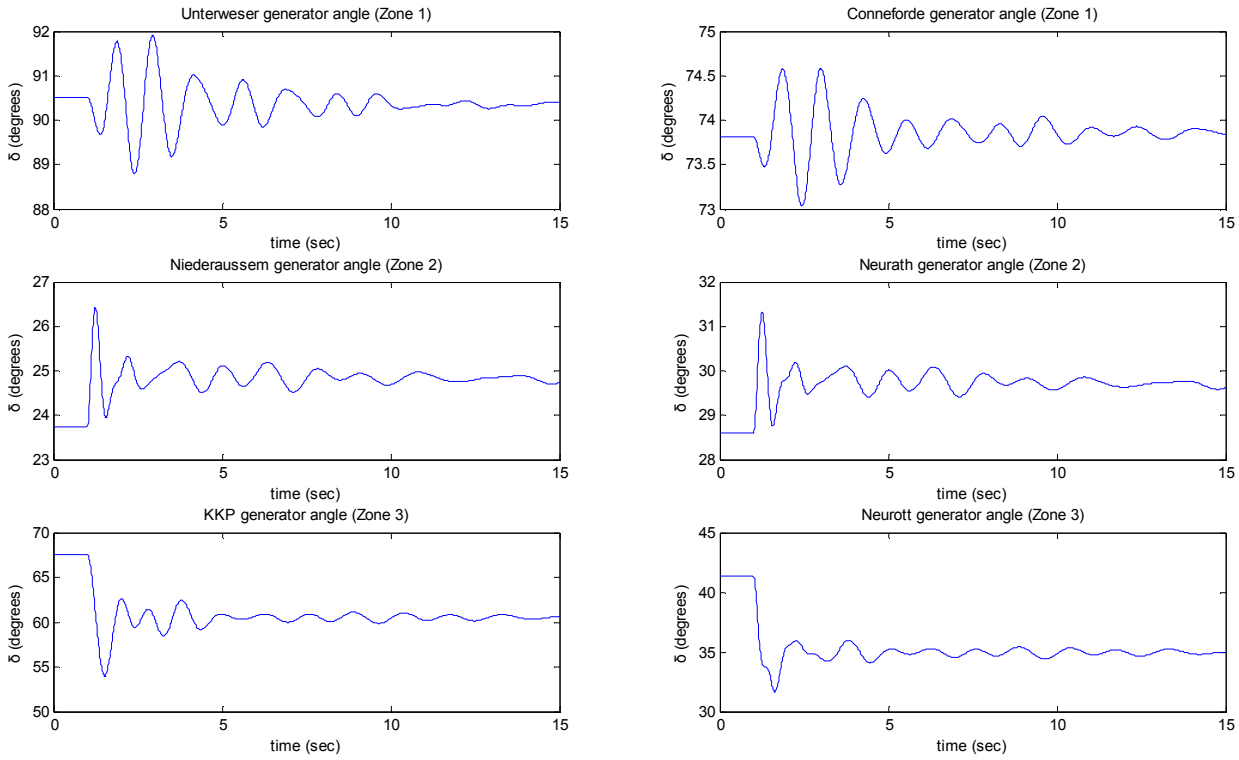

Fig. E.75 Effect of Corridor A's OST-PHLP section loss on the rotor angles in Germany

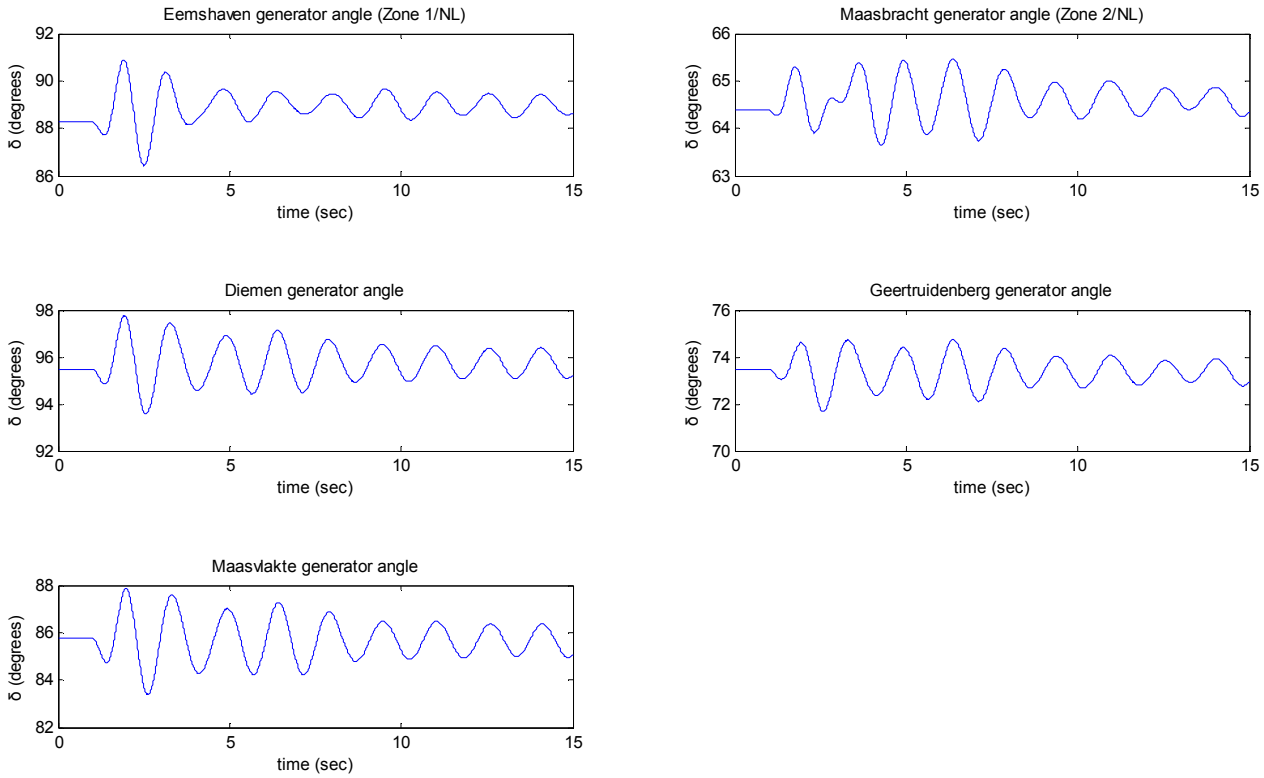

Fig. E.76 Effect of Corridor A's OST-PHLP section loss on the rotor angles in the Netherlands

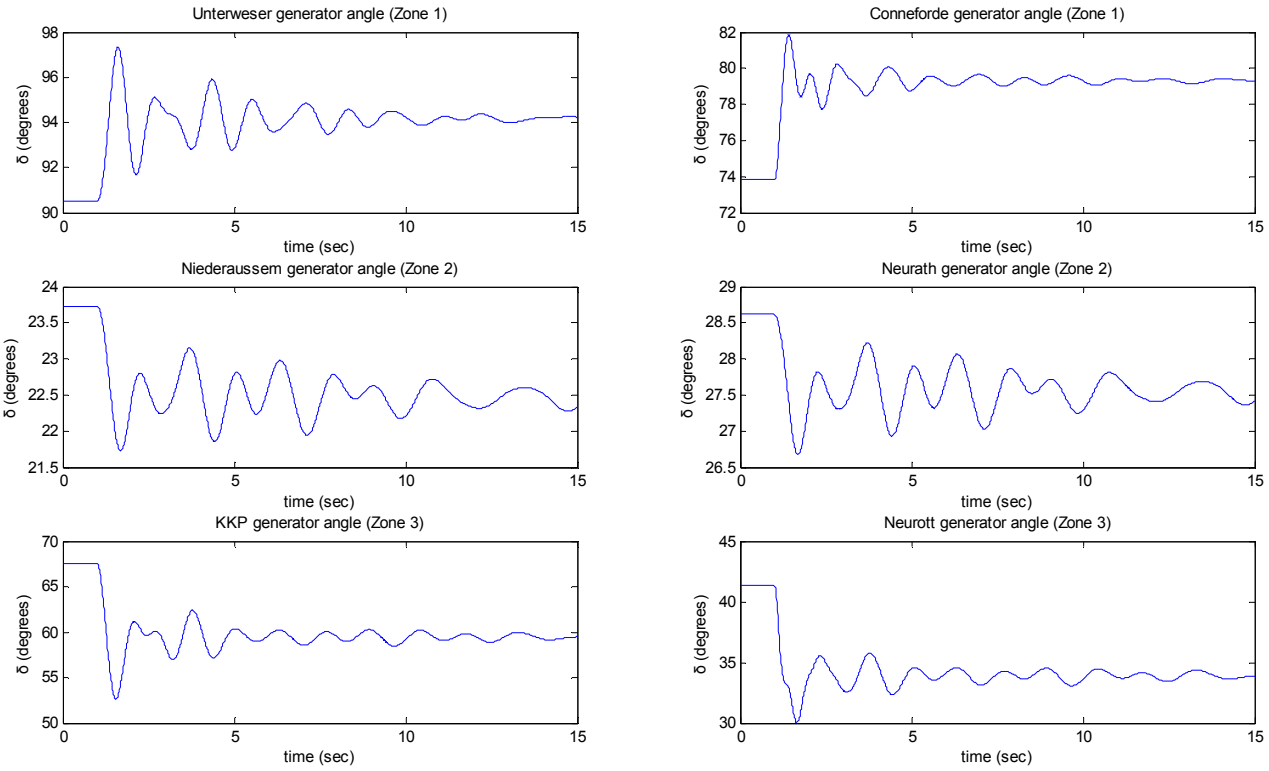

Fig. E.77 Effect of loss of both sections of Corridor A on the rotor angles in Germany

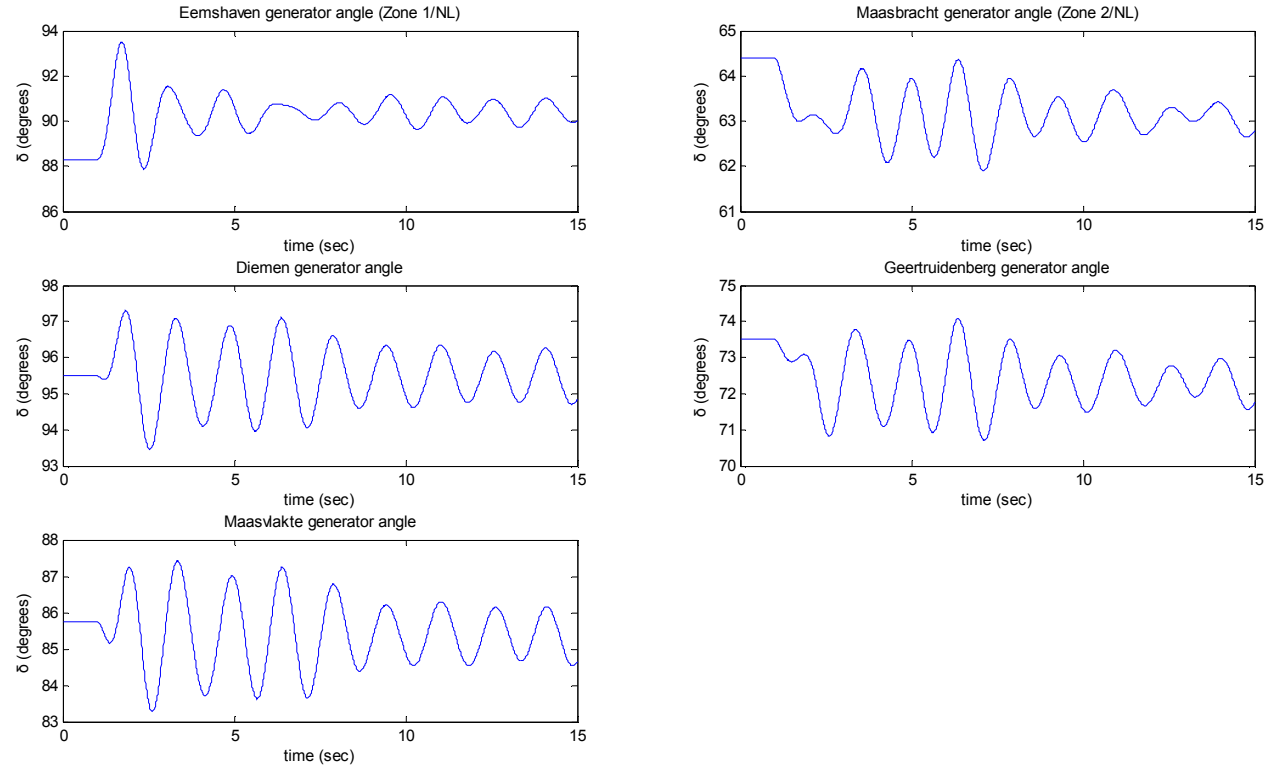

Fig. E.78 Effect of loss of both sections of Corridor A on the rotor angles in the Netherlands

Results of paragraph 4.5.2

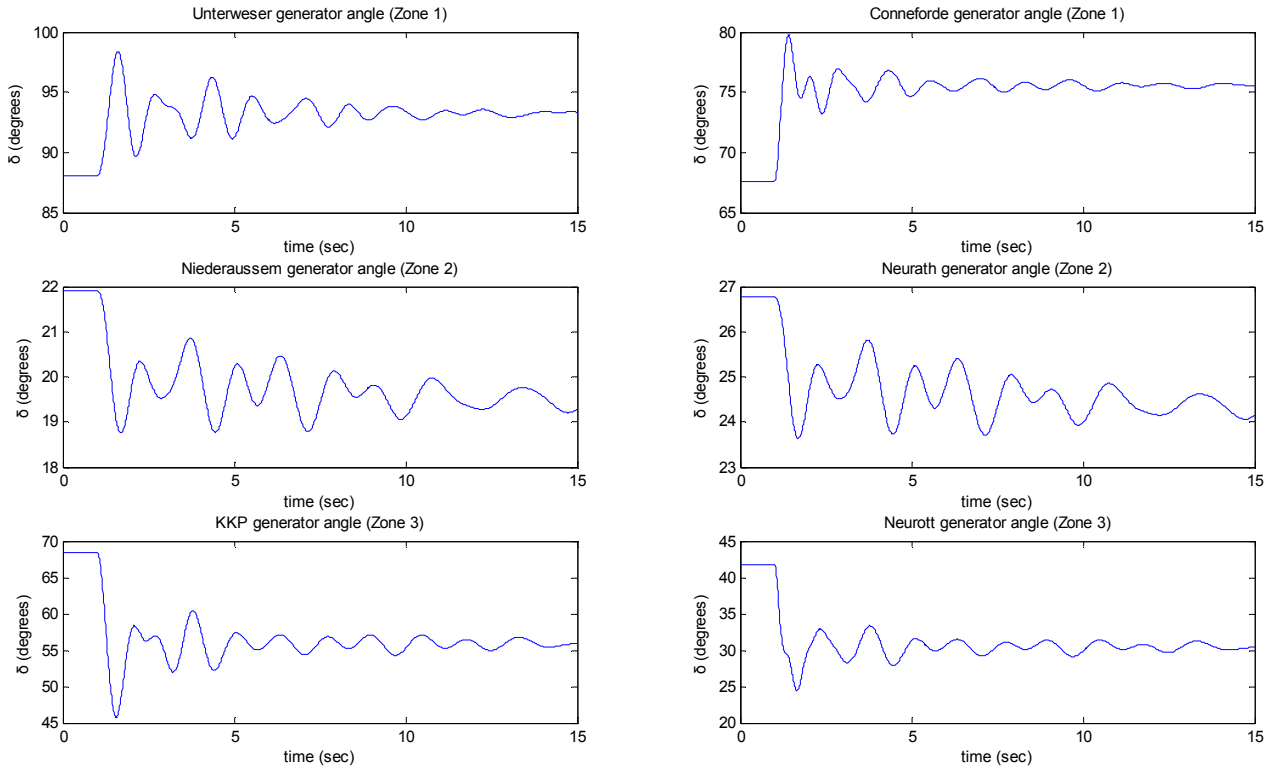

Fig. E.79 Effect of loss of both sections of Corridor A (3000 MW) on the rotor angles in Germany

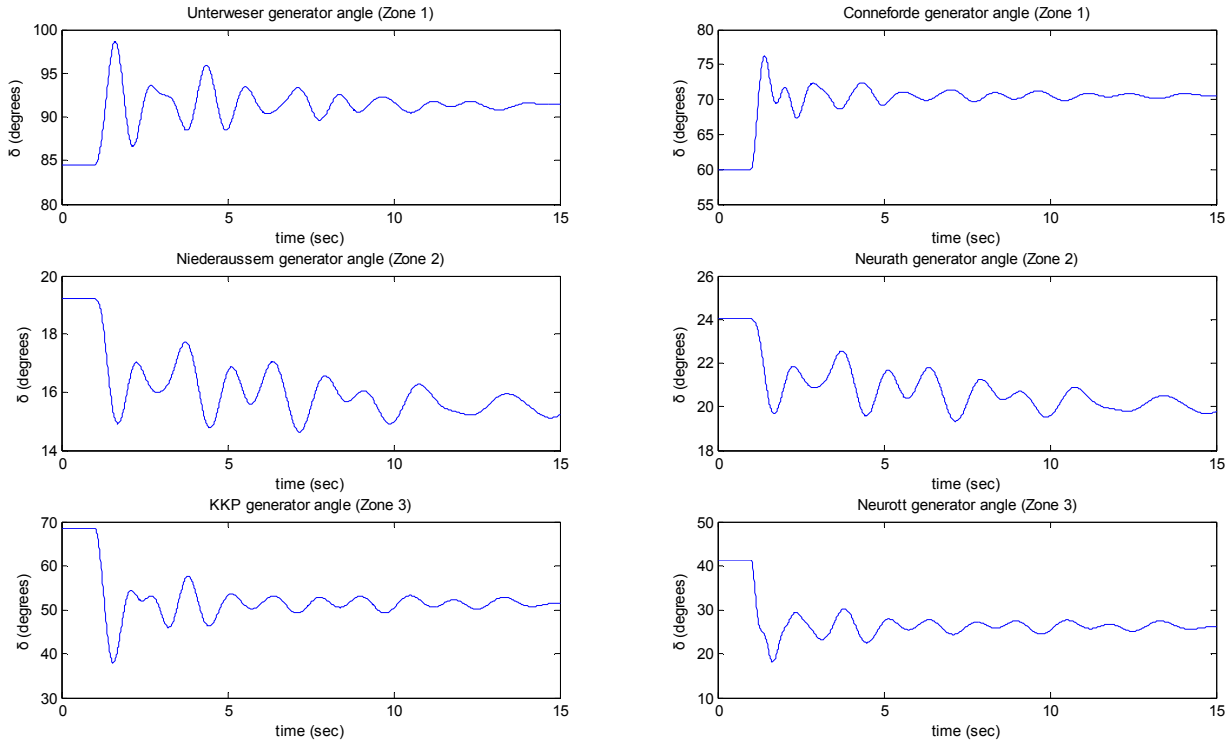

Fig. E.80 Effect of loss of both sections of Corridor A (4000 MW) on the rotor angles in Germany

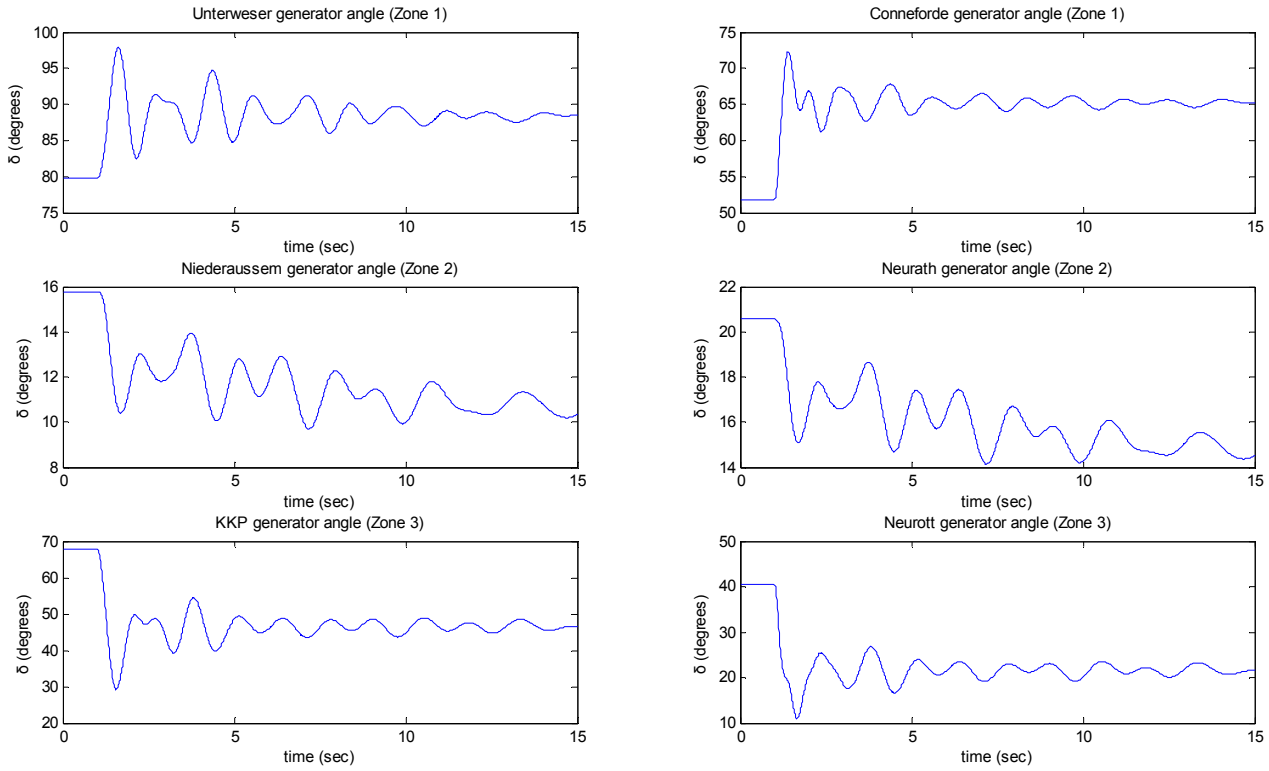

Fig. E.81 Effect of loss of both sections of Corridor A (5000 MW) on the rotor angles in Germany

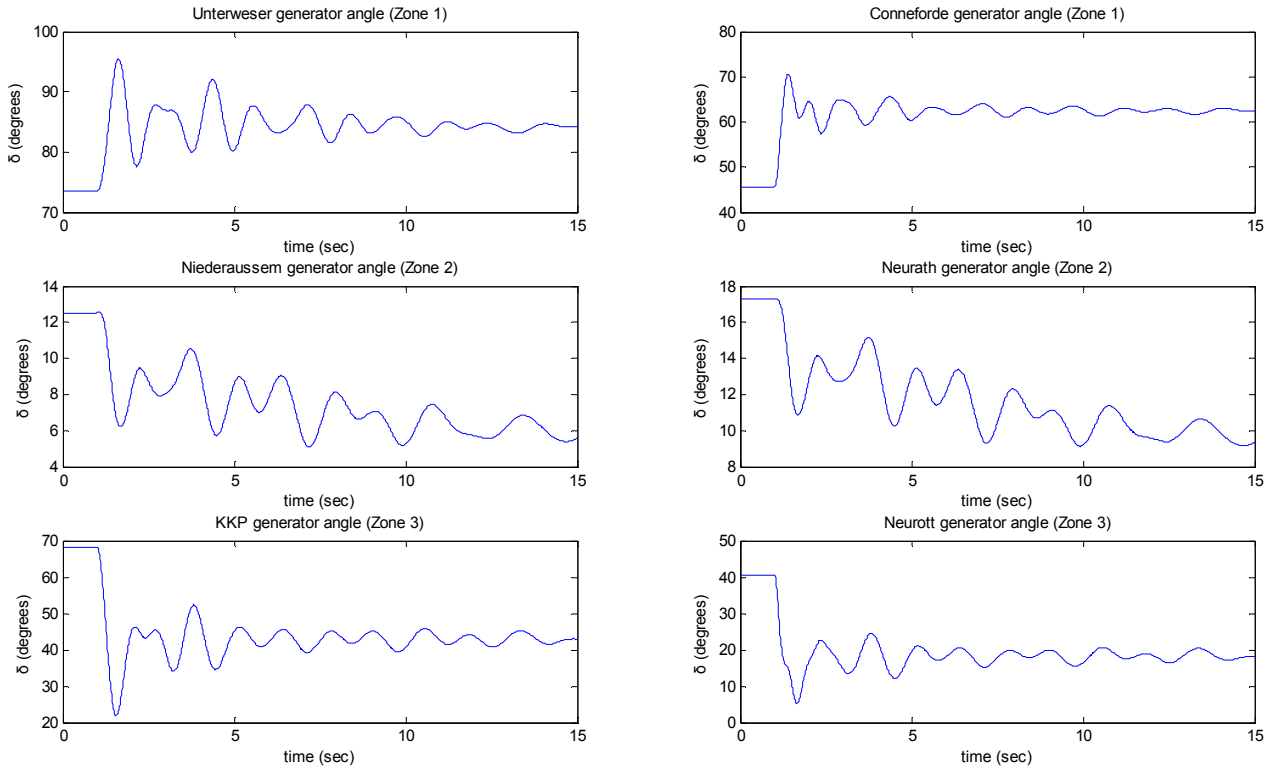

Fig. E.82 Effect of loss of both sections of Corridor A (6000 MW) on the rotor angles in Germany

APPENDIX E: Effect of the wind park modeling on the response of the system

In paragraph 4.1.1 it was mentioned that the behavior of the wind parks, in the transmission system model, is not modeled in an exact way. The wind parks in the Netherlands are modeled as negative static loads while outside of the Netherlands they are modeled as conventional synchronous generators using PSS®E's GENROU model. This modeling choice affects the outcome of the simulations in various ways. First of all in reality wind turbines have a specific fault ride-through characteristic which determines their behavior during and immediately after a fault in the system. This fault ride-through behavior is not modeled. The fault ride-through of a wind turbine determines the reactive power support of the wind turbines during a fault as well as the minimum voltage for which they remain connected to the system.

Secondly, the reactive current support wind turbines offer during a fault is limited by the over-current capability of their VSC converters. The over-current capability of wind turbine converters is much smaller than the reactive power capability of conventional generators. This means that when modeling a wind turbine as a synchronous generator a much more optimistic scenario regarding the voltage profile during the fault, is represented.

Additionally synchronous generators are characterized by an inertia which is much larger than that of wind turbines. This inertia, among other factors, is linked with damping out oscillations that occur after a disturbance in the transmission system.

All the simulations presented in paragraph 4.4 have been run for the aforementioned type of modeling of wind parks. In this paragraph it will be seen how the modeling o the wind parks affects the simulation results. This will be done by replacing the offshore wind turbines in the North Sea area with negative static loads. Only the North Sea wind turbines will be replaced because these are closely related to Corridor A and might affect the most the results.

This scenario will represent a more concervative situation than before or than reality since static loads do not offer reactive current support during the fault and have zero inertia. However this comparison will show the amount by which the results are affected by the wind park modeling. Additionally by reducing the total reactive power support and inertia in the system, any possible stability issues that were previously avoided due to the optimistic modeling of wing parks as conventional generators, will be revealed.

The first step in order to determine how the wind park modeling affects the system's dynamic behavior is to examine the response of the system voltages to a disturbance. In order to do so, a three-phase bus fault will be applied in Dorpen's 380 kV bus. The voltage profile of a selected number of buses in the Dutch and German transmission systems will be shown for the cases where the German wind parks are modeled as synchronous generators and as negative static loads. Corridor A's k gain has been set to zero and therefore its converters do not offer voltage support (k=0) during the fault. The selected buses are in Emden, Conneforde, Osterath, Dulken and Philippsburg from Germany and Meeden, Maasbracht and KIJ from the Netherlands.
The voltages are shown in figure F.1.

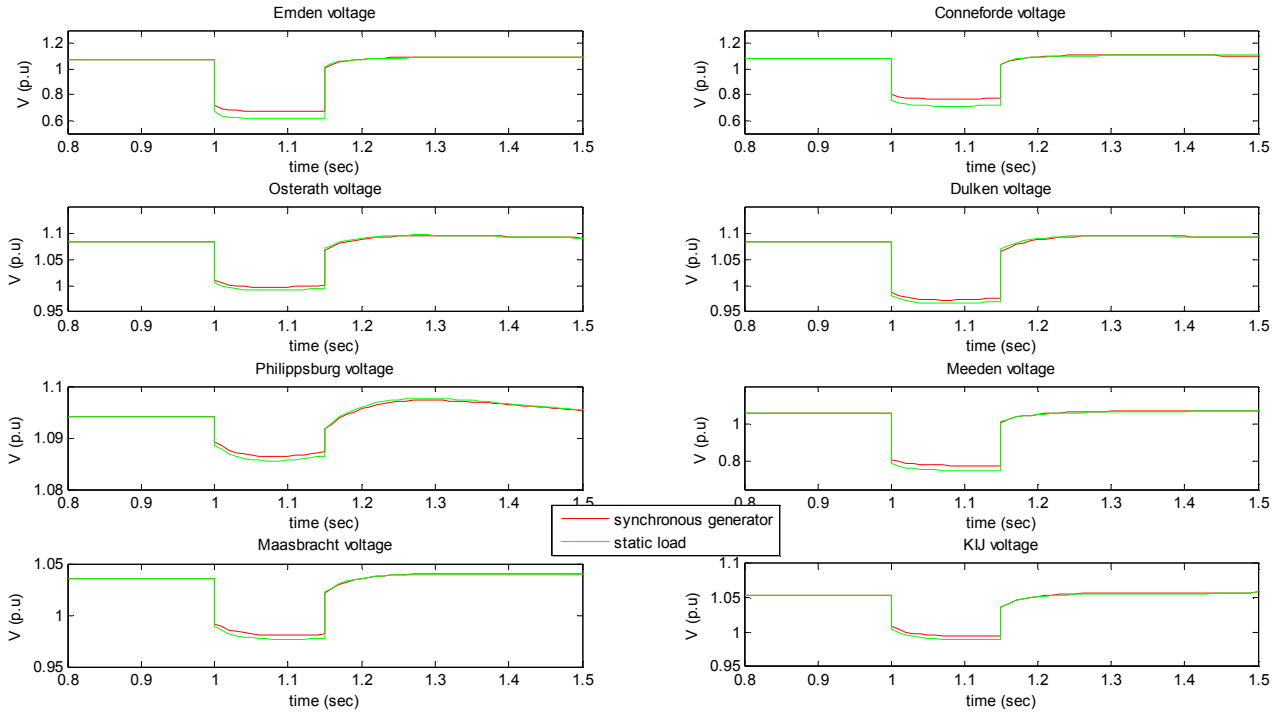

Fig.F.1 Comparison of bus voltages for different wind park modelling

As can be seen from figure F.1 the lack of reactive power support from the wind parks, for the case that they are modelled as static loads, leads to lower voltages during the fault. In order to specify how the difference in modelling affects each area of the system the average voltage dips of the buses above are shown in table F.1.

	Emden	Conneforde	Osterath	Dulken	Philippsburg	Meeden	Maasbracht	KIJ
Wind park model	**ΔV%**	**ΔV%**	**ΔV%**	**ΔV%**	**ΔV%**	**ΔV%**	**ΔV%**	**ΔV%**
synchronous generator	37.023	29.071	7.938	10.122	0.669	26.354	5.202	5.546
static load	42.323	34.122	8.430	10.725	0.741	28.940	5.593	6.052

Table F.1 Comparison of average voltage dips for different wind park modelling

As can be seen from table F.1, the impact of the wind park model is greater in the area close to the North Sea. This makes sense since only the offshore wind parks in the North Sea were replaced. In buses far from the connection points of these offshore wind parks the difference of the voltage profile is quite smaller. For example, the voltage dip in Philippsburg for different wind turbine models is only 0.072% (0.741%-0.669%) while in Emden it is 5.3% (42.323%-37.023%).

Next the effect of the wind park modelling on the rotor angles of generators in the Dutch and German system will be examined. The selected generators are Unterweser, Conneforde, KKP and Neurott from Germany and Eemshaven and Maasvlakte from the Netherlands.

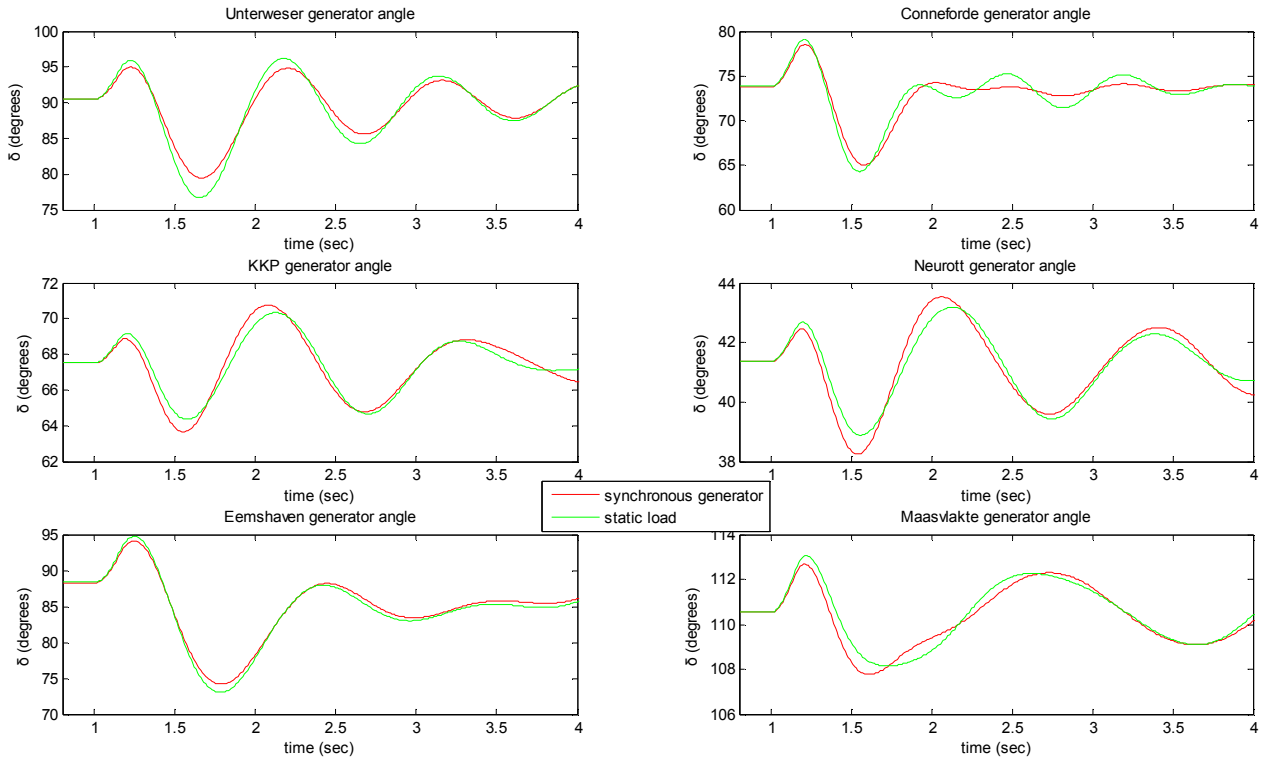

Fig.F.2 Comparison of generator rotor angles for different wind park modelling

As can be seen from figure F.2, by modelling wind parks in the North Sea region as static loads the oscillation of the generator rotor angles becomes larger. This again is due to the lower reactive power support in the system during the fault. The lower voltages that were seen in figure F.1, for the static load wind turbine modelling, will result in higher rotor angle oscillations.

Additionally it can be seen that the lower system inertia doesn't seem to deteriorate the damping of the disturbance induced oscillations. This is probably because only the wind parks of the North Sea were replaced by static loads. Probably if all the wind parks in the transmission system model were replaced by static loads then the effect of reduced inertia would be more noticeable.

Having seen how the wind park modelling affects the voltage profile and damping of the post-fault oscillations, what remains to be seen now is if the results and conclusions of paragraphs 4.3 and 4.4 change by changing the wind park modelling approach.

In order to do so, some of the simulations of paragraph 4.3.1 will be repeated in the case where the wind parks of the North Sea are modelled as negative static loads. There is no need to repeat all the simulations of paragraph 4.3.1 in order to examine the validity of the conclusions. Only the effect of the k gain on the voltage profile and rotor angle stability of the system for a fault in Dorpen will be revisited.

Table F.2 shows the average voltage dip of selected generators for different values of k gain and for the wind parks in the North Sea region modelled as static loads.

	Diele (Zone 1)	Conneforde (Zone 1)	Dulken (Zone 2)	Rommerskirchen (Zone 2)	Meeden (NL)	Diemen (NL)	Maasbracht (NL)	Geertruidenberg (NL)
k	**ΔV%**	**ΔV%**	**ΔV%**	**ΔV%**	**ΔV%**	**ΔV%**	**ΔV%**	**ΔV%**
0	49.365	34.122	10.725	5.485	28.940	9.211	5.593	4.941
2	43.991	26.443	8.741	41.190	25.883	8.309	4.966	4.439
4	41.535	22.776	7.872	3.626	24.423	7.922	4.764	4.268
6	40.702	21.525	7.314	3.260	23.932	7.800	4.674	4.218

Table F.2 Effect of k gain on the average voltage dip for a fault in Dorpen (Zone 1) (North Sea wind parks modeled as static loads)

Comparing the values of tables F.2 and 4.1 it is seen that the same conclusions can be drawn, i.e that higher k gain and thus higher additional reactive current during a fault leads to a better voltage profile in the system's buses. Also one can see that in general, the voltage dips for the static load wind park modeling are higher than those for the synchronous generator wind park modeling. This was seen also from figure F.1 and table F.1 and is due to the lack of reactive power support when the wind parks are modeled as static loads.

Next the rotor angles of selected generators will be examined. Table F.3 shows the rotor angle deviations of generators for the case where wind parks are modeled as static loads.

	Unterweser (Zone 1)	Conneforde (Zone 1)	Niederaussem (Zone 2)	Neurath (Zone 2)	Eemshaven (NL)	Maasbracht (NL)
k	$\Delta\delta_{max\%}$	$\Delta\delta_{max\%}$	$\Delta\delta_{max\%}$	$\Delta\delta_{max\%}$	$\Delta\delta_{max\%}$	$\Delta\delta_{max\%}$
0	5.960	7.104	6.461	4.813	7.213	1.644
2	4.741	5.235	4.327	3.513	6.237	1.515
4	5.352	7.399	7.855	7.609	6.425	1.354
6	5.881	8.807	10.615	9.590	6.654	1.280

Table F.3 Effect of k gain on the maximum rotor angle deviation for a fault in Dorpen (Zone 1) (North Sea wind parks modeled as static loads)

Comparing the values of tables F.3 and 4.5 it can be seen that for both wind park modeling approaches the rotor angle behavior of the generators is similar. In both cases the rotor angle stability of generators in Zones 1 and 2 deteriorates for values of k larger than 2. However it is seen that for wind parks modeled as static loads the rotor angle in Eemshaven deteriorates, for k=4, instead of improving as was seen from table 4.5. The beneficiary effect voltage support had on the rotor angle of Eemshaven's generator for k=4 is decreased due to the lack of voltage support by the wind generators in this modeling approach. Thus the effect of active current reduction on the rotor angles becomes larger resulting on the increase of the first rotor angle peak for k=4. Nevertheless this modeling approach of wind parks does not change the pattern followed by the rotor angles in generators located electrically close to the HVDC converters. This happens because in these generators the effect of active current reduction of the converters is greater than the effect of the voltage.

Looking at the above results it is clear that changing the modeling approach of the wind parks does not change significantly the result analysis and conclusions drawn in paragraphs 4.3 and 4.4. The only way that the wind park modeling affects the results is the amount of voltage dip during the fault. This however does not affect the validity of the conclusions previously drawn.

Bibliography

1) https://www.entsoe.eu/publications/system-development-reports/adequacy forecasts/

2) ENTSO E, “10 year network development plan 2012”, 5 July 2012

3) Netzentwicklungsplan Strom 2013, Zweiter Entwurf der übertragungsnetzbetreiber, 17 July 2013

4) http://spectrum.ieee.org/energy/renewables/germany-takes-the-lead-in-hvdc

5) http://www.world-nuclear.org/info/Country-Profiles/Countries-G N/Germany/#.Uma9vnDwmSo

6) Alstom, “HVDC: Connecting to the future”, Alstom Grid, 2010

7) CIGRE, Ifluenuence of embedded hvdc transmission on system security and ac network performance, 2013

8) J. Arrillaga, Y.H.Liu, N,R.Watson, “Flexible power options: the HVDC solutions”, John Wiley & Sons, LTD, 2007

9) Huang, Z., et al. "Exploiting voltage support of voltage-source HVDC." IEE Proceedings-Generation, Transmission and Distribution 150.2 (2003): 252-256.

10) Latorre, Hector F., and M. Ghandhari. "Improvement of voltage stability by using VSC-HVdc." Transmission & Distribution Conference & Exposition: Asia and Pacific, 2009. IEEE, 2009.

11) Shun, Frederik Leung, et al. "Influence of VSC HVDC on transient stability: Case study of the Belgian grid." Power and Energy Society General Meeting, 2010 IEEE. IEEE, 2010.

12) Liu, Yan, and Zhe Chen. "Transient voltage stability analysis and improvement of a network with different HVDC systems." Power and Energy Society General Meeting, 2011 IEEE. IEEE, 2011.

13) Liu, Yan, and Zhe Chen. "Power control method on VSC-HVDC in a hybrid multi-infeed HVDC system." Power and Energy Society General Meeting, 2012 IEEE. IEEE, 2012.

14) Erlich, I., et al. "Effect of wind turbine output current during faults on grid voltage and the transient stability of wind parks." Power & Energy Society General Meeting, 2009. PES'09. IEEE. IEEE, 2009.

15) ENTSO-E, “Draft Network Code on High Voltage Direct Current Connections and DC-connected Power Park Modules”, 7 November 2013

16) Tennet TSO GmbH, “Grid code: High and extra-high voltage”, December 2012

17) Arrillaga, Jos. High voltage direct current transmission. No. 29. Iet, 1998.

18) Kundur, Prabha. Power system stability and control. Eds. Neal J. Balu, and Mark G. Lauby. Vol. 7. New York: McGraw-hill, 1994.

19) Dorn, J., H. Gambach, and D. Retzmann. "HVDC transmission technology for sustainable power supply." Systems, Signals and Devices (SSD), 2012 9th International Multi-Conference on. IEEE, 2012.

20) ABB, HVDC light-The original VSC technology: Reference list

21) Andersen B.R, Xu and Wong K.T.G, “Topologies for VSC transmission”, AC-DC Power Transmission, 2001. Seventh International Conference , IEEE 2001

22) Flourentzou, Nikolas, Vassilios G. Agelidis, and Georgios D. Demetriades. "VSC-based HVDC power transmission systems: An overview." Power Electronics, IEEE Transactions on 24.3 (2009): 592-602.

23) Rodriguez, Jose, Jih-Sheng Lai, and Fang Zheng Peng. "Multilevel inverters: a survey of topologies, controls, and applications." Industrial Electronics, IEEE Transactions on 49.4 (2002): 724-738.

24) Lesnicar, Anton, and Rainer Marquardt. "An innovative modular multilevel converter topology suitable for a wide power range." *Power Tech Conference Proceedings*. Vol. 3. 2003.

25) Allebrod, Silke, Roman Hamerski, and Rainer Marquardt. "New transformerless, scalable modular multilevel converters for HVDC-transmission." Power Electronics Specialists Conference, 2008. PESC 2008. IEEE. IEEE, 2008.

26) Glinka, Martin, and Rainer Marquardt. "A new AC/AC multilevel converter family." Industrial Electronics, IEEE Transactions on 52.3 (2005): 662-669.

27) Chuco, B., and E. H. Watanabe. "A comparative study of dynamic performance of HVDC system based on conventional VSC and MMC-VSC." Bulk Power System Dynamics and Control (iREP)-VIII (iREP), 2010 iREP Symposium. IEEE, 2010.

28) Friedrich, Kurt. "Modern HVDC PLUS application of VSC in Modular Multilevel Converter topology." Industrial Electronics (ISIE), 2010 IEEE International Symposium on. IEEE, 2010.

29) Kreusel, Jochen, and Dietmar Retzmann. "Integrated AC/DC Transmission Systems–Benefits of Power Electronics for Security and Sustainability of Power Supply." Power System Computation Conference. 2008.

30) Dena Grid Study II, "Integration of Renewable Energy Sources in the German Power Supply System from 2015-2020 with an Outlook to 2025", November 2010

31) http://www.energy.siemens.com/mx/pool/hq/power transmission/HVDC/HVDC_Proven_Technology.pdf

32) Stijn, COLE. *Steady-state and dynamic modelling of VSC HVDC systems for power system Simulation*. Diss. PhD dissertation, Katholieke University Leuven, Belgium, 2010.

33) http://www.offshore-windenergie.net/en/wind-farms/operating-wind-farms

34) MOHAN, Ned; UNDELAND, Tore M. Power electronics: converters, applications, and design. John Wiley & Sons, 2007.

35) M. Davies, M. Dommaschk, J. Dorn, J. Lang, D. Retzmann, D. Soerangr. HVDC PLUS – Basics and principle of operation. Technical article, Siemens, 2011

36) ZHANG, Lidong. Modeling and control of VSC-HVDC links connected to weak AC systems. 2010.

37) Mario Ndreko, Marjan Popov, Jens C. Boemer, Mart A. M. M. van der Meijden. "Sensitivity Analysis on Short-Circuit Current Contribution from VSC-HVDC Systems Connecting Far and Large Offshore Wind Power Plants", IEEE ISGT 2014 Europe, Instanbul. 2014-10-12

38) C. Ismunandur, A. A. van der Meer, R. L. Hendriks, M. Gibescu and W. L. Kling, "Control of multi-terminal VSC-HVDC for Wind Power Intergration using the voltage-margin method," *in in Proc. 9th International workshop on Large Scale Integration of Wind Power into Power systems as well as on Transmission Networks for Offshore Wind Power Plants, Quebec City, Canada*, Oct. 18-19, 2010.

39) P. Kundur, J. Paserba, V. Ajjarapu, G. Andersson, A. Bose, C. Canizares, N. Hatziargyriou, D. Hill, A. Stankovic, C. Taylor, T. van Cutsem and V. Vittal, "Definition and Classification of Power System Stability", *Power Systems, IEEE Transactions, Definition and classification of power system stability IEEE/CIGRE joint task force on stability terms and definitions, vol. 19, no. 3, pp. 1387-1401*, 2004.

40) Van Cutsem, Thierry, and Costas Vournas. *Voltage stability of electric power systems*. Vol. 441. Springer, 1998.

41) Zhang, Lidong. "Modeling and control of VSC-HVDC links connected to weak AC systems." (2010).

42) Li, Guangkai, et al. "Research of nonlinear control strategy for VSC-HVDC system based on Lyapunov stability theory." ***Electric Utility Deregulation and Restructuring and Power Technologies, 2008. DRPT 2008. Third International Conference on*****. IEEE, 2008.**

43) Liang, Haifeng, et al. "Analysis and Design of H Controller in VSC HVDC Systems." ***Transmission and Distribution Conference and Exhibition: Asia and Pacific, 2005 IEEE/PES*****. IEEE, 2005.**

44) Shire, Tamiru Woldeyesus. ***VSC-HVDC Based Network Reinforcement*****. Diss. M. Sc. thesis Electrical power Engineering department, Delft University of Technology, 2009.**

45) Temesgen, Haileselassie. ***Control, Dynamics and Operation of Multi-terminal VSC-HVDC*****. Diss. PhD dissertation, Norwegian University of Science and Technology, 2012.**

46) Du, Cuiqing. "The control of VSC-HVDC and its use for large industrial power systems." Diss. Licentiate dissertation, Chalmers University of Technology, Sweden, 2003.

47) Shewarega, F., I. Erlich, and José L. Rueda. "Impact of large offshore wind farms on power system transient stability." Power Systems Conference and Exposition, 2009. PSCE'09. IEEE/PES. IEEE, 2009.

48) IEC 61400-27-1: Wind Turbines - Part 27-1: Electrical Simulation models for wind power generation," ***IEC,*** **vol. Committee draft (CD), no. Ed.1, 04 2012.**

49) http://ec.europa.eu/clima/citizens/eu/index_en.htm

50) Siemens, "PSS®E 33 user's manual," Siemens Power Transmission and Distribution, Inc., Power Technologies International, January 2012.